SYNAPTOPODIN-2, AN ACTIN-BINDING PROTEIN, IS A PROMYOGENIC FACTOR FOR MYOBLAST FUSION AND MYOFIBRILLOGENESIS IN MOUSE AND ZEBRAFISH

by

Nandini Nagarajan Margam

Submitted in partial fulfilment of the requirements
for the degree of Doctor of Philosophy

at

Dalhousie University
Halifax, Nova Scotia
November 2019

THIS THESIS IS DEDICATED TO:

MY PARENTS

UTHIRA NAGARAJAN AND NAGARAJAN MARGAM

MY SUPERVISOR

DR. ROY DUNCAN

AND

MY MENTOR

DR. FUIBOON KAI

TABLE OF CONTENTS

LIST OF TABLES

LIST OF FIGURES

ABSTRACT

Myogenesis is a differentiation-dependent process involving migration and fusion of uninucleated myoblasts to form multinucleated myotubes, the building blocks of striated, contractile muscle fibers. Several actin-binding proteins are involved in remodeling the actin cytoskeleton and one such protein is synaptopodin-2 (synpo2). Synpo2 binds and polymerizes actin and is upregulated during myogenesis, however, its functional role in the multistep myogenic program is unknown. My objective was to use cell culture and *in vivo* models of myogenesis to determine the roles of SYNPO2 isoforms during myogenesis. The first model used ectopic expression of the three mouse SYNPO2 isoforms (SYNPO2A, SYNPO2B and SYNPO2As) in stably transduced mouse C2C12 myoblasts or shRNA knockdown of endogenous synpo2, and the effects of these isoforms on migration and fusion was assessed using various approaches. Results indicated that only SYNPO2As is upregulated following differentiation and that knockdown of endogenous SYNPO2As inhibits myotube formation. Ectopic overexpression of SYNPO2As increased myotube formation and pharmacological inhibition of the Rho effector kinase ROCK resulted in loss of the enhanced fusion phenotype. Conversely, ectopic expression of SYNPO2A or SYNPO2B inhibited myotube fusion, consistent with the lack of upregulated expression of these isoforms following differentiation. All three isoforms increased C2C12 migration independent of ROCK inhibition indicating SYNPO2As utilizes two different pathways to promote myoblast migration and fusion. To understand the function of synpo2 *in vivo*, studies were carried out using zebrafish embryos. Zebrafish Synpo2 expression was restricted to the musculature of developing embryos and inhibiting Synpo2 expression using morpholino knockdown or CRISPR knockout resulted in abnormal muscle development. Morpholino-injected embryos showed a dramatic curved tail phenotype and immunostaining and electron microscopy revealed disorganized actin fibers, reduced myotube formation and disorganized Z-disk filaments. CRISPR knockout embryos did not show a curved tail phenotype but electron microscopy revealed immature myofilaments and reduced I band width. Loss of the curved tail phenotype and abnormal myotube formation did not reflect upregulated genes that could be compensating for the absence of Synpo2, as assessed by RNAseq analysis, but numerous genes associated with myofibril organization were significantly downregulated. Together, these results identify synpo2 as a new promyogenic factor.

LIST OF ABBREVIATIONS USED

Akt1	Protein kinase B
AMOT	Angiomotin
Abrab	Actin binding Rho activating protein b
Ankrd2	Ankyrin-repeat domain 2
Ants	Antisocial
ARF6	ADP-ribosylation factor 6
Arp2/3	Actin-related protein 2/3
Atp2a1	ATPase sarcoplasmic/endoplasmic reticulum Ca2+ transporting 1
BAG3	Bcl2associated athanogene 3
bHLH	Basic helix-loop-helix
Blow	Blown fuse
BOC	Brother of CDON
BRAG2	IQ motif and SEC7 domain-containing protein 1
CaMKII	Calmodulin-dependent protein kinase II
CaN	Calcineurin
Casq1b	Calsequestrin 1
CDK2	Cyclin-dependent kinase 2
CDK4	Cyclin-dependent kinase 4
CDON	Cell Adhesion Associated, Oncogene Regulated
CHAP	Cytoskeletal heart-enriched actin-associated protein
CKIP	Pleckstrin homology domain-containing protein
CREB	cAMP response element-binding protein
CTGF	Connective tissue growth factor
Dia	Diaphanous
DOCK	Dedicator of cytokinesis
DRF	Diaphanous-related formin
Duf	Dumfounded
DYN2	Dynamin2
FC	Founder cell

FCM	Fusion competent myoblast
FGF	Fibroblast growth factor
FGFR	Fibroblast growth factor receptor
FKHR	Forkhead in human rhabdomyosarcoma
GAP	GTPase-activating protein
GEF	Guanine nucleotide exchange factor
GRAF1	GTPase Regulator Associated with Focal Adhesion Kinase
Hbs	Hibris
ICAM	Intercellular Adhesion Molecule
ID3	Inhibitor of DNA Binding 3
ILK	Integrin-linked kinase
IrreC	Irregular chiasm-C
Kirre	Kin of Irregular chiasm-C
Kirrel	Kin of IRRE-like protein 1
KIRREL3	Kin of IRRE-like protein 3
Klhl40a	Kelch-like family member 40a
LATS1	Large tumor suppressor kinase 1
MARCKS	Myristoylated alanine-rich C-kinase substrate
Mbc	Myoblast city
MHC	Myosin heavy chain
Myhc4	Myosin heavy chain 4
MLC	Myosin light chain
Mlpha	Melanophilin a
MRF4	Myogenic regulatory factor 4
MRTF	Myocardin-related transcription factor
mTOR	Mammalian target of rapamycin
Myf5	Myogenic factor 5
Myh1	Myosin heavy chain 1
Myh2	Myosin heavy chain 2
Myh3	Myosin heavy chain 3
Myh4	Myosin heavy chain 4

Myh7	Myosin heavy chain beta (MHCβ)
Myh7ba	Myosin, heavy chain 7B, cardiac muscle, beta a
Myha	Myosin heavy chain a
Myhz1.1	Myosin, heavy polypeptide 1.1, skeletal muscle
Myhz1.2	Myosin, heavy polypeptide 1.2, skeletal muscle
Myhz2	Myosin, heavy polypeptide 2, fast muscle specific
MyoD	Myogenic differentiation 1
Myog	Myogenin
MyoII/NMII	Non-muscle myosin II
Myom1a	Myomesin 1a
Myoz1b	Myozenin 1b
NAP1	Nck-associated protein1
NCAM	Neural cell adhesion molecule
Nkx3.2	NK3 homeobox 2
p38	p38 MAP Kinase
Parvab	Parvin, alpha b
PAX1	Paired box gene 1
PAX3	Paired box gene 3
PAX7	Paired box gene 7
PDZ	postsynaptic density protein 95/Drosophila disc large tumor suppressor 1/zonula occludens 1
PI3K	Phosphoinositide 3-kinase
PIP2	Phosphatidylinositol 4,5-bisphosphate
PKA	Protein kinase A
PLS	Podosome-like structure
ROCK	Rho-associated coiled-coil containing protein kinase
Rols	Rolling pebbles
Rst	Roughest
SCAR	Suppressor of cAMP receptor
Sltr	Solitary
Sns	Sticks and stones
SRF	Serum response factor

Synpo2b	Synaptopodin2b
TANC1	Tetratricopeptide Repeat, Ankyrin Repeat and Coiled-Coil Containing 1
TAZ	Transcriptional coactivator with PDZ-binding motif
TKS5	Tyrosine kinase substrate with five SH3 domain
Tnni2a.4	Troponin I type 2a tandem duplicate 4
Tnni4b.2	Tnni4b.2 troponin I4b, tandem duplicate 2
Tnnt3a	Troponin T type 3a (skeletal, fast)
Tnnt3b	Troponin T type 3b (skeletal, fast)
VCAM	Vascular cell adhesion protein
Vcla	Vinculin a
WASp	Wiskott–Aldrich Syndrome protein
WAVE	WASp family Verprolin homologue
WIP	WASp-interacting protein
Wnt	Wingless and Int derived from the protooncogene integration 1
YAP	Yes-associated protein

ACKNOWLEDGEMENTS

I would like to first thank my parents who have always been there to support and encourage me in all my success, trials and tribulations. I am greatly indebted to them for giving me a chance to achieve my dream without which I could have never made it here to do my PhD. I would like to thank my sisters and brother for all their support and extended care. I would also like to thank my parents-in-law for giving me my space and time for completing my degree. Without all of you, I could have never made it to what I am today!

My deepest gratitude to my supervisor, Dr. Roy Duncan, for accepting me into his lab and giving me an opportunity to do a PhD in a project that just started when I joined the lab. You have always given me the independence to learn and try new things, and it is because of your belief in me I have been able to achieve this far. Thank you for guiding me to write better and for all the opportunities you have given me throughout my degree.

I would like to especially thank FuiBoon for being a good friend and mentor, in and outside the lab. Right from day one until now, you have always been there to extend a hand and help me troubleshoot so many issues in my project. Your passion for research has inspired and motivated me to contribute more to research in the future.

My sincere thanks to my committee members, Dr. Craig McCormick, Dr. James Fawcett, and Dr. Victor Rafuse, for their continuous support throughout my degree and valuable suggestions to move my research forward. I would also like to thank Dr. Jason Berman for allowing me to collaborate, use the fish facility and lab space to carry out my zebrafish project. I also thank the members of the zebrafish core facility for maintaining my transgenic fish line and for setting up breeding embryos whenever requested. I thank Mary Ann for taking extra effort to, especially section my samples for EM imaging. I would also like to thank Stephen Whitefield and Brianne Lindsay for always being there to set up the microscopes according to the need of my experiments, especially for imaging zebrafish embryos. Without your help, I would have not been able to do any of my live embryo imaging experiments.

Without these people, my lab life would be so boring-Roberto, Nichole, Gerard, Duncan, Yiming, Jacob and Rory. Thank you, Roberto, for making our lab a happy place to work, and always be readily available for any kind of help I have asked for. Thank you, Nichole, for putting up with all my last-minute requests for ordering things, training me to

do a perfect qPCR, and always encourage me to look at things in an optimistic way. Thank you, Gerard, for your timely advice and support both in and outside the lab, and for your constant encouragement at all times. Thank you Yiming for your tireless effort in helping me with the phospho-blots. My special thanks to the honors students, Jacob and Rory. You both have immensely helped and have always been there to extend a hand to help finish my project.

I thank all my friends here in Halifax and back at home for encouraging me throughout my degree. Thank you for putting up with my whining and complaints when my experiments did not work; no matter what, you all helped me smile and laugh at the end of the day. A very special note of thanks and appreciation for my friend Vinoth, who initiated the zebrafish collaboration. Apart from your research, you invested time in training me to handle and work with zebrafish, and for helping me analyze the RNA-seq data. Thank you for all the support, fun times and science conversations we have had all these years- I have learned a lot from you.

Finally, my husband Jude, needs a special mention for putting up with me during my entire Ph.D., late-night waits, and especially being so patient and understanding during my thesis writing days. Thank you for being a wonderful friend and a great pillar of support to help me achieve my goal.

CHAPTER 1: INTRODUCTION

1.1 Overview

Cell fusion is a multistep process that includes: (1) alignment of two cells in close proximity of less that 10 nm; (2) rearrangement of the lipid bilayer to form a transient hemifusion intermediate that results in merging of the outer leaflets; and (3) pore formation and expansion that merges the inner leaflets and completes the fusion reaction allowing cellular content mixing. Proteins that are sufficient to fuse membranes of non-fusing cells are called fusogens (Hernández & Podbilewicz, 2017). Cell-cell fusion occurs in different cell types during development and regeneration and is important to maintain the structural integrity of an organism. Examples of cell-cell fusion processes are gamete fusion during fertilization, cytotrophoblast fusion during placenta formation to generate the syncytiotrophoblast, osteoclast fusion during bone development and maintenance, and myoblast fusion during muscle development (Brukman et al., 2019). Since my project focuses on myoblast fusion, in the following sections I will discuss in detail the steps involved during muscle development and myoblast fusion and the role of several proteins that regulate the different steps of myogenesis.

A simplified model of the different steps involved in myoblast fusion and myofiber formation is depicted in Fig. 1 (top panel). Myoblast fusion begins with uninucleated myoblasts that have a fibroblast-like morphology. External and internal cues trigger expression of differentiation-dependent myogenic factors, mainly transcription regulators, that upregulate expression of proteins needed for myoblast fusion and myofiber organization. Upon differentiation, the cells become elongated and spindle shaped, migrate to facilitate cell-cell contact and fuse to form myotubes. Each myotube contains several myofilaments that are made of actomyosin filaments and sarcomere building proteins that form repeating contractile units called sarcomeres. Several such myotubes align next to one another to form muscle fibers that form the functional unit of the skeletal muscle system. This process is not limited to development but also takes place during muscle injury and regeneration Fig. 1 (bottom panel). In adults, muscle stem cells called satellite cells are activated and differentiate into myoblasts that migrate to the site of muscle damage and fuse to repair the damaged muscle. Migration and fusion of myoblasts both require intense

actin remodelling that is regulated by numerous actin-binding proteins. My Ph.D. research was focused on identifying the role of the actin remodelling protein synaptopodin-2 during myogenesis. Hereinafter, synaptopodin-2 protein will be referred to generically as synpo2, and as SYNPO2 in places referring specifically to human and mouse protein isoforms. The protein and gene names of human, mouse, *Drosophila* and zebrafish will be mentioned according to the nomenclature guidelines mentioned in the respective databases.

Synpo2 is the second member of the podin family and is an actin regulator that promotes actin nucleation, polymerization and bundling. The function of synpo2 has been intensely studied in invasive prostate cancer where human *SYNPO2* gene deletion correlates with increased tumour invasiveness. Functioning as an actin regulator, this invasive cancer biomarker differentially regulates cancer cell migration and invasion and has been implicated in invasive prostate, bladder and breast cancer (Alvarez-Múgica et al., 2010; Arianne De Ganck et al., 2009; Gakis et al., 2012; Jing et al., 2004; Lin et al., 2001; Liu et al., 2018; Xia et al., 2018).

In skeletal muscle, synpo2 has been reported to localize in the nucleus of undifferentiated myoblasts and translocate to the cytoplasm upon differentiation where it localizes in the Z-disc and binds actin filaments (Weins et al., 2001). Synpo2 also binds to other actin-binding proteins such as α-actinin, filamin C and zyxin (Linnemann et al., 2010). Apart from its localization and binding partners in skeletal muscle, the functional role of synpo2 in muscle cells is unknown. In the last decade, the roles of several actin regulating proteins in myoblast fusion was explored in different *in vivo* models, especially in *Drosophila melanogaster*, where the formation of an actin rich structure called an invasive podosome-like structure (PLS) plays an important role during fusion. Adhesion proteins, cytosolic adapter proteins, and actin-regulating proteins all play a role in the formation of such structures. Since synpo2 is expressed in skeletal muscle and binds actin filaments in these tissues, we were interested in determining how synpo2 affects the different steps of myogenesis such as the differentiation program, myoblast migration and myoblast fusion to form multinucleated myotubes.

Before describing the details of what we know about synpo2 in cancer cell migration and skeletal muscle, I will first focus on describing the different steps of myogenesis and how different sets of proteins regulate these processes to bring about

myoblast fusion. Due to the complexity of the different steps, the number of proteins involved and the use of different animal and cell culture models, I will divide the following section into 6 subheadings: 1) Overview of skeletal muscle development; 2) steps involved during myoblast fusion; 3) proteins that regulate myoblast fusion in *Drosophila*; 4) proteins that regulate myoblast fusion in mouse; 5) proteins that regulate myoblast fusion in zebrafish; and 6) actin-regulating proteins. This section will be followed by a detailed description about the synpo family of proteins.

1.2 Myogenesis

Myogenesis or muscle development is a multistep process that is regulated by several transcription factors and proteins. The three types of muscle are skeletal, cardiac and smooth muscles that arise from different segments of the mesoderm. Striated cardiac and skeletal muscle contains repeating units called sarcomeres which consist of thick (primarily myosin) and thin filaments (primarily actin) associated with several other myofibrillar proteins such as α-actinin, filamin, titin, tropomyosin, troponin, etc. Cardiac muscle cells are elongated, branched, mononucleated cells filled with rod-like bundles of myofibrils (myosin and actin) and are separated from each other by intercalated discs. Smooth muscle cells are single cells, divided into two subgroups based on the mode of function. One is referred to as the single-unit type since the entire muscle contracts and relaxes (e.g., blood vessels [except large elastic arteries], urinary tract and digestive tract). The other type is the multiunit type where single cells are innervated (e.g., trachea, large elastic arteries and the iris of the eye). Throughout the rest of the Introduction I will be discussing in detail skeletal muscle development and its regulating proteins, as this is the muscle type germane to my thesis research.

1.2.1 Skeletal muscle development

In vertebrates, the notochord and neural tube form the axis of a developing embryo and the paraxial mesoderm that gives rise to muscle cells flank this axis. The specification and patterning of the paraxial mesoderm is regulated by WNT and FGF signalling (Ciruna & Rossant, 2001; Takada et al., 1994). The paraxial mesoderm has a dorsal and ventral section. The dorsal section is the dermomyotome that gives rise to muscles of the back,

limb, body wall and diaphragm. The cells that reside in this segment express PAX3, PAX7 and MYF5 (Lepper & Fan, 2010). The ventral section is the sclerotome that gives rise to the skeleton, and these cells express pax1 and NKX 3.2 (Zeng et al., 2002). Lateral to the paraxial mesoderm is the intermediate mesoderm that gives rise to kidney and gonads. The final layer is the lateral plate mesoderm that gives rise to tendons, cartilages, smooth muscle and cardiac muscle. The tip of the anterior paraxial mesoderm contains the somites that give rise to skeletal muscle cells. Some of these $PAX7^+$ cells have the capacity to proliferate and renew to become satellite cells (Yin et al., 2013). Most of the other pax7 cells express MYF5, MYOD, slow muscle myosin (MYH7), embryonic myosin heavy chain (MYH3) and skeletal α-actin. These cells form the primary myotome and fuse to form nascent myofibers during the phase of fusion called primary myogenesis. The PAX7 cells further undergo differentiation and express fast myosin heavy chain (MYH2, 4 and 1), myosin light chain 3 and acetylcholine receptors to allow innervation. These cells fuse during the secondary myogenic phase to form mature myofibers (Chal & Pourquié, 2017).

Similarly, in *Drosophila* the mesoderm is located between the ectoderm and endoderm. The mesoderm underdoes segmentation and each segment gives rise to somatic mesoderm and splanchnic mesoderm. The somatic mesoderm gives rise to founder cells (FC) and fusion competent myoblasts (FCM) that fuse to form multinucleated myotubes; the splanchnic mesoderm gives rise to the mesothelial covering of visceral organs. Cardiac muscle cells also develop from the dorsal side of the mesoderm (Baylies et al., 1998). The cell in each segment of the somatic mesoderm expresses the transcription factor twist, important for specification of the cell type. The anterior cells in each mesoderm segment express even-skipped (Eve) and give rise to vascular smooth muscle and fat body, while the posterior cells express sloppy paired (Slp) and give rise to cardiac and somatic muscle (Dobi et al., 2015). Further, the FC and FCM cells specifically expresses lethal of scute (L'sc) and lame duck (Lmd), respectively (Carmena et al., 1995; Duan et al., 2001). Using the two cell system in *Drosophila* (FCs and FCMs), numerous proteins and signaling pathways involved in myotube formation have been identified and informed establishment of a fusion model (Kim et al., 2015) that will be discussed in detail later in the Introduction.

1.2.2 Differentiation of skeletal muscle myoblasts

Myoblast differentiation is an irreversible and important step in myogenesis. The differentiation program induces the expression of muscle-specific genes that help in migration, fusion and myofiber organization. In cell culture, the differentiation program can by turned on by cell to cell contact or by switching culture conditions from growth media (containing 10% fetal bovine serum [FBS]) to differentiation media (containing 2% horse serum). It is still unclear what factors in the differentiation media trigger differentiation. In *in vivo* conditions, cell patterning and signalling molecules trigger the program. Myoblasts in the dermomyotome of vertebrates express PAX7 and MYF5. The expression of these proteins is maintained in proliferative myoblasts by wnt1 and wnt7a that in turn activates protein kinase A (PKA). PKA phosphorylates cAMP response-element binding protein (CREB), which translocates into the nucleus to transcribe PAX7, MYF5 and MYOD (Chen et al., 2005). In these proliferative myoblasts, several proteins involved in cell cycle control such as cyclin-dependent kinases CDK2/4, FGFR, Akt1 are activated (Knight & Kothary, 2011). CDK2/4 phosphorylates myoD (ser200), thereby retaining MYOD in the cytoplasm and inhibiting its transcription activity (Kitzmann et al., 2015).

Mitogen withdrawal or cell-cell contact activates kinases and other proteins to trigger the differentiation program. Cell-cell contact mediated-differentiation is initiated by a multifunctional cell-surface coreceptor, CDON, which interacts in *trans* with N-cadherin to recruit a protein complex including p38 (Krauss et al., 2017). The p38 kinase phosphorylates downstream targets that form a complex with MYOD in the nucleus to transcribe other basic helix-loop-helix (bHLH) myogenic regulatory factors (MRFs) such as MYF5, MYOD, myogenin and MRF4 that regulate expression of skeletal muscle specific genes. Mice with MYF5 or MYOD gene deletions develop normal muscles while a double knockout prevents normal muscle tissue development (Rudnicki et al., 1993) (Kaul et al., 2000; Rudnicki et al., 1992), indicating some redundancy in the function of these two proteins. Tight regulation of these proteins is necessary for the development and maintenance of musculature in different animal models.

1.2.3 Steps involved in myoblast fusion

Once the cells differentiate by the above-mentioned pathways, they are now primed to fuse and form multinucleated myotubes. During myoblast fusion, an actin-rich fusion synapse is formed at the site of cell-cell fusion. To drive fusion synapse formation, the cells need to be brought into close proximity (~10-20 nm) to aid in membrane remodelling and this process is favoured by cell-adhesion proteins. The engagement of cell-adhesion and membrane proteins in *cis* and in *trans* is essential to initiate cell-cell contact and drive downstream signalling and actin remodelling. Our most detailed understanding of the fusion synapse derives from studies in *Drosophila*, where the fusion synapse is termed a podosome-like structure (PLS) (Fig. 2). Several cell adhesion molecules and membrane receptors have been identified that drive downstream signalling, activating actin polymerization via the SCAR-Arp2/3 and Rho-ROCK pathways to form the fusion synapse. The role of these proteins will be explained in the following sections in the order of migration, cell-cell contact, downstream signalling, and fusion synapse formation. The list of the proteins and functions are listed in Tables 1-4.

1.2.4 Proteins that regulate myoblast fusion in Drosophila

During myoblast fusion in *Drosophila*, two different cell types, fusion competent myoblasts (FCMs) and founder cells (FCs), are brought close to one another to initiate cell to cell contact and form a fusion synapse. Some of the proteins involved in this process are specific for one cell type, while others play similar roles in both cell types. The major players involved in this process and the structure of the resulting fusion synapse are illustrated in Fig. 2 (Kim et al., 2015). I will briefly explain the different proteins and their functions during fusion synapse formation and myotube formation.

Formation of the fusion synapse is first initiated by immunoglobulin-domain containing transmembrane receptor proteins (IgSF). The FC expresses Dumfounded (Duf/kin of Irregular-chiasm-C [Kirre]) and its paralogue Roughest (Rst/irregular-chiasm-C[(IrreC]), and the FCM expresses Sticks and Stones (Sns) and its paralogue Hibris (Hbs). Single knockouts of *duf* or *rst* have no effect on muscle development whereas double knockouts fail to form cell-cell adhesion sites and completely block myotube formation (Strünkelnberg et al., 2001). Thus, as with the transcription factors MYF5 and MYOD, there is some redundancy in function between adhesion proteins involved in myoblast

fusion. In contrast, Sns and Hbs paralogs act antagonistically during myoblast fusion (Artero et al., 2001). The *sns* knockout embryos show a complete block of fusion (Bour et al., 2000), whereas *hbs* knockout shows a partial block (Artero et al., 2001), suggesting that Sns and Hbs do not play a redundant function during myoblast fusion. Upon interaction, the cytoplasmic tails of these cell adhesion proteins recruit adaptor proteins that activate downstream signalling. In FCMs, Sns recruits the adapter protein Crk that interacts with Blown fuse (Blow) or Solitary (Sltr) and Wiskott–Aldrich Syndrome protein (WASp) (Kim et al., 2007; Doberstein et al., 1997; Schroter, 2004), and in the FCs adaptor protein Loner/Schizo, is a guanidine exchange factor (GEF) that activates the ARF6-Rac-SCAR pathway (Kim et al., 2007; Rushton et al., 1995; Chen et al., 2003). Loner mutants show irregular Rac localization and abnormally large actin foci that are unfavourable for functional fusion synapse formation (Richardson, Beckett, Nowak, & Baylies, 2007). Together, the WASP/SCAR pathways activate the Arp2/3 complex to remodel the actin cytoskeleton and form the PLS structure. In the FCs, Ants and Rols are recruited to the cytoplasmic tail of Duf after cell-cell adhesion. Ants functions by interacting with Myoblast city (Mbc) to regulate actin cytoskeleton remodelling through an undefined mechanism. Ants deficient mutants show normal cell-cell adhesion and differentiation of myoblasts by they fail to fuse due to abnormal actin cytoskeletal remodelling (Chen & Olson, 2001). Similarly, in FCs Rols7 interacts with Duf and recruits D-titin to form myofibers that connect the actin cytoskeleton to the membrane to enable myoblast fusion (Menon & Chia, 2001). The function of these and other actin regulatory proteins are explained in detail in section 1.2.7.

1.2.5 Proteins that regulate myoblast fusion in mouse

There are several proteins identified to date that play a role in mouse myoblast fusion. However, a defined fusion synapse model or pathways that regulate myoblast fusion as determined in *Drosophila* is yet to be identified. Some of these proteins and their localization on myoblasts is illustrated in Fig. 3. Since, a defined fusion structure is not established in mouse, the function of these proteins is defined based on their effect on differentiation, migration, and myoblast fusion.

1.2.5.1 Myoblast migration

In *in vivo* conditions, migration is assessed by the ability of the myoblasts to migrate from the dermomyotome to the somite or limb to form the specific type of muscle. Live imaging of myoblast migration in mice is challenging due to tissue thickness, whereas *in vitro* culture systems allow easy analyses of migration; however, this method has certain limitations such as 2D culture, absence of extracellular matrix and the affects of external and internal cues. Several of the membrane receptors that play a role in mouse myoblast migration are highlighted in the boxed region in Fig. 3. Knockdown of these proteins inhibits migration and fusion (Jansen & Pavlath, 2006; Bae et al., 2008; Horsley et al., 2003; Lafreniere et al., 2006; Mylona et al., 2006). Prostaglandins are the one example I am aware of where a protein decreases migration and enhances fusion (Bondesen et al., 2007). While most of the above-mentioned proteins show a direct correlation between increased migration and increased fusion, it has not been established whether these processes are directly coupled. Additionally, knockdown of actin binding proteins such as palladin (Nguyen & Wang, 2015) decreases migration and fusion of C2C12 myoblasts. However, these studies did not examine changes in the actin cytoskeleton and how such changes might lead to decreased migration and fusion.

1.2.5.2 Membrane proteins and receptors that regulate fusion

In Drosophila, the Duf and Sns immunoglobulin-domain containing membrane proteins directly regulate myoblast fusion and are indispensable. However, in the mouse model, several membrane proteins play a role in myoblast fusion and the absence of one such membrane protein is compensated by other membrane proteins. In the absence of these proteins, myoblast fusion is usually perturbed but not completely inhibited.

The Duf homolog in mice is KIRREL3. The *in vivo* function of KIRREL3 has not been examined, but KIRREL3 knockdown in C2 myoblasts inhibits cell elongation, induces randomized migration and reduces fusion. In control C2 myoblasts, kirrel3 is localized in the cell front to promote cell-cell adhesion. This localization also enables directed migration of myoblasts and aids in myoblast fusion (Tamir-Livne et al., 2017). The Sns homolog in mice is nephrin. Nephrin knockout in mice is lethal, so the function of nephrin has been assessed in myoblasts isolated from nephrin knockout mice. These cells

differentiate normally but remain mononucleated even after 4 days post-differentiation (Sohn et al., 2009). Although these homologs function to regulate myoblast fusion, it is unclear whether they function in *cis* or *trans*, or whether they interact with each other like Duf and Sns, and their effects on downstream signalling and actin regulation remains an open question (Fig. 3). Apart from KIRREL3 and nephrin, IgSF cell-adhesion molecules NCAM, VCAM and ICAM also play a role in myotube formation (Charlton et al., 2000; Hirayama & Kim, 2008; Pizza et al., 2017; Choo et al., 2017; Rosen et al., 1992). Knockout of NCAM, VCAM and ICAM does not completely block muscle development as these proteins play a redundant role during muscle development *in vivo*.

Several other membrane proteins and receptors have also been implicated in mouse myoblast fusion, including CDON, BOC, cadherins and integrins (Takaesu et al., 2006; Kang et al., 2002; Kang et al., 2004). In cell culture, N-cadherin interacts with CDON and activates the p38 kinase pathway to enhance myogenic differentiation, while M-cadherin interacts in *trans* to activate Rac1 in a Trio-dependent pathway to enhance myotube formation (Charrasse et al., 2007). Knockout of N- or M-cadherin does not affect myoblast differentiation and fusion due to redundancies in their function (Charlton et al., 1997; Hollnagel et al., 2002). Integrins also play a role in myoblast fusion, however, the mechanism by which they regulate fusion is unknown (Schwander et al., 2003; Brzóska et al., 2006; Lafuste et al., 2005).

The long search for the elusive fusogen that mediates the actual membrane fusion reaction recently discovered a two-component membrane protein system that functions as the mouse myoblast fusogen. First discovered was Myomaker, a seven-transmembrane domain-containing protein expressed in skeletal muscle and required for myoblast fusion of vertebrate myoblasts in mouse, zebrafish and chicken (Millay et al., 2013; Goh & Millay, 2017; Landemaine et al., 2014; Luo et al., 2015; Zhang & Roy, 2017). Expression of myomaker in fibroblasts allowed fusion with C2C12 myoblasts but not with other fibroblasts expressing myomaker, indicating that other myogenic proteins are required for myomaker-induced fusion (Millay et al., 2013). The search for the other myogenic fusogen required for myomaker function identified a small, single-pass membrane protein, variously referred to myomerger (Quinn et al., 2017), minion (Zhang et al., 2017), or myomixer (Bi et al., 2017). Expression of myomerger alone in two sets of fibroblasts did

not result in fusion, however, expression of myomerger in only one of two sets of fibroblasts, both of which were expressing myomaker, generated cell-cell fusion and the formation of multinucleated fibroblasts. This indicates that myomaker functions symmetrically while myomerger is required in only one of the two fusing cells (Quinn et al., 2017). A recent study showed that myomaker is important to initiate hemifusion between two fusing cells (i.e., merger of only the outer leaflets of the two plasma membranes) and requires myomerger for pore formation and expansion to complete the fusion process (Leikina et al., 2018). Treatment of C2C12 cells with cytochalasin D to block actin remodelling inhibits myoblast fusion in myomaker transduced myoblasts, clearly indicating the requirement of actin cytoskeleton to drive the fusion process (Millay et al., 2013).

1.2.5.3 Cytoplasmic proteins that regulate mouse myoblast fusion

Several mouse orthologs of *Drosophila* cytoplasmic proteins involved in myoblast fusion have been identified, some of which share similar functions. The *Drosophila* Rols ortholog in mice is tetratricopeptide-repeat, ankyrin-repeat, coiled-coil–containing protein 1 (TANC1). In rhabdomyosarcoma, TANC1 level is upregulated and blocks myoblast differentiation and fusion, retaining the cells in a proliferative state. This function of TANC1 is entirely different from Rols that regulates titin recruitment, and it is not known whether TANC1 is recruited by KIRREL3 during fusion (Avirneni-Vadlamudi et al., 2012). The mammalian ortholog of *Drosophila* Arf6, ARF6, increases PIP2 level in C2C12 myoblasts. This allows the formation of a tertiary complex containing M-cadherin, Trio, and Rac1 at cell-cell contact sites. ARF6 knockdown also reduces PIP2 levels and localization of Trio and Rac at the contact site indicating that ARF6 is required to assemble the protein complex at contact sites to mediate fusion. Alternatively, ARF6 increases phospholipase D (PLD) production, which also increases PIP2 production (Fig. 3) (Bach et al., 2010). This pathway varies slightly in *Drosophila*: PIP2 is recruited to the membrane by an unknown mechanism and triggers Arp2/3-dependent actin polymerization, and Loner activates Arf6-Rac1-Arp2/3 pathway, however, it is unknown whether Drosophila Arf6 activates PIP2 to trigger the Arp2/3 pathway (Fig. 2) (Bothe et al., 2014; Chen et al., 2003). The DOCK180 vertebrate ortholog of *Drosophila* Mbc and BRAG2 are the two GEFs that

serve the same defined function as in Drosophila, to activate the ARF6-Rac-WAVE complex to polymerize actin cytoskeleton (Laurin et al., 2008; Pajcini et al., 2008). There are other cytoplasmic proteins, such as kindlin-2, that regulate actin remodelling and fusion but a defined mechanism is yet to be identified (Dowling et al., 2008). These orthologs function in a similar manner as the *Drosophila* proteins to regulate actin polymerization, based on fusion index and biochemical approaches such as co-IP and GTPase assays. However, it is unclear how these proteins remodel the actin cytoskeleton to regulate fusion.

1.2.6 Proteins that regulate myoblast fusion in zebrafish

The zebrafish is another model that has been used to identify fusion-related proteins in vertebrate. Very few proteins have been identified that play a role in myoblast fusion. Although the identified proteins play a role in myoblast fusion, their interacting partners or the downstream pathways activated by these molecules are yet to be identified. The Duf homolog Kirrel is expressed in zebrafish fast muscle, and Kirrel morphants show normal differentiation but have a fast muscle fusion defect characterized by increased numbers of mononucleated myotubes (Srinivas et al., 2007). It is unclear if Kirrel interacts in *trans* with other receptor proteins. Zebrafish immunoglobulin-domain containing cell adhesion proteins Jamb/Jamc, interact heterotypically or homotypically in *trans*, and mutants show a complete block of fast myoblast fusion but the myoblasts differentiate normally and show no defects in muscle performance (Powell & Wright, 2011). This effect of Jamb and Jamc mutants on myoblast fusion is only observed in early developmental stages, however, adult fast muscle fibers are multinucleated, suggesting a role in early muscle development but not in muscle growth (Si et al., 2019). The Sns homolog in zebrafish is nephrin. Nephrin morphant embryos have a curved tail and abnormal musculature due to inhibited myoblast fusion that results in formation of clusters of mononucleated myoblasts in the somites (Sohn et al., 2009). Apart from these cell adhesion proteins, the only adapter protein identified in zebrafish is Crk-like (Crkl). Crkl is the zebrafish homolog of *Drosophila* Crk, whose knockdown in zebrafish blocks fast muscle cell fusion generating binucleated myoblasts (Moore et al., 2007). Again, whether Crkl drives an actin pathway or activates other downstream signalling pathways is unknown.

1.2.7 Actin-regulating proteins that regulate myoblast fusion

As is evident from the above discussion, numerous steps in the myogenic program are regulated by actin remodelling proteins. Our most detailed understanding of myogenic actin regulators derives from the *Drosophila* field where reverse genetics approaches and *in vivo* imaging have identified several myogenic actin regulators and integrated the function of these different proteins into a fusion synapse model (Fig. 2). The following sections present an overview of normal actin regulatory pathways, followed by discussion of the Drosophila, mouse and zebrafish proteins involved in actin regulation and myoblast fusion.

1.2.7.1 Mechanism of F-actin filament formation

There are the two different types of F-actin filaments, branched and linear F-actin. Branched F-actin filaments are formed by the actin-related protein 2/3 (Arp2/3) complex. This complex is activated by suppressor of cAMP receptor/WASp family Verprolin homologues (SCAR/WAVE) or Wiscott Aldrich syndrome protein (WASp) (Machesky & Insall, 1998; Padrick et al., 2011); the SCAR (in *Drosophila*)/WAVE (in vertebrates) complex is in turn activated by the Rho-GTPase Rac1 (Fig. 4A) (Insall & Machesky, 2009). In contrast, the WASp protein is activated by GTP-bound cdc42 that releases the WIP-WASp interaction. Upon activation both WAVE and WASp expose the VCA domain to bind an actin monomer and the Arp2/3 complex (Higgs & Pollard, 2000). This actin-WASp/WAVE-Arp2/3 complex binds the barbed end of an actin filament and initiates the addition of new actin monomers to build a new filament at an angle of 70° that appears as a branched filament (Pollard et al., 2002) (Fig. 4B). Formation of linear F-actin filaments is dependent on formins such as the Diaphanous homolog (Dia). The formins are activated by Rho GTPase to expose the actin nucleating domain, which binds to the barbed end of actin filaments and recruits G-actin (Vizcarra et al., 2014)(Schönichen & Geyer, 2010).. . Several linear actin filaments can be bundled together in parallel to form linear actin fibers and filopodia at the cell front (Fig. 4C).

1.2.7.2 F-actin foci at the fusion synapse mediate myoblast fusion in *Drosophila*

Several actin-rich structures have been described at the fusion synapse in *Drosophila* FCs and FCMs. These actin-rich foci were first believed to be formed symmetrically in both fusing cells (Kim et al., 2007) and were termed fusion-restricted myogenic-adhesive structures (FuRMAS) (Kesper et al., 2007). Later, the Chen lab identified the nature of these F-actin foci and showed FCMs and FCs make distinct actin structures (Sens et al., 2010) The FCM extends long, finger-like protrusions called podosome-like structures (PLSs) into the receiving FC, which senses the mechanical membrane tension induced by the invading PLS and forms a contractile actomyosin sheath beneath the plasma membrane to resist this force thereby driving close membrane apposition and fusion (Fig. 2) (Kim et al., 2015b; Kim et al., 2015). The actin-regulating proteins that regulate the formation of the PLS are summarized in Table 4.

Formation of the PLS in FCMs is regulated by several pathways. The interaction of Duf with Sns recruits Mbc or Crk to the cytoplasmic tail of Sns. Mbc activates the Rho-GTPase Rac1 which in turn activates the SCAR complex that interacts with the Arp2/3 complex to generate branched actin filaments that form the PLS structures. Rac1-GTP also activates DPak1/3 to polymerize actin in the PLS (Duan et al., 2012). Alternatively, the adapter protein Crk interacts with WIP or Blow to displace WASp which in turn activates the Arp2/3 complex (Berger et al., 2008; Richardson et al., 2007; Massarwa et al., 2007; Schäfer et al., 2007; Berger et al., 2008; Chen et al., 2003; Haralalka et al., 2013).

Protrusion of the PLS from the FCM into the FC generates membrane tension in the FC, resulting in activation of the Rho1 GTPase and its associated kinase, ROK, that are recruited to the cytoplasmic tail of Duf. Activated ROK phosphorylates myosin light chain (MLC) to generate actomyosin contractile filaments and cortical tension to resist the invading FCM (Kim et al., 2015). The adapter protein loner/schizo is also recruited by Duf, which activates the Arf6-Rac-SCAR-Arp2/3 pathway (Chen et al., 2003) (Fig. 2). Knockdown or heterozygous knockout of the above actin-regulating proteins in *Drosophila* inhibits myoblast fusion and myotube formation by ~50-90% (Berger et al., 2008; Richardson et al., 2007; Massarwa et al., 2007; Schäfer et al., 2007).

In addition to F-actin enrichment at the fusion site, the Baylies lab showed the formation of filopodia structures emanating from the actin foci. Formation of these structures is driven by Dia that polymerize actin into linear filaments as opposed to

branched actin filaments (Deng et al., 2015). Dia mutants or embryos expressing constitutively active Dia enhance filopodial protrusion by increasing actin polymerization, leading to increased filopodia numbers and random actin polymerization at sites not involved in the fusion synapse, hindering myoblast fusion (Deng et al., 2015). This data shows compelling evidence for proper spatiotemporal regulation of the actin cytoskeleton to mediate myoblast fusion.

1.2.7.3 Actin-regulators in mouse myoblast fusion

As mentioned before, there is no definite model proposed for mouse myoblast fusion, however, several actin regulators are known to be involved in this process. Table 4 summarizes the actin-regulating proteins identified in mouse myoblast fusion and Fig. 3 outlines the pathways regulated by these actin-regulating proteins. For example, the pleckstrin homology domain containing protein (CKIP-1) (Baas et al., 2012; Safi et al., 2004), the mouse ortholog of Kette (in *Drosophila*), NAP1 (Nowak, Nahirney, Hadjantonakis, & Baylies, 2009), and N-WASp (Gruenbaum-Cohen et al., 2012) are all required for mouse myoblast fusion, though knockdown of these proteins does not completely inhibit fusion. The homologs of Drosophila Mbc are the guanine exchange factors (GEFs), DOCK180, Trio and BRAG2. The role of DOCK is already explained in section 1.2.5.3. Trio interacts with filamin C in membrane ruffles and plays a role in actin remodelling (Dalkilic et al., 2006), and is recruited as a complex with M-cadherin and Rac at cell-cell contact during myoblast fusion in a ARF6-dependent manner (Bach et al., 2010). BRAG2 activates ARF6 GTPase that is required for recruitment of paxillin to focal adhesion sites, which maintains the morphology of differentiated myoblasts needed for myotube formation (Pajcini et al., 2008).

Similar to Rac1-GTPase in *Drosophila* myoblast fusion, Rac1 and Cdc42 are also important for the recruitment of Arp2/3 at cell-cell contacts for mouse myoblast fusion (Vasyutina et al., 2009). In contrast, the RhoA-GTPase level is downregulated during mouse myoblast differentiation and fusion. A canonical Rho-ROCK pathway (Fig. 4D) regulates actomyosin contraction. Constitutively active RhoA levels inhibit differentiation and fusion by promoting interaction of myocardin-related transcription factor (MRTF) with SMAD, which upregulates expression of inhibitor of DNA binding (ID3). ID3 blocks

myoD-dependent transcription (Iwasaki et al., 2008), explaining why the RhoA-ROCK pathway must be down-regulated in differentiating myoblasts. This downregulation dephosphorylates forkhead in human rhabdomyosarcoma (FKHR), a transcription factor that regulates transcription of myogenic genes (Nishiyama et al., 2004). Active RhoA is deactivated by either RhoE-p190RhoGAP or Rho-GTPase-activating protein (GRAF1) that induces the differentiation and fusion program (Doherty et al., 2011; Fortier et al., 2008). Hence, a spatiotemporal regulation of Rho and ROCK is required for myoblast fusion.

There is also evidence that asymmetric actin structures are formed in apposed mouse myoblasts undergoing fusion, similar to the situation in *Drosophila*. The Leu lab recently studied the function of invadopodosome-associated proteins tyrosine kinase substrate with five SH3 domain (TKS5) and dynamin-2 (DYN2) during myoblast fusion. TKS5 and DYN2 accumulate in the tip of an invadopodosome structure in differentiated myoblasts where they bundle actin filaments. This occurs 5-10 mins before fusion, (Chuang et al., 2019), and only in one of the two apposing cells. These filopodial structures contact the other cell, myoblast or myotube, and complete the fusion process. Similar to the actomyosin sheath that forms beneath the membranes of FCs during *Drosophila* myoblast fusion, studies in a mouse myoblast cell line have shown that actomyosin contractile units align parallel and beneath the plasma membrane and accumulate on only one side of the aligning membranes, with non-muscle myosin IIA (NMIIA) being the predominant isoform required for myoblast fusion (Duan & Gallagher, 2009; Swailes et al., 2006). However, it is unknown how these bundles are formed under the membranes and whether these actomyosin units sense cortical tension as seen in *Drosophila* myoblast fusion.

Although several actin-binding proteins are clearly involved in mouse myoblast fusion, it is unclear how these proteins interact with each other to regulate actin-polymerization and drive the fusion process. Further, it is unknown whether these proteins promote linear or branched actin polymerization. The recent identification of an invadopodosome structure in mouse myoblast fusion provides a target for future analysis of localization of these actin-regulating proteins and how they alter the invadopodosome structure for myoblast fusion.

1.2.7.4 Actin-regulators in zebrafish myoblast fusion

The function of actin-regulating proteins in zebrafish has not been studied to the same extent as in the *Drosophila* or mouse models. The two proteins whose functions are determined are Ckip-1 and Rac1. Similar to mouse CKIP-1, Ckip-1 knockdown using morpholinos in zebrafish results in the accumulation of mononucleated myoblasts (Baas et al., 2012). Rac1 knockdown zebrafish embryos also impairs myoblast fusion, with about 35% of myoblasts being mononucleated and 60% binucleated, while expression of a constitutively active form of Rac1 significantly enhances myotube formation (Srinivas et al., 2007). Though the function of these actin-regulating proteins is conserved across organisms, it is unclear whether the same pathways are regulated to mediate fusion in the different model organisms.

As can be appreciated from the above discussion, multiple complex networks are involved in remodelling the actin cytoskeleton to mediate myoblast migration and/or construct a fusion synapse needed for myoblast fusion. It is also apparent that we have an incomplete understanding of how these networks function during myotube fusion, and that additional actin regulators may well be involved in the process. One such protein is synpo2. Synpo2 is an actin binding and polymerizing protein known to regulate cancer cell migration and localize with actin filaments in striated muscle. The following sections will summarize what is known about the different members of the synaptopodin family of proteins and their actin-regulating function in different cell types.

1.3 Synaptopodin family of proteins

The podin family comprises three members, synaptopodin-1 (Synpo1), synpo2 and synaptopodin 2-like (Synpo2L). Each member of the podin family generates different isoforms by alternate splicing. Synpo1 is expressed in telencephalic dendrites and kidney podocytes and produces three isoforms: Synpo-short expressed in neurons (685aa), Synpo-long (903aa) expressed in renal tissue, and Synpo-T (181aa) (Asanuma et al., 2005; Mundel et al., 1997). Synpo2 is expressed primarily in muscle tissues and generates different isoforms in different vertebrates. Human SYNPO2 has five isoforms: SYNPO2A (1093aa), SYNPO2B (1109aa), SYNPO2C (1261aa), SYNPO2D (1230aa) and SYNPO2As (698aa) (Fig. 5A) (Kai et al., 2013). Mouse SYNPO2 has three isoforms: SYNPO2A (1087aa), SYNPO2B (1257aa) and SYNPO2As (757aa) (Fig. 5B). The third member of the podin

family, synpo2L, also known as cytoskeletal heart-enriched actin-associated protein (CHAP), is expressed in heart and skeletal muscle and has two isoforms: CHAPa (978aa) and CHAPb (749aa). The following sections provide a brief overview of the known functions of the founding member of the family, synpo1, followed by a more detailed discussion of synpo2 and its known features and functions.

1.3.1 Actin-regulating ability of synaptopodin-1 in kidney podocytes

Expression of synpo1 is restricted to telencephalic dendrites in the brain and to differentiated podocytes. In both tissue types, synpo1 binds actin filaments and focal adhesion proteins (Mundel et al., 1997). The predicted molecular mass of human SYNPO1 is 74 kDa and the human and mouse homologs share 84% sequence identity. There are three mouse isoforms, SYNPO1-long, -short and -T, all of which interact with α-actinin and enhance actin bundling in podocytes and dendrites. *Synpo1*$^{-/-}$ knockout mice completely lack the dendritic spine apparatus (Deller et al., 2003), whereas the kidneys develop normally (Asanuma et al., 2005). Most of our understanding of synpo1 derives from studies in kidney podocytes. These cells form the filtration barrier and contain foot processes near the basement membrane that are decorated with actin cytoskeletal proteins and actomyosin filaments (i.e., stress fibers). Synpo1 promotes stress fiber formation and podocyte cell migration, and loss of this cellular architecture impairs podocyte migration and leads to proteinuria.

In podocytes, Synpo1 regulates stress fiber formation by competitive binding with RhoA and Nck1. Overexpression of Synpo1 in undifferentiated podocytes significantly enhances active RhoA levels by competing with Smurf1, a HECT domain E3 ubiquitin ligase that degrades RhoA. Thus, Synpo1 interacts with activated Rho-GTP, inhibits Smurf1-mediated RhoA degradation, and increases stress fiber formation (Asanuma et al., 2006). In parallel, Synpo1 also outcompetes binding of c-Cbl, an E3 ubiquitin ligase, to Nck1 thereby preventing Nck1 degradation which activates N-WASp and Arp2/3 to enhance actin polymerization (Buvall et al., 2013).

Synpo1 has also been shown to compensate for the loss of a structurally unrelated protein, tropomyosin. In general, tropomyosin inhibits RhoA ubiquitination and restores stress fibers and cell migration, characteristics shared with Synpo1 in kidney podocytes. In

tropomyosin deficient *Drosophila* and human NIH3T3 fibroblasts, cells exhibited loss of stress fibers and enhanced migration. Overexpression of Synpo1 in a tropomyosin-deficient mutant cell line restored high RhoA levels, stabilized stress fibers and reduced migration (Wong et al., 2012). The concept that non-homologous actin regulatory proteins can serve compensatory functions in mutant cells will appear again later in the thesis.

1.3.2 Synaptopodin-2

Synpo2 is the second member of the podin family. Northern blotting confirmed expression of synpo2 in various muscle tissues including heart, prostate, and colon, with the highest expression in skeletal muscle (Lin et al., 2001). Until a decade ago, the smallest synpo2 isoform, synpo2As, was the only intensely studied synpo2 isoform in both the cancer and muscle fields. The human SYNPO2 isoforms regulate cancer cell migration and invasion, and invasiveness is related to cancer relapse in patients. In the muscle field, the human and mouse SYNPO2As isoforms bind actin and other actin-regulating proteins and localize in the Z-disc of skeletal muscle, however, its functional role remains unknown. The following sections will explain in detail the biophysical characters of synpo2 isoforms and their known functions in cancer and muscle tissues.

1.3.2.1 Synpo2 isoforms and their biophysical properties

The short isoform, synpo2As was first identified in skeletal (80 kDa) and heart muscle (95 kDa) extracts (Weins et al., 2001). In 2008, three human SYNPO2 isoforms were identified in PC3 cells that are generated by alternate splicing: SYNPO2A (1093aa), SYNPO2B (1109aa), SYNPO2C (1261aa) (Ariane De Ganck et al., 2008). In 2013, a fifth isoform was identified by the Duncan lab, named SYNPO2D (1230) (Fui Boon Kai & Duncan, 2013) (Fig. 5A). The long isoforms of both human and mouse SYNPO2 have PDZ domains in the N-terminus whose function is not determined in humans, but in mice it plays a role in the chaperon-assisted selective autophagy (CASA) pathway, that will be discussed later in the thesis. The remaining part of the protein is predicted to be intrinsically disordered, containing basic and proline rich regions with an isoelectric point of ~9.3 (Leinweber et al., 1999). Further, these isoforms also exhibit an aberrant migration phenomenon in SDS-PAGE. For example, the short isoform, synpo2As, has a molecular

mass of 80 kDa but migrates as a 100 kDa band in some studies (Ariane De Ganck et al., 2008). The reason for aberrant migration is speculated to be due to post-translational modification or to the intrinsically disordered nature of the protein.

Apart from the PDZ domain present only in the long isoforms, all five human SYNPO2 isoforms (Fig. 5A) and three mouse SYNPO2 isoforms (Fig. 5B) share a central conserved region encoded by exon 5 in human and exon 4 in mouse. Several interacting partners are identified to bind to this conserved region (Fig. 6A and B). The human SYNPO2As isoform contains two actin binding regions (139-268 and 268-408), a filamin C binding region (240-521aa), three α-actinin binding regions (139-286, 268-521 and 506-698), and an importin-13 binding region (306-698) (Fig. 6A) (A Linnemann & Ven, 2010; Anja Linnemann et al., 2013). Apart from these actin-binding proteins, human SYNPO2As also contains an integrin-linked kinase (ILK)-binding region (82-157) and zyxin binding region (606-624). These regions play a role in prostate cancer cell migration, which will be discussed in the prostate cancer section. Similar truncation analysis of mouse SYNPO2As also identified an actin-binding region from 410-563aa (Weins et al., 2001). Immunofluorescence staining of rat and human skeletal muscle revealed localization of SYNPO2As in the Z-disc and colocalization with known interaction partners such as α-actinin, zyxin and filamin C (A Linnemann & Ven, 2010). Both the human and mouse SYNPO2 isoforms also contain nuclear localization sequences (NLS) whose function will be discussed in the following section (Fig. 6B).

Fesselin, the avian homolog of synpo2, is expressed in chicken gizzard muscle, a type of smooth muscle, as a 79 kDa and 103 kDa protein, and has an isoelectric point of 9.3, similar to synpo1 and 2. It is also expressed in chicken tissue lysates extracted from thigh, breast and heart, and localizes in dense bodies in smooth muscle tissue (Renegar et al., 2009). Experiments with fesselin have been carried out only in *in vitro* conditions. In co-sedimentation assays, fesselin polymerizes G-actin and binds actin and α-actinin (Beall & Chalovich, 2001; Leinweber et al., 1999). The Synpo2 isolated from rabbit stomach muscle also exhibits actin polymerizing property (Schroeter et al., 2008). Fesselin also binds to calmodulin, which inhibits G-actin binding but not F-actin binding and polymerization (M. Schroeter & Chalovich, 2004). Further, fesselin also binds to the S1

ATPase subunit of myosin and inhibits actin and myosin binding. This can be reverted when excess myosin is present (M. M. Schroeter & Chalovich, 2005).

1.3.2.2 Nucleocytoplasmic shuttling property of synpo2

The nuclear-cytoplasmic shuttling property of mouse SYNPO2As has been shown by the Mundel lab, where SYNPO2As resides in the nucleus in undifferentiated myoblasts and translocates to the cytoplasm where it binds actin filaments in differentiated myoblasts and myotubes (Weins et al., 2001). Heat shock treatment of myotubes was also shown to trigger nuclear localization of SYNPO2As, a unique property for a Z-disc protein (Weins et al., 2001). Nuclear localization of endogenous SYNPO2As has been shown only with the mouse isoform, while another group showed that ectopic expression of a V5-tagged human SYNPO2 localizes in the nucleus of PC3 cells (Ariane De Ganck et al., 2008).

Nuclear localization sequences (NLS) are present in the N- and C-termini of both human and mouse SYNPO2As (58-61 and 616-619aa in mouse) (Fig. 6B). However, site-directed mutation of the two NLS sequences in mouse did not inhibit nuclear localization (Weins et al., 2001). Although the two NLS motifs are not required for nuclear localization of mouse SYNPO2As, paradoxically, these motifs are important for importin-α binding, a protein important for nuclear localization. Mouse SYNPO2As also has two 14-3-3β interacting motifs (residues 221-227 and 269-274) (Fig. 6B). Phosphorylation of SYNPO2As at serine-225 and threonine-272 is required for both 14-3-3β and importin-α interaction, and for nuclear localization of SYNPO2As in mouse myoblasts (Christian Faul et al., 2005). The S225 and T272 residues are phosphorylated by PKA and CaMKII, and inhibiting this phosphorylation abrogated nuclear localization and retained SYNPO2As in the cytoplasm where it interacts with several Z-disc associated proteins such as mAKAP, myomegalin, and the catalytic subunit of calcineurin (CnA). The functional importance of this complex remains unknown (Faul et al., 2007). In kidney podocytes, dephosphorylation of synpo1 eventually subjects it to cathepsin-L-mediated degradation, but in skeletal muscle cells dephosphorylation results in interaction with other actin-regulating proteins that might be important to maintain the actin cytoskeleton and Z-disc arrangement. These studies highlight how the same signalling pathway can differentially regulate the function of a protein in a cell-type specific manner.

A motif important for nuclear localization was mapped to the C-terminus of human SYNPO2As (306-698aa) that interacts with importin-13 (Fig. 6A). This interaction was confirmed in HEK293T cells and NIH3T3 fibroblasts, and knockdown of importin-13 inhibited nuclear localization of SYNPO2As by 80% (Liang et al., 2008). The importance of nuclear localization and its functional relevance in myogenesis remains an open question. Nuclear localization of human SYNPO2As has gained importance in the cancer field. Bladder tissues from bladder cancer patients were stained for SYNPO2As and based on the ratio of nuclear-cytoplasmic localization, the grade of the tumor was rated; patients with nuclear localization survived longer and had low grade tumors while those with predominant cytoplasmic staining had high grade tumors (Sanchez-Carbayo et al., 2003).

1.3.2.3 Role of synpo2 in cancer cell migration and invasion

Shortly after the discovery of mouse SYNPO2As expression in skeletal muscle (Weins et al., 2001), human *SYNPO2* gene deletion was identified as a correlate of the severity/stage of prostate cancer patients. Around 84% of individuals with *SYNPO2* gene deletion were shown to be associated with high invasiveness and 78% of patients reported cancer relapse (Lin et al., 2001). As mentioned in the nuclear cytoplasmic shuttling section, bladder cancer patients with cytoplasmic localization of synpo2 had high grade tumors and shorter survival times (Sanchez-Carbayo et al., 2003). Further, the low expression of SYNPO2As in bladder cancer and its relation to the invasiveness of the disease was attributed to the hypermethylation status of the gene (Cebrian et al., 2008). Based on the expression level and methylation status, SYNPO2As is a considered a biomarker of bladder cancer (Gakis et al., 2012).

Several studies support the role of synpo2 as a tumour suppressor. Overexpression of SYNPO2As in PC3 and LNCap prostate cancer cells inhibits proliferation and suppresses invasion in Matrigel assays compared to control cells. Injection of SYNPO2As overexpressing cells into SCID mice reduces tumour size significantly (Jing et al., 2004). Deletion of the zyxin or ILK binding regions in SYNPO2As also increases cancer cell migration, (Y. P. Yu & Luo, 2011; Yan Ping Yu & Luo, 2006). The above data correlates with gene deletion and invasiveness studies in prostate cancer patients (Lin et al., 2001), and supports the concept that SYNPO2As is a tumour suppressor. Two recent studies

further supported the role of SYNPO2 as a tumor suppressor in breast cancer cells. Knockdown of SYNPO2 in several breast cancer cell lines enhanced migration and invasion by increasing the phosphorylated levels of phosphoinositide 3-kinase (PI3K), Akt and mTOR, a critical pathway that regulates cancer progression, and via the YAP-TAZ pathway (Xia et al., 2018; Liu et al., 2018). Contradictory to the previous studies, the Gettemans group reported that siRNA knockdown of SYNPO2As inhibits migration and invasion of PC3 cells (Arianne De Ganck et al., 2009), suggesting synpo2 functions as a tumor promoter.

The contradictory data on the effects of synpo2 on migration was resolved by the Duncan lab. They showed that the human SYNPO2 isoforms differently affect migration and this depends on the external migration stimulus. PC3 cells expressing SYNPO2 isoforms decreased migration when cells were cultured in conditioned media (CM) and enhanced migration in a chemokinetic, rather than chemotactic, manner when cultured in 10% fetal bovine serum (FBS). Under serum stimulation conditions, SYNPO2As was also shown to increase RhoA-GTP levels in PC3 cells, and treatment with the ROCK inhibitor, Y27632, inhibits the enhanced migratory effect of SYNPO2As. This data clearly suggested that SYNPO2 isoforms regulate the migratory response of PC3 cells to external stimuli and enhance migration in response to serum stimulation in a Rho-ROCK dependent manner (Kai et al., 2012).

Consistent with synpo1, SYNPO2As also localizes along actin stress fibers. The five human SYNPO2 isoforms generate different actin structures in PC3 cells. SYNPO2A and As forms thick actin bundles in the cell body, SYNPO2B forms both thick and thin actin bundles in the cell body, SYNPO2C and D stain in a punctate manner with stress fibers along the axis of the cell (Kai & Duncan, 2013). A subsequent study showed that stress fiber formation was due to retrograde flow of F-actin from the cell periphery to the cell body (Kai et al., 2015). The short isoform, SYNPO2As, enhanced non-directional migration by generating large membrane protrusions or lamellipodia formed by branched actin filaments generated by Arp2/3-mediated actin polymerization. SYNPO2As cells treated with the Arp2/3 inhibitor, CK666, lost these membrane protrusions and the enhanced migration phenotype. Videomicroscopy of PC3 cells expressing GFP-tagged SYNPO2As showed that SYNPO2As enhances cancer cell migration by polymerizing

linear actin filaments at the leading edge of cells to generate filopodia-like structures, incorporating these linear F-actin structures into actin stress fibers in the cell body by retrograde flow in a NMII-dependent manner and generating mature focal adhesions (Kai et al., 2015).

1.3.2.4 Role of synpo2 in mouse myoblasts

Our knowledge of the function of synpo2 in the muscle field is very limited. According to the literature, in the proliferative stage of mouse myoblasts SYNPO2As localizes in the nucleus and upon differentiation translocates to the cytoplasm where it binds to actin filaments (Weins et al., 2001). Immunofluorescence staining of rat and human skeletal muscle revealed localization of SYNPO2As in the Z-disc and colocalization with known interaction partners such as α-actinin, zyxin and filamin C (Fig. 6A) (A Linnemann & Ven, 2010). Apart from the above-mentioned roles, the exact function of synpo2 isoforms during myogenesis remains largely unknown,

One exception is the long mouse SYNPO2 isoforms that have a defined role in muscle maintenance. The two main regions of synpo2 that play a role in muscle maintenance are the PPXY motif and the PDZ domain. The human and mouse SYNPO2As isoforms have a PPXY motif (Fig. 6A and B), a motif known to bind proteins that contain a WW domain (Bedford et al., 2000). The two PPXY motifs in synpo1 interact with the WW domain of the tight junction protein MAGI-1 that links the cytoskeleton to tight junctions by interacting with actin-bundling proteins (Patrie et al., 2002). The PPXY motif of mouse SYNPO2 interacts with the WW domain of BCL2-associated athanogene 3 (BAG3) protein (Ulbricht et al., 2013). The BAG3 protein plays a major role in the chaperone-assisted selective autophagy (CASA) pathway. This pathway is activated in striated muscle when mechanical tension-induced damage generates misfolded protein aggregates that need to be degraded. In such a situation, BAG3 forms a complex with heat shock proteins and autophagosome proteins to degrade the damaged proteins by autophagy. PDZ domain-containing proteins link the BAG3 complex and autophagosome complex. Since the long human SYNPO2 isoforms (i.e., SYNPO2A, B, C and D) have a PPXY motif and a PDZ domain they act as a linker protein between the BAG3 and autophagosome complexes (Fig. 7). Interaction of BAG3 with the PPXY motif of large tumour suppressor

kinase 1 (LATS1) or angiomotin (AMOT) releases the Yes-associated protein (YAP)/transcriptional coactivator with PDZ-binding motif (TAZ) transcription factors into the nucleus. Here, YAP/TAZ regulates transcription of connective tissue growth factor (CTGF) genes that play a role in muscle maintenance (e.g.,filamin C). We know from breast cancer studies that SYNPO2, by an unknown mechanism, enhances phosphorylated LATS that in turn regulates YAP localization (J. Liu et al., 2018). It is conceivable that SYNPO2 could interact with BAG3 in these cancer cells to regulate YAP/TAZ localization and thereby regulate cancer cell migration. Although these two studies connect SYNPO2 with YAZ/TAP function, the effects of this relation on the actin cytoskeleton of cancer cells and skeletal muscle remains unknown.

1.4 Hypothesis and objectives

It is evident that the podin family of proteins are important actin regulating proteins. While the expression and localization of synpo2 in skeletal muscle has been examined, and several interacting partners have been identified, the functional role of synpo2 in skeletal muscle development remains unknown. The main objective of my Ph.D. project was to determine the functional role of synpo2 during skeletal muscle development using *in vitro* and *in vivo* models.

Several key results from previous studies provided the rationale for my studies: (1) synpo2 localizes in the nucleus in undifferentiated cells and under stress conditions in differentiated cells (Weins et al., 2001); (2) both synpo1 and synpo2 regulate cell migration by remodelling the actin cytoskeleton; (3) several actin-regulating proteins play a role during myoblast fusion; and (4) synpo2 interacts with several skeletal muscle proteins and localizes in the Z-disc of skeletal muscle cells (C. Faul et al., 2007; A Linnemann & Ven, 2010; Weins et al., 2001). Thus, we hypothesized that synpo2, as a nuclear-cytoplasmic shuttling protein could regulate the differentiation program, and as an actin-remodelling protein could regulate myoblast migration and fusion. Additionally, the human SYNPO2 isoforms differentially remodel actin stress fibers in cancer cells and regulate cell migration, and the PDZ domain containing isoforms play a role in CASA pathway. Therefore, we first wanted to determine whether different isoforms are generated in mouse

myoblasts and whether the different isoforms differentially regulate myogenesis. The results of these objectives are explained in Chapter 3 of the thesis.

We next wanted to determine the mechanism by which synpo2 regulates myoblast migration and fusion. The RhoA-ROCK and Arp2/3 pathways play a specific role in *Drosophila* myoblast fusion (Kim et al., 2015). Both synpo1 and synpo2 enhance the RhoA-ROCK pathway to regulate cell migration, and synpo2 enhances cell migration by generating Arp2/3-dependent membrane protrusions (Kai et al., 2015). We therefore wanted to determine whether synpo2 regulates migration and fusion in RhoA-ROCK and Apr2/3 dependent pathways, and whether these two processes are directly correlated. The results of this objective are also explained in Chapter 3 of this thesis.

My last objective was to determine the function of synpo2 in an *in vivo* model. Synpo2 is expressed in skeletal muscle and localizes in the Z-disc of sarcomeres, suggesting synpo2 knockdown or deletion in an *in vivo* model might lead to muscular dystrophy. Recently, the zebrafish model has gained considerable attention to study myogenesis, with the advantages being different stages of development that can be easily visualized, and larger animal numbers compared to a mouse model. Thus, to understand, the functional role of synpo2, we used zebrafish as an *in vivo* model. The results of the *in vivo* study are explained in Chapter 4 of this thesis.

Table 1: Immunoglobulin superfamily of proteins that regulate myoblast fusion

Drosophila	Function	Mouse	Function	Zebrafish	Function	References
Sns	Interacts with Duf//Rst	Nephrin	No interacting partner	Nephrin	No interacting partner	(Bour et al., 2000; Sohn et al., 2009)
Hbs	Interacts with Duf/Rst					(Artero et al., 2001)
Duf	Interacts with Sns/Hbs	KIRREL3	No interacting partner	Kirrel	No interacting partner	(Srinivas et al., 2007; Strünkelnberg et al., 2001)
Rst	Interacts with Sns/Hbs					(Strünkelnberg et al., 2001)
				Jamb	Interacts with Jamc	(Powell & Wright, 2011)
				Jamc	Interacts with Jamb	(Powell & Wright, 2011)
		ICAM	Interacts in *trans*			(Pizza et al., 2017)
		VCAM	Interacts with α4β1 integrin			(Choo et al., 2017; Rosen et al., 1992)
		NCAM	Interacts with MYONAP			(Charlton et al., 2000; Hirayama & Kim, 2008)

Table 2: Membrane proteins that regulate myoblast fusion

Drosophila	Function	Mouse	Function	Zebrafish	Function	References
		CDON	Interacts with BOC, cadherins and neogenin			(Kang et al., 2002)
		BOC	Interacts with CDON			(Kang et al., 2002)
		Neogenin	Interacts with CDON			(Kang et al., 2004)
		Myomaler	No interacting partner			(Goh et al., 2017; Millay et al., 2013)
		Myomerger	No interacting partner			(Quinn et al., 2017)
		N-cadherin	Interacts with N-cadherin			(Charlton et al., 1997)
		M-cadherin	Interacts with M-cadherin			(Hollnagel at al., 2002)
		ADAM12	Interacts with β1 integrin			(Lafuste et al., 2005)
		α3β1 integrin				(Brzóska et al., 2006)
		α9β1 integrin				(Lafuste et al., 2005)

Table 3: Cytoplasmic proteins that regulate myoblast fusion

Drosophila	Function	Mouse	Function	Zebrafish	Function	References
Crk	Activates Blow or WASp			Crkl		(Erickson et al., 1997; Moore et al., 2007)
Blow	Competes with Sltr for WASp					(Doberstein et al., 1997; Schroter, 2004)
Ants	Interacts with Duf	MANTS1	No function identified			(E. H. Chen & Olson, 2001)
Rols	Interacts with Duf	TANC1	Increases cell proliferation			(Avirneni-Vadlamudi et al., 2012; Menon & Chia, 2001)
		Kindlin-2	Interacts with integrins			(Dowling et al., 2008)

Table 4: Actin-regulating proteins that regulate myoblast fusion

Drosophila	Function	Mouse	Function	Zebrafish	Function	References
Rac1	GTPase and activator of SCAR	Rac1	GTPase	Rac1	GTPase	(Haralalka et al., 2013; Srinivas et al., 2007; Vasyutina et al., 2009)
Kette	SCAR complex	Nap1	WAVE complex			(Nowak et al., 2009; Schröter et al., 2004)
SCAR	Arp2/3 activator					(Berger et al., 2008; Richardson et al., 2007)
WASp	Arp2/3 activator	N-WASp	Arp2/3 activator			(Gruenbaum-Cohen et al., 2012; Massarwa et al., 2007; Schäfer et al., 2007)
Sltr	Binds WASp					(Massarwa et al., 2007; Schäfer et al., 2007)
Arp2/3	Branched actin polymerization					(Berger et al., 2008)
Dia	Linear actin polymerization					(Deng et al., 2015)
Rho	GTPase	RhoA	GTPase			(Iwasaki et al., 2008; Kim et al., 2015; Nishiyama et al., 2004)
MLC	Actomyosin contraction					(J. Kim et al., 2015)

Table 4 (continued): Actin-regulating proteins that regulate myoblast fusion

Drosophila	Function	Mouse	Function	Zebrafish	Function	References
Arf6	GTPase					(Chen et al., 2003)
DPak1/3	Actin bundling					(R. Duan et al., 2012)
Mbc	GEF for Rac	BRAG2	GEF for Rac			(Erickson et al., 1997; Pajcini et al., 2008; Rushton et al., 1995)
		DOCK1 80/5	GEF for Rac			(Laurin et al., 2008; Pajcini et al., 2008)
		Cdc42	GTPase			(Vasyutina et al., 2009)
		Trio	Actin remodelling			(Dalkilic et al., 2006)
		GRAF1	GAP for RhoA			(Fortier et al., 2008)
		Filamin C	Actin binding			(Dalkilic et al., 2006)
		CKIP1	Interacts with Arp2/3	Ckip1		(Dominique Baas et al., 2012; Safi et al., 2004)

Table 4 (continued): Actin-regulating proteins that regulate myoblast fusion

Drosophila	Function	Mouse	Function	Zebrafish	Function	References
		TKS5	Invadopodosome			(Chuang et al., 2019)
		DYN2	Invadopodosome			(Chuang et al., 2019)
		NMIIA	Actomyosin contraction			(Duan & Gallagher, 2009; Swailes et al., 2006)
PIP2	Actin polymerization	PIP2	Actin polymerization			(Bach et al., 2010; Bothe et al., 2014)
Loner	GEF for Arf6					(E. H. Chen et al., 2003)

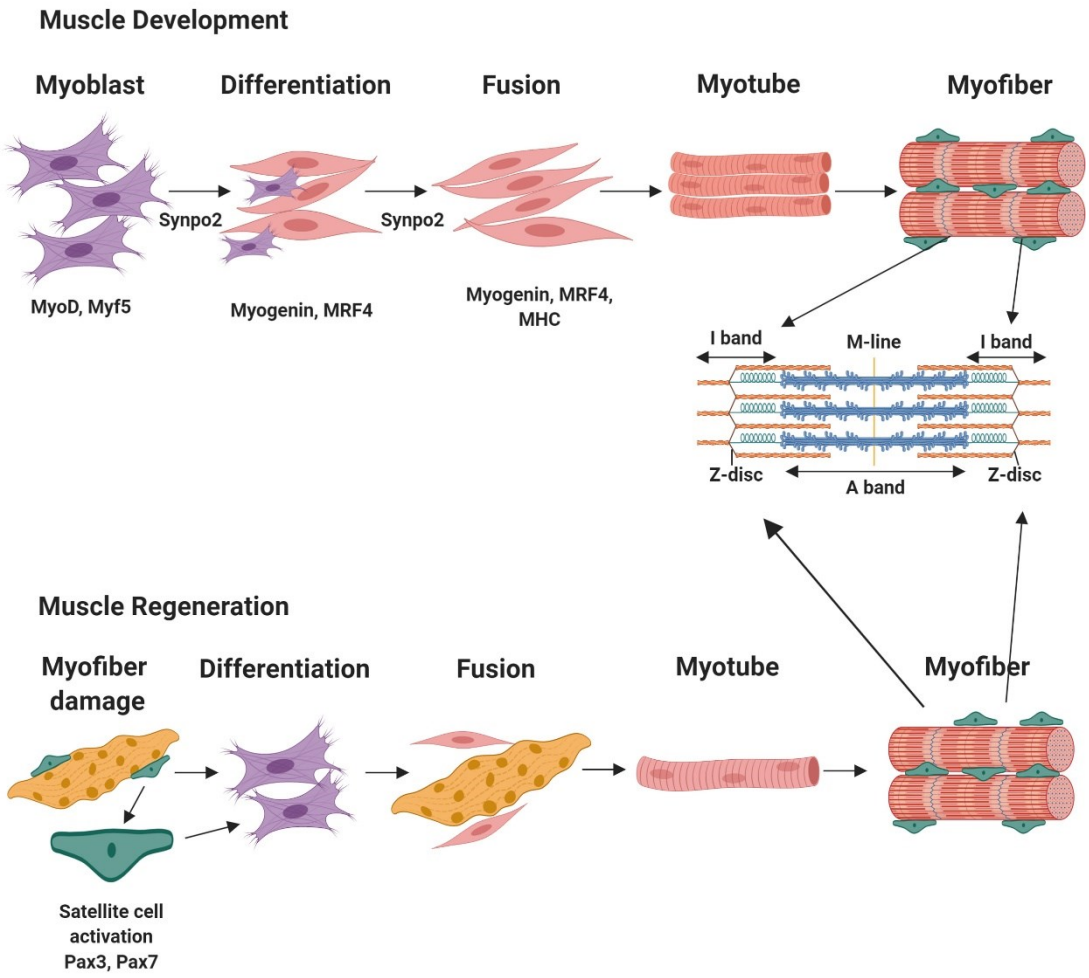

Figure 1: Myogenesis during muscle development and regeneration.
The upper panel depicts the steps involved during skeletal muscle development and the lower panel depicts the steps involved during muscle regeneration. Proteins expressed in each step of the myogenic program are mentioned below each cell type. The center panel represents one sarcomeric unit of skeletal muscle. The lower panel depicts muscle regeneration where myofiber damage activates muscle stem cells (green), called satellite cells, that differentiate and fuse to repair the damaged muscle fiber.

Fusion competent myoblast (FCM)

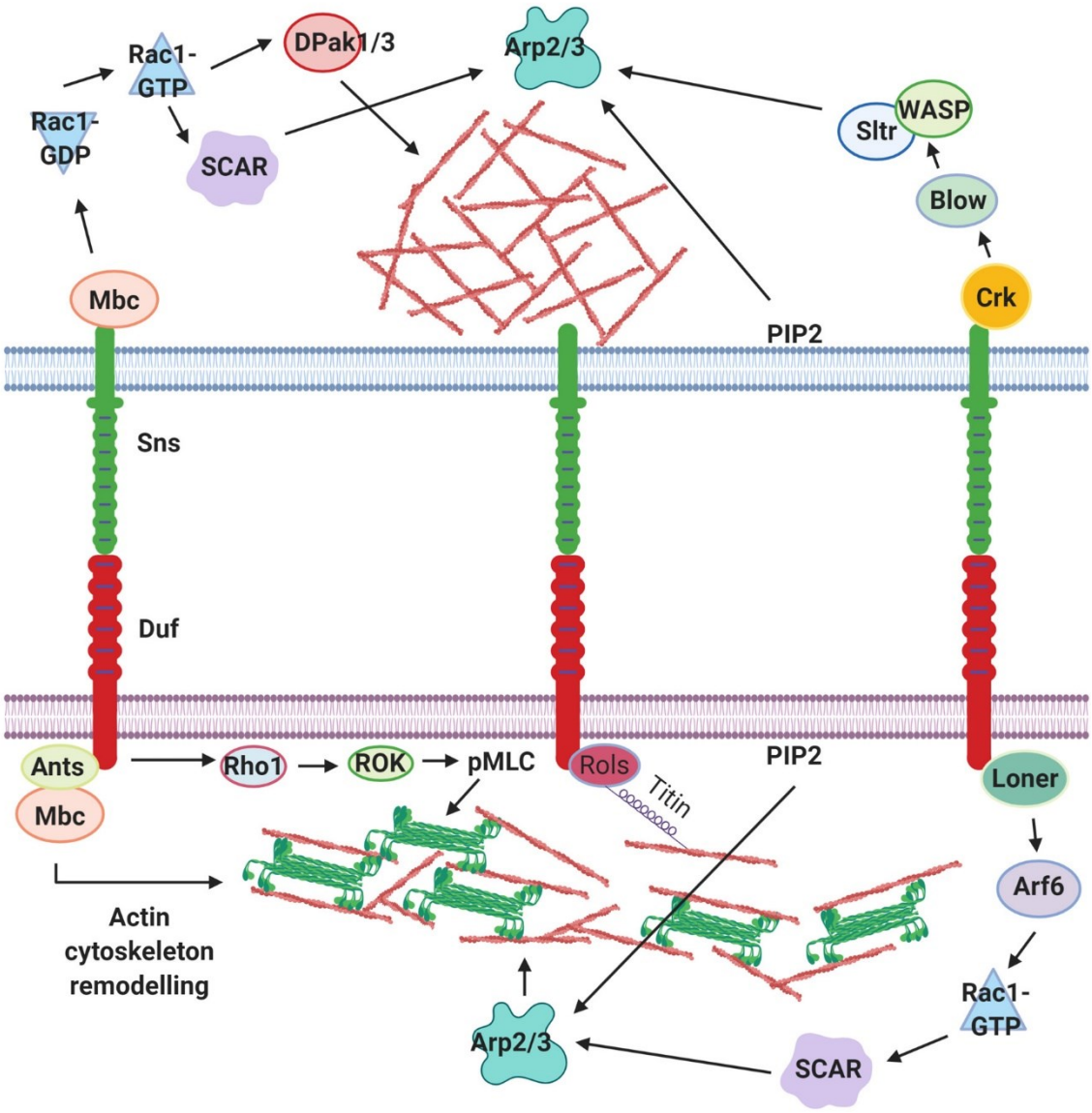

Founder cell (FC)

Figure 2: Model of drosophila myoblast fusion.
The founder cell (FC) and fusion competent myoblast (FCM) interact via cell adhesion proteins Duf and Sns. This interaction drives the following downstream signalling pathway in each cell type. FCM specific signalling: adapter proteins Crk and Mbc are recruited to the cytoplasmic region of Sns. Mbc activates the Rho-GTPase, Rac1, which in turn activates SCAR and the Arp2/3 complex to initiate actin polymerization. Activated Rac1 also activates DPak3 to initiate actin polymerization. The adapter protein Crk recruits Blow that competes for Sltr to bind to WASp. The WASP-Sltr complex activates the Arp2/3 complex to initiate actin polymerization. All these signalling pathways drive the formation of extensive branched actin filaments that form the invasive podosome-like structure (actin core of podosome) that invades the FC. FC specific signalling: adapter proteins Ants, Mbc and loner are recruited to the cytoplasmic region of Duf. Loner activates Arf6 GTPase to activate Rac1. Similar to the role in FCM, Rac1 activates SCAR-Arp2/3 to polymerize actin; Ants and Mbc bind to Duf to polymerize actin and form an actin sheath beneath the plasma membrane. Simultaneously, Rho1 is recruited to the cytoplasmic tail of Duf and activates the Rho-ROK-MyoII pathway to form actomyosin fibers to resist the invading podosome. Phosphatidylinositol 4,5-bisphosphate (PIP2) is recruited to the membrane and initiates Arp2/3-mediated actin polymerization in both the FCM and FC.

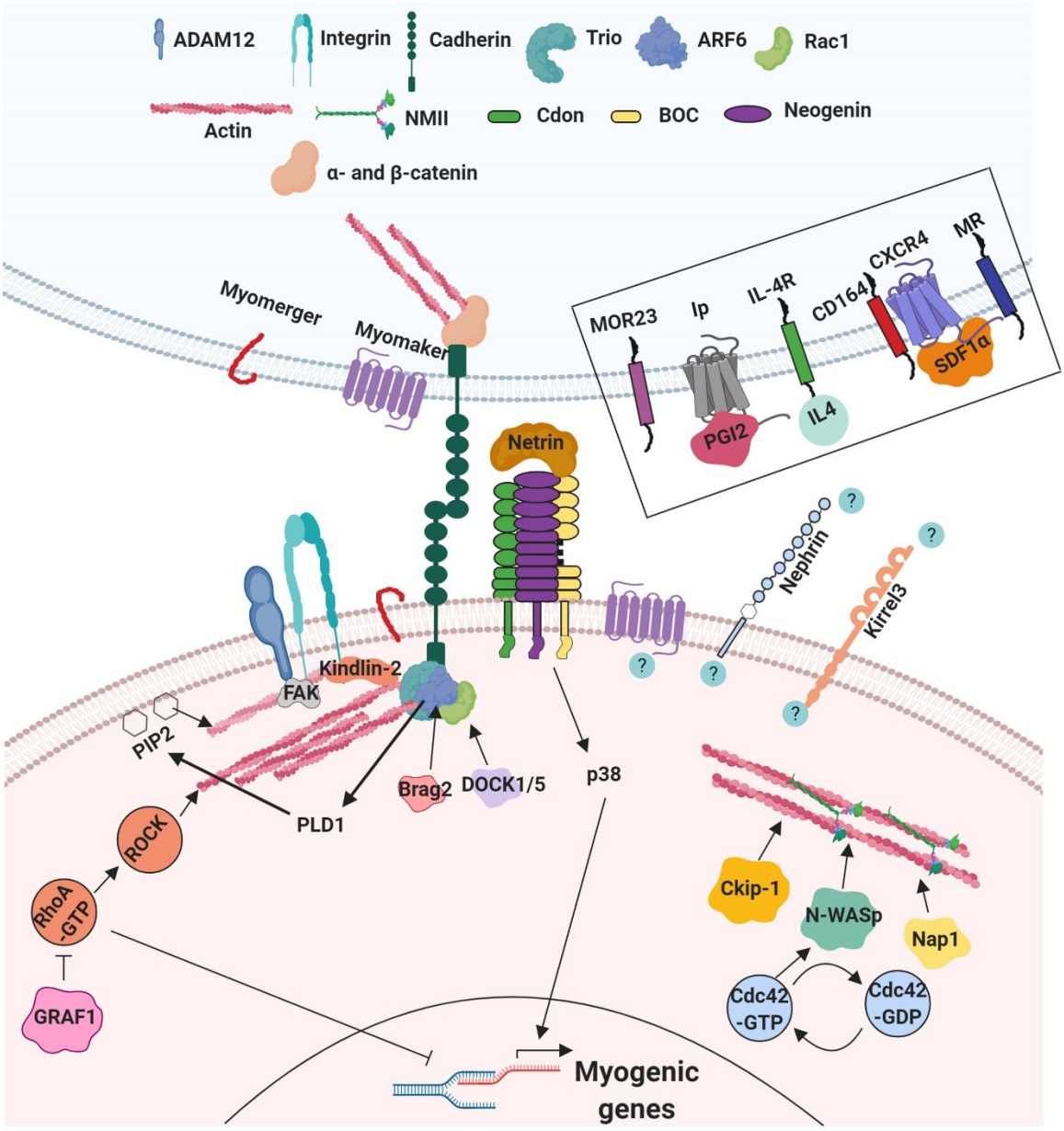
ADAM12
Integrin
Cadherin
Trio
ARF6
Rac1
Actin
NMII
Cdon
BOC
Neogenin
α- and β-catenin
Myomerger
Myomaker
MOR23
Ip
IL-4R
CD164
CXCR4
MR
PGI2
IL4
SDF1α
Netrin
Nephrin
Kirrel3
FAK
Kindlin-2
PIP2
PLD1
Brag2
DOCK1/5
p38
ROCK
RhoA -GTP
GRAF1
Ckip-1
N-WASp
Nap1
Cdc42 -GTP
Cdc42 -GDP
Myogenic genes

Figure 3: Pathways and protein that regulate mouse myoblast fusion.
Three different membrane complexes drive actin polymerization in myoblasts. (1) CDon/BOC/Neogenin forms a complex in the membrane of fusing cells. This complex drives the p38 kinase pathways to activate muscle-specific gene transcription. (2) *Trans* interaction of cadherins recruits α- and β-catenin to initiate actin-polymerization. Alternatively, the cytoplasmic domain of cadherins binds to a protein complex containing Trio, ARF6 and Rac1. The two GEFs, Brag2 and Dock, activate ARF6-GTPase and Rac1-GTPase, respectively, that initiate actin polymerization. Activated ARF6 also activates phospholipase D-1 (PDL1). Both ARF6 and PDL1 increase PIP2 production that plays a role in actin polymerization. (3) Integrin binds to ADAM12 that recruits focal adhesion kinase (FAK) for actin polymerization. Integrin-associated protein kindlin-2 also initiates actin polymerization. Nephrin, kirrel3, myomaker and myomerger are membrane associated proteins required for myoblast fusion. Actin regulating proteins Ckip1, Nap1, N-WASp, and RhoA-ROCK initiate actin polymerization, and Cdc42 GTPase activates N-WASp. The Rho-ROCK pathway also blocks muscle-specific gene transcription in proliferating myoblasts. The GRAF1 GAP inactivates RhoA to initiate muscle-specific gene transcription during differentiation. Proteins that regulate myoblast migration and fusion are highlighted in the black box: odorant receptor, MOR23, PGI2-Ip, IL4-ILR4, CD164-CXCR4-SDF1α and mannose receptor (MR). The question marks are unanswered questions that remain to be explored.

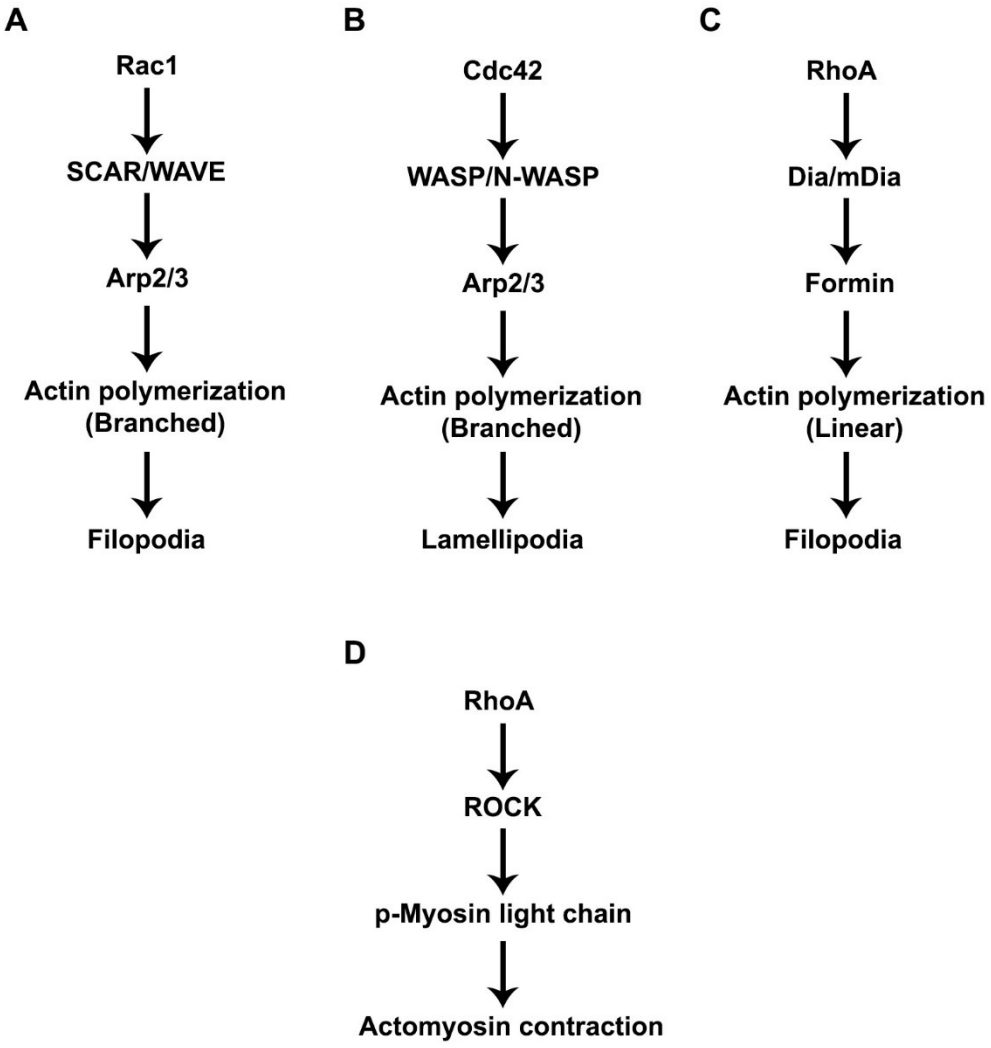

Figure 4: Actin regulating pathways.
(A) Branched F-actin polymerization initiated by the active Rac1 pathway. (B) Branched F-actin polymerization initiated by the active Cdc42 pathway. (C) Linear F-actin polymerization initiated by the RhoA pathway. (D) The canonical RhoA-ROCK pathway that initiates actomyosin contraction.

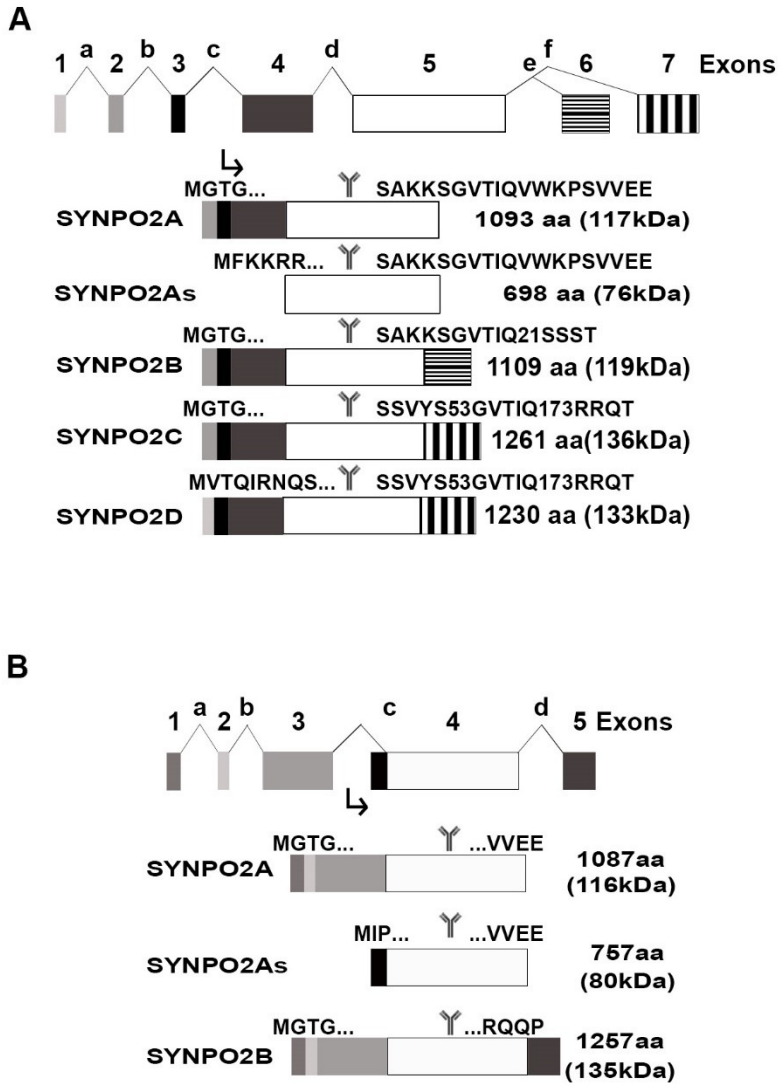

Figure 5: Human and mouse SYNPO2 isoforms.
Exon arrangements of the human (A) and mouse (B) SYNPO2 genes and protein isoforms. The protein isoforms are translated from alternatively spliced mRNAs generated from an upstream promoter, or in the case of the short isoforms (As suffix) from an internal promoter (downward arrow in each panel). Upper panels depict the gene, with exons indicated by numbered shaded rectangles and introns by alphabetically labelled chevrons. Amino acid sequences above each protein isoform indicate the N- and C-terminal sequences. The number of amino acid residues and predicted molecular mass (in brackets) for each isoform are indicated. The centrally located conserved exon (white rectangle) contains the epitope recognized by the commercial antiserum (indicated by the Y symbol) and several protein interaction motifs described in the text.

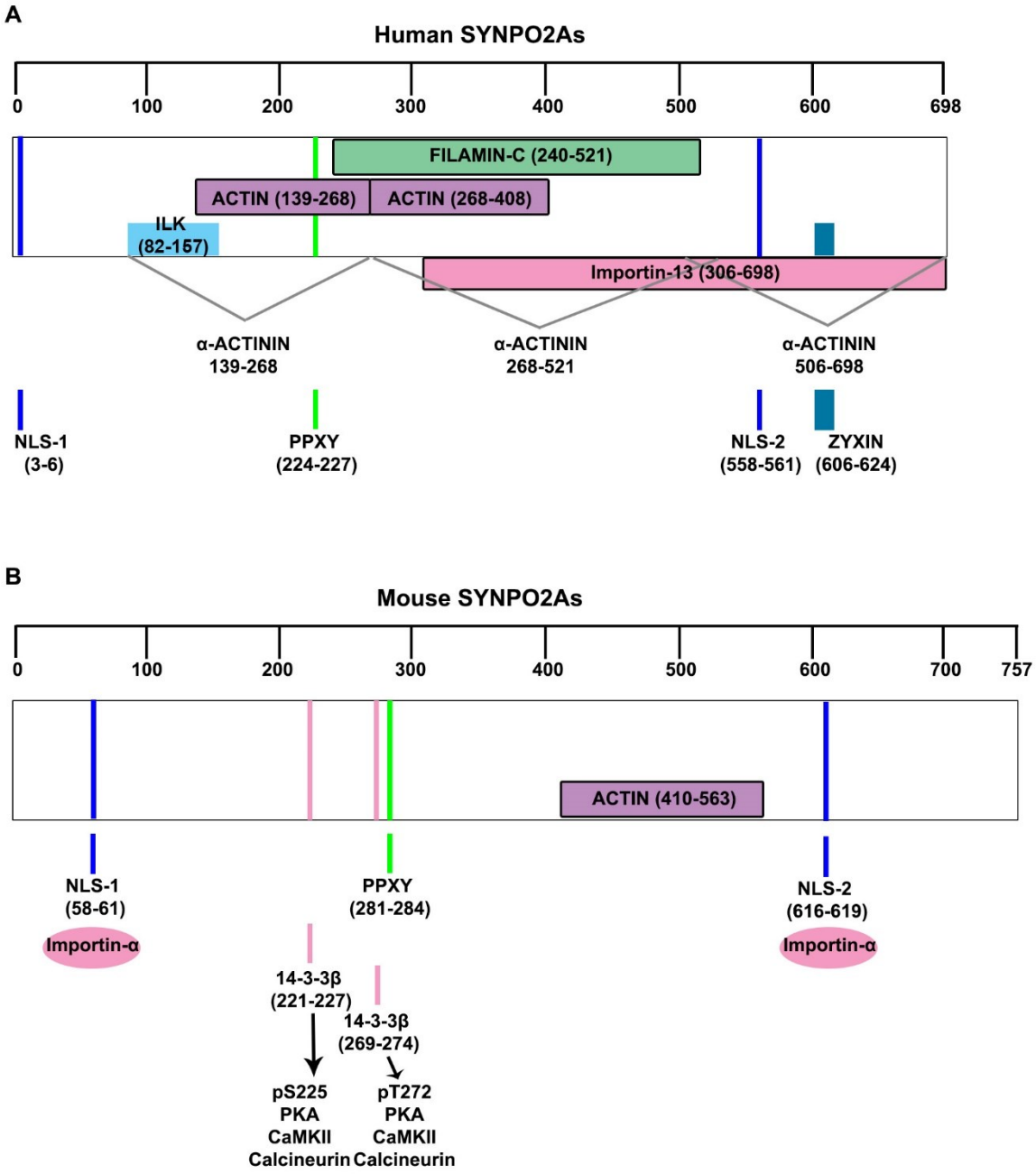

Figure 6: Interacting partners of human and mouse synpo2As.
(A) Human SYNPO2As and (B) mouse SYNPO2As interacting proteins are highlighted in different colors. The α-actinin binding regions are denoted by chevrons. The bracketed numbers are the amino acid residue boundaries of the indicated binding motifs.

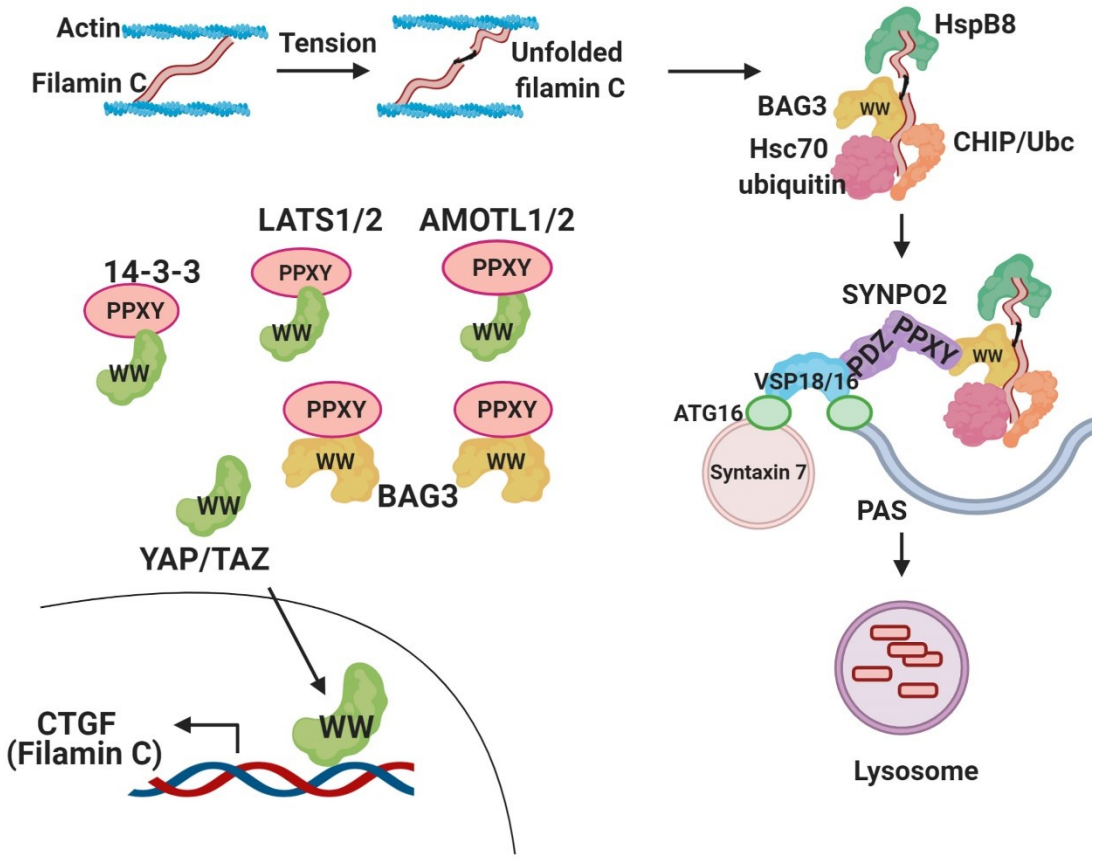

Figure 7: Role of SYNPO2 in chaperone-assisted selective autophagy.
Image modified from Ulbricht et al., 2013. On the right: Schematic presentation of the BAG-3-containing chaperone complex. Filamin is damaged during migration due to mechanical stress and is ubiquitinated and degraded by the CASA complex. BAG3 uses its BAG domain to bind to the N-terminal ATPase domain of Hsc70, while at the same time CHIP occupies the C-terminal domain that covers the peptide-binding region of the chaperone. BAG-3 provides a physical link between HspB8 and the Hsc70/CHIP complex. The WW domain of BAG3 binds the PPPY motif of SYNPO2. The PDZ domain of SYNPO2 binds vacuolar protein sorting 18/16 (Vps18/16), which in turn interacts with ATG16 and syntaxin 7 to form the pre-autophagosomal structure (PAS). The PAS engulfs the CASA complex and fuses with lysosomes to degrade the ubiquitinated substrate. On the left: BAG3 when localized in the cytoplasm binds the PPXY motif of large tumor suppressor (LATS1/2) or angiomotin-like (AMOT1/2), releasing the YAP/TAZ transcription factor into the nucleus. YAP/TAZ transcribes target genes such as filamin and connective tissue growth factor (CTGF).

CHAPTER 2: MATERIALS AND METHODS

2.1. Cells, Antibodies and Reagents

Cells: C2C12 (CRL-1772) mouse myoblast cells were obtained from the American Type Culture Collection (ATCC). Phoenix cells were kindly provided by Craig McCormick (Dalhousie University). Cells were grown in Dulbecco Modified Eagle Medium (DMEM) supplemented with 10% fetal bovine serum (FBS) and 25 mM 4-(2-hydroxyethyl)-1-piperazineethanesulfonic acid (HEPES) at 37ºC with 5% CO_2. HEK293T cells used for generating lentivirus were grown in Dulbecco Modified Eagle Medium (DMEM) supplemented with 10% fetal bovine serum (FBS) at 37ºC with 5% CO^2. For differentiation experiments, growth medium was replaced with Dulbecco Modified Eagle Medium (DMEM) supplemented with 2% horse serum (HS).

Antibodies: Primary antibodies against synpo2 (Abcam Ab103710 and Abcam Ab50192), c-myc (Sigma M4439), myosin heavy chain (MF-20, Developmental Studies Hybridoma Bank), MyoD (Santa Cruz Biotechnology M-318; Dako M3512), myogenin (Sigma-Aldrich F5D), Pax7 (Developmental Studies Hybridoma Bank), Troponin T (Sigma-Aldrich T6277), LC3-II (3868, Cell signalling), NMIIA (M8064, Sigma), and actin (A2066, Sigma), and secondary antibodies goat-anti-rabbit HRP (474-1506, KPL), goat-anti-mouse HRP (sc-2005, Santa Cruz), and goat-anti-mouse Alexa 488, 568 (Molecular Probes) were purchased from the indicated suppliers.

Reagents: DRAQ5 (Cell Signalling) or Hoechst 33342 (Thermo Fischer Scientific) were used interchangeably for nuclear staining. Alexa fluor-555 phalloidin (A34055, Thermo Fischer Scientific) for actin staining. 0.1% naphthol blue solution was prepared in-house and used for total protein loading.

2.2. Molecular cloning

RNA was extracted from proliferating C2C12 cells using the RNeasy Mini Kit (Qiagen) as per manufacturer's instructions and used as a template for cDNA synthesis using an oligo(dT) primer, and cDNA was amplified using isoform specific primers and PfuUltra High Fidelity DNA polymerase (Agilent Biotechnologies). The primers used for PCR amplification flanked the translation start and stop sites in the mouse mRNA

sequences for SYNPO2A (Accession #Q91YE8.2), SYNPO2B (Accession #NM_080451.2) and SYNPO2As (Accession #AJ306625.1). Amplicons were cloned into the BamHI-NotI sites in the pBMN retrovirus plasmid vector. All cDNA clones were sequenced in their entirety in both directions, and confirmed to agree with those deposited in the database.

2.3. Transfections

Phoenix cells were seeded at $3x10^6$ cells per 100mm dish in DMEM medium containing 25 mM HEPES and 10% FBS. The cells were then transfected with an empty pBMN retrovirus plasmid vector (kindly provided by Dr. Craig McCormick, Dalhousie University) or with the same vector containing the SYNPO2 cDNAs using poly(ethylenimine) (PEI) transfection reagent. After 22 h of seeding, growth medium was replaced with serum-free medium. Six µg of plasmid DNA was added to 600 µl of Opti-MEM I Reduced Serum Media (31985070, Thermo Fisher Scientific) and 18 µl of PEI was added to 600 µl of Opti-MEM and incubated separately at room-temperature (RT) for 5 min, and then mixed together and incubated for another 15 min at RT. The DNA-PEI mix was added to the cells and after 6 h post-transfection serum-free medium was replaced with growth medium.

To determine the knockdown efficiency of shRNA2, the shRNA2 plasmid construct was transiently transfected into HEK293T cells along with the pBMN plasmids expressing the SYNPO2A or SYNPO2B isoforms using PEI reagent in serum-free medium using the above-mentioned transfection protocol. Briefly, HEK293T cells were seeded in a 6-well plate in growth medium. One µg of pSMN-shRNA2 plasmid and 1 µg of pBMN-SYNPO2A or pBMN-SYNPO2B plasmid was added to 100 µl of Opti-MEM and 6 µl of PEI was added to 100 µl of Opti-MEM and incubated separately at room-temperature (RT) for 5 min, and then mixed together and incubated for another 15 min at RT. The DNA-PEI complex was added to cells in serum-free medium. After 24 h post-transfection, cells were lysed and processed for western blotting.

2.4 Generation of stable SYNPO2 overexpression cell lines

For generation of retroviruses, Phoenix cells were transfected as mentioned above. After 48 h post-transfection, cell culture supernatants were collected and filtered through a 0.45 μM filter to remove cell debris. Sequabrene (S2667, Sigma) was added at a final concentration of 4 μg/ml to the supernatant to increase the efficiency of viral infection. C2C12 cells ($0.36x10^6$) were infected with the retrovirus-containing supernatant for 24 h and then cultured in fresh growth medium containing 1 μg/ml puromycin (Invitrogen) for 3 days to select pBMN-SYNPO2 transduced cells.

2.5. Generation of knockdown cell lines

Two short hairpin RNAs, one targeting the unique 5'-exon of SYNPO2As (shRNA1) and the other targeting the conserved exon present in all SYNPO2 isoforms (shRNA2), were designed using RNAi Central software (http://cancan.cshl.edu/RNAi_central/RNAi.cgi?type=shRNA) and cloned into the pSMN retroviral plasmid (kindly provided by Dr. Craig McCormick, Dalhousie University). For stably transducing C2C12 cells with the two shRNAs to knockdown endogenous SYNPO2, the above-mentioned protocol was used and cells were selected using 2 mg/ml G418 (Sigma) for 5 days. Western blotting with anti-SYNPO2 antibody was used to determine the knockdown efficiency of the shRNAs.

2.6. Western blotting

Cells were trypsinized, harvested by centrifugation at 500xg for 5 min, washed with phosphate buffered saline (PBS), and cell pellets were stored at 80°C until analyzed. Cell pellets were lysed in cell lysis buffer (50 mM Tris, 10 mM MgCl2, 0.5 M NaCl, 2% Igepal, pH 7.5) containing protease inhibitor cocktail (Pierce), sonicated using a stainless-steel probe sonicator, and insoluble debris removed by centrifugation at 15000xg for 10 min. An aliquot of each sample was used to determine protein concentration using the Bio-Rad DC™ protein assay kit, as per manufacturer's instructions, and the remaining sample was frozen using liquid nitrogen until further processing. Frozen samples were thawed, diluted with cell lysis buffer, 5X protein sample buffer (5% sodium dodecyl sulfate, 0.25% bromophenol blue and 50% glycerol [2X buffer was used]), and 500 mM dithiothreitol (DTT [50 mM was used]) to equalise the protein concentration, boiled at 95°C

for 5 min, and equal protein loads were fractionated by SDS-PAGE (7.5% polyacrylamide). Fractionated samples were transferred onto polyvinylidene difluoride (PVDF) membranes, blocked for 1 h at room temperature (RT) using 5% skim milk in TBST (50 mM Tris-HCl, 150 mM NaCl, 0.1% Tween 20), and probed with the respective primary antibodies diluted in TBST at the following dilutions: synpo2, 1:2500; MHC, 1:250; myoD, 1:250; myogenin, 1:100; LC3-II, 1:1000; and actin, 1:5000. Blots were washed extensively with TBST, treated with horseradish peroxidase-conjugated secondary antibody (1:5000), developed using ECL-Plus reagent (GE Healthcare) and visualized on a Typhoon 9410 multi-mode imager, or developed using Clarity western ECL substrate (Bio-Rad) and visualized on a Bio-Rad ChemiDoc imaging system. Western blots to examine any changes in the differentiation program were performed in triplicate and relative expression levels were normalized to protein loads detected by staining blots with 0.1% naphthol blue for 30 min prior to blocking and imaged using the Bio-Rad ChemiDoc calorimetry setting.

2.7. Satellite cell isolation and immunofluorescence microscopy

Care and handling of animals were in accordance with the federal Health of Animals Act, as practiced by McGill University and the Lady Davis Institute for Medical Research. Satellite cells were prepared by Dr. Colin Crist (McGill University) from abdominal muscles and diaphragms of 8–12-week old *Pax3*$^{GFP/+}$ mice by enzymatic dissociation as previously described (Zismanov et al., 2016). For live cell sorting, single cells were stained with 1 μg/ml propidium iodide (PI) to exclude PI+ dead cells. Cell sorting was performed with a FACSAria Fusion Cell Sorter (BD). Isolated *Pax3*$^{GFP/+}$ satellite cells were resuspended in 39% DMEM, 39% F12 (Gibco) growth medium containing 20% FBS (Gibco) and 2% Ultroser G (Pall, Port Washington, NY). Cells were cultured in 35-mm dishes coated with 0.2% gelatin at a density of 7500 cells per dish. For immunocytochemical analysis, cultured cells were fixed with 10% formalin and permeabilized with 0.2% Triton X100, 50 mM NH_4Cl in PBS. Cells were incubated with 0.2% fishskin gelatin in PBS (Sigma). The following antibodies were used as primary antibodies: anti-MyoD (1:100, Santa Cruz Biotechnology, Santa Cruz, CA), anti-Troponin T (1:300, Sigma) and anti-synpo2 (1:100, Abcam Ab103710). Secondary antibodies were coupled to flurochromes Alexa 488 or 594 (1:500, Molecular Probes, Carlsbad, CA). 4,6-

Diamidino-2-phenylindole (DAPI, 1:500, Molecular Probes) was used to counter-stain nuclei. All images were captured at the same microscope settings so that fluorescence intensity was representative of detection levels.

2.8. Indirect immunofluorescence microscopy

To observe endogenous SYNPO2 subcellular localization, C2C12 cells were seeded at 40% or 80% confluency on coverslips and induced to differentiate using medium containing 2% horse serum until 2- or 3-days post-induction of differentiation (dpi). Cells were fixed with 4% paraformaldehyde, permeabilized with 0.25% triton X-100 in 1x PBS and blocked with 1% BSA in 1x PBS at RT. Cells were then incubated with anti-synpo2 antibody (1:500) overnight at 4◦ C. Cells were washed and incubated with goat anti-rabbit secondary antibody (Alexa fluor 488), and Alexa-555 conjugated phalloidin for 1 h at RT, and cell nuclei were stained using DRAQ5 (1:1000) for 10 min. A similar protocol was used for detecting ectopically expressed myc-tagged SYNPO2 isoforms using anti-c-myc primary antibody. A Z-stack of the cells were imaged using a 63X 1.4 NA oil-immersion objective on a Zeiss LSM 510 Meta laser scanning confocal microscope. To quantify the cortex/cytoplasm ratio of actin and NMIIA, cells were fixed with the above protocol and stained using phalloidin or anti-NMIIA (1:50). Images were acquired using Zen software (Zeiss) and a single slice from each Z-stack was used. The orthogonal view of the Z-stack was obtained by selecting the slice of interest and the images were processed using linear adjustments with Photoshop CS6 (Adobe).

2.9. Quantification of myotube formation

Duplicate or triplicate wells in a 12-well plate were seeded with C2C12 cells at 80% confluency ($1.5x10^5$ cells), cultured in growth medium for 24 h, and then induced to differentiate using medium containing 2% horse serum until 3-4 dpi. Cells were fixed with methanol for 15 min and stained with Wright-Giemsa stain (Siemens). A total of 10-12 random fields from each well were imaged using a 10x objective. For the actin inhibitor studies, 10 μM ROCK-inhibitor (Y-27632) or 20 μM Arp2/3 inhibitor (CK666) were added to cells 8 h after differentiation (to ensure the inhibitors did not affect the differentiation program), and media containing the inhibitors or solvent control was replaced every 24 h

until 3 dpi. Cells were methanol fixed, permeabilized with 0.25% triton X-100 in 1x PBS, blocked with 1% BSA in 1x PBS at RT, and immunostained with anti-MHC and nuclei stained with Hoescht. Plates were imaged at 10X using the EVOS FL cell imaging system (Thermofisher). All experiments were repeated three times and the fusion index was quantified as the percent of the total number of nuclei in a field present in MHC+ myotubes containing 3 or more nuclei to the total number of nuclei present in a field. All results are presented as the mean ± SEM of two or three experiments.

2.10. Live cell fluorescence video microscopy and cell migration analysis

For determining migration parameters post-differentiation, mock- and SYNPO2-transduced C2C12 cells, or C2C12 cells transduced with control shRNA or SYNPO2 shRNA, were seeded at 70% confluence ($0.43x10^5$ cells) in tissue culture treated glass bottom quadrant dishes (Greiner bio-one, #627870), cultured for 24 h in growth medium, and differentiated with 2% horse serum. For the ROCK and Arp2/3 studies, cells were treated with the inhibitors starting at 8 h post-differentiation. Before imaging, nuclei were stained with 0.2µg/ml Hoechst (Invitrogen;) to facilitate tracking by fluorescence video microscopy. Cell migration at 2 dpi was recorded for 3 h capturing images every 5 min using the 20x objective of a Zeiss Cell Observer Spinning Disk Confocal System, and cells from each experiment were tracked using IMARIS version 9.1.2 software to determine velocity (µm/min). The data were analyzed using GraphPad Prism version 6.

2.11. Zebrafish husbandry

Adult zebrafish (Danio rerio), both AB strain and c*asper*, and *synpo2b*$^{-/-}$ knockout lines were housed and maintained in the zebrafish core facility, Dalhousie University. Fish were grown in fish water and maintained at 28˚C. All experiments were carried out with the approval of Dalhousie University Animal Care Committee (protocol no. 17-134). Adult male and female zebrafish were set in breeding tanks separated by a divider the day before breeding in the ratio 1:2. The following morning, the dividers were removed, and embryos were collected in a 10 cm dish in egg water (5 mM NaCl, 0.17 mM KCl, 0.33 mM CaCl2, 0.33 mM MgSO4). The embryos were grown in a 28˚C incubator and used for downstream analysis.

2.12. Synpo2b morpholino treatment

A morpholino oligonucleotide was designed to target the 5'UTR/ATG sequence of *synpo2b* and was purchased from GENE TOOLS, LLC. The morpholino was resuspended in DNAse and RNAse free water and a 500 nM concentration of the morpholino was injected into the yolk-sac of the embryos along with phenol red to make sure the oligonucleotide was injected. A scrambled morpholino was injected as a control. Embryos were fixed in 4% paraformaldehyde (PFA) for immunofluorescence analysis.

2.13. Generation of *synpo2b*$^{-/-}$ knockout fish line

Design and synthesis of sgRNA and cas9 mRNA: The *synpo2b*$^{-/-}$ knockout line was generated using the clustered regularly interspaced short palindromic repeat (CRISPR)/CRISPR-associated endonuclease (cas9) system. Guide RNAs (sgRNAs) were designed using the Sequence Scan for CRISPR (SSC) (http://cistrome.org/SSC/) (Xu et al., 2015) and six sgRNAs were chosen based on the score that predicts specificity and off-target effects. Each sgRNA was designed with a T7 promoter, target sequence and a 20-nucleotide sequence that overlaps with the sgRNA scaffold sequence. The sgRNAs were synthesized by carrying out overlap-extension PCR using each of the forward sgRNA oligonucleotides with the reverse scaffold oligo (rev-sgRNA-scaffold). The PCR products were gel extracted and transcribed by *in vitro* transcription using the MEGAshortscript T7 kit (AM1354, Thermo Fisher Scientific). The cas9 mRNA was prepared from pT3TS-nCas9n plasmid (Prykhozhij et al., 2018) (Addgene, 46757) using the mMassage mMachine T3 kit (AM1348, Thermo Fischer Scientific) and purified using LiCl as per the kit's instruction.

synpo2b targeted sgRNA injection: The six gRNAs along with cas9 mRNA were injected in the one-cell stage *casper* embryos. The embryos were grown for one month and genotyped using primers targeting the 5'- and 3' UTRs of the gene. The F0 containing gene knockouts were grown to adulthood. The knockout fish were outbred with wild-type fish to remove off-target effects of the gRNAs, and to determine germline transmission of the gene knockout. One out of 11 F0 fish was able to transfer the gene knockout (1720bp deletion) to F1 off-spring. These heterozygotes were then in-crossed and screened for

homozygous knockouts (F2). The F2 knockout were in-crossed to obtain the F3 generation that were used for breeding F4 embryos for all downstream experiments.

2.14. Protocol for genotyping knockout fish

Genotyping was carried out on one-month olf fish. Each fish was anesthetized in water containing 4% Tricaine-MS-222. The caudal fin was clipped using a surgical blade and added to an 8-strip PCR tube that contained 50 µl of lysis buffer (10 mM Tris pH 8, 2 mM EDTA, 0.2% Triton X-100, and 200 µg/ml Proteinase K). The tubes were incubated at 98◦C for 10 min, briefly vortexed and 5 µl (20 mg/ml) of proteinase K was added to each tube and incubated at 55◦C for 20 min, and then incubated at 98◦C for 10 min and vortexed again. The extracted genomic DNA was diluted 1:20 in elution buffer and PCR was carried out using Hot-start Taq polymerase (abm, G011) as per the manufacturer's instruction.

2.15. Whole-mount *in situ* hybridization of zebrafish embryos

Generation of Digoxigenin (DIG)-labelled RNA probe: The N-terminus of *synpo2b*-S exon 1 (ENSDART00000137869.2) comprising a 1000 bp fragment and the unique region of *synpo2b*-L exon 2 (ENSDART00000193375.1) comprising a 460 bp fragment were PCR amplified from cDNA. The fragments were amplified using a forward primer and a T7 promoter-containing reverse primer. The DIG-labelled RNA probes were generated using an *in vitro* transcription kit with DIG RNA labeling mix (#11277073910, Roche).

In situ hybridization protocol: Embryos at different stages of development (8 hours post-fertilization [hpf]), 12 hpf, 18 hpf, 25 hpf, 48 hpf, and 72 hpf) were fixed with 4% PFA overnight at 4°C, washed twice with 1x PBST (PBS with 0.1% Tween-20) and stored in methanol at -20°C. Embryos were rehydrated with a series of methanol washes (95/75/50/25% methanol in PBST) and washed three times for 5 min with 1x PBST. The 48hpf and 72hpf embryos were treated with a bleaching solution (1% KOH and 3% H_2O_2 in H_2O) at RT until embryos appeared bleached (decolorization of the eye). The embryos were then washed in 1x PBST three times every 5 min. *In situ* hybridization was performed as described in (Lauter et al., 2011) with modifications. Briefly, after washing with 1x PBST, embryos were treated with proteinase K (10 µg/ml in PBST) to enhance accessibility

of probes. Embryos younger than 24 hpf were not treated with proteinase K, while 25 hpf, 48 hpf and 72 hpf embryos were treated for 1, 10 or 30 min, respectively. Treated embryos were then post-fixed with 4% PFA for 20 min at RT and washed with 1x PBST four times for 5 min. Embryos were transferred into 1 ml of pre-hybridization buffer (Hb4) and incubated at 60˚C in a hybridization oven. The buffer was replaced with 200 µl of Hb4D5 (Hb4 containing 5% dextran sulfate) containing 200 ng of DIG-labelled RNA probe and embryos were incubated at 60˚C overnight for 16 h. Embryos were then subjected to a series of washes with saline sodium citrate at different concentrations at 60˚C. After the final wash with PBST at RT, embryos were incubated in 8% sheep serum for 1 h at RT by gently rocking on a shaker. The blocking solution was completely removed and replaced with alkaline phosphatase (AP) anti-DIG antibody (1:2000) in blocking solution and incubated overnight at 4˚C without agitation. The embryos were then washed with PBST six times for 15 min at RT, and then washed with alkaline tris buffer three times for 5 min. The antibody was detected by adding 5-bromo-4-chloro-3-indolyl phosphate/nitroblue tetrazolium (BCIP/NBT) alkaline phosphatase (AP) substrate (SK-5400, Vector Laboratories) as per protocol. The embryos were incubated in the dark at 37˚C until staining was visible. The reaction was stopped by washing in PBS and fixing embryos again in 4% PFA. During imaging, embryos were suspended in 80% glycerol and imaged using a Zeiss V20 stereo microscope.

2.16. Quantitative PCR

Around 30 embryos each at different stages of development (4-72 hpf) were snap-frozen for qPCR analysis. RNA was extracted using Trizol reagent (#15596026, Invitrogen) according to the protocol. Briefly, 500 µl of Trizol reagent was added and the tissue was homogenized using a 25-gauge needle. The homogenized samples were centrifuged at high speed to remove fat content and transferred to Phasemaker (A33248, Invitrogen) tubes. 100 µl of chloroform was added and the tubes were shaken vigorously. Upon centrifugation, the mixture separated into three phases, and the aqueous phase was transferred to new tubes. RNA was precipitated by adding 250 µl of isopropanol and centrifuging at high speed. The pelleted RNA was washed with 500 µl of 75% ethanol, centrifuged and resuspended with DNAse and RNAse free water. cDNA synthesis was carried out using RNA to cDNA

EcoDry™ Premix kit. Briefly, 2 µg of RNA was added to the mix and incubated at 42°C for 1 h. A standard curve was performed for primer validation. The synthesized cDNA was diluted 1:40 and used for qRT-PCR analysis.

2.17. Whole-mount immunofluorescence of zebrafish embryos

Embryos at 48 hpf were fixed with 4% PFA overnight at 4°C, washed twice with 1x PBST and stored in methanol at -20°C. Embryos were rehydrated with a series of methanol washes (95-25% methanol in PBST), and washed three times for 5 min in 1x PBST. Embryos were permeabilized in 2% Triton-X100 in PBS for 2 h at RT and stained for actin with Alexa Fluor 555 phalloidin (1:20) in 2% Triton X-100 overnight at 4°C for actin. Following staining, embryos were washed in 1x PBST three times for 15 min at RT and stored in PBS at 4°C until imaging.

For MHC staining, permeabilized embryos were blocked for 2 h at RT with blocking solution, 2% BSA, 5% goat serum, 0.1% Triton X-100 in PBS, and for β-dystroglycan staining, permeabilized embryos were washed in a solution containing 0.1% PBST, 0.1% Tween-20 and 0.3% saponin for 10 min at RT. The embryos were then blocked in a blocking solution containing 0.1% PBST, 0.1% Tween-20, 0.3% saponin and 1% BSA. Primary antibody anti-MHC (MF20, 1:10) or β-dystroglycan (Novocastra, #NCLbDG, 1:250)) was added in the blocking solution and incubated overnight at 4°C. Embryos were then washed six times for 15 min in 1x PBST and incubated with Alexa Fluor-488 conjugated secondary antibody (1:250) in blocking solution overnight at 4°C. Embryos were again washed six times for 15 min in 1x PBST and treated with 1 µg/ml DAPI in 1x PBS for 30 min at RT. Finally, embryos were washed in 1x PBS three times for 15 min. During imaging, embryos were embedded in 1% low melting agarose in a glass bottom dish and imaged using the 20X 1.5 NA objective on a Zeiss Axioplan II fluorescent microscope.

2.18. Electron microscopy

Embryos at 48 hpf were fixed in 2.5% glutaraldehyde diluted with 0.1 M sodium cacodylate buffer for 2 h at RT. Samples were then rinsed three times for 10 min with 0.1 M sodium cacodylate buffer. Samples were then fixed in 1% osmium tetroxide for 2 h and

rinsed with distilled water, and then incubated in 0.25% uranyl acetate at 4°C overnight. Embryos were dehydrated with a graduated series of acetone treatment and infiltered with epon araldite resin in a 3:1 ratio (3 parts dried 100% acetone, 1 part resin) for 3 h; 1:3 ratio (1 part dried 100% acetone: 3 parts Resin) overnight and 100% Epon araldite resin two times for 3 h. Curing was performed by embedding the embryos in 100% Epon araldite resin at 60°C for 48 h. Thin sections (approximately 100 nm thick) were obtained using a Reichert-Jung Ultracut E Ultramicrotome with a diamond knife and placed on formvar grids (#FF200-Cu, EMS) and stained with 2% aqueous uranyl acetate for 10 min, washed with distilled water two times for 5 min each, treated with lead citrate for 4 min, quickly rinsed with distilled water and air dried. The samples were then viewed using a JEOL JEM 1230 Transmission Electron Microscope at 80kV and imaged using a Hamamatsu ORCA-HR digital camera.

2.19. Laser-inflicted muscle injury

Embryos were maintained until 3 dpf (days post-fertilization) in egg water at 28°C. Before injuring, the embryos were anesthetized in egg water containing 0.02% tricaine-MS-222 and then transferred onto 8-chamber glass slide (#C7182, Nunc Lab-Tek) in 1% low melting agarose. Each chamber contained one embryo oriented in such a way to allow the laser to cut the muscle fibers. The Zeiss photoactivated localization microscopy (PALM) was set at 20X and to excite laser power intensity set to 55%. The same somite number was chosen for each of the embryos to be injured. Upon activation of the laser, the muscle fibers in the somite were cut and the injury was evident from curled up fibers. Injured embryos were then gently removed from the agarose and placed in separate wells in a 12-well dish in egg water, and allowed to recover at 28°C.

The injured embryos were imaged on a Zeiss V20 stereo microscope at 89% zoom. The damaged somite along with surrounding healthy somites were imaged using birefringence. Images were taken at 0, 2, 3- and 4-days post-injury and regeneration of the damaged somite was quantified using image J. The birefringence of the injured somite, somite 12 in this case, and uninjured somite number 10, was obtained as the mean grey value. The value of the injured somite was then normalized to an uninjured somite to report regeneration.

2.20. Touch response assay

Embryos were maintained until 2 dpf in egg water at 28°C. Unhatched embryos were dechorionated with pronase and the embryos allowed to recover for 30 min before imaging. During imaging, a 36 mm dish with a 10 mm diameter circle was placed on the illuminated stage of a Zeiss Axiovert 200M stereo microscope. Live imaging was acquired using a Hamamatsu Orca R2 Camera at 25 frames per second. Each embryo was placed in the center of the 10 mm circle and the tail was touched using an insect pin. Video was acquired until the fish swam out of the field of view. The time taken in seconds for each embryo to swim outside the circle after the touch stimulus was quantified and reported as the escape time.

2.21. RNA sequencing

RNA sequencing: Three sets containing 30 embryos each of WT and *synpo2*$^{-/-}$ KO were snap frozen at 22hpf. The frozen tissue samples were shipped to Genewiz, New Jersey, USA, for RNA-seq analysis. Briefly, RNA was extracted from the tissues and an RNA-seq library was prepared as described by the company as follows: (1) fragmentation and enrichment of RNA; (2) synthesis of first strand cDNA and double stranded cDNA; (3) end repair, 5' phosphorylation and dA-Tailing; and (4) adaptor ligation, PCR amplification and sequencing.

RNA sequencing data analysis: The obtained reads were trimmed to remove adaptor sequences and mapped to the Danio rerio GRCz10.89 reference genome on ENSEMBL using the STAR aligner v.2.5.2b to obtain the raw counts. A Bioconductor platform, edgeR, was used for determining the differentially expressed genes. The raw counts were processed in the edgeR platform, where the counts were first filtered to remove very low and no value counts, and then normalized to the total read counts. The normalized counts were subjected to the Fisher exact test to determine the fold change and pValue. From the data obtained, a volcano plot was generated using the log2 fold change and -log10 pValue.

Gene set enrichment analysis (GSEA) and pathway analysis: The edgeR platform generates a file containing the significantly regulated genes, and this data was subjected to GSEA, pathway analysis, and gene ontology (GO) enrichment analysis using the

ClusterProfiler and ReactomePA Bioconductor platforms. The data generated from this analysis was used for generating the *cnet* plot and heat map.

2.22. Statistical analysis

All results reported herein are the mean ± SEM of duplicate or triplicate experiments as indicated. Statistical significance was determined using an unpaired Student *t* test ($p < 0.05$) as indicated in the figure legends.

CHAPTER 3: SYNAPTOPODIN-2As IS A NOVEL PROMYOGENIC MARKER THAT DIFFERENTIALLY REGULATE MYOBLAST MIGRATION AND FUSION USING TWO DISTINCT PATHWAYS

3.1 Introduction

In the fruit fly, intense research has been done to identify the players of cell fusion during muscle development and regeneration. As mentioned in the Introduction, *Drosophila* myoblast fusion comprises a two-cell system, founder cell (FC) and fusion competent myoblast (FCM), and the difference in their genetic makeup has made it easy to study the effect of each protein in these specific cell types. Early screens identified cell recognition and adhesion molecules, cell signalling, and actin remodelling proteins required for myoblast fusion (Kim et al., 2015). More recently, the Chen lab identified the formation of actin-rich invadopodosomes in the FCM (Sens et al., 2010) and mechanical tension put forth by actomyosin contraction in the FC against the invading podosomes of FCMs at the fusion site as key features of *Drosophila* myoblast fusion (Kim et al., 2015). In vertebrates, actin cytoskeleton remodelling proteins such as Nck-associated protein 1 (Nap1), SCAR/WAVE complex, Arp2/3, Rac1 and RhoA (Nishiyama et al., 2004; Nowak et al., 2009; Richardson et al., 2007; Vasyutina et al., 2009) are all involved in muscle cell fusion. These studies highlight the importance of actin remodelling proteins during myoblast fusion.

The aim of my PhD project was to determine the function of one such actin binding protein, synpo2, in vertebrate myoblast fusion. The function of human SYNPO2 has been studied in-depth in the prostate cancer field, however, very little is known about the role of synpo2 in myogenesis. In the cancer field, human SYNPO2As (Fig. 5A) is a biomarker for invasive prostate cancer as its deletion correlates with increased invasiveness of the tumour, however it is not clinically used as a biomarker (Lin et al., 2001). The nuclear-cytoplasmic ratio of SYNPO2 is also related to the grade and stage of bladder cancer (Sanchez-Carbayo et al., 2003). In addition to the above-mentioned SYNPO2As isoform, the Gettemans lab isolated three other transcripts from human prostate cancer cells, SYNPO2A, B and C (Fig. 5A), all containing a PDZ domain in the N-terminus that is absent in the short SYNPO2As isoform. These long isoforms bind actin fibers in the cytoplasm, but only the short isoform showed some localization in the nucleus (Ariane De Ganck et al., 2008). A fourth isoform,

SYNPO2D (Fig. 5A) was later isolated from PC3 cells, and the functional role of all the isoforms was reported by the Duncan lab (Kai et al., 2013). The different isoforms all induce formation of actin stress fibers (SF) and either enhance or supress PC3 cell migration depending on the external stimuli (Kai et al., 2012). The formation of SFs and enhanced migration were both shown to be ROCK-dependent (Kai et al., 2013).

Almost all studies in the myogenesis field use the short isoform, SYNPO2As (Fig. 5A and B). Mouse and human SYNPO2As are both 80 kDa nuclear-cytoplasmic shuttling proteins that bind actin (Weins et al., 2001). In human skeletal muscle, SYNPO2As interacts with other actin-binding proteins such as filamin C and α-actinin, and with focal adhesion proteins such as zyxin (A Linnemann & Ven, 2010). *In vitro* studies report the actin binding and actin polymerization property of SYNPO2As (Chalovich & Schroeter, 2010; Schroeter et al., 2013). Apart from the above-mentioned studies, the functional role of synpo2 isoforms during myogenesis remains largely unknown. My project aimed to decipher the functional role of mouse SYNPO2 isoforms during myoblast migration and myotube formation.

In addition to SYNPO2As that is expressed in differentiated mouse and human skeletal muscle, we isolated two additional long isoforms, SYNPO2A and B from the C2C12 mouse myoblast cell line, and I examined the functional role of all three isoforms in myogenesis. Consistent with results from the prostate cancer field, overexpression of all three mouse isoforms significantly enhanced myoblast migration whereas knockdown significantly reduced migration. Contrary to the human SYNPO2 isoforms in prostate cancer cells, the mouse SYNPO2As isoform enhanced myoblast migration in a ROCK-independent manner. Most notably, SYNPO2As enhanced myotube formation while SYNPO2A and B inhibited myogenesis, and SYNPO2As promoted myotube formation in an Arp2/3-independent and ROCK-dependent manner. These results provide the first evidence that mouse SYNPO2 isoforms exert differential effects on myoblast fusion, and they identify SYNPO2As as a new promyogenic factor that regulates two actin remodelling processes, cell migration and fusion, using two independent pathways.

3.2 Results

3.2.1 Isolation of SYNPO2 isoforms from C2C12 myoblasts

To determine the functional role of SYNPO2 isoforms on myogenesis, we used the well-established C2C12 mouse myoblast cell line (Blau et al., 1985) throughout this study. The *Synpo2* gene is located in the reverse strand of chromosome 3 and the gene contains 5 exons. In addition to the known short isoform, SYNPO2As, we found sequences of two long isoforms annotated in the NCBI database. The larger isoforms, SYNPO2A and SYNPO2B, have the same N-termini but different C-termini while the smaller isoform, SYNPO2As, has the same C-terminus as SYNPO2A and a unique N-terminus that is transcribed from the intron region of the gene (Fig. 5B), similar to human SYNPO2As (A Linnemann & Ven, 2010). The difference in the N- and C-termini between the isoforms was used to design isoform-specific PCR primers and the cDNAs were cloned from RNA extracted from undifferentiated C2C12 myoblasts.

3.2.2 SYNPO2As is upregulated during myogenic differentiation

SYNPO2As is the only isoform reported to be expressed during differentiation (Weins et al., 2001). We wanted to determine the expression pattern of all the three SYNPO2 isoforms in C2C12 myoblasts. Throughout this study, we followed the below protocol to differentiate C2C12 myoblasts, and a representative Giemsa-stained image of the morphology of the cells during different stages of myogenesis is shown in Fig. 8A. The C2C12 myoblasts are mononucleated in growth/proliferation media (Day 0). C2C12 myoblasts were seeded at 70% confluence and differentiated in 2% horse serum (HS). Two days post-induction of differentiation (dpi), the fibroblast shaped mononucleated cells elongate and appear spindle shaped and align next to one another. By 3-4 dpi, differentiated myoblasts have fused to form multinucleated myotubes. Western blots of cell lysates from different days post-differentiation were probed with a commercial anti-synpo2 antiserum raised against a peptide from the conserved exon 4 region present in all isoforms (Fig. 5B). As previously reported (Linnemann et al., 2010; Weins et al., 2001), we were only able to detect upregulated expression of the small isoform, SYNPO2As, which appeared as a 80 kDa band (Fig. 8B). We were not able to detect the long isoforms, SYNPO2A and B whose predicted molecular weights are 116 kDa and 135 kDa, respectively (Fig. 8B). To determine whether the antibody could detect the long isoforms, we cloned the cDNAs of the three isoforms into retroviral plasmids and generated stably transduced C2C12 cell

lines: mock, SYNPO2A, SYNPO2B and SYNPO2As. As shown (Fig. 8C), western blotting of cell lysates collected from undifferentiated, stably transduced C2C12 myoblasts readily detected all three isoforms. We noted the large two isoforms migrated aberrantly in SDS-PAGE, with calculated molecular masses of ~160 kDa and ~170 kDa, considerably larger than the predicted molecular masses of 116 kDa and 135 kDa. This aberrant migration of the long isoforms is consistent with the aberrant migration of human SYNPO2 isoforms reported in PC3 cells (Ariane De Ganck et al., 2008). Furthermore, SYNPO2As, when ectopically expressed migrated as a predominant band at ~110 kDa and faint band at 80 kDa (Fig. 8C), contrary to endogenous expression where a 110 kDa band was not readily detected (Fig. 8B).

A recent publication reported that the long isoforms, SYNPO2A and B that contain a PDZ domain play a role in chaperone assisted selective autophagy (CASA) and are detected in differentiated C2C12 myoblasts and A7r5 rat smooth muscle cells (Ulbricht et al., 2013). To determine if we could detect the long isoforms by inhibiting autophagy, C2C12 myoblasts were treated with bafilomycin A1 (autophagy inhibitor) in both growth media and differentiated media. Cell lysates were collected both before and after differentiation, and with and without the treatment. Irrespective of the treatment, we were only able to detect expression of SYNPO2As, but not SYNPOA and B, by western blotting (Fig. 8D).

3.2.3 Mouse SYNPO2 isoforms associate with cytoplasmic actin filaments

To examine subcellular localization of endogenous SYNPO2, parental C2C12 cells at 3 dpi were imaged by immunofluorescence using anti-synpo2 antibody. As previously reported (A Linnemann & Ven, 2010; Weins et al., 2001), SYNPO2 associated with actin filaments in the cytoplasm of myotubes displaying a punctuated staining pattern along these filaments (Fig. 9). To examine the staining pattern of the different isoforms, stably transduced C2C12 cells expressing myc-tagged versions of the SYNPO2 isoforms at two dpi were similarly imaged. The ectopically expressed myc-tagged SYNPO2As isoform showed a similar punctuated staining pattern along cytoplasmic actin fibers as endogenous SYNPO2As (Figs. 10C). SYNPO2A and SYNPO2B also showed a similar punctuated staining pattern along actin filaments as SYNPO2As, although the intensity of the

fluorescent foci varied qualitatively between the different isoforms (Figs. 10A and B). The human SYNPO2 isoforms also show different staining patterns along actin fibers in PC3 cells, even though all of these isoforms have similar effects on PC3 cell migration (Fui Boon Kai & Duncan, 2013).

In collaboration with Colin Crist (McGill University), we further used satellite cells isolated from *Pax3*$^{GFP/+}$ mice and immunofluorescence staining to confirm expression of SYNPO2 in primary cells. Freshly isolated cells were stained with Pax7 antibody, a satellite-cell specific marker, to confirm they were satellite cells (Fig. 11A). Cells were then cultured for three days during which time they differentiated into myoblasts, as evident from positive immunostaining for MyoD. By five days post-culture, cells had differentiated into myotubes and stained positively for troponin T (Fig. 11A). At all stages of pre- and post-differentiation, cells were co-stained with anti-synpo2 antibody to confirm its localization in primary cells. Cells at day 0 stained positively for SYNPO2, with apparent nuclear staining although the small size of the cells made it difficult to differentiate between nuclear and cytoplasmic localization. At three dpi SYNPO2 staining was more evident in the cytoplasm of the myoblasts, and by 5 dpi in the myotubes (Fig. 11A), showing similar colocalization with actin filaments in the cytoplasm as observed in C2C12 myoblasts (Fig. 9).

To determine if the primary satellite cells expressed the three SYNPO2 isoforms, satellite cell lysates at 3 dpi and 5 dpi were examined by western blotting using anti-synpo2 antibody. We were able to detect clear upregulation of an 80 kDa band that was presumably the short isoform, SYNPO2As, but were unable to detect expression of the other two long isoforms, SYNPO2A and B (Fig. 11B). Cell lysates were also probed with myosin heavy chain (MHC) (Fig. 11C) and myoD (Fig. 11D) to confirm myogenic differentiation of satellite cells. These results demonstrated that all three mouse isoforms of SYNPO2 associate with actin fibers in differentiated myoblasts and that only the short isoform, SYNPO2As, is upregulated following myoblast differentiation.

3.2.4 SYNPO2As promotes myotube formation

To determine the function of the SYNPO2 isoforms during myotube formation, stably transduced C2C12 myoblasts expressing the individual SYNPO2 isoforms were

seeded at 70% confluency, differentiated with 2% HS, then fixed at 4 dpi and Giemsa-stained to visualize myotubes. Cells were imaged by bright field microscopy and images from five random fields per well (triplicate samples) were used to quantify the fusion index, which is the ratio of the total number of syncytial nuclei in myotubes (i.e., cells with ≥ 3 nuclei) to the total number of nuclei in the field. A representative image of each isoform at 4 dpi is shown in Fig. 12A. Overexpression of SYNPO2A and B significantly reduced myotube formation by ~50% compared to mock-transduced cells whereas SYNPO2As effectively doubled myotube formation (Fig. 12B).

These ectopic expression results were confirmed using RNA inhibition. We designed two short-hairpin RNAs (shRNAs) to knockdown the three isoforms; shRNA1 was designed to target the unique N-terminus of SYNPO2As while shRNA2 targeted the conserved region of all the three isoforms (Fig. 13A). The shRNAs were cloned into retroviral plasmids and used to generate stable cells lines. As shown by western blotting, both shRNAs decreased endogenous SYNPO2As expression at 3 dpi by ~50-80%, with shRNA2 showing the most pronounced effect (Fig 13B). Since endogenous SYNPO2A and B were undetectable in C2C12 myoblasts, HEK293T cells were used to determine knockdown efficiency of the long isoforms. HEK293T cells were co-transfected with SYNPO2A or B along with shRNA2, which reduced expression of both SYNPO2A and B to beyond detectable limits (Fig. 13C).

To determine the effect of endogenous SYNPO2 knockdown on myotube formation, C2C12 myoblasts stably transduced with the shRNAs or a control shRNA were differentiated, fixed on 3 dpi and Giemsa-stained to visualize myotubes, and the fusion index was quantified as described above. As noted from Fig. 13D, the fusion index showed that knockdown of SYNPO2As using shRNA1 and shRNA2 significantly inhibited myotube formation by 50% on 3 dpi. Analysis of a time course from 2 dpi to 4 dpi showed a significant reduction of myotube formation by ~50% until 3 dpi, which was reduced to ~25% inhibition by 4 dpi in knockdown cells (data not shown), indicating SYNPO2 knockdown delays fusion kinetics. Targeting all three SYNPO2 isoforms with shRNA2 gave approximately the same reduction in myotube formation as shRNA1, consistent with the western blotting results indicating the long isoforms are not expressed following early

differentiation. This is the first data to show that SYNPO2As is a promyogenic factor that enhances early myotube formation.

Since SYNPO2 is an actin polymerizing and bundling protein, we hypothesized that knockdown of SYNPO2 would alter actin structures, which could affect myoblast fusion. Knockdown cells were fixed at 3 dpi and stained with phalloidin to image filamentous actin structures. Contrary to our hypothesis, we did not observe any significant change in cell morphology or in the overall appearance of the actin cytoskeleton in the knockdown cells compared to control cells post-differentiation (Fig. 14). If SYNPO2As functions as an actin regulator to enhance myotube formation, then its affects on actin dynamics do not alter the gross actin cytoskeleton structure.

3.2.5 SYNPO2 isoforms overexpression or knockdown does not affect the overall myogenic differentiation program

To determine whether ectopic expression or knockdown of SYNPO2 isoforms affected the myogenic differentiation program, C2C12 myoblasts expressing mock and SYNPO2 isoforms or expressing control or shRNAs were differentiated. Cell lysates were collected at various days-post induction and western blots were probed using antibodies against myogenic differentiation (myoD), myogenin (myoG), and myosin heavy chain (MHC); myoD and myogenin are early differentiation markers and MHC is a late differentiation marker. Ectopic expression of SYNPO2 isoforms or shRNA knockdown of endogenous SYNPO2 did not affect expression of the above-mentioned myogenic proteins (Figs. 15A and B). These results show that the effect of SYNPO2As on myotube formation is independent of the differentiation program.

3.2.6 SYNPO2As significantly enhanced migration post-differentiation

Human SYNPO2 can increase or decrease prostate cancer cell migration depending on the external stimuli, and the enhanced cell migration is influenced by the Rho/ROCK pathway (Kai et al. 2012). We know that migration is an important step in myogenesis as the cells need to migrate close to one another to enable cell-cell contact and initiate fusion. However, it is unknown whether mouse SYNPO2As exerts any effect on myoblast migration and whether altered migration has a direct effect on myotube formation. To

quantify migration, cells were differentiated and videomicroscopy was used to quantify the migration of individual cells at 48 hours post-induction of differentiation (hpi), just prior to the first appearance of myotubes. To more easily track the migration of individual cells, cell monolayers were stained with 0.2 μg/ml of Hoechst to visualize nuclei, and migration was recorded for 3 hours, taking an image every five minutes using a spinning-disc confocal microscope. The velocity of the migrating cells was quantified using IMARIS software. Overexpression of all three mouse SYNPO2 isoforms significantly enhanced the velocity of the migrating cells compared to mock-transduced cells (Fig. 16A), while knockdown of endogenous SYNPO2As had the converse effect, significantly reducing cell velocity compared to cells expressing control shRNA (Fig. 16B). Specifically, in the knockdown studies control cells migrated with an average velocity of 0.153μm/min while SYNPO2 knockdown cell migrated with an average velocity of 0.143μm/min. In addition, only 23% of SYNPO2 knockdown cells migrated faster than this average velocity. Thus, all SYNPO2 isoforms have modest, though statistically significant effects on upregulating C2C12 migration but only SYNPO2As enhances myotube formation.

3.2.7 Converse effects of ROCK inhibition on SYNPO2As-enhanced migration and myotube formation

Myoblast fusion in *Drosophila* is controlled by two actin-regulatory pathways, the Arp2/3 and the Rho-ROCK pathways. The Arp 2/3 pathway is required to form actin foci made up of branched actin filaments in the invading myoblast, whereas the Rho-ROCK pathway is required to form a contractile actomyosin sheath beneath the membrane of the receiving myoblast/myotube (Kim et al., 2015). From the prostate cancer field, we know that human SYNPO2 polymerizes actin at the leading edge of the cell favouring cell migration by utilizing the Rho-ROCK pathway (Kai et al., 2012), and promotes lamellipodia formation in an Arp 2/3-dependent manner (Kai et al., 2015). Therefore, we used pharmacological inhibitors of Arp 2/3 and ROCK to determine whether SYNPO2As influenced migration and fusion of myoblast using these actin-regulatory pathways that are known to be involved in *Drosophila* myoblast fusion. Mock and SYNPO2As transduced cells were induced to differentiate in the presence or absence of the Arp 2/3 inhibitor, CK666 (20μM). Cells were fixed at 3 dpi and myotubes were stained with anti-MHC

antibody and Hoechst to quantify the fusion index. Treatment with CK666 reduced the overall fusion efficiency of mock and SYNPO2As transduced cells compared to DMSO treated cells. However, SYNPO2As significantly enhanced myotube formation compared to mock-transduced cells to approximately the same extent both in the presence and absence of CK666, suggesting that SYNPO2As enhances myoblast fusion in an Arp 2/3-independent manner (Fig. 17A). Similarly, the fusion index was quantified for both mock- and SYNPO2As-transduced C2C12 cells treated with the ROCK inhibitor Y27632 (10μM). Treatment with the ROCK inhibitor increased myotube formation of mock transduced cells, as reported previously (Nishiyama et al., 2004). However, Y27632-treated SYNPO2As cells did not significantly enhance myotube formation compared to treated mock-transduced cells (Fig. 17B), indicating SYNPO2As-enhanced fusion is sensitive to ROCK inhibition.

To determine whether SYNPO2As-enhanced fusion and cell migration were both sensitive to ROCK inhibition and possibly causally related the cell migration experiments were repeated in the presence and absence of the ROCK inhibitor. As observed before, untreated SYNPO2As cells significantly enhanced the velocity of the migrating cells compared to mock transduced cells, and the same results were obtained in cells treated with the ROCK inhibitor, implying SYNPO2As enhances myoblast migration independent of ROCK (Fig. 17C). Thus, SYNPO2As influences myoblast migration and myotube formation using different actin regulating pathways. Coupled with the data indicating that SYNPO2A and B also increase migration but decrease fusion, these results suggested the SYNPO2As-enhanced migration and myotube phenotypes may not be causally linked.

3.2.8 SYNPO2As does not alter the actomyosin levels to mediate myoblast fusion

A recent study revealed that a reduced cortical to cytoplasmic ratio of actin and NMIIA leads to uncontrolled C2C12 myoblast fusion leading to the formation of massive myotubes (Tsuchiya et al., 2018). Studies in *Drosophila* have also shown that a contractile layer of cortical actomyosin in FCs is needed to appose the protrusive forces of invadopodia from adjoining FCMs (Kim et al., 2015). Therefore, we used anti-pMLC and phalloidin to stain actomyosin fibers in differentiated C2C12 cells (Fig. 18B) and used immunofluorescence microscopy to quantify the ratio of cortical to cytoplasmic

actomyosin fibers (Fig. 18C and D). A Z-stack of myotubes at random fields were imaged using confocal microscopy and the fluorescence intensity for actin and NMIIA staining was quantified separately using imageJ software. Briefly, two equal-sized rectangular boxes were drawn, one on the membrane and the other in the cytoplasm, and the mean grey value was determined (Fig. 18A). This was done on several regions of each myotube and the average ratio of pixels in the cortex to cytoplasm was calculated for each myotube to determine changes in distribution of NMIIA and F-actin. As shown (Fig. 18C and D), knockdown of SYNPO2 had no effect on the distribution of filamentous actin or actomyosin fibers between the cortex and cytoplasm. This data suggested that, if SYNPO2As enhances myotube formation via alterations to actin dynamics, then it does so without inducing detectible changes in the overall architecture of the actin or actomyosin cytoskeleton.

3.3 Discussion

Myogenesis is a multi-step process that turns uninucleated myoblasts into multinucleated myotubes. Two crucial processes for myoblast fusion are: (a) the differentiation program that converts myoblasts to myocytes that encode proteins required for muscle development and function; and (b) actin remodelling to enable the cells to migrate and fuse to make myotubes. A detailed list of myogenic proteins and actin remodelling proteins that play a role during myoblast fusion is mentioned in the Introduction of this thesis. During development several myotubes align next to one another to form myofibrils that form the contractile units of muscle. These myofibrils contain repeating sarcomeric units made of actin and myosin fibrils and several actomyosin regulating proteins. Each sarcomere is bordered by a Z-disc and further contains an A-band, I band and M-line. Some proteins in the Z-disc and M-line act as mechanosensory and signalling molecules shuttling between the nucleus and cytoplasm (Knöll et al., 2011).

Of the many proteins in the Z-disc, the protein of interest to us is synpo2. Mouse SYNPO2As is a nuclear-cytoplasmic shuttling protein that localizes in the nucleus in the myoblast stage and shuttles to the cytoplasm upon differentiation, binding to actin filaments and localizing in the Z-disc of skeletal muscle fibers. Nuclear accumulation of SYNPO2As in myotubes can also be triggered by heat shock (Weins et al., 2001). Additionally,

SYNPO2As binds actin and other actin-related proteins in differentiated myoblasts and myotubes (Linnemann et al., 2010). The above-mentioned studies report the localization and actin-binding ability of the short isoform SYNPO2As, however, its functional role during muscle development is unknown.

My research focused on studying the functional role of mouse SYNPO2 during myogenesis. We have for the first time identified a functional role for SYNPO2As as a promyogenic marker required for myoblast fusion. This study was carried out using three mouse isoforms, SYNPO2A, B and As (Fig. 5B), to understand how the different isoforms affect myotube formation. As reported previously, SYNPO2As is the only endogenously expressed isoform we were able to detect during myoblast differentiation (A Linnemann & Ven, 2010; Weins et al., 2001). Upregulated SYNPO2As expression coincided with increased myotube formation while inhibiting endogenous SYNPO2As expression had the opposite effect. Unlike filamin C and drebrin, two actin-regulating proteins that reduce differentiation markers and fusion when knocked down in C2C12 myoblasts (Dalkilic et al., 2006; Mancini et al., 2011), SYNPO2 knockdown or over-expression regulated myotube formation independent of the differentiation pathway, similar to other actin-regulating proteins such as Brag2, ARF6, ELMO and BAI3 (Bach et al., 2010; Hamoud et al., 2014; Pajcini et al., 2008). Conversely, and consistent with their lack of upregulated expression during early myotube formation, ectopic expression of SYNPO2A and B significantly inhibited myoblast fusion. Like the human SYNPO2 isoforms that enhanced PC3 cell migration, the mouse SYNPO2 isoforms also significantly enhanced migration. Studies aimed at identifying the mechanism by which SYNPO2As enhanced migration and fusion clearly showed that migration was ROCK-independent, whereas the enhanced myoblast fusion phenotype was sensitive to ROCK inhibition. Though the two processes, migration and fusion, are regulated by independent mechanisms, this does not exclude the possibility that these processes may be causally related, as I discuss further below. Thus, we have determined that only the SYNPO2As isoform exerts an effect on the early steps of myogenesis, functioning as a pro-myogenic factor in a ROCK-sensitive manner to enhance myotube formation.

SYNPO2As is the only detectable endogenous isoform in primary and C2C12 myoblasts

The NCBI database has three annotated mouse SYNPO2 isoforms. To date, studies have reported the actin binding property of only the smallest isoform, SYNPO2As, which lacks the N-terminal PDZ domain present in the longer SYNPO2A and B isoforms. Cell lysates from C2C12 myoblasts and primary satellite cells confirmed the presence of the 80 kDa protein, SYNPO2As, but not SYNPO2A and B (Fig. 8B and Fig. 11B). In the prostate cancer field, a commercial antibody or an in-house polyclonal antibody raised against the actin binding region of human SYNPO2 isoforms both detected the ectopically expressed, but not the endogenous, long SYNPO2 isoforms (Ariane De Ganck et al., 2008). A study carried out by the Höhfeld group identified that the PDZ-domain containing long SYNPO2 isoforms play a role in the CASA pathway (Ulbricht et al., 2013). This CASA complex degrades the damaged muscle filaments that are generated during mechanical tension, and the PDZ domain containing Synpo2 isoforms are also degraded during this process leading to reduced steady-state levels of Synpo2. In the same study they showed expression of the longer isoforms in differentiated mouse C2C12 myoblasts and A7r5 rat smooth muscle cells by western blotting (Ulbricht et al., 2013). This is the only report of upregulated expression of the long isoforms in differentiating myoblasts.

The results of Ulbricht et al. (Ulbricht et al., 2013) are contradictory to our result as we were not able to detect expression of the long isoforms in differentiated C2C12 myoblasts, even in the presence of an inhibitor of autophagic flux, bafilomycin A (Fig. 8D), and even though the commercial antisera was clearly capable of detecting the long isoforms when they were ectopically expressed in cells (Fig. 8C). The basis for this discrepancy is not clear but may reflect differences in the antibodies used to detect SYNPO2 since we used a commercial antiserum while the Höhfeld group used a monoclonal antibody. We note that the same group used the same monoclonal antibody to detect upregulated expression of the longer SYNPO2 isoforms in differentiated C2C12 myoblasts but failed to detect these isoforms in differentiated human skeletal muscle extracts (Linnemann et al., 2010; Ulbricht et al., 2013). As we have now shown, upregulated expression of the longer isoforms actually impedes early myotube formation, which seems more consistent with our results that the longer SYNPO2 isoforms are not expressed at early stages post-differentiation in C2C12 myoblasts or in primary satellite cells. However, we were able to clone the long isoforms from mRNA extracts of undifferentiated C2C12 myoblasts,

implying the long isoforms are post-transcriptionally downregulated during early steps of myogenesis in C2C12 myoblasts.

It is conceivable that the long isoforms may play a role in muscle maintenance rather than muscle development. Our western blot results, and those of others, only examined expression patterns until day 6 post-differentiation, which might be an early time-point to determine expression of the long isoforms. Thus, it would be reasonable to run western blots with samples from adult mice under normal and stressed conditions to assess the presence of the larger isoforms. Regardless of the above discrepancies, SYNPO2As is the only readily detectible isoform during early muscle development and the only isoform that exerts a positive effect on myotube formation.

Aberrant migration of synpo2 isoforms

All SYNPO2 isoforms showed anomalies in their gel migration patterns, a phenomenon noted in some previous studies. We showed that the ectopically expressed SYNPO2A and B long mouse isoforms, which have predicted molecular masses of 117 kDa and 136 kDa, respectively, migrate more like 150-160 kDa proteins in SDS-PAGE (Fig. 8C). This aberrant migration on SDS-PAGE is also reported in the prostate cancer field with respect to the human SYNPO2 isoforms (De Ganck et al., 2008; Kai et al., 2012). This could be attributed to post-translation modifications; synpo2 is known to be phosphorylated (Faul et al., 2007; Faul et al., 2005), but no other post-translational modifications have been reported. A second possibility is the intrinsically disordered nature of the protein. From prediction databases, mouse SYNPO2 contains several disordered regions and intrinsically disordered proteins have been shown to migrate aberrantly during SDS-PAGE (Iakoucheva et al., 2001).

Another migration anomaly was noted for SYNPO2As, which is expressed as an 80 kDa protein in both mouse and human skeletal muscle and as a 95 kDa protein in human heart muscle (Linnemann et al., 2010; Weins et al., 2001). We, and others (Linnemann et al., 2010; Weins et al., 2001), detected endogenous SYNPO2As in muscle cells as only an 80 kDa polypeptide but during ectopic expression, SYNPO2As migrated predominantly as a 110 kDa polypeptide with lesser amounts of the 80 kDa polypeptide (Fig 8C). Similar expression of both 110 kDa and 80 kDa polypeptides was previously noted following

ectopic expression of human SYNPO2As in PC3 prostate cancer cells (De Ganck et al., 2008; Kai & Duncan, 2013; Kai et al., 2012). A ~110 kDa SYNPO2 polypeptide was also detected in normal differentiated mouse C2C12 myoblasts and A7r5 rat smooth muscle cells by western blotting (Ulbricht et al., 2013). The origin of the 110 kDa species is unclear, as is an explanation for why this species is only readily detected following ectopic expression. Expression of the 110 kDa SYNPO2As species was cause for concern when analyzing our stably transduced cells, but this concern was mitigated using our knockdown cell lines that gave the opposite results of the over expression system, confirming a promyogenic function for SYNPO2As in myogenesis Additional studies are needed to define the basis for the appearance of the 110 kDa SYNPO2As polypeptide and whether this species has any biological relevance to myotube formation.

Is SYNPO2As a nucleocytoplasmic shuttling protein?

Another interesting anomaly was the absence of preferential nuclear localization of both endogenous and ectopically expressed SYNPO2As in C2C12 cells. The Mundel group first reported nuclear localization of SYNPO2As in undifferentiated C2C12 myoblasts using their in-house antibody (Weins et al., 2001), and the same antibody was used by the same group in subsequent studies (Faul et al., 2007; Faul et al., 2005; Weins et al., 2001). Other groups have shown EGFP-tagged constructs of human Synpo2As in the nucleus in HEK293 cells and bladder cancer cell lines (De Ganck et al., 2005; Liang et al., 2008; Sanchez-Carbayo et al., 2003; Van Impe et al., 2003). In our hands, GFP-tagged human SYNPO2As in PC3 cells showed staining in the nucleus as large bundled threads (Dr. FuiBoon Kai, personal communication), similar in appearance to the nuclear "actin whorls" reported by Weins et al. in C2C12 cells when using EGFP-tagged SYNPO2As (Weins et al., 2001). The Getteman lab showed nuclear localization of V5-tagged human SYNPO2As in prostate cancer cells, however, they did not show endogenous staining of SYNPO2As (Ariane De Ganck et al., 2008). Thus, the nuclear localization of endogenous synpo2 has only been shown by one group using their in-house antibody.

My results indicated that undifferentiated C2C12 cells stained with the commercial anti-synpo2 antibody showed a faint speckled staining pattern throughout the cytoplasm with some evidence of nuclear localization, as shown by co-staining with the nuclear stain

DRAQ5 (Fig. 19B). However, there was no evidence of co-localization of this speckled staining pattern with cytoplasmic F-actin (Fig. 19A), a hallmark feature of SYNPO2. We believe this faint speckled staining pattern in the cytoplasm and nucleus reflects cross reaction with another protein present in undifferentiated myoblasts since the staining was not associated with actin filaments and was unchanged by knockdown of endogenous SYNPO2 (Fig. 19A). Moreover, SYNPO2As expression in undifferentiated myoblasts was undetectable by western blotting with the same antiserum (Fig. 8B), suggesting limited amounts of SYNPO2As are present in these cells. We did note, however, numerous cross-reacting bands in most western blots of 0 dpi cell lysates probed with the anti-synpo antiserum (Fig. 8B and D). The speckled, possibly nuclear, staining pattern observed in satellite cells at day 0 in the absence of detectable SYNPO2As expression assessed by western blotting (Fig. 8B) may reflect a similar cross reaction. It is notable that the Mundel group also showed no 80 kDa band detectable in samples extracted from C2C12 lysates at 0 dpi but still detected nuclear localization at this time using immunofluorescence microscopy. The issue of whether the description of SYNPO2 as a nucleocytoplasmic shuttling protein is relevant to myogenesis remains debatable. However, we did observe an increase in the staining intensity of endogenous SYNPO2As following differentiation with increased punctuated staining along cytoplasmic actin fibers (Fig. 19C), the expected staining pattern for SYNPO2As, suggesting this antiserum does recognize SYNPO2 by immunofluorescence microscopy in addition to western blotting. The apparent cross-reaction of this only available commercial antiserum limited its use in further immunofluorescence analyses.

The overall architecture of the actin cytoskeleton is not altered by overexpression or knockdown of SYNPO2 isoforms

While SYNPO2As is a known actin effector protein and actin dynamics is a key feature of myoblast fusion, it remains unclear if and how the actin remodelling capacity of SYNPO2As directly influences myotube formation. *In vitro* analysis confirms the actin bundling and polymerizing ability of SYNPO2As (Linnemann et al., 2013; Schroeter et al., 2013), and the human isoforms induce formation of different types of F-actin structures in PC3 cells (Kai & Duncan, 2013). However, we did not observe any conspicuous changes

in the overall architecture of filamentous actin following ectopic expression of the different isoforms, where all isoforms colocalized in the cytoplasm with actin filaments (Fig. 10) in a similar staining pattern as observed for endogenous SYNPO2 in differentiated myotubes (Fig. 9). Knockdown of endogenous SYNPO2 expression also did not alter the overall appearance of F-actin in differentiated myotubes (Fig. 14). The cortical actomyosin cytoskeleton is also important to regulate myoblast fusion (Tsuchiya et al., 2018; Kim et al., 2015). Quantification of the cortical vs cytoplasmic ratio of actin and NMII in SYNPO2 knockdown cells (Fig. 18C) suggested SYNPO2As does not alter actomyosin levels and is enhancing myotube formation using an alternate mechanism. F-actin stained human SYNPO2 expressing PC3 cells did increase F-actin stress fiber formation (Kai & Duncan, 2013), and videomicroscopy showed that SYNPO2 enhances actin polymerization at the cell front and these actin filaments flow centripetally into the cell body to be incorporated into stress fibers (Kai et al., 2015). In earlier studies, this actin dynamic regulation of SYNPO2 at the cell front was masked by cytoplasmic staining of F-actin. Similarly, the lack of appreciable differences in the actin cytoskeleton, as detected by phalloidin staining of C2C12 cells with perturbed SYNPO2 expression, could reflect a role for SYNPO2 in regulating actin dynamics near the cell periphery that are not detectable by imaging fixed cells. The spatiotemporal regulation of F-actin by SYNPO2 should be determined using live imaging.

Though we did not observe gross actin cytoskeleton changes, we hypothesize that SYNPO2As could be playing a role at the fusion synapse and may be involved in recruiting other fusion-related proteins. Apart from the known PLS and FuRMAS structures in *Drosophila* myoblast fusion, (Kim et al., 2015), studies have also highlighted the importance of actin-rich filopodial structures during *Drosophila* myoblast fusion (Segal et al., 2016; Girardi et al., 2019; Nowak et al., 2009). A heterotypic, two-cell system equivalent to FCMs and FCs in Drosophila has not been identified in vertebrate myoblasts, but a recent study did identify an asymmetric F-actin structure in the invading mouse myoblast cell (i.e, equivalent to the FCM in *Drosophila*) that uses TKS5 and DYN2 to generate an actin-enriched invadosome (Chuang et al., 2019). In my search for actin-rich structures during fusion, at higher magnification I was able to detect actin-rich protrusions in some of the SYNPO2As expressing differentiated myoblasts and SYNPO2As

colocalized at the tips of these protrusive structures (Fig. 20A). These structures were also observed in differentiated mock-transduced cells, lesser in number with faint staining at the tips (qualitative data, not shown). However, using fixed cells we were unable to confirm whether cells with such actin structures were fusing with neighbouring cells or not. These structures were not apparent during live cell imaging of GFP-tagged actin at a lower magnification (data not shown).

Finding such actin structures is challenging when using fluorescently tagged constructs in a confluent layer of cells since the cell boundaries tend to overlap in different planes, making it difficult to focus on a particular cell. Expressing the SYNPO2 constructs under a differentiation-related gene promoter such as MHC would allow analysis to focus only on the differentiated cells. Fluorescently-tagged actin constructs under an MHC promoter can also be used to understand actin dynamics during mouse myoblast fusion. With the recent discovery of asymmetric actin structures in differentiated mouse myoblasts, it could be interesting to study whether SYNPO2As knockdown myoblasts contain persistently longer actin-rich protrusions that prevent cell fusion, as occurs in some Drosophila actin regulatory mutants, or to determine the dynamic recruitment of proteins such as TKS5, DYN2, or DOCK180 to fusion sites. Such studies should be done by live imaging to study the spatiotemporal changes that take place during fusion (Fig. 20B).

Is SYNPO2As an accessory or essential promyogenic factor?

The inhibitory effect of SYNPO2As knockdown on myoblast fusion was partial and merely delayed the rate of myotube formation, suggesting SYNPO2As may be more of an accessory than an essential promyogenic factor. However, information from the mouse genome informatics (MGI) database indicates *Synpo2* mutant mice are lethal at the preweaning stage, suggesting SYNPO2 could be an essential regulator of myotube formation and muscle development. Similarly, N-WASP and filamin C knockout mice die at the embryonic stage due to reduced skeletal muscle mass and improper lung function (Dalkilic et al., 2006; Gruenbaum-Cohen et al., 2012), and *Drosophila* null mutants of kette, SCAR or Arp2/3 lose the ability to dissolve the actin-foci at the fusion synapse resulting in a complete block of fusion (Richardson et al., 2007). However, a careful review of the literature revealed the effects of SYNPO2As knockdown on myotube formation in

cell culture are comparable to levels observed when the functions of other actin-regulating proteins considered important in myotube formation are perturbed. For example, homomorphic and maternal/zygotic mutants of *Drosophila* proteins kette, WASp, WASP-interacting protein (WIP/sltr), SCAR, mDia, and Rho1 and ROK reduce myotube formation by ~30-80% and slow down, but do not eliminate, muscle development (Schroter, 2004; S. Kim et al., 2007; Massarwa et al., 2007; Deng et al., 2015; J. Kim et al., 2015; Duan et al., 2012). Knockdown of regulators of actin remodelling pathways such as ARF6, Brag2 or DOCK180 in C2C12 myoblasts also show a partial, 50-80% decrease in myoblast fusion (Bach et al., 2010; Nowak et al., 2009; Pajcini et al., 2008). Pathways that regulate actin polymerization are complex and several proteins play redundant role in this process. Thus, knockdown or partial loss of function of such proteins does not necessarily completely block fusion but perturbs myotube formation and muscle development. Similar to the above-mentioned proteins, SYNO2As also appears to be an important actin remodeler required for efficient myotube formation at early stages of muscle development.

SYNPO2As upregulates myoblast migration

As explained in Fig. 1, myogenesis is a multi-step process involving migration of myoblasts to initiate cell-cell contact, formation of a fusion synapse and subsequent myoblast fusion, all of which require actin remodelling. In prostate cancer cells, human SYNPO2As can either enhance or inhibit cell migration in response to different external stimuli (Kai et al., 2012). We hypothesized that SYNPO2 isoforms could similarly regulate myoblast migration, either by increasing migration to promote initial cell-cell contact or by inhibiting migration to promote fusion synapse formation. We therefore determined the effect of SYNPO2 over expression and knockdown on migration of myoblasts post-differentiation. Our data showed that all three isoforms increased myoblast migration irrespective of whether they increased or inhibited myotube formation, indicating no direct correlation between migration and fusion exerted by the three SYNPO2 isoforms.

Like SYNPO2As, there are several examples of proteins that show a direct correlation between enhanced myoblast migration and fusion (Bae et al., 2008; Jansen & Pavlath, 2006; Lafreniere et al., 2006; Griffin et al., 2010), including actin-regulating proteins such as casein kinase 2 interacting protein-1 (CKIP-1) (D. Baas et al., 2012) and

palladin (Nguyen & Wang, 2015). In these instances, knockdown of the protein decreased migration by 25-50%, while SYNPO2As knockdown inhibited migration by only 10% compared to control cells. If SYNPO2As is altering actin dynamics to promote both migration and fusion, and if these two processes are causally related, then why do SYNPO2A and B increase migration but decrease fusion? Possible explanations include small changes in actin dynamics exerted by SYNPO2A and B that alter formation of a fusion synapse and decreased fusion, perhaps reflecting recruitment of a different set of actin effectors by the PDZ domain present in these long isoforms. As discussed above, whatever effects the SYNPO2 isoforms might have on actin dynamics that affect migration and/or fusion were not apparent in immunofluorescence images showing the gross actin cytoskeleton architecture. Conversely, the migration phenotype may be unrelated to the fusion phenotype, as suggested by the very small differences in migration velocity between control cells and SYNPO2-expressing cells and by the lack of a direct correlation between migration and fusion. Additional studies using live imaging with fluorescently tagged actin probes could provide more insight into the spatiotemporal changes in actin dynamics favouring the migration and fusion phenotypes and whether these processes are coupled.

SYNPO2As regulates migration and fusion by using distinct actin remodelling pathways

As discussed in the introduction of this thesis, the fusion synapse formed between a founder cell (FC) and fusion competent myoblasts (FCMs) during myotube formation involves the role of several cell adhesion proteins, adapter proteins, GTPases, and actin-regulating proteins. Of interest to us, the podosomes in the FCM at the fusion synapse are driven by branched actin structures that are polymerized by the Arp2/3 complex, and the actomyosin resisting sheath formed in the FC by the Rho-ROCK-MLC pathway (Kim et al., 2015). Furthermore, human Synpo2 enhances migration in a Rho-ROCK-dependent manner that triggers Arp2/3-dependent formation of lamellipodia-like protrusions (Kai et al., 2015; Kai et al., 2012). Therefore, we used inhibitors against Arp2/3 and ROCK to determine if SYNPO2As was dependent on these pathways to enhance myotube formation and migration.

Treatment with the Arp2/3 inhibitor CK666 inhibited the basal level of fusion of both mock and SYNPO2 cells but treated SYNPO2As cells still significantly enhanced

myotube formation compared to treated mock cells (Fig. 17A). This suggested that SYNPO2As significantly enhanced myotube formation via an Arp2/3-independent pathway. Treatment with a ROCK inhibitor significantly enhanced myotube formation of mock treated cells (Fig. 17B), consistent with decreased activation of the Rho-ROCK pathway upon differentiation-dependent nuclear translocation of the FHKR (Forkhead in human rhabdomyosarcoma) transcription factor to upregulate transcription of myogenic related proteins, as reported previously (Nishiyama et al., 2004). Under conditions that limited the levels of activated ROCK, SYNPO2As cells fused at the same rate as inhibitor-treated mock cells, indicating the ability of SYNPO2As to enhance myoblast fusion is sensitive to the levels of ROCK in cells during the fusion process.

The level of activated ROCK in cells and its effect on fusion remains contradictory. Treatment with the Y27632 ROCK inhibitor was shown to enhance myotube formation in C2C12 myoblasts, whereas knockdown using siRNA transfection had no affect on fusion efficiency (Pelosi et al., 2007), while ROK knockout *Drosophila* mutants inhibit myotube formation by 30% (Kim et al., 2015). The ROCK inhibitor Y27632 is known to exert several off-target effects, such as on protein kinase C-related kinase and citron kinase (Davies et al., 2000; Ishizaki et al., 2000). Therefore, the increased fusion phenotype of mock cells seen with the ROCK inhibitor could be due to off target effects. Further, there are two isoforms of ROCK, ROCK-1 and ROCK-2, of which ROCK-2 is the skeletal muscle-specific isoform, and the ROCK inhibitor is more specific to ROCK-1 than ROCK-2 (Pelosi et al., 2007). Therefore, it remains unclear whether the loss of the enhanced fusion phenotype in SYNPO2As cells reflects off-target effects of the drug or is due specifically to one of the two ROCK isoforms. This data needs to be reassessed using specific shRNAs and/or transient CRISPR knockouts for the two different ROCK isoforms.

While the enhanced fusion phenotype was sensitive to ROCK inhibition, such was not the case for the enhanced migration phenotype. Treatment of mock and SYNPO2As C2C12 cells with the ROCK inhibitor reduced the basal velocity of both cell types compared to untreated cells, showing the importance of ROCK to myoblast migration. However, unlike the situation with human SYNPO2As in PC3 cells (Kai et al., 2012), mouse SYNPO2As still increased migration relative to mock cells under limiting ROCK conditions (Fig. 17C), indicating SYNPO2As enhances migration in a ROCK-independent

manner. The disconnect between the sensitivity of the SYNPO2As-enhanced migration and fusion phenotypes suggested these two processes are not directly coupled. It is conceivable that SYNPO2As functions through a ROCK-dependent pathway to alter the actin cytoskeleton and enhance fusion but can alter the actin cytoskeleton independent of ROCK to enhance migration. The specific mechanism by which SYNPO2As regulates these two processes remains unknown, but some potential models are discussed in Chapter 5 of this thesis.

As I have shown, whatever effects SYNPO2As might be having on actin dynamics in C2C12 post-differentiation, these effects are not apparent in gross changes to F-actin or actomyosin structures in cells (Figs. 14 and 18). Phalloidin staining of C2C12 cells also did not reveal intense actin foci or increased numbers of filopodia at sites of cell-cell contact and fusion, as reported during *Drosophila* fusion (Kesper et al., 2007; Kim et al., 2015; Segal et al., 2016). Human SYNPO2 polymerizes actin at the leading edge of migrating cells to enhance the migratory phenotype of PC3 cells (Kai et al., 2015). This phenotype was originally missed by simple phalloidin staining of the actin cytoskeleton that stained the predominant F-actin stress fibers present in PC3 cells (Kai & Duncan, 2013), and only became apparent using live cell imaging and conditions that inhibited stress fiber formation (Kai et al., 2015). We speculate that mouse SYNPO2As could be similarly regulating actin dynamics at the cell periphery of uninucleated migrating cells, facilitating the organization of other fusion-related proteins into a fusion synapse. As discussed above, additional studies using videomicroscopy to image actin dynamics at the cell periphery could be used to test this hypothesis. Additional interrogation of factors that function downstream, or in parallel, to the ROCK pathway, and determining subcellular localization of SYNPO2As with other actin-regulating proteins during myoblast fusion might also shed more light on the effects of SYNPO2As on actin dynamics and myotube formation.

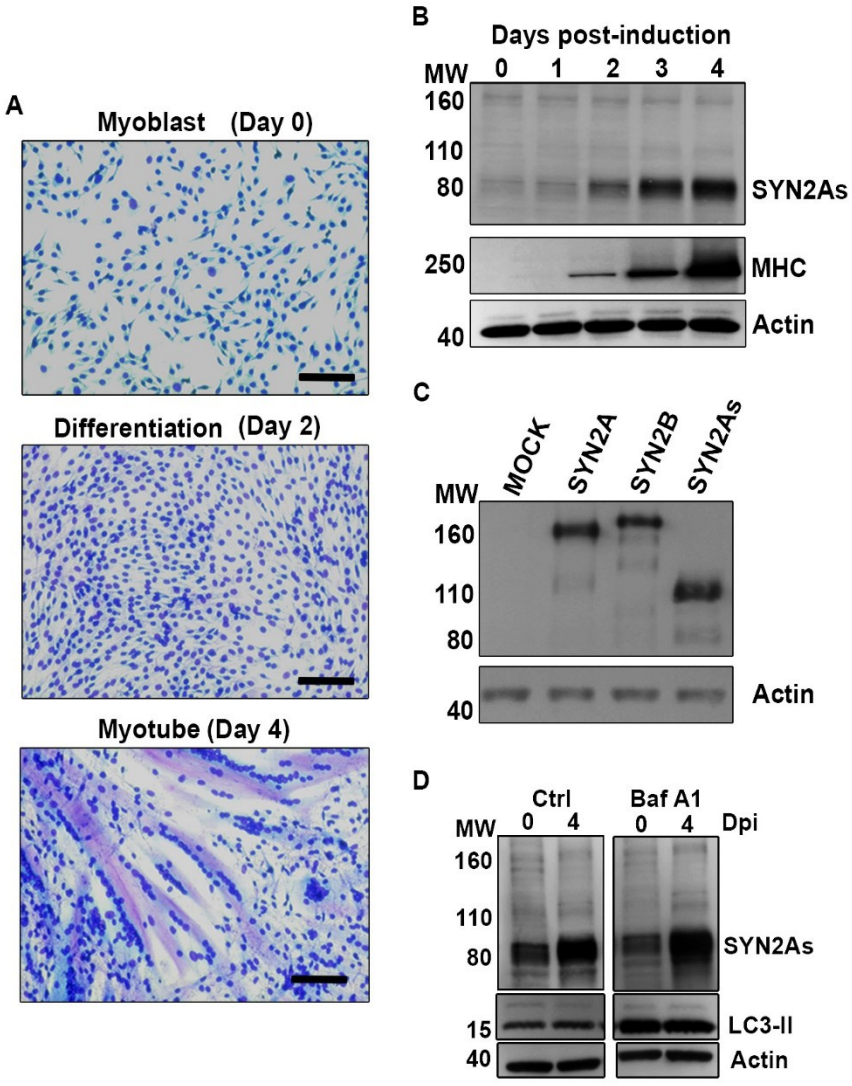

Figure 8: SYNPO2As expression is upregulated following myoblast differentiation. (A) Representative microscopic images of Giemsa-stained C2C12 mouse myoblasts cultured in growth medium (Day 0) or following 2 or 4 days growth in differentiation medium. Scale bars = 2µm. (B) Western blot of C2C12 cell lysates collected at 1-4 dpi and probed with anti-SYNPO2. (C) Western blot of C2C12 cell lysates from transduced cells stably expressing the three mouse SYNPO2 isoforms (SYN2A, SYN2B and SYN2As) collected at 3 or 4 dpi and probed with anti-SYNPO2. (D) C2C12 cells at 0 or 4 dpi were treated with DMSO (Ctrl) or bafilomycin A1 (BafA1) to inhibit autophagic flux, and western blots of cell lysates were probed with antibodies specific for SYNPO2 (SYN2As) or LC3-II as a marker of autophagic flux. Molecular weight markers in kDa (MW) are indicated on the left of each blot and naphthol blue (NB) stained membranes were used as loading controls.

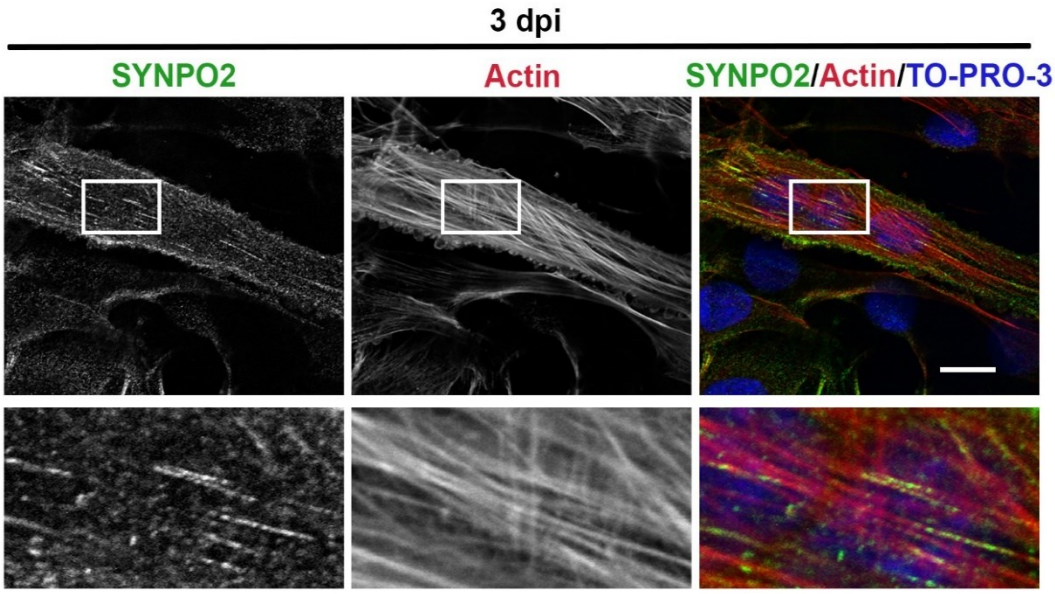

Figure 9: Endogenous SYNPO2 binds actin filaments in myotubes.
Top panel: Parental C2C12 cells were fixed at 3 dpi and stained with anti-SYNPO2 antibody and Alexa fluor 488-conjugated secondary antibody (green). Actin stress fibers were stained with phalloidin (red) and the nucleus stained with TO-PRO-3 (blue). Bottom panel is the magnified image of the white inset box. Scale bar = 10µm.

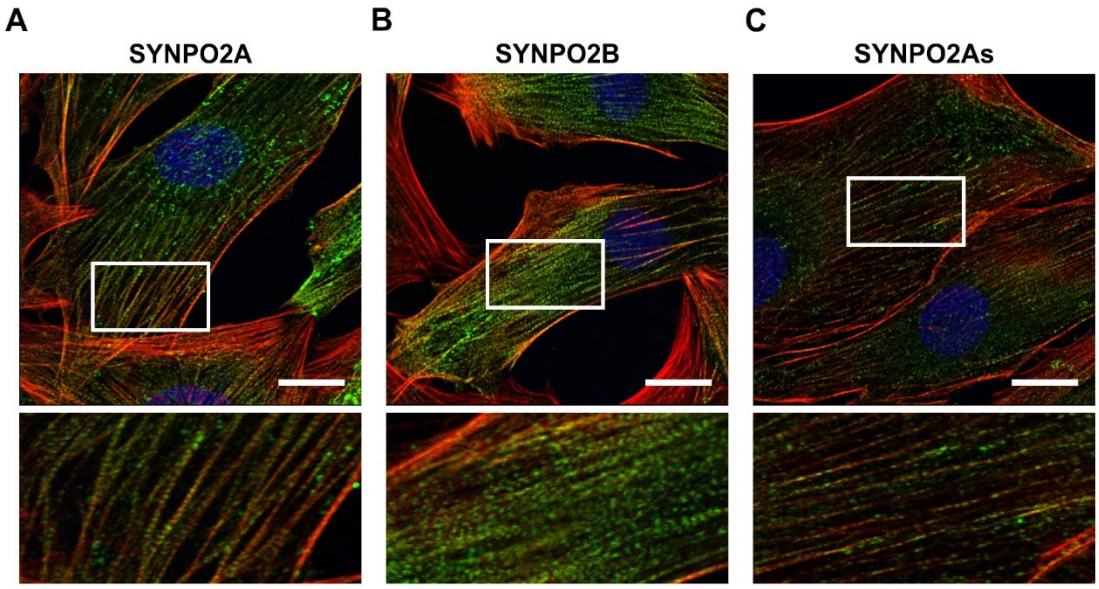

Figure 10: SYNPO2 isoforms associate with cytoplasmic actin filaments post-differentiation.
Top panel: C2C12 cells stably transduced with N-terminally myc-tagged SYNPO2 isoforms (SYNPO2A, SYNPO2B, SYNPO2As) were induced to differentiate for 2 dpi and stained with anti-myc antibody and Alexa fluor 488-conjugated secondary antibody (green). Filamentous actin was stained with Alexa-555 conjugated phalloidin (red) and nuclei were stained with DRAQ5 (blue). Images are one slice from a z-stack. Bottom panel is the magnified image of the white inset box. Scale bar = 10μm.

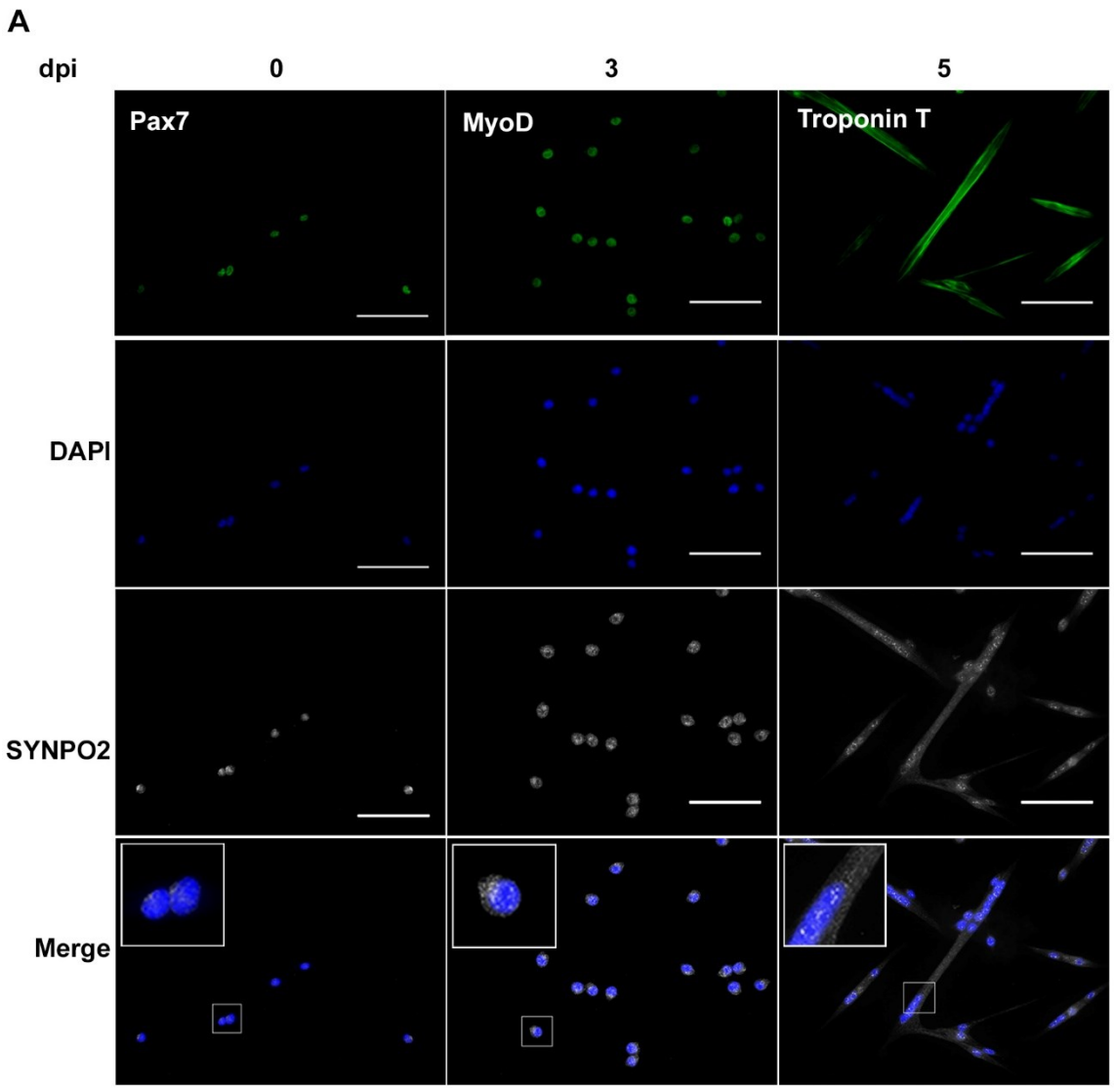
A
dpi
0
3
5
Pax7
MyoD
Troponin T
DAPI
SYNPO2
Merge
B
MW
dpi
0
5
160
110
80
SYNPO2As
250
160
MHC
50
40
MyoD

Figure 11: SYNPO2As expression is upregulated following differentiation of primary satellite cells.
(A) Satellite cells from $Pax3^{GFP/+}$ mice were sorted and immunostained at 0, 3 or 5 dpi. Cells were immunostained with antibodies against SYNPO2 (black and white) and either Pax7, a satellite cell marker (0 dpi), MyoD, a myoblast differentiation marker (3 dpi), or Troponin T, a late myogenic marker (5 dpi) (all green). Nuclei were stained with DAPI (blue). Merge is an overlay of the DAPI and SYNPO2 images. (B) Western blots of $Pax3^{GFP/+}$ satellite cell lysates at 0 or 5 dpi and probed with antibodies against SYNPO2 (SYN2As), myosin heavy chain (MHC) or MyoD. Molecular weight markers in kDa (MW) are indicated on the left of each blot. Scale bars = 2μm.

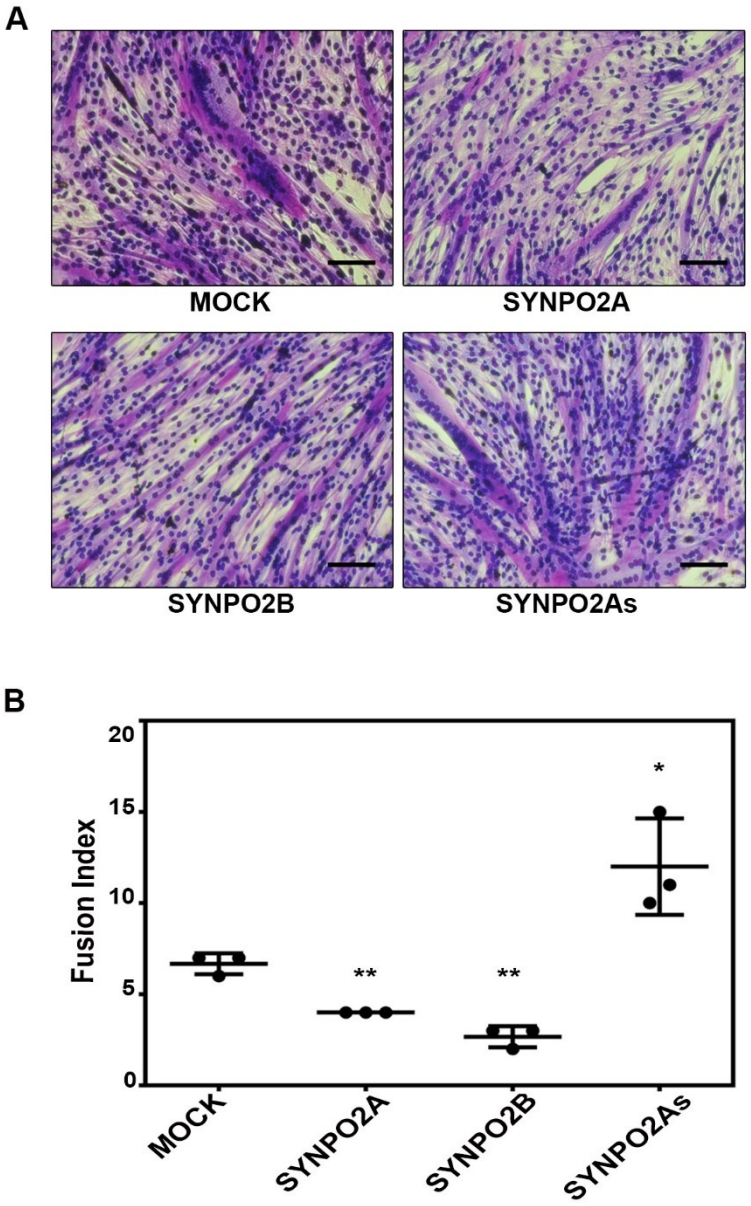

Figure 12: Differential effect of SYNPO2 isoforms on C2C12 myotube formation.
(A) Giemsa-stained microscopic images of C2C12 cells stably expressing the indicated SYNPO2 isoforms at 4 dpi. Scale bars = 2µm. (B) C2C12 cells stably transduced with an empty retrovirus vector (Mock) or with retrovirus vectors expressing the indicated SYNPO2 isoforms were induced to differentiate, and the fusion index of cells at 4 dpi was quantified from the Giemsa-stained microscopic images. Results are presented as the mean ± SEM of the fusion index (percent of nuclei present in syncytia) from triplicate samples in three independent experiments. Statistical significance: * $p < 0.05$; ** $p < 0.01$.

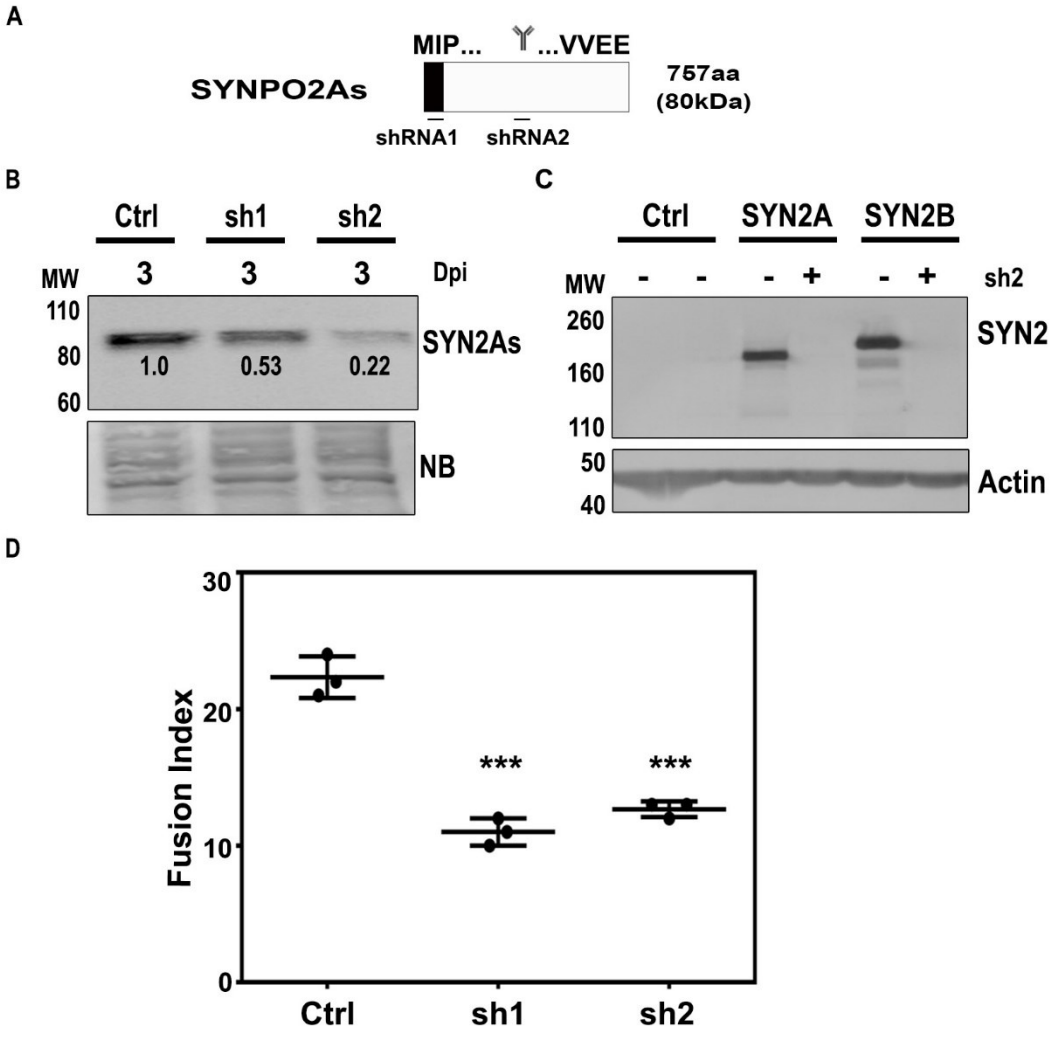
A
MIP...
...VVEE
SYNPO2As
757aa
(80kDa)
shRNA1
shRNA2
B
Ctrl
sh1
sh2
MW
3
3
3
Dpi
110
80
60
1.0
0.53
0.22
SYN2As
NB
C
Ctrl
SYN2A
SYN2B
MW
- - - + - +
sh2
260
160
110
50
40
SYN2
Actin
D
Fusion Index
30
20
10
0
***
***
Ctrl
sh1
sh2

Figure 13: Knockdown of SYNPO2As inhibits myotube formation.
(A) Diagram of the SYNPO2As isoform. The black box represents the unique N-terminus and the white box represents the conserved region of the SYNPO2 isoforms. The N- and C-terminal amino acid sequence is indicated above. The Y symbol represents the commercial antibody binding region. The number of amino acid residues is indicated on the right and the predicted molecular weight in brackets. The two black lines below the boxes represent the regions targted by the two shRNAs. (B) Western blot of cell lysates from C2C12 cells at 3 dpi stably expressing shRNA1 or 2 (sh1, sh2) that target the regions encoding the unique N-terminus of SYNPO2As isoform or the conserved region present in all isoforms, respectively, or a non-targeting control shRNA (Ctrl), probed with anti-SYNPO2. Numbers indicate the fold change of the SYNPO2As polypeptides relative to cells transduced with the non-targeting shRNA at 3 dpi. Naphthol blue (NB) stained membrane was used as a loading control. (C) Western blot of cell lysates from HEK293 cells transiently transfected with empty plasmid (Ctrl) or with plasmids expressing SYNPO2A or SYNPO2B (SYN2A and SYN2B) and co-transfected with plasmids expressing the non-targeting shRNA (-) or expressing shRNA2 (sh2) that targets all three SYNPO2 isoforms, probed with anti-SYNPO2 (top panel) or actin (loading control). Molecular weight markers (MW) are indicated on the left of each blot. (D) Data represents the fusion index of cells at 3 dpi. Results are presented as the mean ± SEM of the fusion index (percent of nuclei present in syncytia) from triplicate samples in three independent experiments. Statistical significance: ** $p < 0.01$; *** $p < 0.005$; **** $p < 0.001$; NS = non-significant.

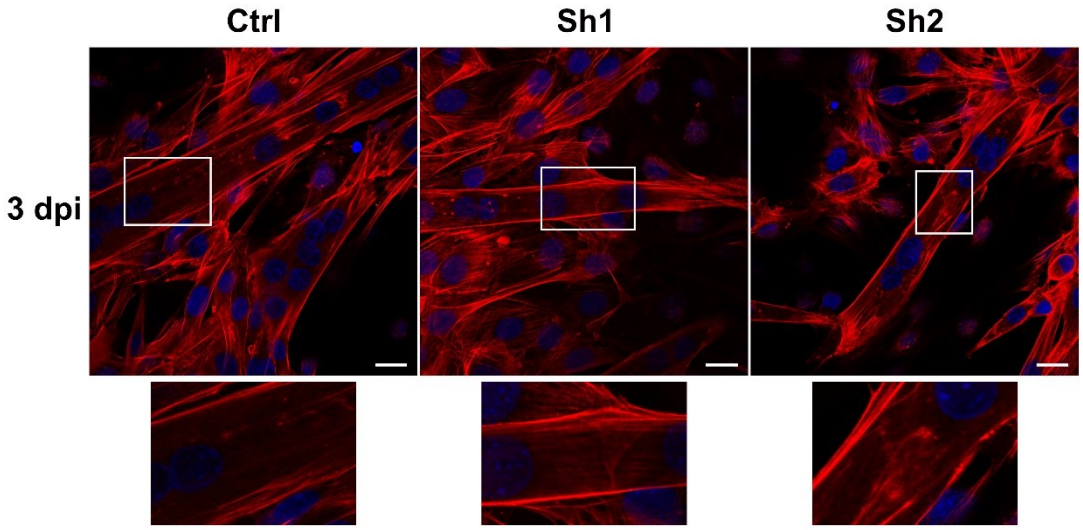

Figure 14: SYNPO2 knockdown does not alter the actin cytoskeleton.
C2C12 cells stably expressing control, shRNA1 and shRNA 2 constructs were differentiated until 3 dpi (upper panel) and stained for actin filaments using phalloidin (red), and the nucleus stained with DRAQ5 (blue). Bottom panel is the magnified image of the white inset box. Scale bar = 10μm.

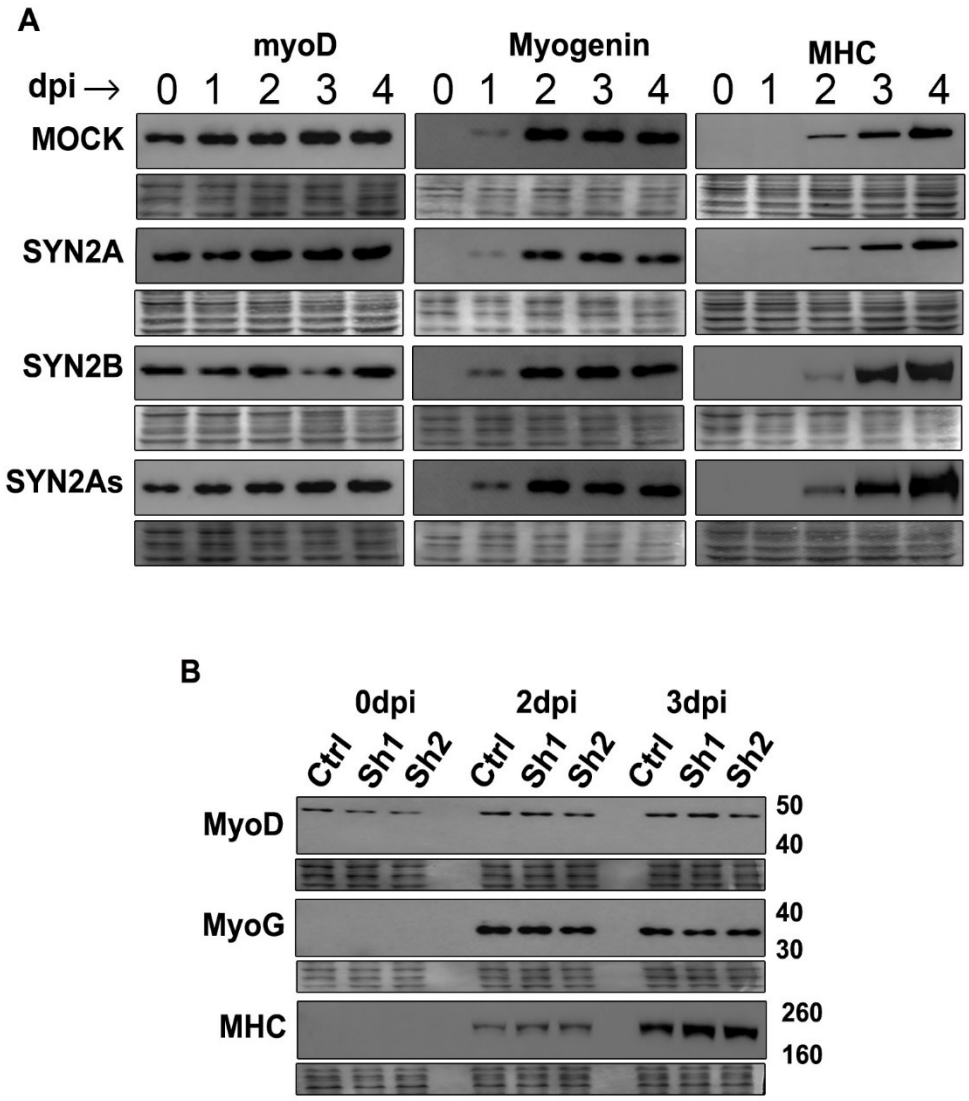

Figure 15: Knockdown or ectopic expression of SYNPO2 isoforms does not affect differentiation.

Western blots of C2C12 cells mock-transduced or transduced with retrovirus vectors expressing the indicated SYNPO2 isoforms (SYN2A, SYN2B, SYN2As) (A) or stably expressing shRNA1 (Sh1) that targets SYNPO2As or shRNA2 (Sh2) that targets all SYNPO2 isoforms (B) were harvested at the indicated dpi and blots were probed with antibodies specific for MyoD, myogenin or myosin heavy chain (MHC). Molecular weight markers are indicated on the right, and naphthol blue stained blots (lower panels below each of the antibody probed blots) were used as a loading control.

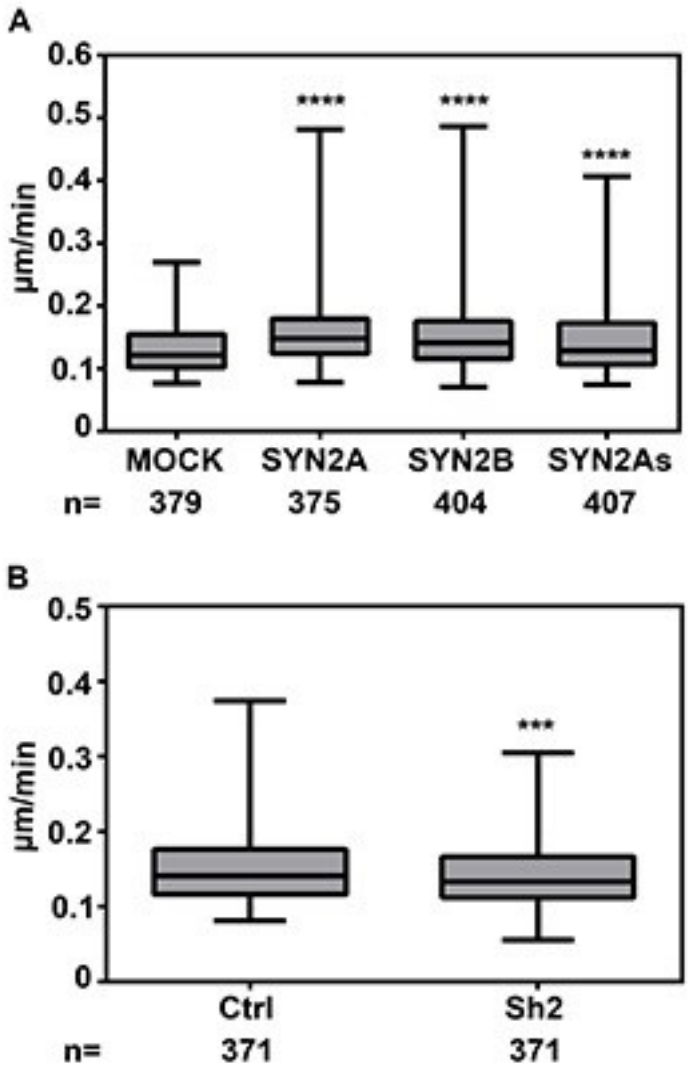

Figure 16: SYNPO2As enhances C2C12 cell migration post-differentiation.
(A) C2C12 cells transduced with the indicated SYNPO2 isoforms (SYN2A, SYN2B, SYN2As) were monitored for cell migration by videomicroscopy at 2 dpi. The velocity of cells from three independent experiments was calculated, and results are presented as the mean (horizontal line), standard deviation (shaded rectangles), and maximum and minimum (whiskers). (B) As in panel A, except using C2C12 cells transduced with non-targeting control shRNA (Ctrl) or shRNA2 targeting SYNPO2 (Sh2). The velocity of cells from two independent experiments was calculated. The numbers below each panel represents the total number of cells analyzed from the three independent experiments. Statistical significance: ***p value < 0.005; ****p value < 0.001.

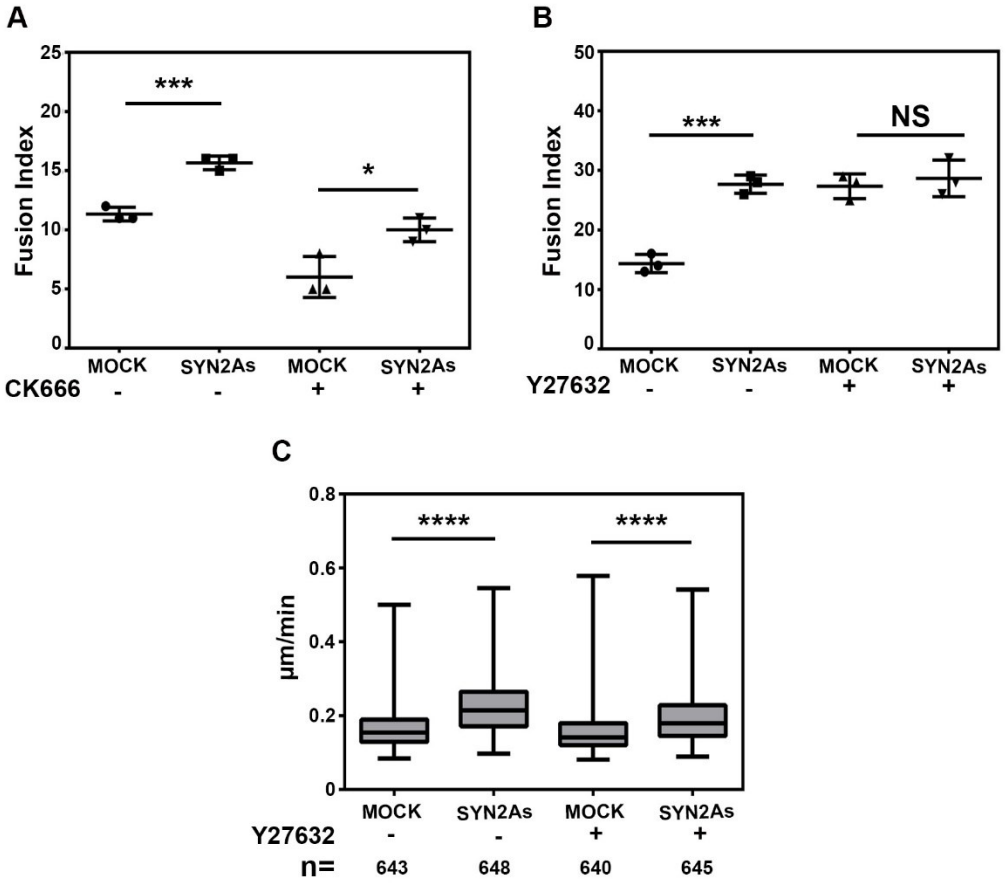

Figure 17: Ectopic expression of SYNPO2As enhances myotube formation in a ROCK-dependent manner and enhances migration in a ROCK-independent manner. C2C12 cells stably transduced with an empty retrovirus vector (Mock) or SYNPO2As (SYN2As) were induced to differentiate in the presence or absence of the Arp2/3 inhibitor CK666 (A) or the ROCK inhibitor Y27632 (B). The fusion index was quantified at 3 dpi and results are presented as the mean ± SEM from triplicate samples in three independent experiments. (C) C2C12 cells transduced with empty (Mock) or SYNPO2As (SYN2As) retrovirus vectors were monitored for cell migration by videomicroscopy at 2 dpi in the presence or absence of the ROCK inhibitor Y27632. The velocity of cells from each of three independent experiments was calculated and results are presented as the mean (horizontal line), standard deviation (shaded rectangles), and maximum and minimum (whiskers). The numbers below panel C represents the total number of cells quantified from three independent experiments. Statistical significance: *p value < 0.05; ***p value < 0.005; ****p value < 0.001; NS not significant.

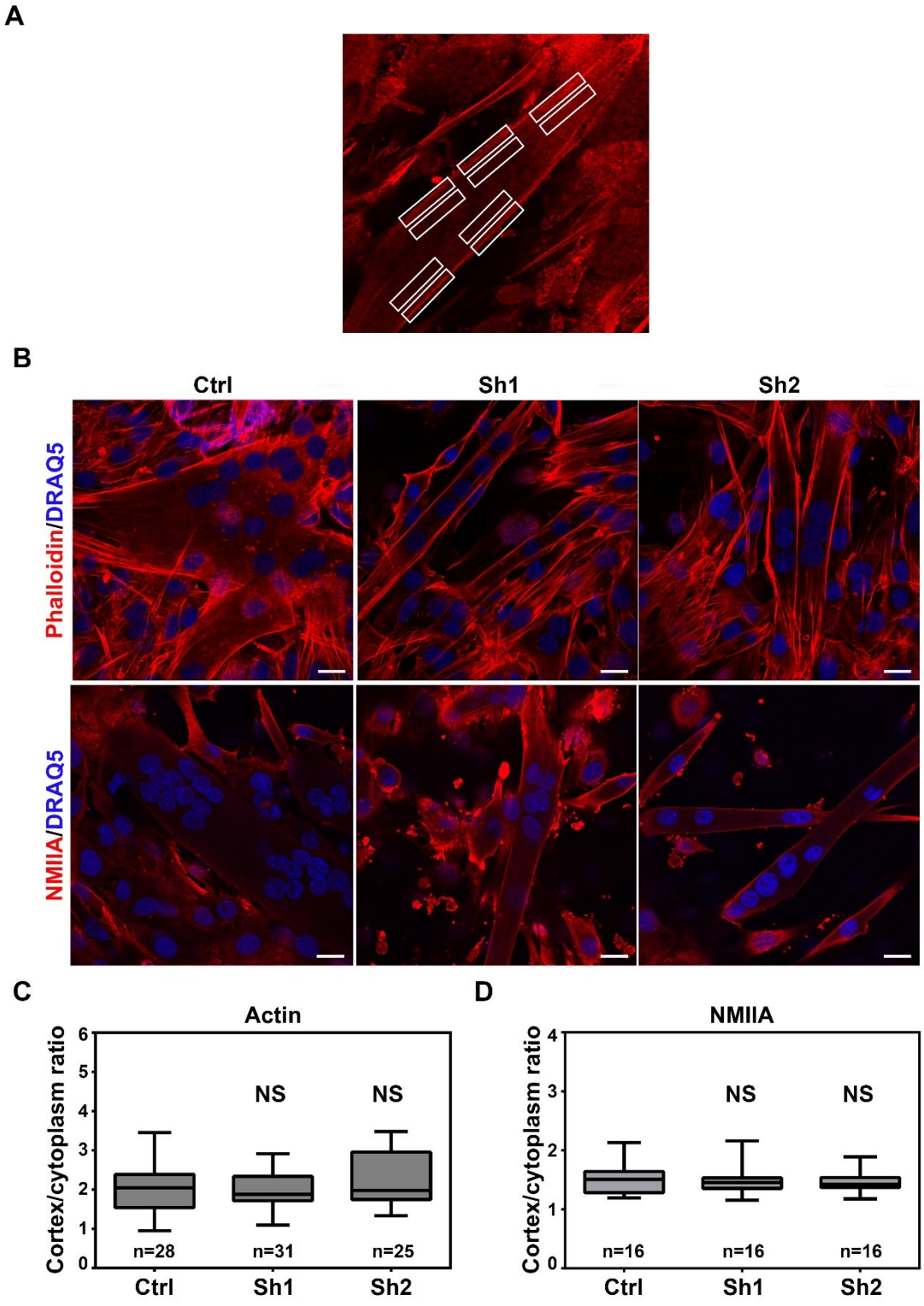
A
B
Ctrl
Sh1
Sh2
Phalloidin/DRAQ5
NMIIA/DRAQ5
C
Actin
Cortex/cytoplasm ratio
NS
NS
n=28
n=31
n=25
Ctrl
Sh1
Sh2
D
NMIIA
Cortex/cytoplasm ratio
NS
NS
n=16
n=16
n=16
Ctrl
Sh1
Sh2

Figure 18: SYNPO2 knockdown does not alter cortical actomyosin levels in myotubes. (A) Representative image of actin stained myotubes. The white boxes represent the area measured for determining the staining intensity at the cortex and cytoplasm. C2C12 cells stably transduced with control and SYNPO2 targeted shRNAs were seeded at high density and induced to differentiate for 3 dpi. Actin was stained with Alexa-555 conjugated phalloidin (red, top panel), non-muscle myosin IIA (red, bottom panel) and nuclei were stained with DRAQ5 (blue). (B and C) Cortex vs cytoplasmic ratio quantified from actin and NMIIA fluorescent signal. Images are one slice from a z-stack. Scale bar = 10μm. Statistical significance: NS = not significant.

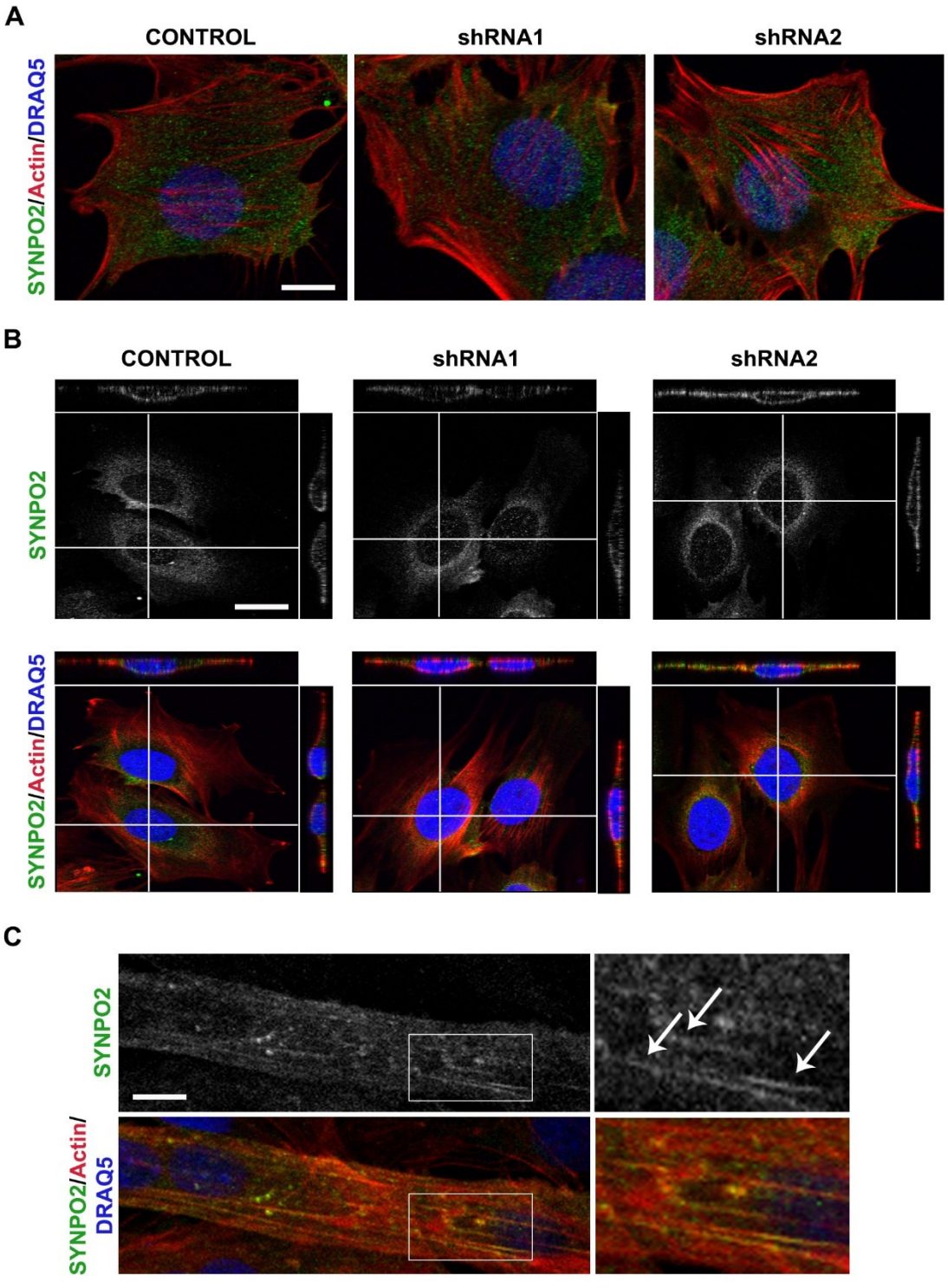
A
CONTROL
shRNA1
shRNA2
SYNPO2/Actin/DRAQ5
B
CONTROL
shRNA1
shRNA2
SYNPO2
SYNPO2/Actin/DRAQ5
C
SYNPO2
SYNPO2/Actin/
DRAQ5

Figure 19: SYNPO2As specifically binds actin filaments in myotubes but not in myoblasts.
C2C12 cells stably expressing control, shRNA1 and shRNA 2 constructs were fixed at 0 dpi and 3 dpi, and stained with anti-synpo2 antibody and Alexa fluor 488-conjugated secondary antibody (green); actin filaments were stained using phalloidin (red), and nuclei stained with DRAQ5 (blue). (A) A representative merged image of a myoblast fixed and stained at 0 dpi. (B) The top panel is a representative image of SYNPO2As stained myoblasts at 0 dpi, and the bottom panel is a merged image. The image is one slice from a z-stack and orthogonal views (white lines depict the xz and yz slice) are shown on the top and right of each image. (C) Top panel is a representative image of SYNPO2As stained myotube of control cells at 3 dpi, and the bottom panel is a merged image. Images on the right are the magnified images of the white inset box. Scale bar = 20μm.

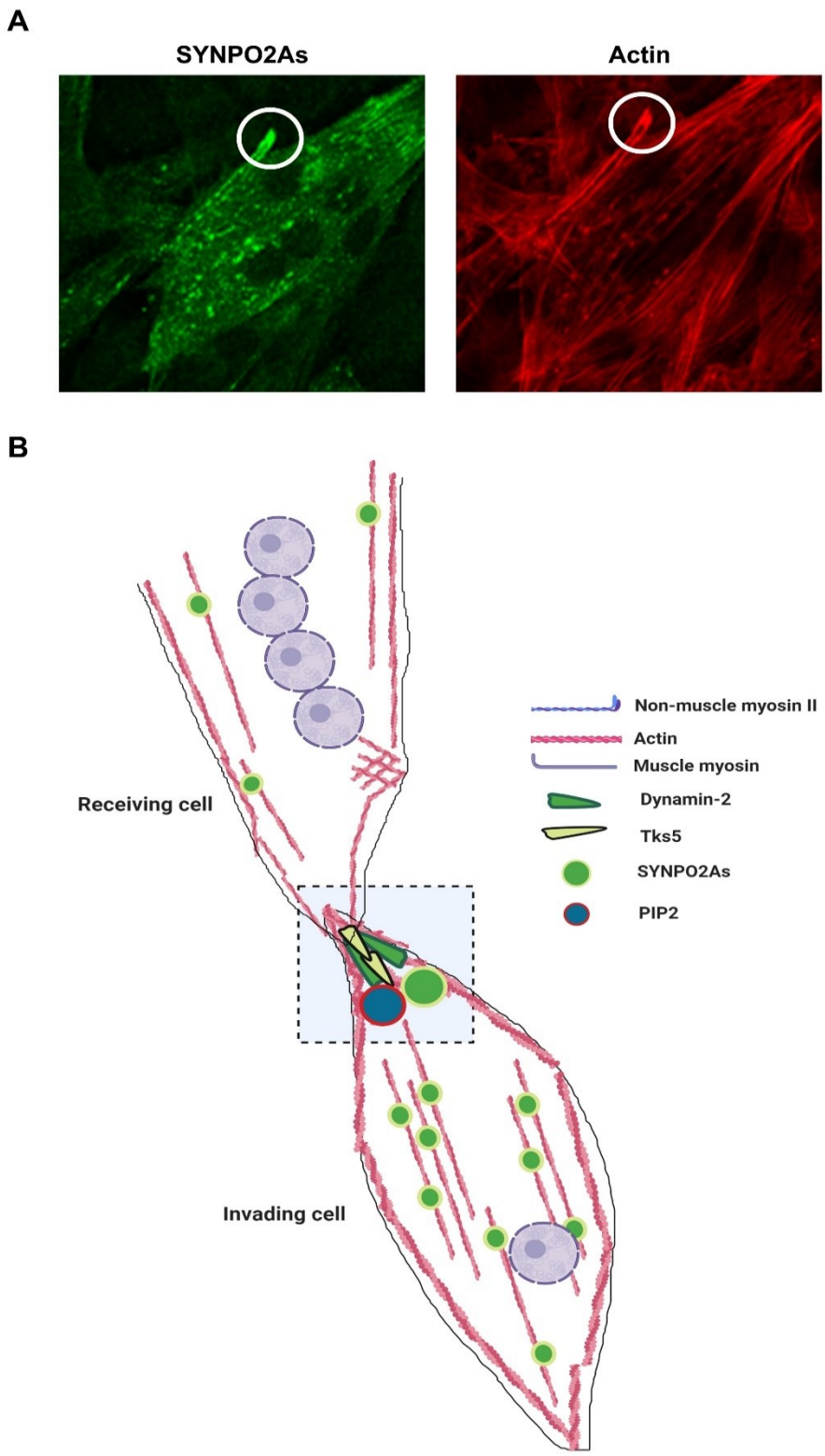
A
SYNPO2As
Actin
B
Receiving cell
Invading cell
Non-muscle myosin II
Actin
Muscle myosin
Dynamin-2
Tks5
SYNPO2As
PIP2

Figure 20: Model depicting possible mechanism of SYNPO2As during myoblast fusion.
(A) SYNPO2As overexpressing C2C12 myoblasts were differentiated and fixed at 3 dpi and stained with anti-SYNPO2 antibody and Alexa fluor 488-conjugated secondary antibody (green), and actin filaments were stained with phalloidin (red). The white circle shows the accumulation of SYNPO2As and actin in filopodial-like tip. (B) Diagram of two fusing cells. The invading cell recruits actin, Tks5, Dyn2, and PIP2 to invadopodosome tips during fusion. As seen in (A), SYNPO2As could also be recruited to invadopodosomes during fusion.

CHAPTER 4: IN VIVO ANALYSIS OF THE BIOLOGICAL FUNCTION OF SYNAPTOPODIN-2B IN DANIO RERIO ANIMAL MODEL

4.1 Introduction

To examine the influence of synpo2 on muscle development *in vivo* I turned to the zebrafish model. The following brief introduction to zebrafish muscle development and how it relates to mouse muscle development provides some context for my studies. Mouse muscle development takes place from embryonic day 8 (E8.0), when the somites start forming. Primary myogenesis takes place from E10.5 to 12.5 followed by secondary myogenesis from E13.5 to 17.5 (G. Rossi & Messina, 2014). In zebrafish, muscle development takes places from 10.5 hours post-fertilization (hpf) to 48 hpf, regulated by the hedgehog signalling pathway. Hedgehog signalling regulates expression of Prdm1a and MyoD/Myf5 expression. Prdm1a is a zinc-finger DNA-binding protein that mediates expression of slow-twitch specific muscle genes such as Prox1a, Smyhc1 and slow troponin c. The Prdm1a protein does not directly regulate expression of these genes but instead represses the function of the Sox6 transcription factor that inhibits expression of slow-twitch specific muscle genes (von Hofsten et al., 2008). On the other hand, MyoD/Myf5 regulates the expression of fast-twitch muscle genes Mylz2, fast-MyHCx, Tnnt3a and Tnni2 (G. Rossi & Messina, 2014).

Similar to mouse skeletal muscle development, the somites in zebrafish arise from the paraxial mesoderm. Each somite is an arrangement of cuboidal cells containing medially located slow-twitch muscle cells, laterally located fast-twitch muscle cells and anterior border cells (ABC) (Goody et al., 2017). Zebrafish muscle development takes place as myogenic waves. First, the anterior border cells migrate laterally to form the external layer of fast precursor/satellite cells ($Pax3^+$ and $Pax7^+$). Then, the medial slow-twitch cells elongate and migrate laterally through the fast-twitch cells to form the superficial layer of the skeletal muscle. This medial to lateral migration of slow-twitch cells is necessary to induce the elongation of fast-twitch cells that forms the inner mass of the skeletal muscle (Henry & Amacher, 2004). As the migration of slow-twitch cells take place, the fast-twitch cells elongate and adhere to the myotendinous junction. Simultaneously, these cells fuse to form multinucleated fast-twitch myofibers (Snow et al., 2008). In zebrafish, the fast muscle

cells are multinucleated and slow muscle cells are mononucleated. As summarized in Tables 1-4, there are several zebrafish proteins that regulate fast-muscle fusion. We took advantage of the rapid and external development of zebrafish embryos to study the function of Synpo2 during skeletal muscle development.

I identified two synaptopodin-2b (Synpo2b) isoforms in zebrafish that are differentially expressed during zebrafish development via alternate splicing, one of which, Synpo2b, is an apparent homolog of mouse SYNPO2As. My initial studies using Synpo2b targeted- morpholinos were promising, with embryos showing deleterious phenotypes such as a curved tail, inability to swim, and disorganized myofibrils. I then used the CRISPR/cas9 system to knockout the gene, and the F0 generation showed similar phenotypes as seen in the morpholino injected embryos. However, in homozygous mutants we were unable to recapitulate the morpholino data; the embryos developed normally with no obvious muscle deformities. Ultrastructural analysis of the skeletal muscle in these knockout embryos, however, showed the presence of immature myofibers in addition to reduced sarcomere unit length and significantly reduced I band length. RNA seq analysis of *synpo2b*$^{-/-}$ knockout embryos also showed significantly reduced mRNA transcript levels of muscle contractile proteins. Though the contractile protein mRNAs were significantly downregulated, the knockout embryos did not delay muscle regeneration following laser injury and swimming behaviour assessed by touch response was unaffected. Though we did not observe gross morphological muscle deformities, the presence of immature myofilaments and reduced I band length suggested that Synpo2b in zebrafish acts as an important factor required for normal muscle development and/or muscle maintenance.

4.2. Results

4.2.1 Zebrafish Synpo2b isoforms are spatiotemporally expressed during zebrafish development

Using the ZFIN and ENSEMBLE websites I identified two isoforms of zebrafish Synpo2b generated by alternate splicing (Fig. 21A). The mouse SYNPO2As ortholog of zebrafish Synpo2b has a sequence identity of 40%. This short isoform encodes a 617 amino acid polypeptide named Synpo2b-S, and the long isoform encodes a 660 amino acid polypeptide named Synpo2b-L. The short isoform is encoded from a single exon, exon 2,

and the long isoform shares the N-terminal region encoded by exon 2 and a unique C-terminal region encoded by exon 3. Since there is no antibody against zebrafish Synpo2b, I used *in situ* hybridization on different stages of *casper* embryos (8, 12, 18, 25, 48 and 72 hpf) to determine expression of Synpo2b. For each time point, 12-15 embryos from each of the three breeding sets were pooled and fixed. Each time point was then separated into two sets and probed for the two isoforms separately. The probe for Synpo2b-S was designed to target the conserved 5' region of exon 2 and the probe for Synpo2b-L was designed to target the unique 3'-region of exon 3 (Fig. 21B). Expression of the short isoform, Synpo2b-S, was evident from the 6-somite stage (12 hpf) and expression increased during development along the skeletal muscle of the embryos. At 72 hpf, Synpo2b-S was localized in myofibers and in the chevron/myotome boundary (Fig. 22A). Synpo2b-S expression was not observed in the heart of the embryos. Expression of the long isoform, Synpo2b-L, was transient, only becoming evident in embryos at 25 hpf and decreasing at 48 and 72 hpf embryos (Fig. 22B). Most notably, the staining pattern of Synpo2b-L, which localized particularly strongly in the notochord and was absent from muscle sarcomeres, was quite distinct from that observed for Synpo2b-S. To quantify the expression levels of the two isoforms, embryos were pooled from three breeding sets and a quantitative PCR was performed on 4, 9, 12, 25, 48 and 72 hpf embryos. Two primer sets, one targeting the conserved region in exon 2 and the other targeting the unique region in exon 3 were designed (Fig. 23A). Similar to the *in situ* hybridization data, expression levels of Synpo2b-S increased significantly from 1-fold at 9 hpf to 21-fold at 72 hpf, whereas Synpo2b-L was expressed only around 1 fold at 12 and 24 hpf and the expression diminished at 48 and 72 hpf (Fig. 23B). These results are the first report of expression of the two Synpo2b isoforms in zebrafish during development.

4.2.2 Zebrafish Synpo2b knockdown disorganizes myofibril arrangement

Since knockdown of SYNPO2As in C2C12 myoblasts significantly inhibited myotube formation during development, we examined whether Synpo2b-S was similarly required for myoblast fusion of fast myocytes during zebrafish muscle development. To study the functional role of Synpo2b-S in zebrafish, we designed an antisense morpholino oligonucleotide targeting the 5' region of exon 2 to knockdown Synpo2b expression (Fig.

24A). The control morpholino and Synpo2b-targeted morpholino were injected separately in the single-cell stage of AB strain embryos. The AB strain was originally generated by crossing two groups purchased from a pet store in 1970. The AB strain is the regular striped fish used for generating all the transgenic laboratory lines (Holden & Brown, 2018; Meyer et al., 2013). Interestingly, Synpo2b-targeted morpholino injected embryos exhibited pronounced bent and curved tail phenotypes at 48 hpf compared to embryos injected with a control morpholino (Fig. 24B), and visual examination showed the Synpo2b knockdown embryos had reduced swimming capability (data not shown).

The knockdown embryos were fixed at 48 hpf and stained with phalloidin to determine whether there were changes to the actin cytoskeleton by confocal microscopy. The knockdown embryos contained loosened myofibrils, evident by the wavy pattern of phalloidin-stained myofibers compared to the compact and rigid myofibers seen in the control embryos (Fig. 24C, top panel). Embryos were also stained for myosin heavy chain (MHC) to determine if Synpo2b knockdown inhibited myotube formation. The synpo-2b knockdown embryos exhibited an irregular staining pattern of MHC compared to control embryos, and qualitatively it appeared as if Synpo2b knockdown reduced myotube formation (Fig. 24C, bottom panel), suggesting a role for Synpo2b in normal zebrafish muscle development or maintenance.

4.2.3 Zebrafish *synpo2b* knockout recapitulates Synpo2b knockdown morpholino data at the F0 and F1 generation

The morpholino data was very promising, however, it is known that morpholinos are prone to off-target effects and toxicity. We therefore used the CRISPR/cas9 system to generate a *synpo2b*-null mutant to confirm the morpholino data. To generate the knockout fish line, I generated six guide RNAs targeting different regions of exon 2 (Fig. 25A). These gRNAs along with cas9 mRNA were injected into the single cell stage of *casper* embryos. The *casper* strain is a double mutant line devoid of genes encoding melanocytes and iridophores, making it transparent for easy imaging of internal tissues (White et al., 2008).

To confirm deletion of the *synpo2b* gene, primers (P1 and P2) were designed to flank exon 2 (Fig. 25A). Heterozygous mutants contained both the wild-type (1851 bp) and knockout (359 bp) PCR amplicons (Fig. 25B, lane 2). Approximately 75% of the gRNA-

injected embryos were shorter in length and had curved tails showing aberrant musculature (Fig. 27). These embryos were unable to swim and died 5 dpf. The curved tail phenotype seen in the F0 generation was the same phenotype observed in the morpholino-injected embryos (Fig. 24B). The remaining 25% of the gRNA injected embryos were normal and comparable to uninjected embryos. These viable embryos were grown to adulthood (1-month old) and each embryo was genotyped for the heterozygous gene knockout. Fig. 26 shows an outline of the different steps carried out to generate the homozygous mutant line. Briefly, the F0 embryos were genotyped and 11 fish were screened for heterozygosity. Each of the 11 fish were out-crossed with WT fish to remove off-target effects of the gRNAs and to identify fish with the germline mutation that were able to transfer the gene knockout to the F1 offspring. Only one fish of the 11 fish screened at one month old for germline transfer was able to transfer the gene knockout to the offspring. The F1 fish were grown to 3 months old and in-crossed to generate homozygous F2 mutants. The F2 generation was then screened for homozygous mutants and the homozygous F2 mutants were in-crossed to produce F3 homozygous mutants. The F3 generation was further screened to confirm gene deletion, and the F3 adult fish were in-crossed to produce homozygous F4 animals.

Only 20% of the F1 embryos at 48 hpf had the curved tail phenotype (Fig. 28A) while the remaining embryos appeared normal. Several of the curved tail embryos were fixed at 48 hpf for ultrastructural analysis. Compared to the wild-type embryos that had highly organized and compact sarcomeric units, the heterozygous F1 mutants (*synpo2b*$^{+/-}$) had reduced myofilaments and the myofilaments that formed appeared disorganized and loosely packed (Fig. 28B). These mutant embryos also showed increased accumulation of double membrane vacuoles, empty vacuoles and vacuoles similar in appearance the glycogen storage vacuoles seen in pompe disease (Lim et al., 2014), all features of a muscular dystrophy phenotype (Domingo-Horne & Salajegheh, 2018) (Fig. 29A). When quantified in six heterozygous mutant embryos, the total number of empty vacuoles ranged from 40 to 100 compared to 10 vacuoles in WT embryos, autophagic vacuoles ranged between 50 to 125 compared to 20 in WT embryos, and lipid storage-like vacuoles ranged between 15 to 35 compared to 1 in WT embryos (Fig. 29B). The accumulation of such vacuoles suggested that there could be constant turnover of damaged myofibrils. Hence,

both the morpholino and heterozygous F1 mutant results suggested zebrafish Synpo2b is required for efficient muscle development or maintenance.

4.2.4. Zebrafish *synpo2b*$^{-/-}$ KO embryos (F4 generation) develop normally without muscular defects

The morpholino and F1 heterozygous mutants showed promising and exciting results, so we moved forward to generate homozygous mutants. The F1 fish (12 out of 45) were grown to 3 months old and in-crossed to generate homozygous F2 mutants. PCR screening identified 24 out of 53 F2 fish that were homozygous mutants. The homozygous F2 mutants were in-crossed to produce F3 homozygous mutants and the F3 adult fish were in-crossed to produce F4 offspring that were used for all subsequent experiments.

Surprisingly, we were not able to reproduce the morpholino and F1 data in the F4 generation. All the F4 embryos had straight tails like the WT embryos and did not show the swimming disability observed in the morpholino injected or heterozygous F1 mutant embryos. To confirm the genotype of the F4 embryos, the *synpo2b*$^{-/-}$ F3 line was set as three breeding pairs and in-crossed. Around 30 embryos from each set were pooled, genomic DNA was extracted and used for PCR, and the single amplicon product was sequenced, which confirmed a homozygous Synpo2b gene deletion of 1720 bp that removed almost all of exon 2 (Fig. 30A and 30B-lane 2). Additionally, *in situ* hybridization was carried out using both WT and *synpo2b*$^{-/-}$ KO embryos at different stages of development (8-, 12-, 18-, 25-, 48- and 72-hours post-fertilization (hpf)). There was no detectible expression of Synpo2b-S in the knockout embryos compared to WT embryos that showed clear skeletal muscle expression (Fig. 31A). Thus, two different methods confirmed homozygous gene deletion of the central region of Synpo2b despite loss of the curved tail phenotype and any obvious muscular defects. As an aside, similar *in situ* analysis of Synpo2b-L expression showed the same notochord expression pattern as the WT embryos. Since the *in situ* probe for Synpo2b-L recognizes the unique exon 3 present in this longer isoform (Fig. 21), which is still present in the homozygous F4 deletion mutant (Fig. 31B), this result suggests these mutants are expressing a truncated Synpo2b-L transcript, although it is unclear whether this transcript is a functional mRNA.

4.2.5 Zebrafish *synpo2b*$^{-/-}$ KO embryos have ultrastructural defects in myofibril organization

Loss of the curved tail phenotype in the homozygous F4 knockout embryos was unexpected but did not exclude the possibility that muscle defects might exist at the cellular level. To explore this possibility, both WT and *synpo2b*$^{-/-}$ embryos were fixed at 48 hpf and stained for myosin heavy chain (MHC) or phalloidin to observe myofibril organization. The myofibers of the knockout embryos appeared indistinguishable from the WT embryos, with well-organized, multinucleated myofibers that were indistinguishable from the myofibers in WT embryos (Fig. 32), but quite distinct from the loosely packed myofibrils present in the morpholino-treated embryos (Fig. 24C). Thus, knocking out *synpo2b* in zebrafish did not affect myotube formation during development as it did in mouse C2C12 myoblasts, nor did it grossly alter myofibril organization as seen in the morpholino treated embryos.

I did, however, note several changes to myofibril organization at the ultrastructural level. During zebrafish development, the fast muscle myoblasts become elongated and fuse with one another, and these fused myofibrils span between myotome boundaries. To examine the muscle ultrastructure in more detail, thirty WT and KO embryos were stained with anti-β-dystroglycan and somites 15, 16, and 17 were imaged by fluorescence microscopy. Visually, the KO embryos did not appear to be different from the WT embryos (Fig. 33A). However, quantifying the angle of the myotome boundaries for each embryo between somites 15, 16 and 17 using image J revealed knocking out *synpo2b* significantly increased the angle of the myotome boundaries (Fig. 33B). This change did not result in gross muscle deformities, but it could affect muscle performance at later stages of development.

Additional changes were noted in the myofibers of *synpo2b*$^{-/-}$ KO embryos when compared to WT embryos using electron microscopy. Ten WT and eight KO 48 hpf embryos were fixed and processed for ultra thin, longitudinal sectioning such that each section covered from head to tail of a fish. Using this method, it was easy to count the somite number and compare somites between the WT and KO embryos. Electron microscopic images of WT embryos showed highly organized sarcomeric units with well formed Z-discs (Fig. 34, top panel), whereas the *synpo2b*$^{-/-}$ KO embryos contained regions

with loosely packed myofilaments and these abnormal myofilaments lacked a well-defined Z-disc (Fig. 34, bottom panel), similar to the appearance of immature myofilaments. I quantified the percentage of somites that had immature myofilaments in each fish by counting the total number of somites having immature myofilaments and normalizing this value to the total number of somites imaged in each fish. The number of somites imaged for each embryo ranged from 10-27, depending on the preparation. There was a statistically significant 3-4-fold increase in the number of somites that had immature myofilaments in the KO embryos when compared to the WT embryos, where <10% of somites in the WT embryos had immature myofilaments (Fig. 35A).

During muscle contraction and relaxation, the distance between two Z-discs that flank each sarcomere shortens and expands during every cycle of contraction and relaxation. Since mouse and human SYNPO2As are Z-disc associated proteins, I wanted to determine whether *synpo2b*$^{-/-}$ KO embryos altered the length between Z-discs. Sarcomere length, which is the length between two Z-discs in electron microscope images, of random sarcomeric units from different myofilaments was measured and an average sarcomere length quantified. Compared to WT embryos, the average sarcomere length of *synpo2b*$^{-/-}$ KO embryos decreased from 1.5 µm to 1.29 µm, although this difference was not statistically significant (Fig. 35B). From the same images we also quantified the I band length, which is the narrow region between two A-bands and consists of a single Z-disc. The *synpo2b*$^{-/-}$ KO embryos showed significantly reduced I-band lengths compared to the WT embryos (Fig. 35C), with average I band lengths ranging between 0.23µm to 0.29µm for WT embryos and 0.19µm to 0.26µm for KO embryos. Thus, three different data sets (i.e., presence of immature myofilaments, reduced sarcomere length and reduced I band length) all suggest that Synpo2b is required for the efficient formation and/or maintenance of sarcomere organization in myofilaments.

4.2.6 *Synpo2b*$^{-/-}$ knockout embryos did not show any defective swimming behaviour

Zebrafish embryos show spontaneous tail coiling by 17 hpf, and by 21 hpf they respond to mechanical stimuli. Both these types of tail coiling require muscles to contract and relax normally. Actin and myosin make the thin and think filaments, respectively, of myofibers, and are the most important proteins required for muscle contraction. To

determine whether the ultrastructural defects observed in *synpo2b*$^{-/-}$ embryos affected muscle contraction or function, I performed a touch-evoked response assay on both WT and KO embryos. Individual embryos were analyzed by placing them in a 10 mm diameter circle, and the tail of the embryo was touched using an insect pin. Representative images from the video recorded at 25 frames per second (fps) show that both the WT and KO embryos exited the field of view within approximately the same time frame (Fig. 36A). The time taken to exit the circle (~260 milliseconds) was noted from the video, and the escape time was calculated by subtracting the exit time from the start time. The escape time ranged from 114-374ms for WT embryos and between 187-337ms for KO embryos, except for three KO embryos that had escape times of 524, 562, and 599ms (Fig. 36B). Therefore, the majority of *synpo2b*$^{-/-}$ embryos displayed no defect in their muscle contraction capability.

4.2.7 *Synpo2b*$^{-/-}$ knockout does not delay muscle regeneration following laser injury

To determine whether *synpo2b*$^{-/-}$ embryos had any defect in muscle regeneration, as opposed to muscle development, I used the 355 nm laser on a PALM laser dissection microscope to inflict muscle injury in 72 hpf WT and KO embryos. The same laser intensity was used to injure the same somite in all embryos. Each injured embryo was placed in a separate well of a 12-well plate and imaged every 24 hours using birefringence under polarized light to observe myofibril repair. Qualitatively, as seen in the birefringence images, both the WT and *synpo2b*$^{-/-}$ embryos regenerated the damaged somite efficiently and to the same extent (Fig. 37A). I further analyzed the birefringence data of 4 dpi embryos with imageJ, using increased light refraction as an indicator of more organized myofibers and regeneration. As shown (Fig. 37B), there was no difference in the relative intensity of both WT and *synpo2b*$^{-/-}$ embryos, suggesting loss of Synpo2b does not adversely affect zebrafish muscle regeneration.

4.2.8 Muscle contractile-specific proteins are downregulated in *synpo2b*$^{-/-}$ KO embryos

While the morpholino, F0 and F1 *synpo2b*$^{+/-}$ embryos showed gross muscle defects, this phenotype was lost in the homozygous mutants. The loss of phenotype by gene deletion could be attributed to compensatory genes that get upregulated upon gene deletion but not

upon knockdown (A. Rossi et al., 2015). To understand whether the loss of phenotype in our *synpo2b*$^{-/-}$ embryos was reflected in a compensatory change in the expression of other genes, I performed RNAseq analysis of both the WT and KO embryos. Since Synpo2b-S is expressed in developing somites, three sets each of 22 hpf WT and KO embryos were analyzed as described in detail in the Method's section of this thesis.

The differentially regulated genes list generated by the edgeR platform was used to generate a volcano plot (Fig. 38). The differentially expressed genes were plotted based on the false discovery rate (FDR) values and the pValue cutoff was set to <0.05. Based on the FDR value, 404 gene transcripts out of the 21358 gene transcripts detected were significantly differentially regulated (orange dots in Fig. 38). These genes are listed in the Appendix A. A few of the significantly up-and down-regulated genes of interest are marked on the plot. The significantly differentially regulated genes were then subjected to GSEA and GO analysis using ClusterProfiler and ReactomePA platforms to group the gene list based on the gene ontology term (GO terms) that represents a biological process. From our analysis, we were not able to identify any gene(s) that was both significantly upregulated and had defined muscle-specific functions that could potentially compensate for the loss of Synpo2b.

Interestingly, several downregulated genes that clustered together based on their annotated biological function as muscle contractile proteins were all significantly downregulated (Fig. 38). As shown more clearly in a category network (CNet) plot (Fig. 39), these downregulated genes involved in muscle development and maintenance grouped together under different processes such as sarcomere, contractile fiber part, myofibril, contractile fiber and actin cytoskeleton. The gene names involved in each of these processes are detailed in Table 5. Genes that were downregulated more than 4-fold included ankyrin-repeat domain 2 (Ankrd2), actin binding Rho activating protein b (Abrab) and melanophilin a (Mlpha), where Ankrd2 and Abrab are proteins localized in the I band of skeletal muscle. Genes that were downregulated 2-3-fold included myosin heavy chain 4 (Mhc4), myosin heavy chain a (Myha), troponin I type 2a (skeletal, fast), tandem duplicate 4 (Tnni2a.4), and troponin T type 3b (skeletal, fast) (Tnnt3b), that function as a part of the contractile fiber. Other genes that were significantly downregulated, but less than 2-fold, included Synpo2b itself, as well as other genes that regulate the actin cytoskeleton and/or the

function of fast skeletal muscle fibers (Table 5). The differential expression of these genes across the three different sets of samples for both the WT and KO embryos is plotted as a heat map, normalizing the p value of each gene to only the gene set included in the heat map (Fig. 40). Hence, deletion of Synpo2b results in ultrastructural changes to myofiber organization in zebrafish embryos that do not affect overall muscle performance as analyzed, but which paradoxically have significant deleterious effects on maintaining the transcript levels of numerous muscle contractile proteins.

4.3 Discussion

I identified two Synpo2b isoforms in zebrafish, Synpo2b-S and Synpo2b-L, that are differentially expressed during zebrafish development (Fig. 21A). Since SYNPO2As localizes in the Z-disc (Weins et al., 2001) and is required for myoblast fusion (our data), we hypothesized that knocking down Synpo2b should cause defects in fast muscle cell fusion and therefore affect muscle performance. As predicted, morpholino injected embryos and heterozygous F0 and F1 mutant embryos showed gross muscle defects such as curved tails and an inability to swim properly, and myofibers appeared abnormal when examined by fluorescence microscopy. Unexpectedly, the gross muscle defect phenotype did not persist in the homozygous F2 generation or subsequent generations, although ultrastructural changes in myofilament organization were observed in the homozygous deletion mutants. Furthermore, RNAseq analysis revealed substantial downregulation of numerous factors and pathways controlling the formation and function of actomyosin fibers in the homozygous deletion mutants. Despite these changes in muscle architecture and actomyosin pathways we did not observe any functional defects when quantifying muscle regeneration or swimming performance. This is the first direct evidence that Synpo2 is a promyogenic factor that influences normal muscle development *in vivo*.

Spatiotemporal expression of Danio rerio Synpo2b isoforms

There is not much known about the expression profile of synpo2 in muscle tissue, other than information contained in curated large-screen databases that report the mRNA expression levels of synpo2 in several tissues isolated from human and mouse. In human fetal samples between week 10-20, SYNPO2 transcripts increase in the heart, intestine and

stomach with low levels of mRNA expression detected in adrenal glands and kidneys (Szabo et al., 2015). Human SYNPO2 mRNA expression is also reported to be increased in human prostate, skeletal muscle, small intestine, stomach, uterus and heart tissues with very low expression detected in other tissues (Duff et al., 2015; Lin et al., 2001). Similar mouse gene expression databases report SYNPO2 mRNA expression in the intestine, bladder, colon, genital fat pad, heart, mammary gland, ovary, stomach and subcutaneous fat pad in adult mice (Yue et al., 2014). In both the human and mouse databases, it is not clear which of the several synpo2 isoforms are specifically detected.

To examine the *in vivo* effects of synpo2 on muscle development I exploited the advantages of the zebrafish model system which include a 70% similarity to the human genome, external fetal development, transparency in the case of *casper* fish for easy imaging, fecundity, and easy genetic manipulation. I identified two isoforms of Synpo2b in the ZFIN database, which we named Synpo2b-S (short isoform) and Synpo2b-L (long isoform) (Fig. 21A). These isoforms share 43% and 38% sequence identity, respectively, to mouse SYNPO2As. Zebrafish is well known for gene duplication events, and the ZFIN database has an annotated sequence named Synpo2a that is 491bp mRNA. However, this sequence is annotated as a cDNA clone with no reference to the sequence being Synpo2a, it is not mapped to a chromosome, and it is not known to encode a protein. Thus, we identified only one Synpo2b gene in zebrafish.

As shown by *in situ* hybridization, Synpo2b-S mRNA is strongly expressed in skeletal muscle by 25 hpf and this staining pattern was maintained (at reduced levels) through 72 hpf, while Synpo2b-L staining was much fainter and more transient, localizing in the notochord of zebrafish at 25 hpf (Fig. 22A and B). There are other examples of muscle specific proteins whose different isoforms are expressed in different regions of the fish during development, including fast muscle myosin heavy chain isoforms 1 and 2 (fmyhc1 and 2) (Nord et al., 2014), and ankyrin repeat protein isoforms ankrd1a and b (Boskovic et al., 2018). The tissue-specific localization of these different isoforms, and of Synpo2b-S and Synpo2b-L, suggests they have different functional roles. These results are the first to show tissue-specific expression of two Synpo2b isoforms in an *in vivo* model during development.

Synpo2b knockdown and synpo2b$^{+/-}$ heterozygous mutants mimic a muscular dystrophy phenotype

To examine the role of Synpo2b-S in zebrafish muscle development, I began by knocking down Synpo2b expression using morpholinos targeting the N-terminus of the mRNA (Fig. 24A). Morpholino injected embryos exhibited curved tails and a short body axis, typical of a dystrophy model (Fig. 24B). Immunofluorescence staining for actin and myosin showed loosely packed myofibrils between myosepta boundaries (i.e., the chevrons) and a disorganized myosin staining pattern with most myofibers containing only 1 or 2 nuclei (Fig. 24C), similar to the reduced myotube formation noted when mouse SYNPO2As was knocked down in C2C12 cells. The extent of disrupted myotube formation induced by Synpo2b-S knockdown was comparable to that observed when some other proteins considered essential for myoblast fusion are knocked down using morpholinos. For example, knockdown of cell adhesion proteins such as Kirre-like (Kirrel), the *Drosophila* homolog of Kin of irre (Kirre)/Duf, increases the number of mononucleated muscle fibers to ~80% compared to ~10% of WT mononucleated fibers (Srinivas et al., 2007). Similarly, knockdown of actin-regulating proteins such as Rac1, DOCK180 and DOCK5 reduces myotube formation by ~30-50% (Pajcini et al., 2008; Vasyutina et al., 2009). Morpholino knockdown of some of these actin-regulating proteins in zebrafish resulted in the same curved tail phenotype and increased numbers of mono- and bi-nucleated myofibers I observed following Synpo2b knockdown (Srinivas et al., 2007; Moore et al., 2007).

The morpholino results were initially supported by results obtained using the CRISPR/cas9 system to knockout the *synpo2b* gene, with the F0 embryos showing the same curved tail phenotype observed in the MO treated embryos (Fig. 27). This phenotype could be attributed due to mosaicism, that is gene deletion in both somatic and germline cells. To determine if the mutation was a germline mutation, the heterozygous F0 mutants were outcrossed with a WT fish. Ultrastructural analysis of the muscle of curved F1 embryos showed reduced myofilament content, increased vacuole accumulation, granular material, and mitochondria accumulation between myofibers (Figs. 28 and 29). These phenotypic changes are similar to those seen in myofibrillar myopathy (MFM) patients, a condition caused by mutations in sarcoplasmic and cytoskeletal proteins (Schröder & Schoser, 2009).

Morpholino knockdown of MFM-related genes in zebrafish also elicited the same MFM symptoms (Bührdel et al., 2015). Thus, like some other cytoskeletal proteins, knockdown of Synpo2b reduced fast muscle myotube formation and replicated the symptoms seen in MFM. However, Mendelian genetics predicted 50% of the F1 offspring should have had a curved tail phenotype but we only observed 20% of the embryos with this phenotype. In a second cross of F0 with WT none of the embryos had a curved tail phenotype suggesting the curved tail embryos in the first cross could have been due to breeding conditions or first-time breeding. These initial studies therefore failed to define the relative role of Synpo2b in zebrafish muscle development.

Knockdown phenotype versus Knockout phenotype

According to the MGI database, *Synpo2* knockout mice are lethal at the preweaning stage. Additionally, we observed in our *in vivo* model that Synpo2b morphants and heterozygous mutants showed striking muscular defect phenotypes. We were therefore surprised when the F2, F3 and F4 embryos screened for homozygosity by PCR displayed no curved tail phenotype or any obvious muscular defects. Furthermore, *in situ* hybridization confirmed the Synpo2b-S isoform was not expressed in the skeletal muscle of KO embryos (Fig. 31A). The loss of phenotype was discouraging, but phenotypic discrepancies between morphants and zygotic mutants have been previously reported in zebrafish and in other models like *Arabidopsis*, yeast and mice (El-Brolosy & Stainier, 2017). For example, zebrafish embryos with morpholino knockdown of the Fus gene display symptoms of amyotrophic lateral sclerosis (ALS) but zygotic mutants remain normal (Lebedeva et al., 2017). Similarly, embryos with individual morpholino knockdowns of 10 genes (Amot, Ccbe1, Elmo1, Ets1, Flt4, Fmnl3, Gata2a, Mmp2, Nrp1a, Pdgfrb) display vascular or lymphatic defects, but this phenotype is only observed in zygotic mutants of three of these genes (Flt4, Ccbe1 and Gata2a); the remaining seven mutants develop normally (Kok et al., 2015). Lastly, morpholino knockdown of muscle specific genes Kirrel and Ckip1 significantly reduces fusion of fast muscle cells (D. Baas et al., 2012; Srinivas et al., 2007), however, a recent study showed that *kirrel3*, *ckip1* and *iqsec1b* mutants did not show any fusion defect and were able to swim and regenerate muscle normally (Hromowyk, 2017). Aberrant morphant phenotypes have been attributed

to off-target effects or MO-toxicity. Studies such as these led to the development of guidelines to follow when publishing morpholino data, including the need to show a zygotic mutant phenocopies the morphant (Stainier et al., 2017). Despite the loss of a gross muscle defect in Synpo2b zygotic mutants, ultrastructural analysis of muscle tissues did reveal increased numbers of immature myofilaments and decreases in sarcomere length and I band width, indicating zebrafish Synpo2b plays a role in the efficient formation and/or maintenance of myofilaments.

Does synpo2b gene deletion trigger compensatory changes in gene expression?

Zygotic deletions can trigger genetic compensation where altered expression of other genes can compensate for loss of the deleted gene. Other instances include RNAi depletion of Tet1 in mice reduces leukemia inhibitory factor (LIF)/STAT3 signaling (Freudenberg et al., 2011), whereas increased Tet2 expression compensates for the loss of Tet1 in knockout mice, which do not show any phenotype (Dawlaty et al., 2011). Similarly, EGF-like-domain multiple 7 (Egfl7) morphants in zebrafish have vascular defects that are not present in *egfl7*$^{-/-}$ mutants due to upregulated expression of a compensatory gene, Emilin3a (A. Rossi et al., 2015), while muscle α-actin (Actc1b) morphants show nemaline bodies and poor muscle performance, phenotypes not observed in *act1b*$^{-/-}$ mutants where upregulation of Actc1a compensates for the absence of actc1b (Sztal et al., 2018).

To determine whether genetic compensation contributed to the loss of the morphant phenotype in the zygotic *synpo2b* mutants, I used RNAseq analysis to look for upregulated expression of compensatory genes. Results did not identify a single gene or cluster of genes with a particular function that could compensate for the loss of phenotype in *synpo2b*$^{-/-}$ embryos. According to set pValue cutoffs and FDR calculations, expression of 404 genes were significantly altered in the *synpo2b*$^{-/-}$ embryos compared to WT embryos. Unfortunately, the majority of genes that were the most significantly upregulated (e.g., si:dkey-42i9.7 was upregulated 9-fold) or significantly downregulated (e.g., si:ch1073-190k2.1 was downregulated by 11-fold) are those yet to be annotated and whose functions in zebrafish have not been defined.

One gene of potential interest was shisa family member 4 (Shisa4) that was upregulated 8.8-fold. The shisa family of proteins are ER-localized transmembrane proteins

best known for playing a role in head formation by inhibiting Wnt and FGF signalling (Yamamoto et al., 2005). However, a very recent paper showed that knockdown of SHISA2 significantly inhibits fusion of C2C12 and primary myoblasts (Liu et al., 2018). As an ER protein, shisa4 might also localize in the muscle sarcoplasmic reticulum to regulate muscle contraction and somehow compensate for the loss of Synpo2b. The localization or function of Shisa4 in zebrafish muscle is unknown, and further studies are needed to establish the role of Shisa4 in WT skeletal muscle and in *synpo2b*$^{-/-}$ embryos.

Since most of genes were not annotated with a gene name, I analyzed all 404 hits by individually searching with the available name (e.g., si:dkey-42i9.7) or Ensemble ID in the PANTHER classification system. This process allowed us to group each gene based on the PANTHER protein class, family and function. The only notable result was a few genes involved in immune system processes or transcription factor signaling, but different genes in these pathways were either upregulated or downregulated (Appendix A). While the PANTHER classification system did not identify an upregulated pathway likely to compensate for loss of Synpo2b, I did identify clusters of genes that regulate the actin cytoskeleton and muscle contraction that were significantly downregulated in *synpo2b*$^{-/-}$ embryos (Table 5). These genes were categorized as sarcomere, contractile fiber, myofibril, contractile fiber and actin cytoskeleton proteins. As can be seen, several major components required for the organization and function of myofilaments in myofibers were significantly downregulated in the *synpo2b*$^{-/-}$ embryos, despite the absence of any gross morphological muscular defects. Why loss of Synpo2b might lead to downregulated muscle specific gene transcripts is discussed further in Chapter 5 of this thesis.

Synpo2b$^{-/-}$ *knockout embryos exhibit defects in myofilament organization*

Knockout of Ig domain containing transmembrane proteins JamB and JamC (Powell et al., 2011), transmembrane protein myomaker (Zhang et al., 2017), or the micropeptipe myomixer (Shi et al., 2017) completely blocks multinucleated myotube formation, generating myofibers with a single, centrally located nucleus. Despite this complete block to myoblast fusion, these zebrafish embryos remain viable and exhibit normal twitching and swimming behaviour. To determine whether the *synpo2b*$^{-/-}$ embryos that lacked any obvious muscle or swimming defects had ultrastructural changes in their

myofiber organization, 48 hpf embryos were examined by fluorescence microscopy using phalloidin to stain F-actin, anti-MHC to stain fast muscle fibers, or anti-β-dystroglycan to image myosepta, and whole mount embryos were also examined by electron microscopy. As shown (Figs. 32 and 33), the *synpo2b*$^{-/-}$ embryos formed normal multinucleated myotubes but displayed several defects in their myofiber organization, including changes to the organization of myosepta boundaries, Z-discs and I bands. Regions of loosely packed myofilaments resembling immature myofibrils and reduced (approaching statistically significant) sarcomere length were also noted in the *synpo2b*$^{-/-}$ embryos, indicating Synpo2b is required for efficient formation of normal myofibrils in zebrafish.

During embryo development, muscle contraction is required for proper myotome development. For example, treatment of embryos with blebbistatin (non-muscle myosin II inhibitor) to reduce actomyosin contraction reduces localization of paxillin to focal adhesion sites and these embryos have wider myosepta boundaries. Paxillin mutants also exhibit wider myosepta boundaries (Jacob et al., 2017). The effects of *synpo2b* deletion on myosepta boundaries correlated with significantly downregulated muscle contractile proteins, and the KO embryos also exhibited reduced sarcomere length suggesting muscle contraction could be affected.

The possible role of Synpo2b in myofilament maturation (Fig. 34) is somewhat similar to the role the PDZ domain containing mouse isoforms, SYNPO2A and B, play in regulating the CASA pathway for muscle maintenance (Ulbricht et al., 2013). However, zebrafish Synpo2b-S shows only 40% sequence similarity to SYNPO2A and B and this sequence conservation is only in the conserved actin-binding region encoded by exon 4 in mouse and does not align with the PDZ domain. Thus, Synpo2b in zebrafish seems unlikely to play a role in the CASA pathway but may be required for maintaining actomyosin contraction and myosepta stability.

Several additional hits from our RNA sequencing data were also consistent with the ultrastructural changes observed in the myotome of *synpo2b*$^{-/-}$ embryos. The fast muscle myosin heavy chain genes *myhz1.1* and *myhz1.2* were significantly downregulated, and Myhz1.1 is known to be expressed in somites 1 to 17 while and Myhz1.2 is expressed in somites 1-11 (Nord et al., 2014). Downregulated expression of these genes correlated with the presence of immature myofilaments in *synpo2b*$^{-/-}$ embryos, especially in the mature

somites present in the anterior region of the embryo. Similarly, the KO embryos exhibited significantly reduced I band length compared to WT embryos (Fig. 35C), and two hits were I-band localized proteins ankyrin repeat domain 2 (Ankyrd2) and actin binding Rho activating protein b (Abrab). Ankyrd localizes in the I-band of skeletal muscle and upon cardiotoxic injury in mice translocates to the nucleus and localizes with euchromatin (Tsukamoto et al., 2008). Abrab, also known as striated muscle activator of Rho signalling (STARS), localizes in the I-band in COS cells and polymerizes actin thereby sequestering G-actin. Decreased levels of G-actin releases the myocardin-related transcription factor (MRTF) that translocates into the nucleus and along with serum response factor (SRF) increases transcription of downstream targets (Arai et al., 2002). Down-regulation of both Ankrd2 and Abrab in the *synpo2b*$^{-/-}$ embryos could explain the significantly reduced I-band length, and downregulation of Abrab could also downregulate other muscle specific contractile proteins by interfering with MRTF/SRF signaling. Downregulation of muscle contractile proteins and I-band proteins may explain the need for Synpo2b in the formation and maintenance of normal, mature myofilaments, even though altered myofilament organization due to *synpo2b* deletion did not affect the overall morphology, regenerative capacity or function of zebrafish muscle.

All of my studies were carried out in embryos less than 6 dpf. It may be possible that knockout of *synpo2b* could affect muscle regeneration during aging as seen in *cavin4b/murcb* mutants, where only the 10 week post-fertilized fish or older show muscle defects and swimming deficiency (Housley et al., 2016). Even in the case of Synpo1 mutant models, *Synpo1*$^{-/-}$ mutant mice show normal kidney structures during development but treatment of knockout mice with protamine sulphate significantly reduced podocyte foot processes leading to nephrotic syndrome (Asanuma et al., 2005). Similarly, it would be interesting to asses the function of Synpo2b in zebrafish at later stages of development or by placing the fish under stressed conditions.

Possible role of Synpo2b in myofibrillogenesis

The arrangement of different proteins into contractile units is myofibrillogenesis. Striated muscle contains repeating sarcomeric units, and each unit is flanked by electron dense Z-discs, I Band, A band and M-line (Fig. 34 top panel). The organization of these

sarcomeres begin with nascent myofibrils made of actin and NMII, later replaced by muscle myosin to form mature myofibers (Sanger et al., 2010) (Fig. 41). There is a potential link between the apparent effects of Synpo2b on transcriptional regulation and myofibrillogenesis. The downregulation of muscle-specific transcripts, especially myosin isoforms, in *synpo2b* knockout fish likely lead to reduced myosin protein levels, which could have an impact on the dynamics of muscle myosin incorporation into nascent myofibrils and thereby delay myofiber maturation (Fig. 41). It would be interesting to study the staining pattern of sarcomeric proteins at different stages of myofibrillogenesis to determine whether *synpo2b* deletion delays this process.

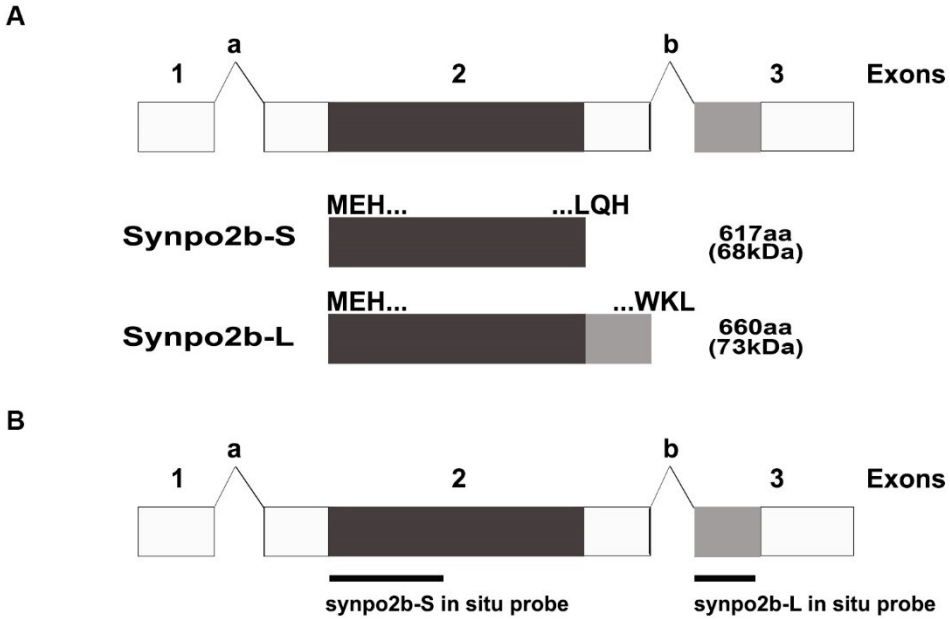

Figure 21: Zebrafish Synpo2b isoforms.
(A) Exon and protein arrangement of synpo2b gene and protein isoforms. The protein isoforms, Synpo2b-S (short) and Synpo2b-L (long) are generated from alternatively spliced mRNAs generated from an upstream promoter. The exons are indicated by numbers and introns by alphabetically labelled chevrons. Amino acid sequences above each protein isoform indicate the N- and C-terminal sequences. The number of amino acid residues and predicted molecular mass (in brackets) for each isoform are indicated. (B) The black line under exon 2 and 3 shows the region used for designing *in situ* probes for whole mount *in situ* hybridization (Figs. 20A and 20B).

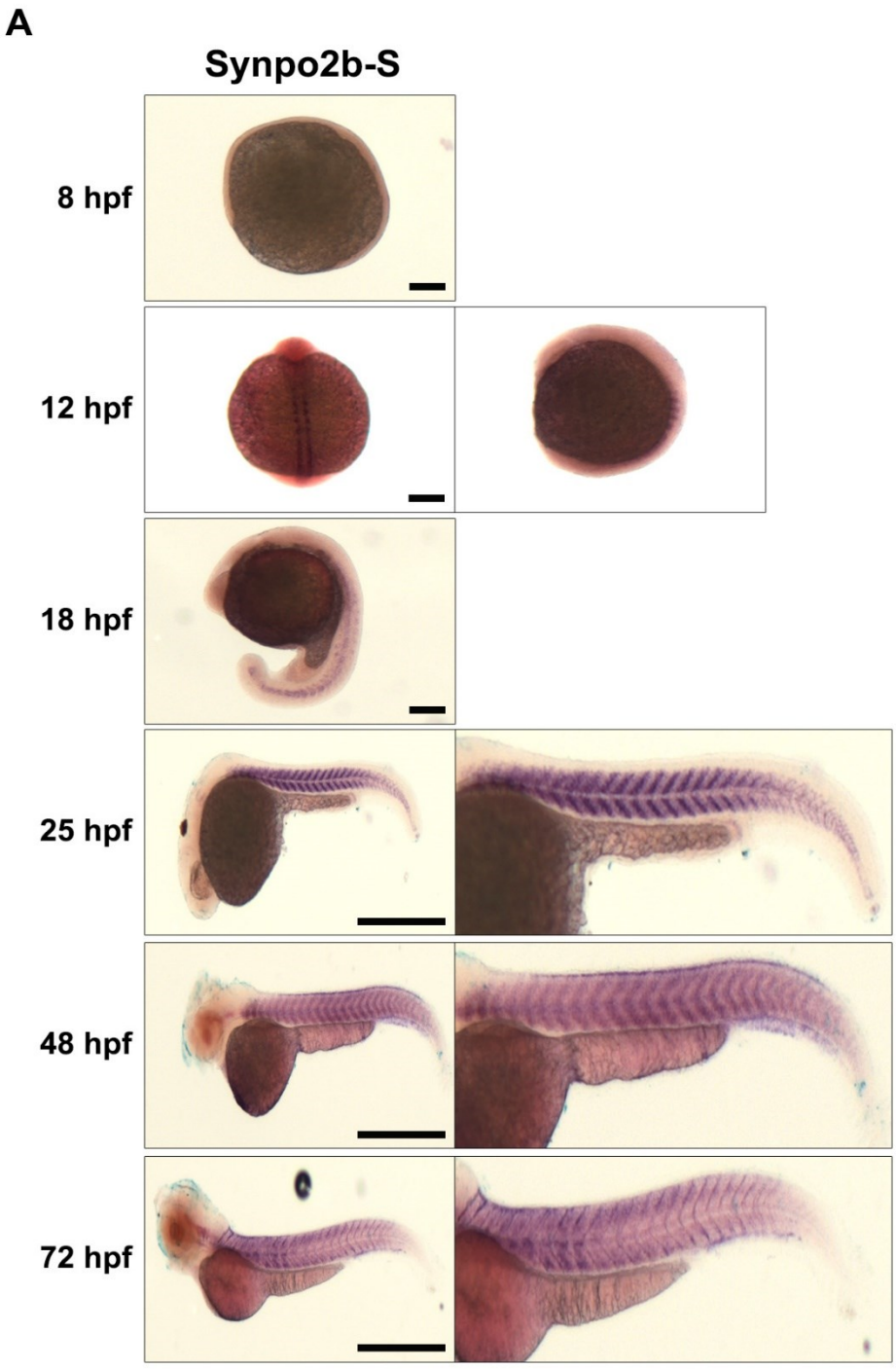
A
Synpo2b-S
8 hpf
12 hpf
18 hpf
25 hpf
48 hpf
72 hpf

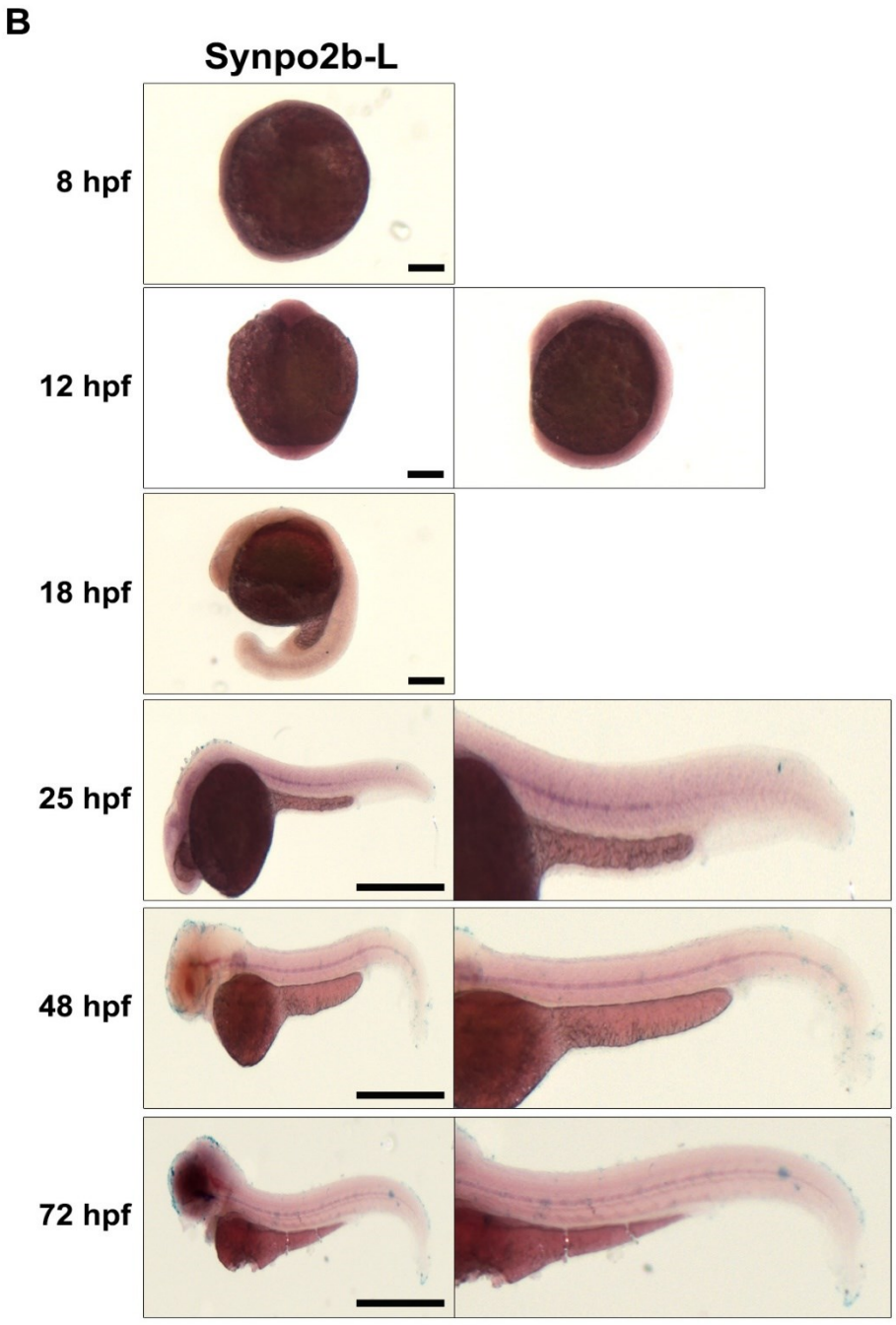

Figure 22: Synpo2b isoforms are differentially expressed during development.
(A) Whole mount *in situ* hybridization of synpo2b-S during different stages of development. (B) Whole mount in situ hybridization of synpo2b-L during different stages of development. In both figures, the side view of 12 hpf embryo is shown on the right. Magnified region of the skeletal muscle of 25, 48 and 72 hpf embryos is shown on the right. Scale bar = 200 µm (8, 12 and 18 hpf) and 500µm (25, 48 and 72 hpf).

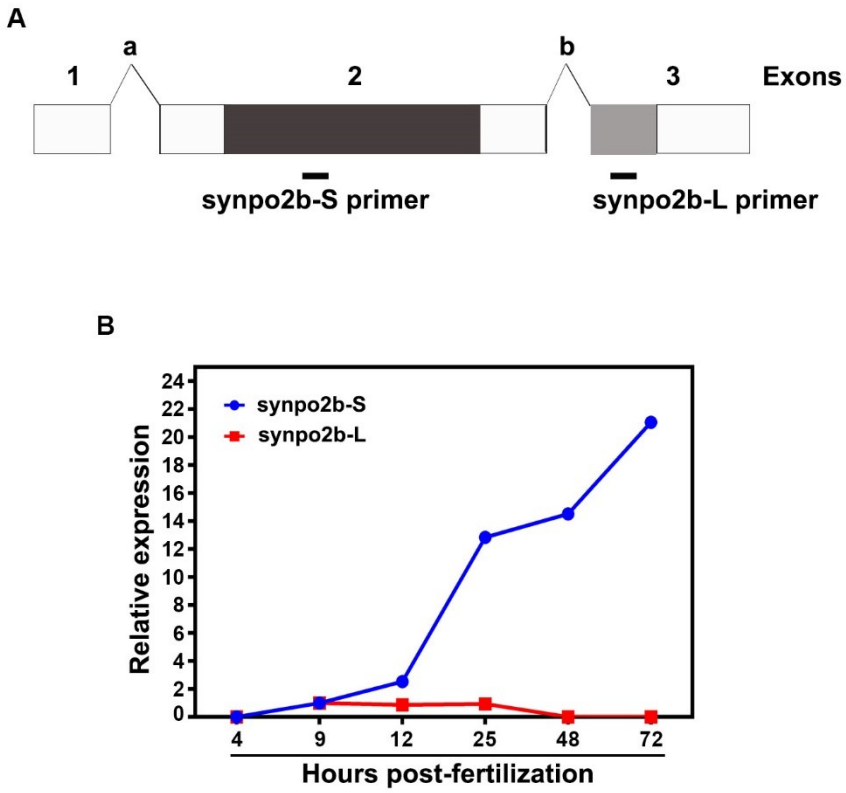

Figure 23: Synpo2b-S is upregulated during development.
(A) Exon arrangement of synpo2b gene. The black line under exon 2 and 3 highlights the region amplified for quantitative RT-PCR. (B) Quantitative RT-PCR of synpo2b-S and synpo2b-L during different stages of embryo development.

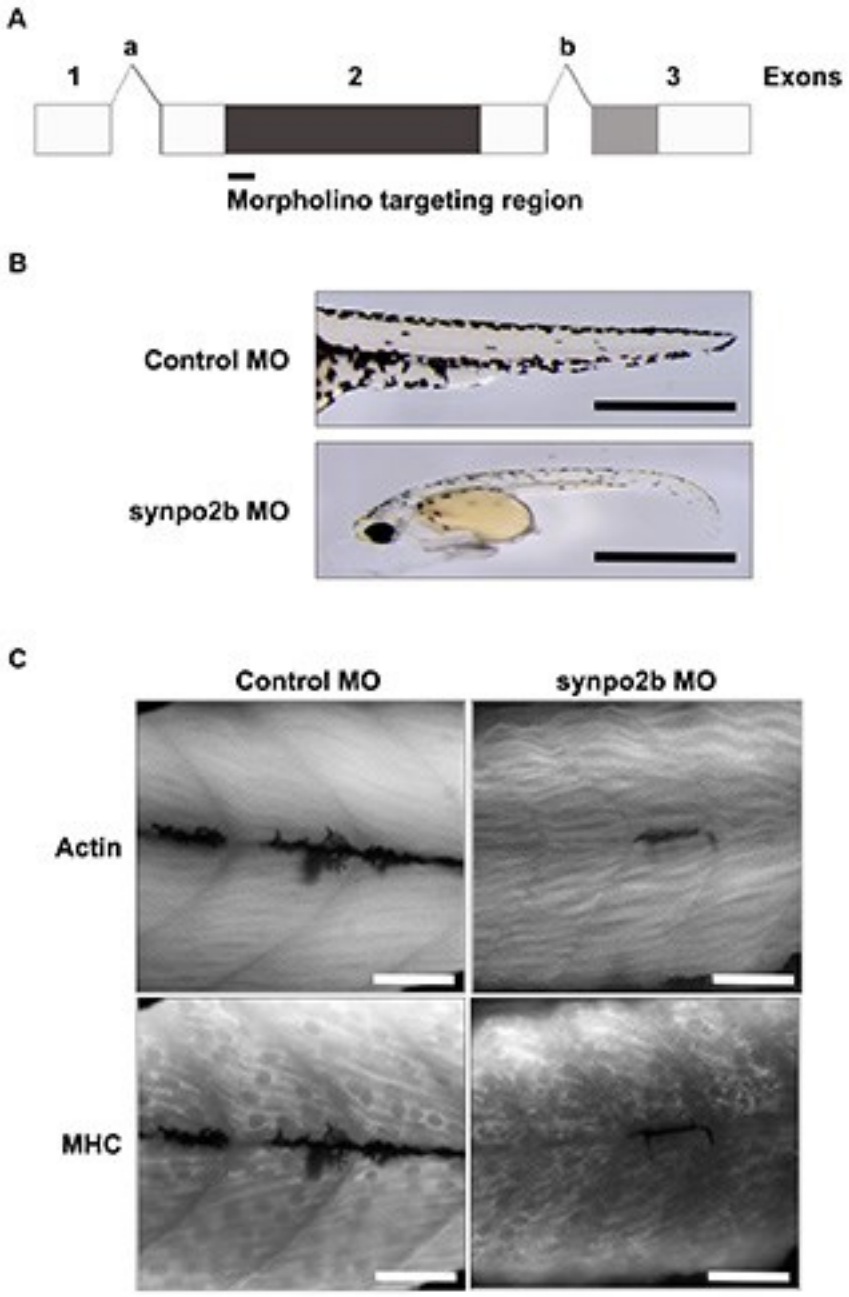

Figure 24: Synpo2b knockdown disorganizes skeletal muscle fiber organization.
(A) Exon arrangement of synpo2b gene. The black line under exon 2 shows the region targeted by the morpholino. (B) Control morpholino (top panel) and synpo2b-targeted morpholino (bottom panel) injected AB strain embryos at 48 hpf. (C) Actin and myosin heavy chain (MHC) staining of control and synpo2b-targeted morpholino injected 48 hpf AB strain embryos. Scale bar = 200μm (B) and 20μm (C).

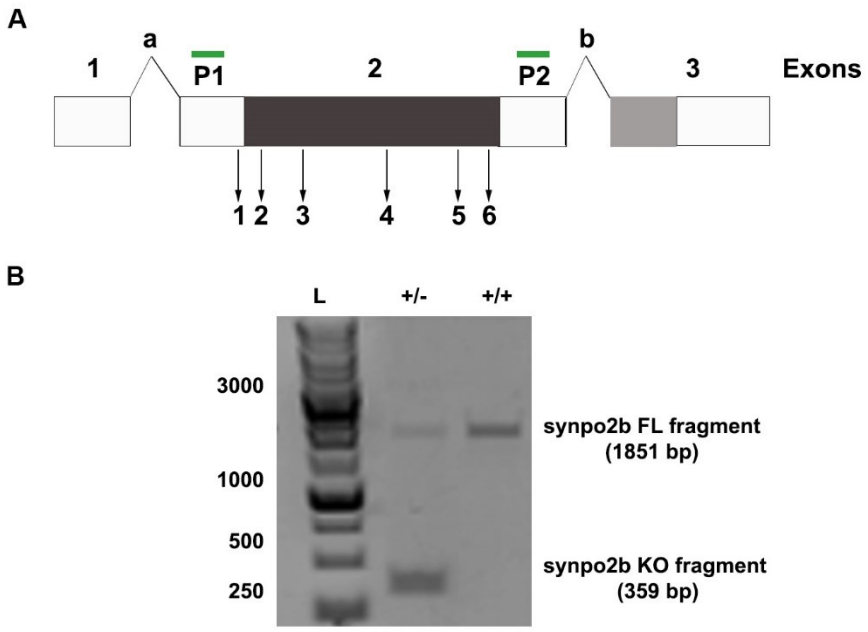

Figure 25: *Synpo2b* gene deletion using CRISPR system.
(A) Exon arrangement of synpo2b gene. The green lines above exon 2 (P1 and P2) show the primer binding regions. The arrows and numbers 1 to 6 show the gRNA targeting regions. (B) PCR gel image showing the regions amplified by primers P1 and P2. Lane 1: ladder; lane 2: two amplicons, the wild-type (1851bp) and mutant band (359bp) from heterozygous fish (+/-); and lane 3: single amplicon of the full-length gene from wildtype.

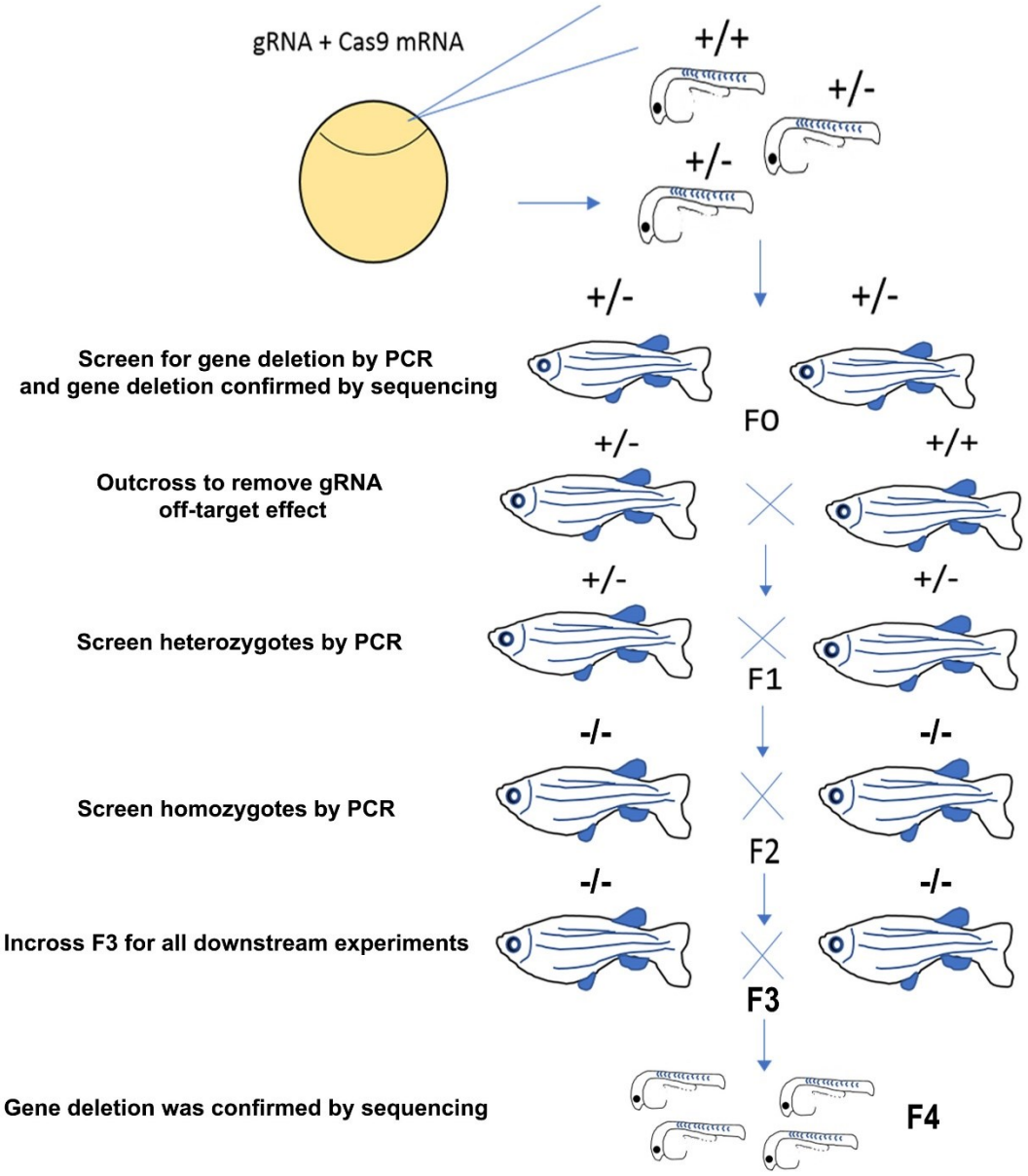

Figure 26: Flowchart depicting the generation of the *synpo2b*$^{-/-}$ knockout fishline.
The six gRNAs (shown in Figure 23A) were injected in the single-cell stage of casper embryos. The injected embryos were grown for 1 month and genotyped for gene deletion (F0 generation). The F0 embryos carrying the *synpo2b* gene deletion were grown to 3 months old and out-crossed with a wild-type casper fish. This removes off-target effects of the gRNAs and confirms germline transmission of the mutation. The FI embryos were screened for the gene deletion (+/-) and in-crossed to obtain the F2 generation. F2 embryos were genotyped for the homozygous gene deletion (-/-) and further in-crossed to obtain the F3 generation that was used for breeding the F4 generation for downstream analysis.

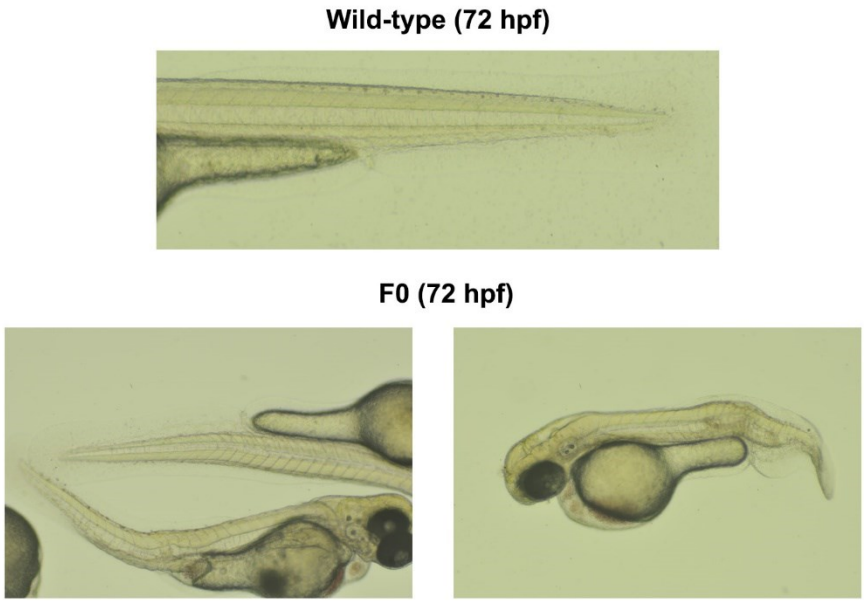

Figure 27: *Synpo2b* knockout embryos develop abnormally (F0).
Top panel represents an uninjected casper embryo (WT), and the bottom panel represents embryos injected with synpo2b targeted gRNAs.

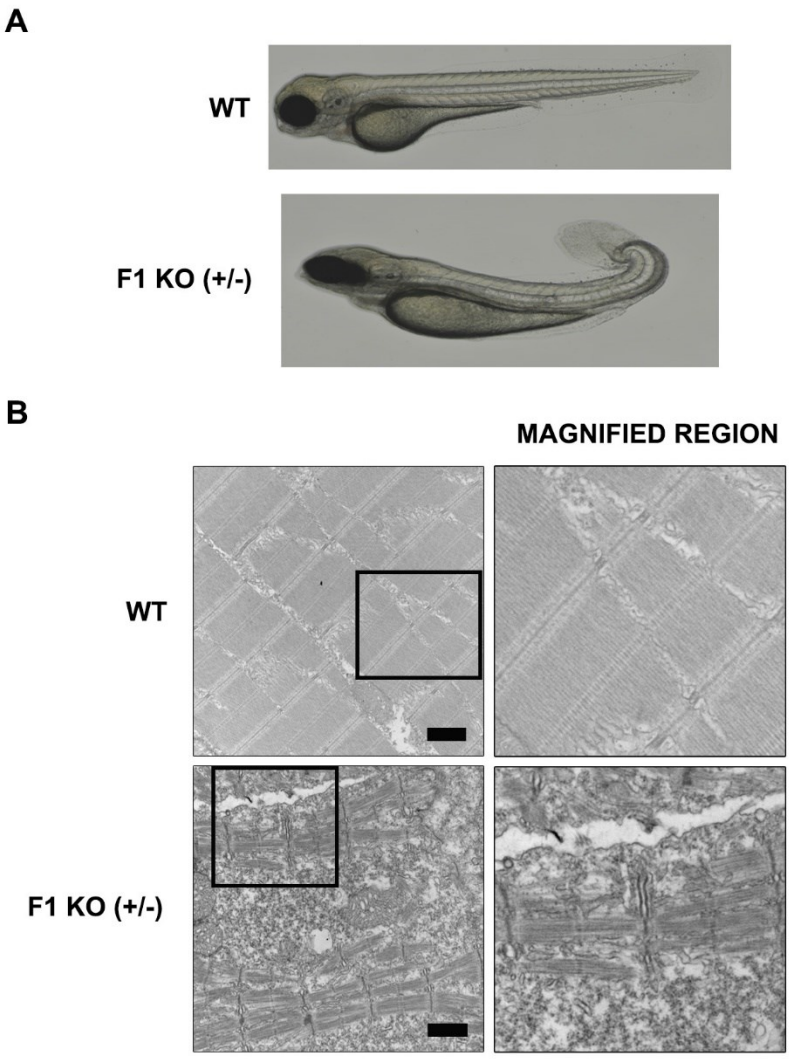

Figure 28: *Synpo2b* F1 knockout embryos have abnormal muscle function and architecture.
(A) The top panel is an uninjected casper embryo (WT), and the bottom panel an F1 embryo (+/-) raised from an F0 mutant and wild-type out-cross. (B) Left panel is the electron microscopic images of WT and heterozygous mutant (+/-) embryos. The right panel is the magnified image of the black inset box. Scale bar = 800nm.

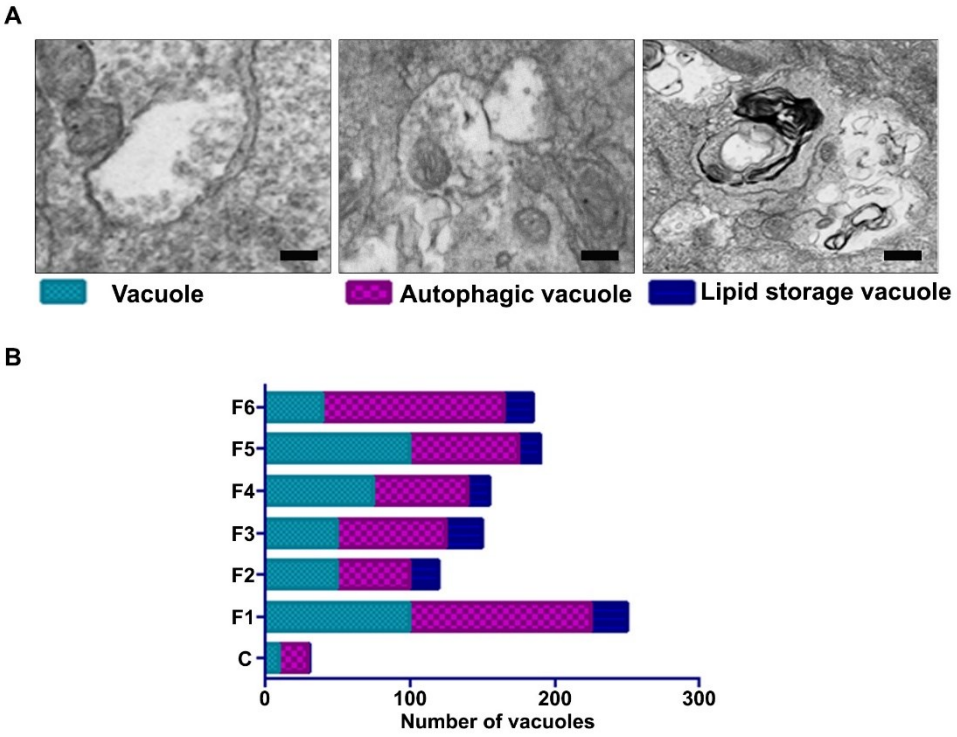

Figure 29: Synpo2b F1 knockout embryos accumulate aberrant vacuoles in the skeletal muscle.
(A) Electron microscopic images of different types of vacuoles. The colored box corresponds to panel B. Scale bar = 1µm. (B) Quantification of the different types of vacuoles. C-control fish, F1 to F6- heterozygous mutants.

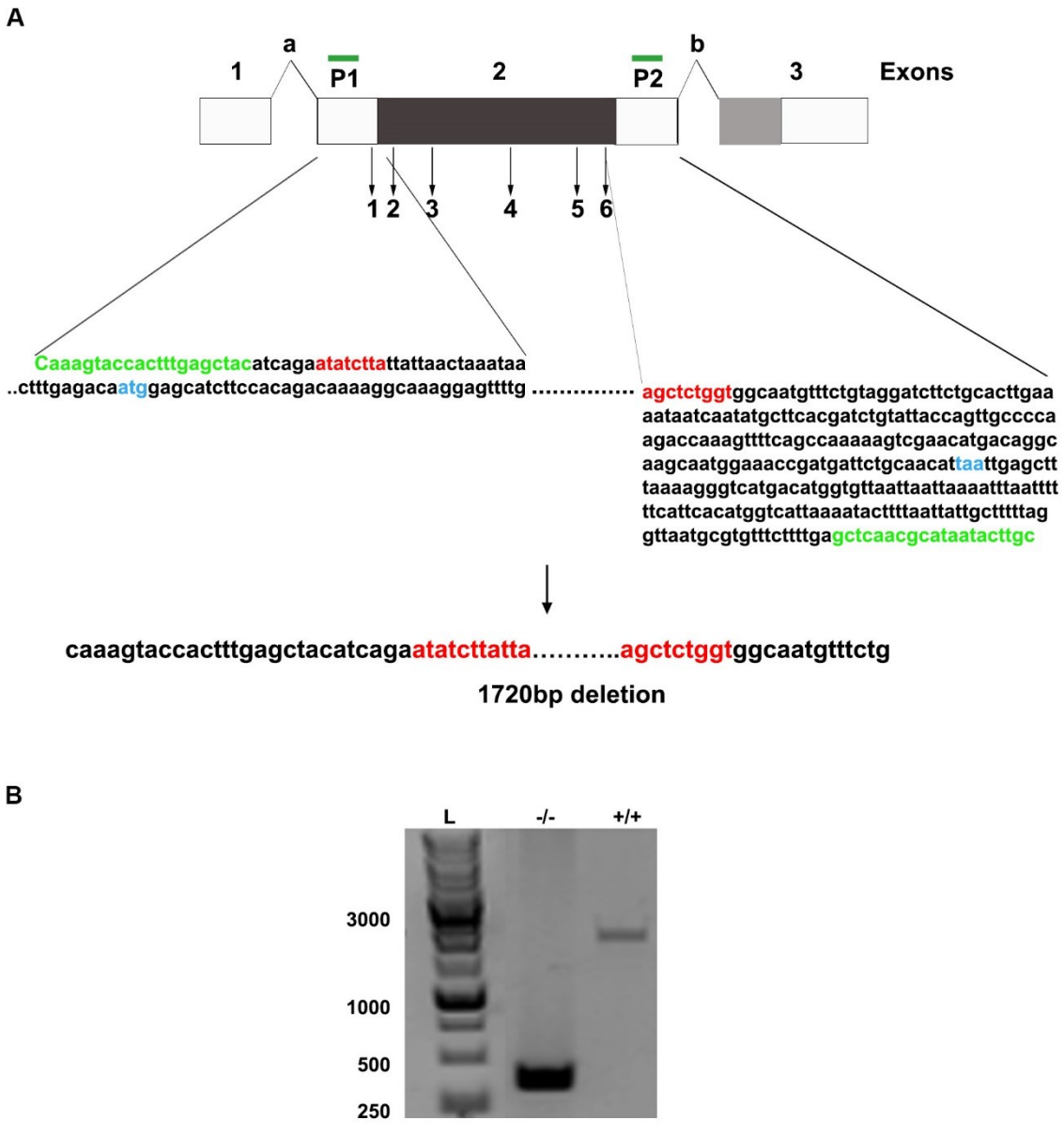

Figure 30: Generation of *synpo2b* homozygous mutants using the CRISPR system. Exon arrangement of the *synpo2b* gene. P1 and P2 show the primer binding regions. The arrows and numbers 1 to 6 show the gRNA targeting regions. The sequence on the left is the 5' UTR with the start codon shown in blue letters, and the sequence on the right is the 3' UTR with the stop codon shown in blue letters. Bases highlighted in green are the P1 and P2 regions (i.e., the primers used for amplifying exon 2). The gRNAs delete a 1720 bp region of exon 2. Bases highlighted in red are the region flanking the deleted region. (B) PCR gel image: lane 1: ladder; lane 2: single amplicon of the mutant band from homozygous fish (-/-); and lane 3: single amplicon of the full-length gene from wildtype.

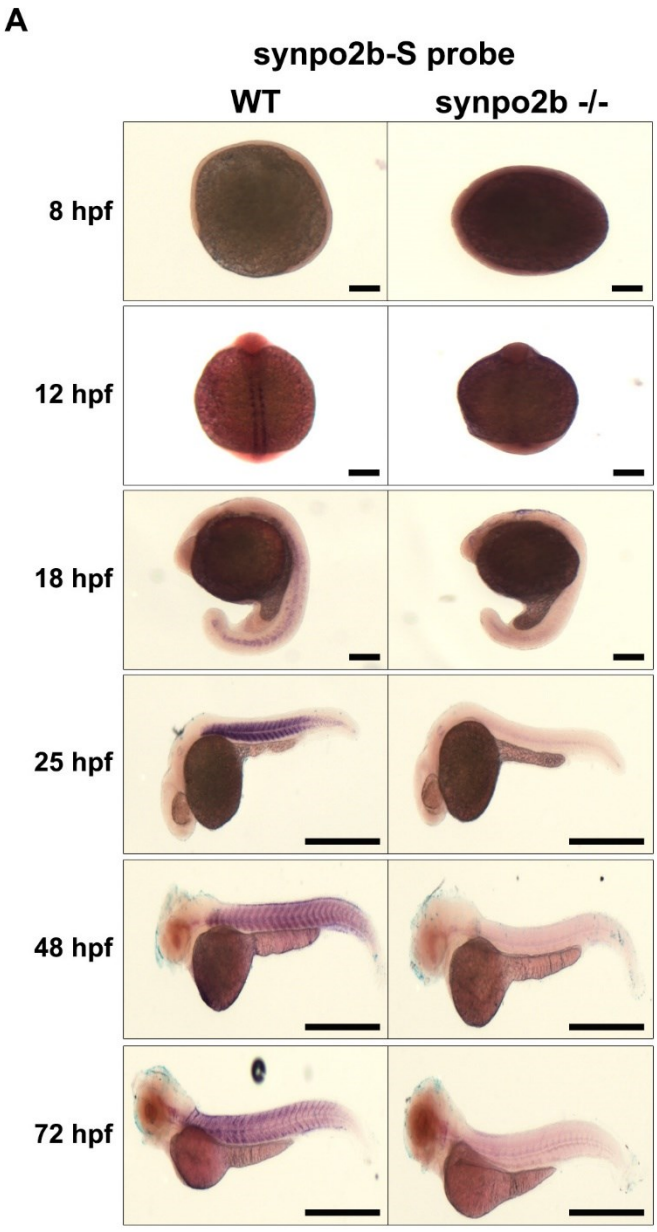
A
synpo2b-S probe
WT
synpo2b -/-
8 hpf
12 hpf
18 hpf
25 hpf
48 hpf
72 hpf

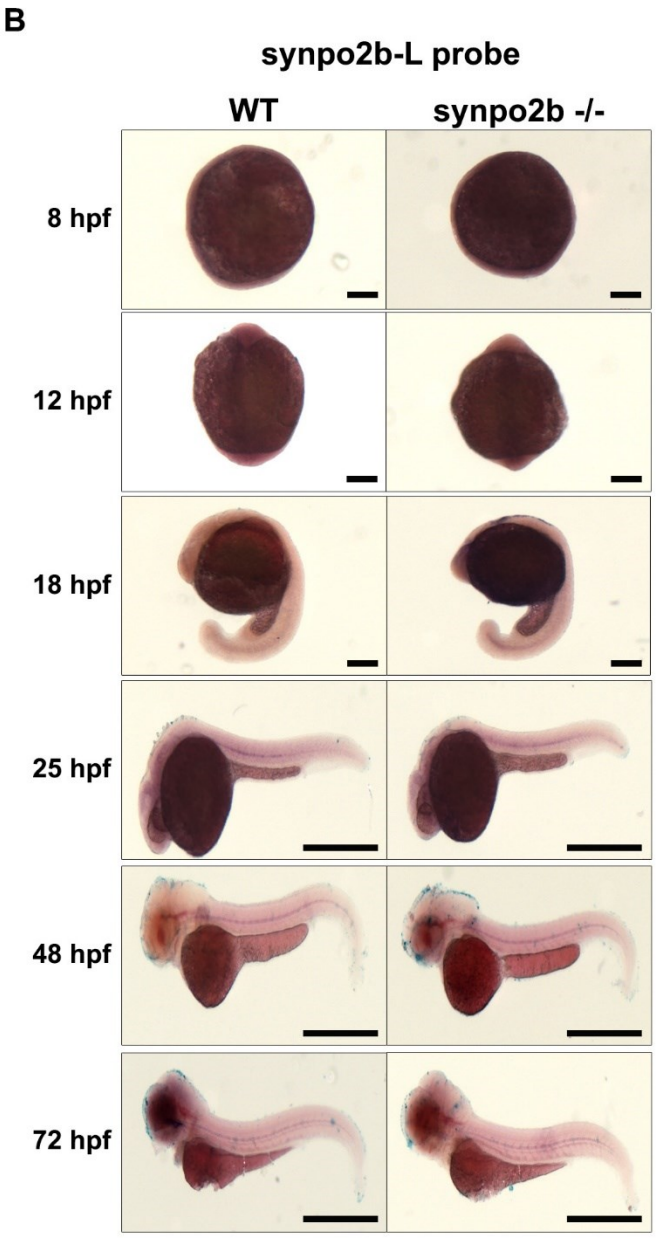

Figure 31: Synpo2b knockout embryos develop normally.
(A) Whole mount *in situ* hybridization of synpo2b-S during different stages of development. (B) Whole mount in situ hybridization of synpo2b-L during different stages of development. In both figures, the left panel represents images of WT embryos and the right panel represents the knockout embryos. Scale bar = 200 μm (8, 12 and 18-hpf) and 500 μm (25, 48 and 72 hpf).

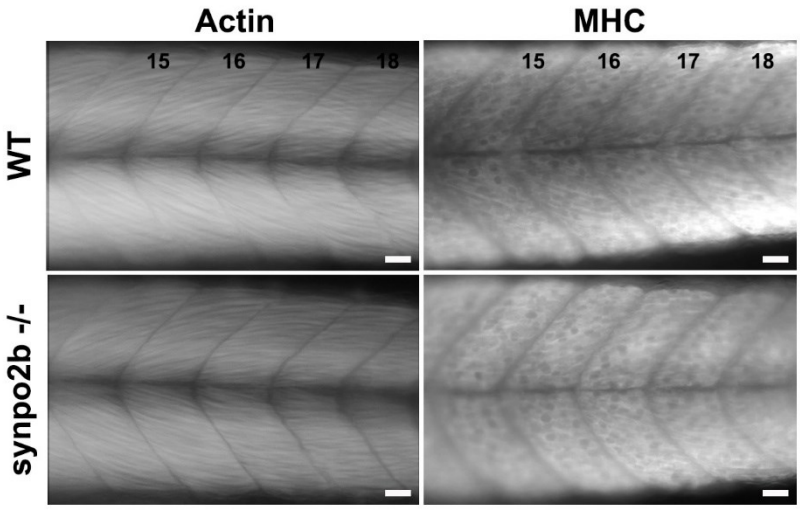

Figure 32: *Synpo2b* knockout does not inhibit myoblast fusion.
Actin and myosin heavy chain (MHC) staining of WT and synpo2b$^{-/-}$ knockout embryos at 48 hpf. The numbers in the images represent the somite number. Scale bar = 20μm.

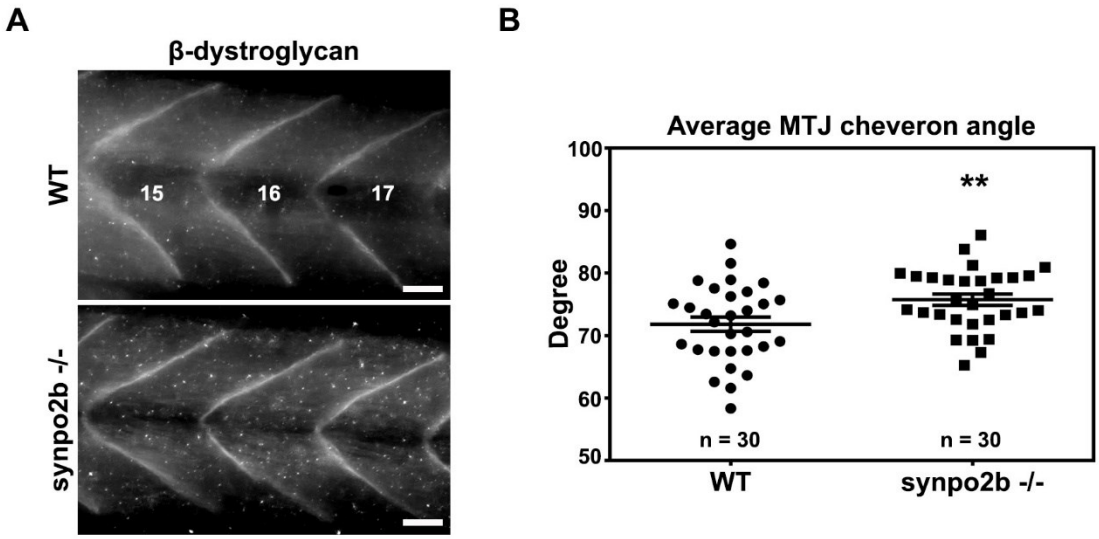

Figure 33: *Synpo2b* knockouts exhibit myotome developmental defects.
(A) β-dystroglycan staining of WT and *synpo2b*$^{-/-}$ knockout embryos at 48 hpf. The numbers in the images represent the somite number. (B) Measurements of the chevron angles from the stained images (A). Numbers in the graph represents the number of embryos quantified. Scale bar = 20 μm. Statistical significance: ** $p < 0.01$.

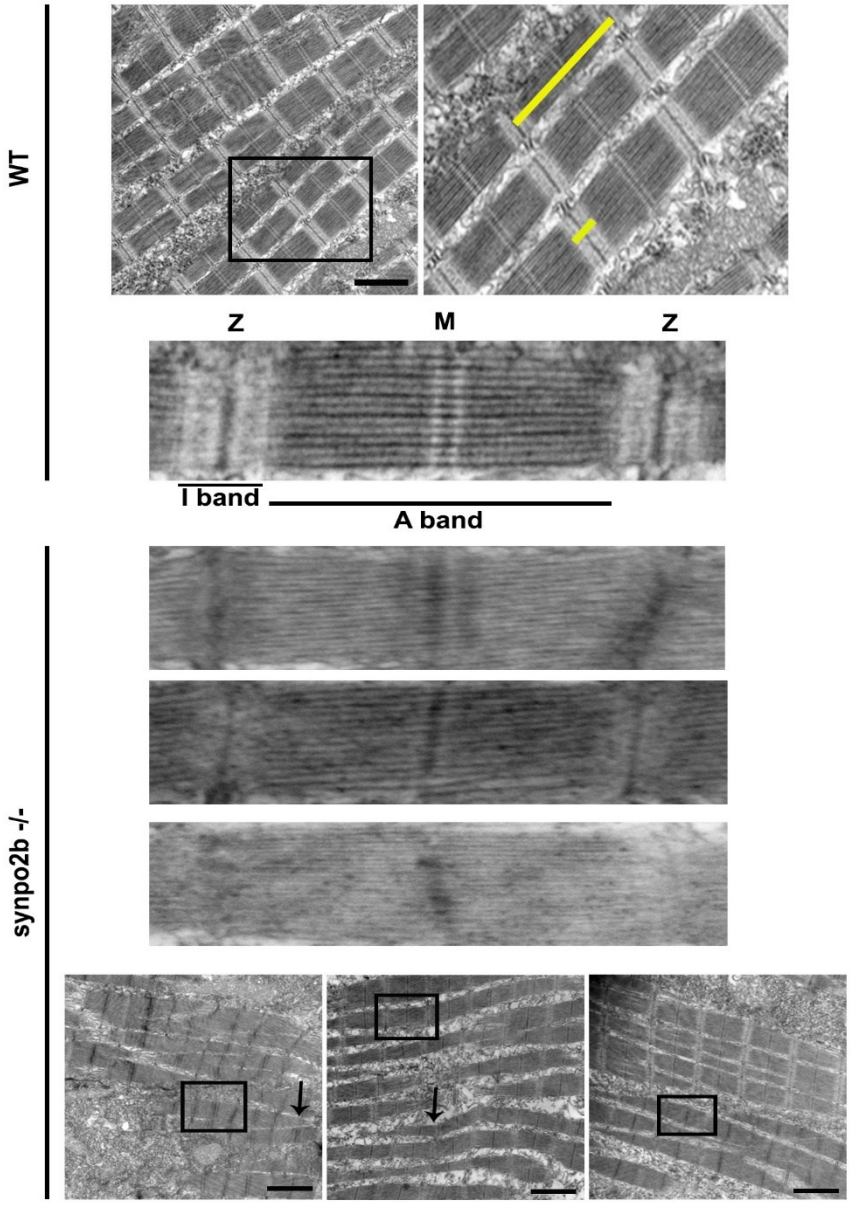

Figure 34: Synpo2b knockout causes ultrastructural changes in myofiber organization.
Electron microscopic images of WT (top panel) and homozygous mutant (-/-) embryos (bottom panel). The right panel of the WT image is the magnified image of the black inset box. The big yellow line in the magnified WT image represents a sarcomere unit, and the small yellow line represents the I-band. The magnified image is a sarcomere of a WT embryo showing the different regions of a sarcomere. The three magnified images of a sarcomere of synpo2b$^{-/-}$ mutant from three different fish; the bottom panel is a zoomed-out image of three mutant fish. The black arrow shows disorganized myofilaments. The black inset box shows the region magnified above.

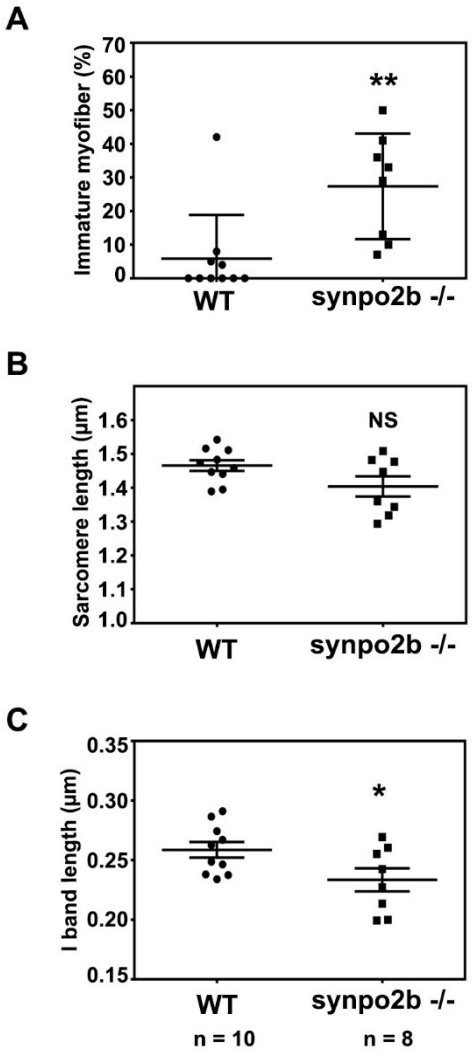

Figure 35: Synpo2b knockout disrupts sarcomeric unit organization.
(A) Percentage of somites containing immature myofibers to the total number of somites imaged in each embryo. (B) Measurements of the sarcomere length from Z-disc to Z-disc in different embryos. (C) Measure of I band length from one I band to the adjacent I band in different embryos. Numbers (n= 10 and n= 8) represent the number of embryos quantified for B, C and D. Scale bar = 800 nm. Statistical significance: * $p < 0.05$; ** $p < 0.01$; NS = Not significant.

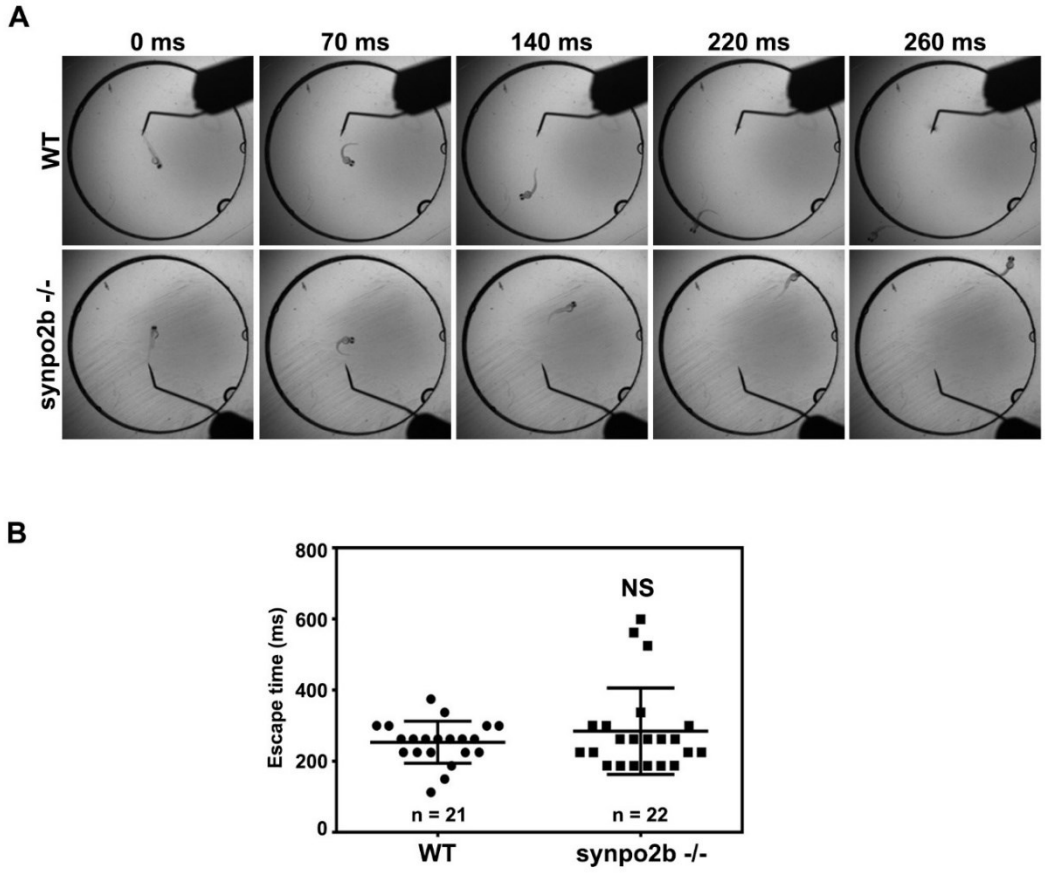

Figure 36: *Synpo2b* knockout does not affect swimming behavior of embryos.
(A) Video frames from a touch-response swimming analysis of WT (top panel) and *synpo2b*$^{-/-}$ knockout (bottom panel) embryos at 48 hpf. Time in milliseconds is shown above each image. (B) Measure of time taken by each embryo to exit the 10 mm diameter circle. The numbers in the graph represent the number of embryos measured. Statistical significance: NS = Not significant.

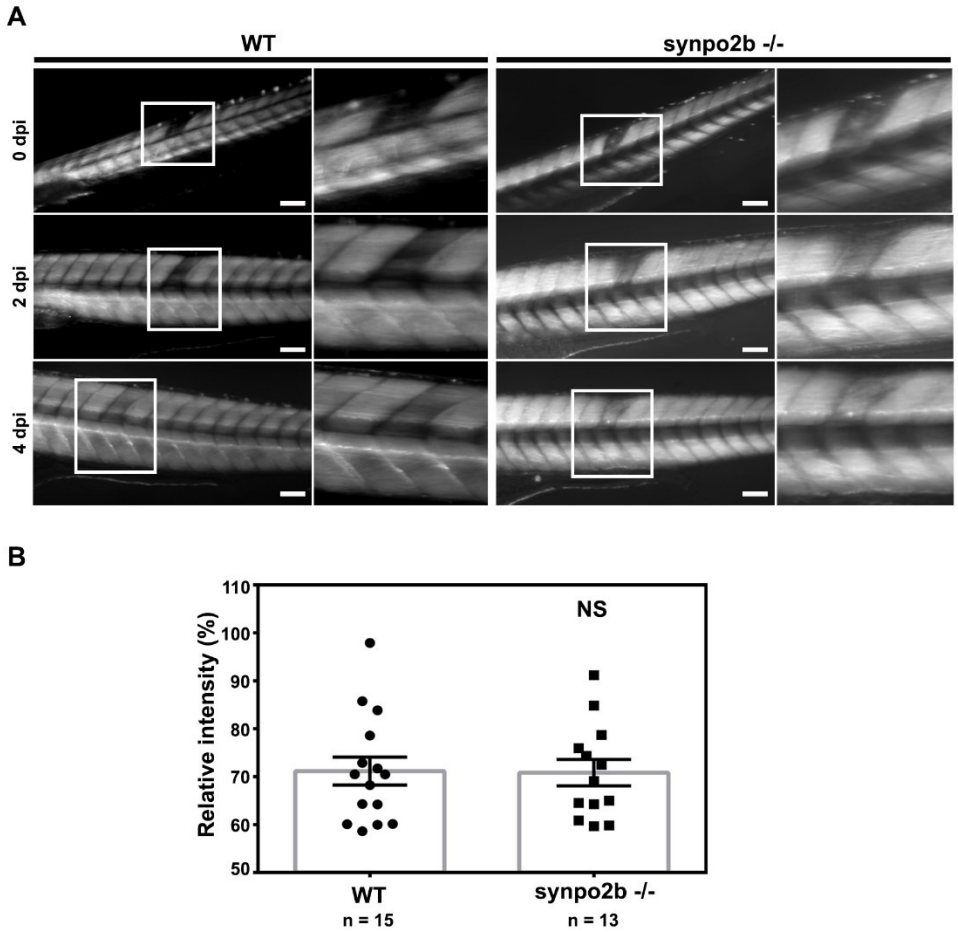

Figure 37: *Synpo2b* knockout does not delay muscle regeneration.
(A) Representative images of laser injured WT and *synpo2b*$^{-/-}$ knockout embryos imaged by birefringence at 0, 2 and 4 days post-injury. (B) Normalized mean grey value of injured somite to an uninjured somite in the same embryo. The numbers in the graph represent the number of embryos measured. Scale bar = 200µm. Statistical significance: NS = Not significant.

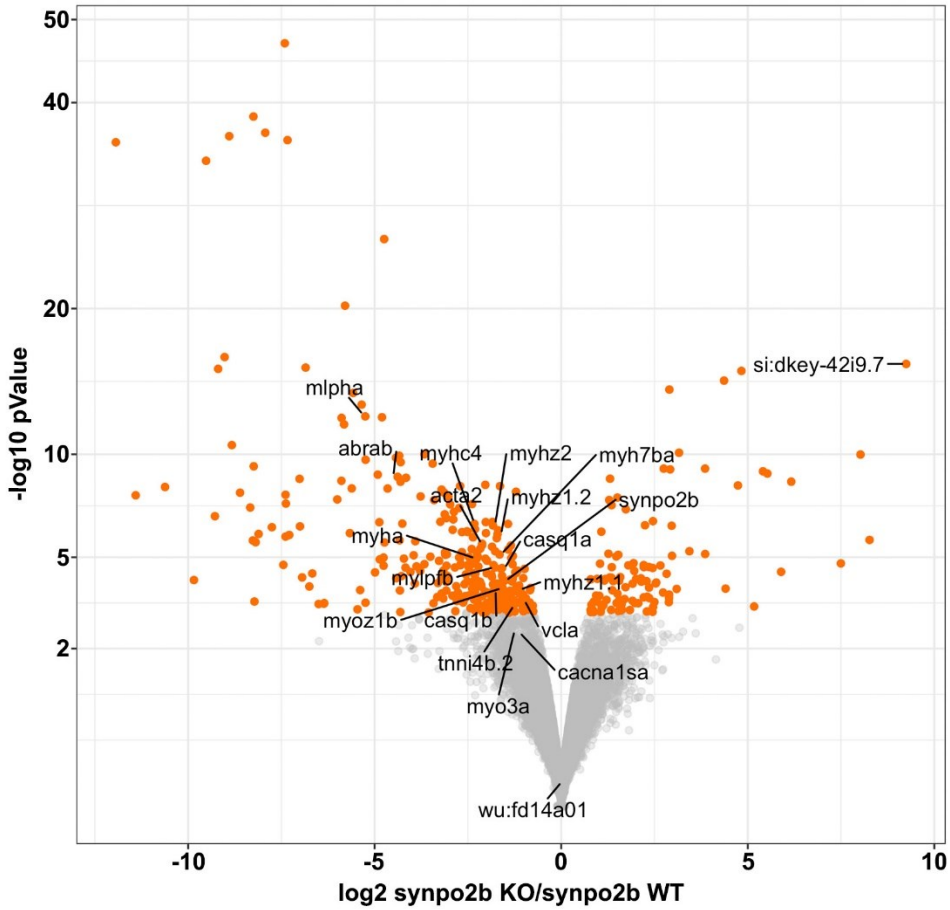

Figure 38: Volcano plot showing the differentially expressed genes.
The grey dots represent the genes not regulated. Orange dots represent the genes significantly up- or downregulated and the dots are plotted based on FDR values. A few of the most significant genes are highlighted.

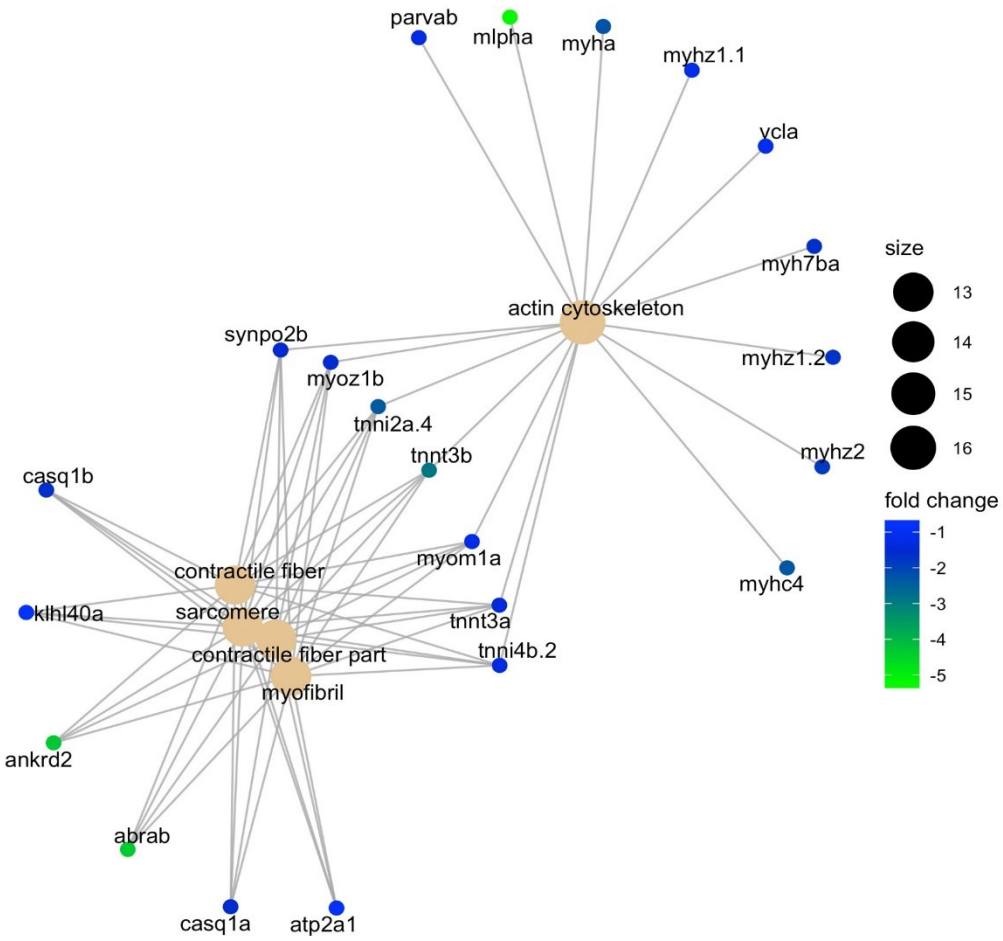

Figure 39: Enrichment GO plot showing the significantly downregulated genes.
The different genes are connected to multiple biological processes by the grey lines. The size of the dots represents the number of genes included in a pathway. For example, dot size 16 represents the actin cytoskeleton dot comprising 16 genes. The color of the dots represents the fold change from -1 to -5. Ankyrin-repeat domain 2 (ankrd2), actin binding Rho activating protein b (Abrab), melanophilin a (Mlpha), myosin heavy chain 4 (Mhc4), myosin heavy chain a (Myha), troponin I type 2a (skeletal, fast) tandem duplicate 4 (Tnni2a.4), troponin T type 3b (skeletal, fast) (Tnnt3b), calsequestrin 1a (Casq1a), Casq1b, synaptopodin2b (Synpo2b), myozenin 1b (Myoz1b), Tnni4b.2, Tnnt3a, myomesin 1a (Myom1a), parvin alpha b (Parvab), myosin heavy polypeptide 1.1 skeletal muscle (Myhz1.1), myosin heavy polypeptide 1.2 skeletal muscle (Myhz1.2), vinculin a (Vcla), myosin heavy chain 7B cardiac muscle beta a (Myh7ba), and myosin heavy polypeptide 2 fast muscle specific (Myhz2).

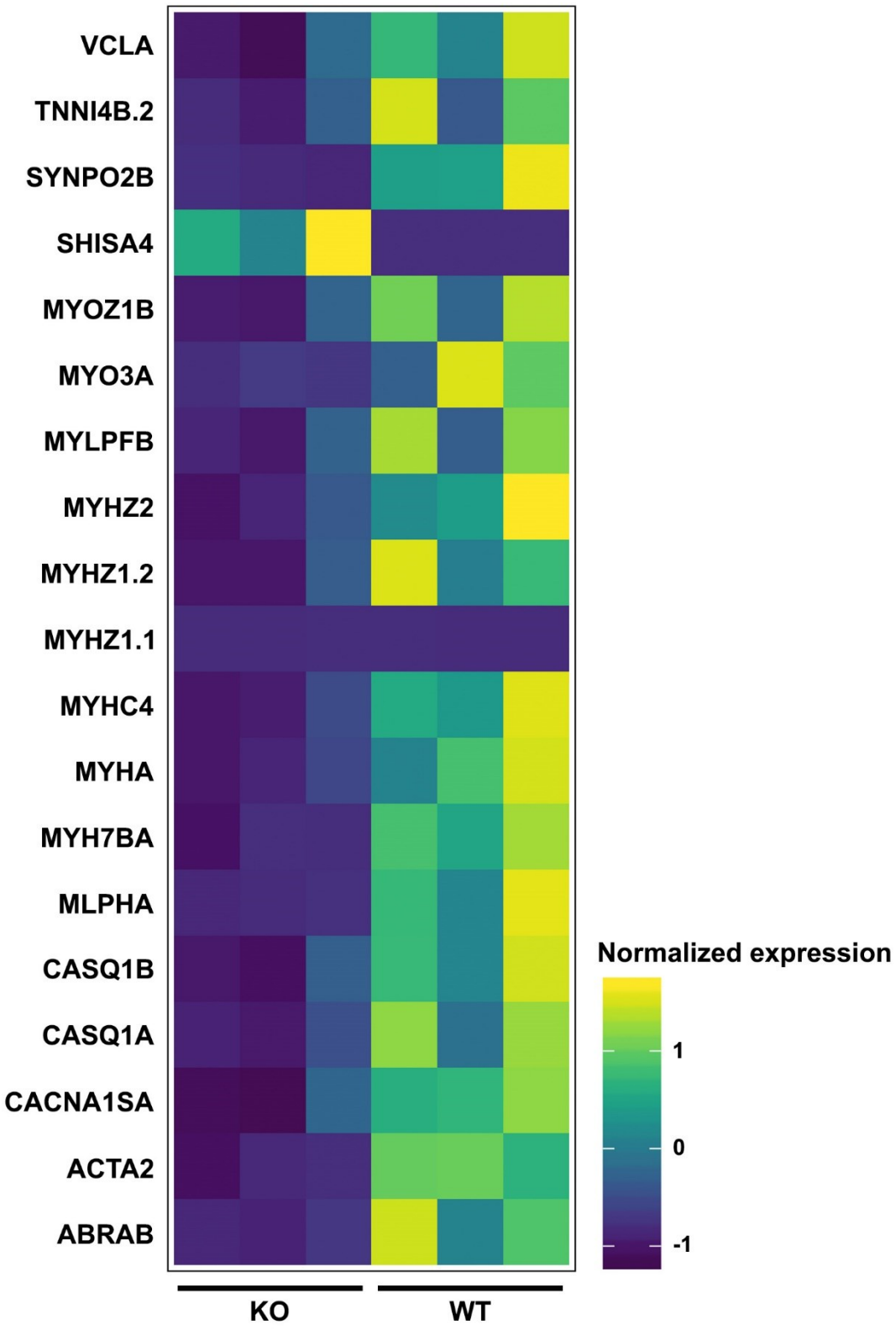
VCLA
TNNI4B.2
SYNPO2B
SHISA4
MYOZ1B
MYO3A
MYLPFB
MYHZ2
MYHZ1.2
MYHZ1.1
MYHC4
MYHA
MYH7BA
MLPHA
CASQ1B
CASQ1A
CACNA1SA
ACTA2
ABRAB
KO
WT
Normalized expression
1
0
-1

Figure 40: Heat map of the significantly downregulated muscle specific genes.
The first three columns represent data from three different sets of synpo2b KO embryos and the next three columns represent data from three different sets of WT embryos. The color corresponds to normalized gene expression. The different genes are: vinculin a (Vcla), troponin I4b tandem duplicate 2 (Tnni4b.2), synaptopodin2b (Synpo2b), shisa family member 4 (Shisa4), myozenin 1b (Myoz1b), myosin IIIA (Myo3a), myosin light chain phosphorylatable fast skeletal muscle b (Mylpfb), myosin heavy polypeptide 2 fast muscle specific (Myhz2), myosin heavy polypeptide 1.2 skeletal muscle (Myhz1.2), myosin heavy polypeptide 1.1 skeletal muscle (Myhz1.1), myosin heavy chain 4 (Mhc4), myosin heavy chain a (Myha), myosin heavy chain 7B cardiac muscle beta a (Myh7ba), melanophilin a (Mlpha), calsequestrin 1a (Casq1a), Casq1b, calcium channel voltage-dependent L type alpha 1S subunit a (Cacna1sa), actin alpha 2 smooth muscle (Acta2), and actin binding Rho activating protein b (Abrab).

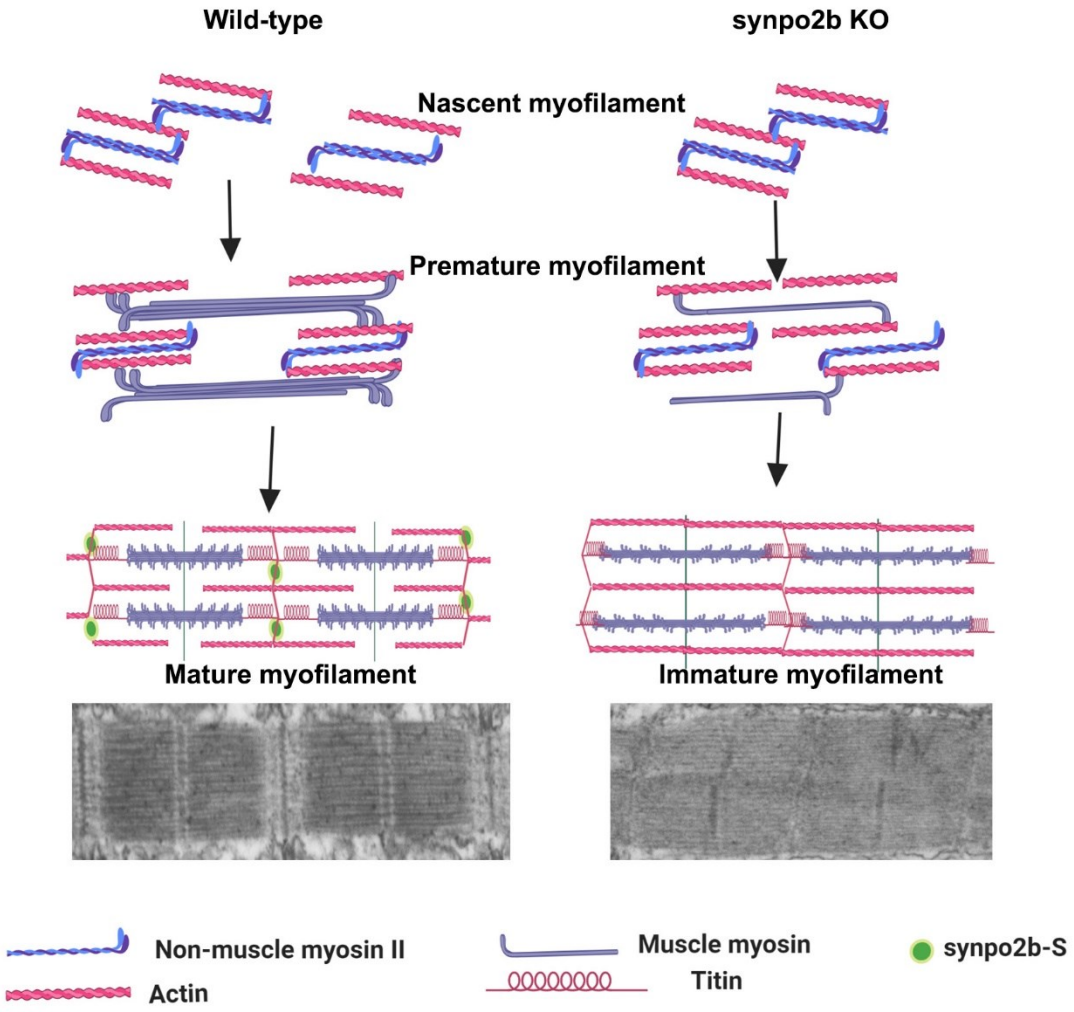

Figure 41: Steps involved during myofibrillogenesis.
Mature myofilaments are formed by building nascent actomyosin filaments containing actin and non-muscle myosin. Muscle myosin arranges between actin filaments to form premature myofilaments along with non-muscle myosin. The final step is the complete replacement of non-muscle myosin with muscle myosin to form mature myofilaments. Panel on the left represents steps involved in wild-type embryos and panel on right represents synpo2b knockout embryos. The electron microscopy image represents properly formed mature myofilaments in wild-type (left) and immature myofilaments in knockout (right) embryos.

Table 5: List of muscle-specific genes that regulate the actin cytoskeleton and muscle contraction which were significantly down-regulated in *synpo2b*$^{-/-}$ embryos

Gene ID	AC	CF	CFP	M	S	Function
Ankrd2		Y	Y	Y	Y	Localize in I band; skeletal muscle development
Abrab		Y	Y	Y	Y	Actin-binding activity
Atp2a1		Y	Y	Y	Y	ATPase activity; contraction and relaxation of skeletal muscle
Mlpha	Y					Actin- and myosin-binding activity
Myhc4	Y					Actin filament-binding activity
Myha	Y					Actin filament-binding activity
Tnni2a.4	Y	Y	Y	Y	Y	Myofibril assembly; troponin complex
Tnnt3b	Y	Y	Y	Y	Y	Calcium-dependent ATPase activity; troponin complex
Casq1b		Y	Y	Y	Y	Skeletal muscle contraction
Casq1a		Y	Y	Y	Y	Skeletal muscle contraction
Synpo2b	Y	Y	Y	Y	Y	Actin-binding and bundling activity
Myoz1b	Y	Y	Y	Y	Y	Localize in Z-disc; Actin-, telethonin-, and FATZ binding activity
Tnni4b.2	Y	Y	Y	Y	Y	Skeletal muscle contraction; troponin complex
Tnnt3a	Y	Y	Y	Y	Y	Sarcomere organization; Calcium-dependent ATPase activity; troponin complex
Myom1a	Y	Y	Y	Y	Y	Muscle contraction
Parvab	Y					Actin-binding activity
Myhz1.1	Y					Somite specification; actin-binding
Myhz1.2	Y					Actin filament-binding activity
Vcla	Y					Sarcomere organization; Heart muscle contraction
Myh7ba	Y					Actin filament-binding activity; cardiac muscle development
Myhz2	Y					Actin filament-binding activity; skeletal muscle development
Klhl40a		Y	Y	Y	Y	Skeletal muscle fiber development

AC: Actin cytoskeleton; CF: Contractile fiber; CFP: Contractile fiber part; M: Myofibril; S: Sarcomere; Y: Yes.

CHAPTER 5: CONCLUSION

The podin family of proteins, synpo1 and synpo2, are proline rich actin-binding proteins reported to specifically regulate kidney podocyte migration and cancer cell migration, respectively. Human SYNPO2 is a biomarker for prostate cancer and exerts variable effects on cancer cell migration depending on the cell type and external stimuli. The known key features of synpo2 in the myogenesis field are as follows: (1) human and mouse SYNPO2 are expressed in both skeletal and smooth muscle; (2) SYNPO2 binds, polymerizes and nucleates actin to form F-actin filaments; (3) human and mouse SYNPO2 has been shown to localize in the nucleus of undifferentiated C2C12 myoblast cells and along actin filaments in differentiated myoblasts and myotubes; (4) mouse SYNPO2 has also been shown to shuttle from the cytoplasm to nucleus under stress conditions in myotubes: and (5) in mature skeletal muscle fibers, synpo2 localizes in the Z-disc. Though synpo2 is known to be expressed in skeletal muscle, its exact function during myogenesis has not been examined. My project aimed to investigate the functional role of different synpo2 isoforms during myogenesis using an *in vitro* mouse model of early myogenesis and an *in vivo* zebrafish model of muscle development, maintenance and regeneration. My results established that expression of only the short isoform of mouse SYNPO2 is differentially regulated and is required for efficient myotube formation in mouse myoblasts, and that the short zebrafish Synpo2b-S isoform is required for efficient myofiber maturation and organization.

From the *in vitro* ectopic studies, I showed that the short isoform, SYNPO2As, increased migration in a ROCK-independent manner but increased fusion in a ROCK-sensitive manner (Fig. 17B and C). Further, I also showed that migration and fusion are not directly correlated, since all SYNPO2 isoforms increased myoblast migration but only SYNPO2As increased fusion. From the literature, the lack of a correlation between migration and fusion is an unusual phenotype for an actin remodelling protein involved in myoblast fusion. The canonical RhoA-ROCK pathway is a major pathway regulating cell migration whereby ROCK phosphorylates MLC that participates in actomyosin contraction. In fibroblasts, increased pMLC levels and increased pMLC turnover leads to membrane ruffles at the cell front and enhanced migration (Matsumura & Hartshorne,

2008; Totsukawa et al., 2004). However, MLC can also be phosphorylated by MLCK in a ROCK-independent non-canonical pathway (Fig. 42 top panel), a possible mechanism by which SYNPO2As could be upregulating migration. Since migration is not directly correlated with fusion, I will focus the remainder of this discussion on possible mechanisms by which SYNPO2As could be regulating myoblast fusion.

To help frame this discussion I propose a hypothetical model of how synpo2 could promote myoblast fusion (Fig. 42). This model incorporates the known function of synpo2 as an actin remodeller with my results showing synpo2 does not grossly alter the actin or actomyosin cytoskeleton. As discussed in Chapter 3, we hypothesized that SYNPO2As could be regulating myoblast fusion by regulating actin dynamics and recruiting other actin-regulating proteins at the fusion synapse (Fig. 20). A recent study showed the formation of an actin focus along with actin-regulating protein such as TKS5 and DYN2 in mouse myoblasts undergoing fusion to myotubes in an asymmetric manner (Chuang et al., 2019). However, I hypothesize that SYNPO2As, via its effects on F-actin, might also enhance myoblast fusion by increasing transcription of late-differentiation genes to accelerate the downstream myogenic program. While carefully analyzing the data, I noticed that overexpression of SYNPO2As increased the number of differentiated cells observed by MHC staining on 2 dpi compared to mock cells (Fig. 43A). To determine whether the increase in the fusion phenotype was due to increased levels of the differentiation-related proteins, we carried out western blotting for MYOD, myogenin and MHC. Qualitatively, there was no appreciable change in the levels of these proteins (Fig. 15A). However, quantification of blots from three independent experiments showed that on day 2 post-differentiation, ectopic expression of SYNPO2A and B increased MHC levels by ~2-fold while SYNPO2As increased MHC levels by ~4-fold compared to mock cells (Fig. 43B). MHC levels were not increased in cells where SYNPO2 expression was knocked down, and similar analysis showed the SYNPO2 isoforms did not alter the levels of the early myogenic proteins MYOD and myogenin (Fig. 43B). These results suggest SYNPO2 expression may accelerate the downstream myogenic program resulting in more efficient myotube formation.

How might SYNPO2, an actin remodelling protein, regulate expression of a late differentiation protein such as MHC? Although SYNPO2As has been reported to localize

in the nucleus of undifferentiated myoblasts (Weins et al., 2001), we did not observe strong nuclear localization with the available commercial antibody (Fig. 19B), suggesting that if SYNPO2 does affect the transcription pattern in cells, it may do so functioning as an indirect transcriptional regulator. However, SYNPO2As is also a Z-disc associated protein and some such proteins are known to be involved in signalling through downstream effectors to maintain muscle integrity. I hypothesize that SYNPO2As could act as an indirect transcriptional regulator by polymerizing actin or regulating other actin-regulating pathways, as diagrammed in Fig 42.

Apart from MYOD and MYF5 that play a role in transcription of early differentiation-related genes, there are few known proteins that regulate transcription of late differentiation genes. The two known pathways are an actin polymerization-dependent pathway involving serum response factor (SRF) and myocardin-related transcription factor (MRTF), and an actin-independent pathway involving down regulation of the RhoA-ROCK pathway to activate the forkhead in rhabdomyosarcoma (FKHR)/forkhead box protein O1 (FOXO1) pathway. Both these pathways are involved in specifically transcribing late differentiation genes such as MHC, creatine kinase, prosaposin, frizzled-4 and others (Bois & Grosveld, 2003; Wallace et al., 2016) that increase the rate of myoblast fusion. Similarly, SYNPO2As could be increasing transcription of late differentiation genes by regulating one or both of the above-mentioned pathways, as discussed below.

Increased levels of G-actin sequester the transcription factor MRTF in the cytoplasm. Actin polymerization depletes G-actin levels in the cytoplasm and releases myocardin-related transcription factor (MRTF) into the nucleus that binds serum response factor (SRF) to initiate muscle-specific gene transcription (Sotiropoulos et al., 1999). Several actin regulating proteins such as the Rho-GTPases, LIMK1 and mDIA can activate SRF by polymerizing actin (Miralles et al., 2003). The coactivator of SRF, MRTF, is a heart muscle specific protein, however, it has been shown to play a role with SRF in several normal and cancerous cell lines (Gau & Roy, 2018); MRTF is phosphorylated and sequestered by G-actin in the cytoplasm; increased G-actin uptake to form F-actin by actin-binding proteins and the Rho-ROCK pathway releases MRTF into the nucleus to bind SRF and initiate transcription (Duggirala et al., 2015). In myoblast cell lines, the striated muscle activator of Rho signalling (STARS) protein, an actin-binding protein that activates RhoA-

ROCK to polymerize actin also activates SRF but in a MRTF-independent mechanism to transcribe genes such as creatine kinase mitochondrial 2 (CKM2), creatine kinase muscle (CKM), myosin heavy chain 4 (MHC-IIb), MYF5 and MYF6 but not myogenin (Arai et al., 2002; Wallace et al., 2016). Both STARS and SYNPO2As are actin-binding and polymerizing proteins that are transcriptionally regulated by SRF (Arai et al., 2002; Turczyńska et al., 2015). Thus, SYNPO2As could regulate the MRTF-SRF pathway by nucleating or polymerizing G-actin in a Rho-ROCK-dependent manner thereby releasing MRTF to transcribe late differentiation genes and increase the rate of myoblast fusion, or SYNPO2As could activate SRF via Rho signalling independent of MRTF, similar to STARS (Fig. 42 right panel).

We did not observe gross F-actin changes in knockdown cells or cells ectopically expressing SYNPO2As. In such a case, how could SYNPO2As utilize G-actin levels to regulate transcription? SYNPO2As could be polymerizing actin at the periphery of cells to promote fusion synapse formation, similar to how human SYNPO2As in PC3 cells polymerizes actin at the leading cell edge to promote migration. Such localized actin polymerization or nucleation events may be enough to release sufficient MRTF into the nucleus to drive late myogenic gene transcription (Fig. 42 right panel). As previously discussed, a careful spatiotemporal analysis of actin dynamics in fusing mouse myoblasts, as recently employed to identify a TKS5-DYN2 actin fusion foci in C2C12 cells (Chuang et al., 2019), is needed to test this hypothesis.

The other pathway that regulates transcription of late differentiation genes is the Rho-ROCK pathway via FKHR. The RhoA-ROCK pathway is a canonical pathway that regulates actomyosin contraction and cell migration but is inhibitory to fusion. Activated ROCK phosphorylates FKHR and retains it in the cytoplasm. Down regulation of ROCK post-differentiation dephosphorylates FKHR, resulting in nuclear localization and transcription of late-differentiation genes such as prosaponin, frizzled-4, slow myosin heavy chain, procollagen types V and XVIII, fibulin-2 and ankyrin-3 that play a role in myoblast fusion (Bois & Grosveld, 2003; Nishiyama et al., 2004). We showed that SYNPO2As-enhanced fusion was sensitive to ROCK inhibition (Fig. 17B and C), consistent with a role for the Rho-ROCK pathway in the mechanism by which SYNPO2As enhances myotube formation. I hypothesize that SYNPO2As might block ROCK

activation, thereby promoting activation of the FKHR pathway and accelerating the late differentiation program. In mock-transduced cells, the inhibitory role of ROCK on fusion is removed by treatment with the ROCK inhibitor and fusion increases (Fig. 17B). In SYNPO2As cells, if early SYNPO2As overexpression itself inhibits ROCK activity, then the ROCK inhibitor would be ineffective (Fig. 17B). In this scenario, SYNPO2As functions as a promyogenic factor by blocking a myogenic repressor, ROCK. This hypothesis is, however, at odds with the demonstrated ability of both Synpo1 and Synpo2 to stimulate the Rho-ROCK pathway in podocytes and prostate cancer cells.

An alternative hypothesis is that ROCK somehow activates synpo2 and increases the MRTF/SRF pathway (Fig. 42). Studies have shown that Synpo2 is phosphorylated by several kinases such as PKG, ERK, PKC and ROCK (Huang et al., 2006; Reimann et al., 2017; Yura et al., 2016). The function of such phosphorylation sites is yet to be determined, especially for ROCK. ROCK could phosphorylate SYNPO2As, thereby inhibiting the ability of synpo2 to activate the MRTF pathway. The ROCK inhibitor alone would increase FKHR nuclear localization and transcription, increasing fusion and masking the enhancing effects of synpo2 functioning through the MRTF pathway. Conversely, ROCK phosphorylation of synpo2 could be a positive regulator of the MRTF pathway, in which case ROCK inhibition would prevent synpo2 activation of this pathway and enhanced myogenesis. Since several open questions need to be answered with respect to ROCK and SYNPO2As during myoblast fusion, I use the term ROCK-sensitive rather than ROCK-dependent (Fig. 42 left panel). Clearly, a detailed analysis of the effects of synpo2 on the Rho-ROCK, FKHR and MRTF pathways is warranted and might be informative.

There are two potential inconsistencies between my data and the hypothetical model. First, the two long isoforms SYNPO2A and B also increased MHC expression, albeit to much lower levels than induced by SYNPO2As (i.e., 2-fold versus 4-fold, respectively) but decreased myoblast fusion. The slight increase in MHC induced by the long isoforms could possibly be because of the conserved actin binding regions present in all three isoforms that lead to actin polymerization and sequestering of G-actin, thereby releasing MRTF into the nucleus to transcribe late differentiation genes. However, due to possible recruitment of unique cofactors by the PDZ domain present in the long synpo2 isoforms, these isoforms may generate a multiprotein complex that regulates actin

dynamics in a manner incompatible with fusion synapse formation or myoblast fusion. The second inconsistency was quantification of MHC expression from western blots of lysates from synpo2 knockdown cells did not show any difference in the MHC levels compared to cells treated with a non-targeting shRNA (Fig. 15B and 43C). The absence of a significant reduction of MHC in the knockdown cells could be due to only partial knockdown of SYNPO2As (Fig. 13B). Moreover, western blots are difficult to accurately quantify, and I only examined expression of MHC, not other late differentiation markers that could also be upregulated. In addition, the myosin antibody I used (MF-20) is a pan antibody that recognizes all myosin isoforms. Hence, further studies such as quantification of nuclear localized MRTF and FKHR levels, qRT-PCR analysis of several late differentiation transcripts, and/or the use of isoform-specific myosin antibodies are needed to test the above assumptions and establish whether SYNPO2As utilizes one or both of above-mentioned pathways to regulate transcription and myoblast fusion.

My proposed transcriptional regulatory role for synpo2 in myogenesis is also compatible with my zebrafish knockout model in which several late differentiation related/myofibril proteins are downregulated. Like the upregulation of MHC in mouse myoblasts in an ectopic system, most of the significantly downregulated muscle specific genes in the zebrafish knockout model are different types of myosin isoforms (Fig. 39 and 40). One of the most interesting hits from the RNA seq data is the zebrafish actin binding Rho activating protein b (Abrab), whose mouse ortholog is STARS. As mentioned before, STARS plays an essential role in the SRF pathway during myogenesis and STARS localizes in the I-band of skeletal muscle (Arai et al., 2002; Wallace et al., 2016), one of the muscle regions that showed abnormal development in the knockout embryos. Assuming Abrab also localizes to the I-band in zebrafish muscle, downregulated Abrab expression could result in atypical I-band formation. Furthermore, the downregulation of numerous myofibrillar genes in the knockout embryos is consistent with a role for synpo2 in regulating late myogenic gene expression to promote efficient, normal myofibrillogenesis (Figs. 34 and 35A). The relationship, if any, between Synpo2b and Abrab is unknown. The absence or reduced expression of two actin-polymerizing proteins, Synpo2b and Abrab, could restrain the SRF pathway resulting in significant downregulation of myofibril genes.

A qRT-PCR analysis should be carried out in the knockout model for Abrab and other down-regulated transcripts to confirm the RNA-seq data.

The data obtained from ultrastructural analysis of *synpo2b*$^{-/-}$ knockout embryos clearly suggested that Synpo2b is required for myofibril organization during development of zebrafish skeletal muscle. This developmental defect did not affect muscle performance as assessed from the swimming and injury assay. However, these experiments were carried out on 2 dpf and 4 dpf, respectively. At these time points the embryos are not actively swimming when compared to adult fish. Therefore, these experiments should be carried out in older fish to assess if the myofibril defects affect muscle performance leading to muscle damage. This data would further strengthen our understanding whether Synpo2b is required for muscle maintenance, as muscle fibers could be constantly damaged during active muscle usage and regeneration during aging.

Thus, both my *in vitro* and *in vivo* studies identified synpo2 as a new promyogenic factor and suggested a potential role for Synpo2 as an actin-mediated transcriptional regulator, a new function for synpo2 in muscle cells.

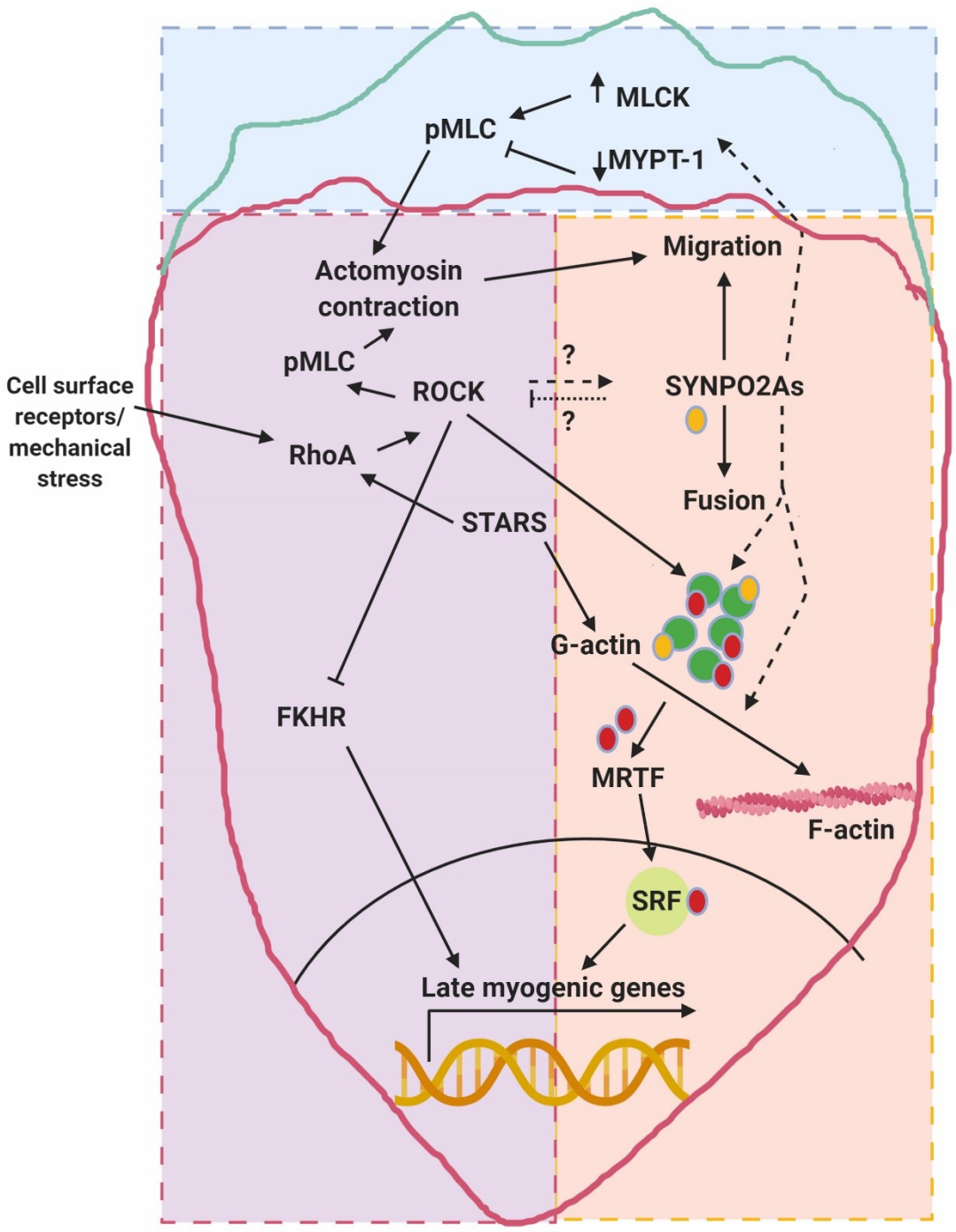
MLCK
pMLC
MYPT-1
Migration
Actomyosin
contraction
pMLC
?
ROCK
?
SYNPO2As
Cell surface
receptors/
mechanical
stress
RhoA
Fusion
STARS
G-actin
FKHR
MRTF
F-actin
SRF
Late myogenic genes

Figure 42: Model depicting possible roles of SYNPO2As during myogenesis.
Black arrows are known functions and dotted arrows are possible functions. Top panel: Possible mechanism by which SYNPO2As regulates myoblast migration. Synpo2As could increase myosin light chain kinase (MLCK) levels and/or decrease myosin phosphatase target subunit-1 (MYPT-1) in the cell front which in turn increases pMLC levels. This increased pMLC levels could increase actomyosin contractility and influence myoblast migration. Left panel: Canonical RhoA-ROCK pathway: RhoA can be activated by cell surface receptors or mechanical stress. RhoA activates ROCK that in turn phosphorylates myosin light chain (pMLC); pMLC plays a role in actomyosin contraction. RhoA-ROCK pathway can activate the SRF pathway by polymerizing G-actin to F-actin. STARS, an actin-binding protein, can activate Rho-ROCK mediated actin polymerization and in turn activate SRF mediated transcription. ROCK kinase also phosphorylates forkhead in rhabdomyosarcoma (FKHR) and inhibits nuclear translocation. Dephosphorylated FKHR translocate to nucleus and transcribes late-differentiation genes. SYNPO2As might inhibit ROCK activity to enhance FKHR-mediated transcription, and/or ROCK could phosphorylate SYNPO2As to inhibit the inhibitory effect. Right panel: Another pathway that regulates transcription of late myogenic genes is the myocardin-related transcription factor (MRTF)-serum response factor (SRF) complex. MRTF is sequestered by G-actin in the cytoplasm. Activation of actin polymerization releases MRTF which translocates into the nucleus and interacts with SRF to drive transcription. SYNPO2As could directly be involved in actin polymerization to activate the MRTF-SRF pathway or sequester G-actin to initiate nucleation thereby releasing MRTF into the nucleus.

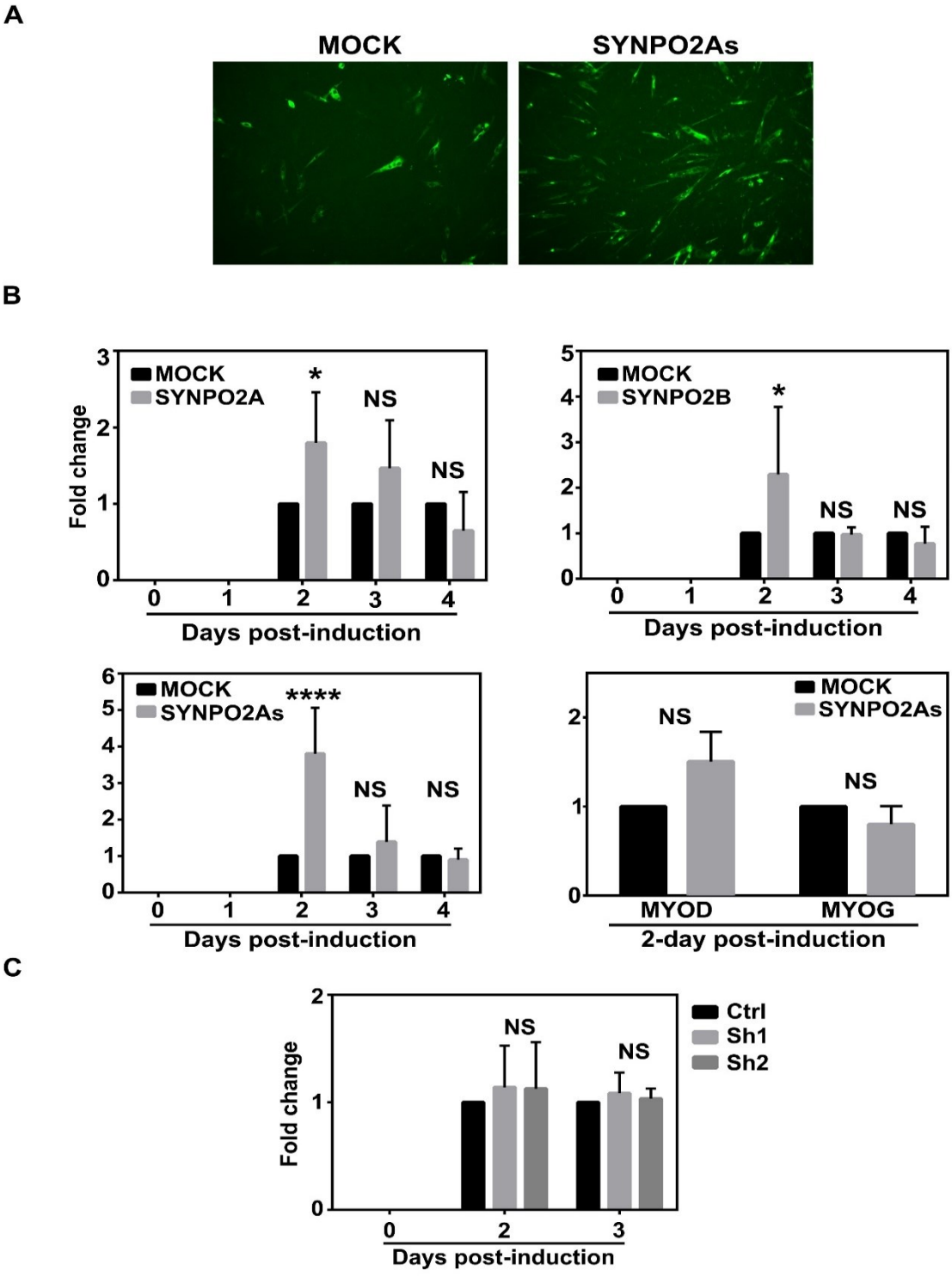
A
MOCK
SYNPO2As
B
MOCK
SYNPO2A
Fold change
Days post-induction
MOCK
SYNPO2B
Days post-induction
MOCK
SYNPO2As
Days post-induction
MOCK
SYNPO2As
MYOD
MYOG
2-day post-induction
C
Ctrl
Sh1
Sh2
Fold change
Days post-induction

Figure 43: SYNPO2 isoforms enhances MHC expression post-differentiation.
(A) Representative images of mock and SYNPO2As cells fixed on 2 dpi and stained with anti-MHC antibody and Alexa fluor 488-conjugated secondary antibody (green). (B) Quantified data of MHC western blots of SYNPO2A, B and As cell lysates collected at 0-4 dpi and probed with anti-MHC antibody (blot images in Fig. 13A), and MYOD and MYOG blots of SYNPO2As at 2 dpi. (C) Quantified data of MHC western blots of control, shRNA1 (Sh1) and shRNA2 (Sh2) cell lysates collected at 0, 2 and 3 dpi and probed with anti-MHC antibody (blot images in Fig. 13B). Statistical significance: *p value < 0.05, ****p value < 0.001, and NS = Not significant.

BIBLIOGRAPHY

Alvarez-Múgica, M., Cebrian, V., Fernández-Gómez, J. M., Fresno, F., Escaf, S., & Sánchez-Carbayo, M. (2010). Myopodin methylation is associated with clinical outcome in patients with T1G3 bladder cancer. *Journal of Urology*. https://doi.org/10.1016/j.juro.2010.05.085

Arai, A., Spencer, J. A., & Olson, E. N. (2002). STARS, a striated muscle activator of Rho signaling and serum response factor-dependent transcription. *Journal of Biological Chemistry*. https://doi.org/10.1074/jbc.M202216200

Artero, R. D., Castanon, I., & Baylies, M. K. (2001). The immunoglobulin-like protein Hibris functions as a dose-dependent regulator of myoblast fusion and is differentially controlled by Ras and Notch signaling. *Development (Cambridge, England)*.

Asanuma, K., Kim, K., Oh, J., Giardino, L., Chabanis, S., Faul, C., … Mundel, P. (2005). Synaptopodin regulates the actin-bundling activity of α-actinin in an isoform-specific manner. *Journal of Clinical Investigation*. https://doi.org/10.1172/JCI200523371

Asanuma, K., Yanagida-Asanuma, E., Faul, C., Tomino, Y., Kim, K., & Mundel, P. (2006). Synaptopodin orchestrates actin organization and cell motility via regulation of RhoA signalling. *Nature Cell Biology*. https://doi.org/10.1038/ncb1400

Avirneni-Vadlamudi, U., Galindo, K. A., Endicott, T. R., Paulson, V., Cameron, S., & Galindo, R. L. (2012). Drosophila and mammalian models uncover a role for the myoblast fusion gene TANC1 in rhabdomyosarcoma. *Journal of Clinical Investigation*. https://doi.org/10.1172/JCI59877

Baas, D., Caussanel-Boude, S., Guiraud, A., Calhabeu, F., Delaune, E., Pilot, F., … Goillot, E. (2012). CKIP-1 regulates mammalian and zebrafish myoblast fusion. *Journal of Cell Science*. https://doi.org/10.1242/jcs.101048

Baas, Dominique, Caussanel-Boude, S., Guiraud, A., Calhabeu, F., Delaune, E., Pilot, F., … Goillot, E. (2012). CKIP-1 regulates mammalian and zebrafish myoblast fusion. *Journal of Cell Science*. https://doi.org/10.1242/jcs.101048

Bach, A.-S., Enjalbert, S., Comunale, F., Bodin, S., Vitale, N., Charrasse, S., & Gauthier-Rouviere, C. (2010). ADP-Ribosylation Factor 6 Regulates Mammalian Myoblast Fusion through Phospholipase D1 and Phosphatidylinositol 4,5-Bisphosphate Signaling Pathways. *Molecular Biology of the Cell*. https://doi.org/10.1091/mbc.e09-12-1063

Bae, G. U., Gaio, U., Yang, Y. J., Lee, H. J., Kang, J. S., & Krauss, R. S. (2008). Regulation of myoblast motility and fusion by the CXCR4-associated sialomucin, CD164. *Journal of Biological Chemistry*. https://doi.org/10.1074/jbc.M706730200

Baylies, M. K., Bate, M., & Gomez, M. R. (1998). Myogenesis: A view from Drosophila. *Cell*. https://doi.org/10.1016/S0092-8674(00)81198-8

Beall, B., & Chalovich, J. M. (2001). Fesselin, a synaptopodin-like protein, stimulates actin nucleation and polymerization. *Biochemistry*. https://doi.org/10.1021/bi011806u

Bedford, M. T., Sarbassova, D., Xu, J., Leder, P., & Yaffe, M. B. (2000). A novel Pro-Arg motif recognized by WW domains. *Journal of Biological Chemistry*. https://doi.org/10.1074/jbc.275.14.10359

Berger, S., Schafer, G., Kesper, D. A., Holz, A., Eriksson, T., Palmer, R. H., … Onel, S.-F. (2008). WASP and SCAR have distinct roles in activating the Arp2/3 complex during myoblast fusion. *Journal of Cell Science*. https://doi.org/10.1242/jcs.022269

Bi, P., Ramirez-Martinez, A., Li, H., Cannavino, J., McAnally, J. R., Shelton, J. M., … Olson, E. N. (2017). Control of muscle formation by the fusogenic micropeptide myomixer. *Science*, *356*(6335), 323–327. https://doi.org/10.1126/science.aam9361

Blau, H. M., Pavlath, G. K., Hardeman, E. C., Chiu, C. P., Silberstein, L., Webster, S. G., … Webster, C. (1985). Plasticity of the differentiated state. *Science*. https://doi.org/10.1126/science.2414846

Bois, P. R. J., & Grosveld, G. C. (2003). FKHR (FOXO1a) is required for myotube fusion of primary mouse myoblasts. *EMBO Journal*. https://doi.org/10.1093/emboj/cdg116

Bondesen, B. A., Jones, K. A., Glasgow, W. C., & Pavlath, G. K. (2007). Inhibition of myoblast migration by prostacyclin is associated with enhanced cell fusion. *The FASEB Journal*. https://doi.org/10.1096/fj.06-7070com

Boskovic, S., Marín-Juez, R., Jasnic, J., Reischauer, S., Sammak, H. El, Kojic, A., … Kojic, S. (2018). Characterization of zebrafish (Danio rerio) muscle ankyrin repeat proteins reveals their conserved response to endurance exercise. *PLoS ONE*. https://doi.org/10.1371/journal.pone.0204312

Bothe, I., Deng, S., & Baylies, M. (2014). PI(4,5)P2 regulates myoblast fusion through Arp2/3 regulator localization at the fusion site. *Journal of Cell Science*. https://doi.org/10.1242/jcs.157057

Bour, B. A., Chakravarti, M., West, J. M., & Abmayr, S. M. (2000). Drosophila SNS, a member of the immunoglobulin superfamily that is essential for myoblast fusion. *Genes and Development*.

Brukman, N. G., Uygur, B., Podbilewicz, B., & Chernomordik, L. V. (2019). How cells fuse. *Journal of Cell Biology*. https://doi.org/10.1083/jcb.201901017

Brzóska, E., Bello, V., Darribère, T., & Moraczewski, J. (2006). Integrin α3 subunit participates in myoblast adhesion and fusion in vitro. *Differentiation*. https://doi.org/10.1111/j.1432-0436.2005.00059.x

Bührdel, J. B., Hirth, S., Keßler, M., Westphal, S., Forster, M., Manta, L., … Just, S. (2015). In vivo characterization of human myofibrillar myopathy genes in zebrafish. *Biochemical and Biophysical Research Communications*. https://doi.org/10.1016/j.bbrc.2015.03.149

Buvall, L., Rashmi, P., Lopez-Rivera, E., Andreeva, S., Weins, A., Wallentin, H., … Mundel, P. (2013). Proteasomal degradation of Nck1 but not Nck2 regulates RhoA activation and actin dynamics. *Nature Communications*. https://doi.org/10.1038/ncomms3863

Carmena, A., Bate, M., & Jimenez, F. (1995). lethal of scute, a proneural gene, participates m the specification of muscle progenitors during Drosophila embryogenesis. *Genes and Development*. https://doi.org/10.1101/gad.9.19.2373

Cebrian, V., Alvarez, M., Aleman, A., Palou, J., Bellmunt, J., Gonzalez-Peramato, P., … Sánchez-Carbayo, M. (2008). Discovery of myopodin methylation in bladder cancer. *Journal of Pathology*. https://doi.org/10.1002/path.2390

Chal, J., & Pourquié, O. (2017). Making muscle: skeletal myogenesis in vivo and in vitro . *Development*. https://doi.org/10.1242/dev.151035

Chalovich, J. M., & Schroeter, M. M. (2010). Synaptopodin family of natively unfolded, actin binding proteins: Physical properties and potential biological functions. *Biophysical Reviews*. https://doi.org/10.1007/s12551-010-0040-5

Charlton, C. A., Mohler, W. A., & Blau, H. M. (2000). Neural cell adhesion molecule (NCAM) and myoblast fusion. *Developmental Biology*. https://doi.org/10.1006/dbio.2000.9654

Charlton, Carol A., Mohler, W. A., Radice, G. L., Hynes, R. O., & Blau, H. M. (1997). Fusion competence of myoblasts rendered genetically null for N-cadherin in culture. *Journal of Cell Biology*. https://doi.org/10.1083/jcb.138.2.331

Charrasse, S., Comunale, F., Fortier, M., Portales-Casamar, E., Debant, A., & Gauthier-Rouviere, C. (2007). M-Cadherin Activates Rac1 GTPase through the Rho-GEF Trio during Myoblast Fusion. *Molecular Biology of the Cell*. https://doi.org/10.1091/mbc.e06-08-0766

Chen, A. E., Ginty, D. D., & Fan, C. M. (2005). Protein kinase A signalling via CREB controls myogenesis induced by Wnt proteins. *Nature*. https://doi.org/10.1038/nature03126

Chen, E. H., & Olson, E. N. (2001). Antisocial, an Intracellular Adaptor Protein, Is Required for Myoblast Fusion in Drosophila. *Developmental Cell*. https://doi.org/10.1016/S1534-5807(01)00084-3

Chen, E. H., Pryce, B. A., Tzeng, J. A., Gonzalez, G. A., & Olson, E. N. (2003). Control of myoblast fusion by a guanine nucleotide exchange factor, loner, and its effector ARF6. *Cell*. https://doi.org/10.1016/S0092-8674(03)00720-7

Choo, H.-J., Canner, J. P., Vest, K. E., Thompson, Z., & Pavlath, G. K. (2017). A tale of two niches: differential functions for VCAM-1 in satellite cells under basal and injured conditions. *American Journal of Physiology-Cell Physiology*. https://doi.org/10.1152/ajpcell.00119.2017

Chuang, M. C., Lin, S. S., Ohniwa, R. L., Lee, G. H., Su, Y. A., Chang, Y. C., … Liu, Y. W. (2019). Tks5 and dynamin-2 enhance actin bundle rigidity in invadosomes to promote myoblast fusion. *Journal of Cell Biology*. https://doi.org/10.1083/jcb.201809161

Ciruna, B., & Rossant, J. (2001). FGF Signaling Regulates Mesoderm Cell Fate Specification and Morphogenetic Movement at the Primitive Streak. *Developmental Cell*. https://doi.org/10.1016/S1534-5807(01)00017-X

Dalkilic, I., Schienda, J., Thompson, T. G., & Kunkel, L. M. (2006). Loss of FilaminC (FLNc) Results in Severe Defects in Myogenesis and Myotube Structure. *Molecular and Cellular Biology*. https://doi.org/10.1128/mcb.00243-06

Davies, S. P., Reddy, H., Caivano, M., & Cohen, P. (2000). Specificity and mechanism of action of some commonly used protein kinase inhibitors. *Biochemical Journal*. https://doi.org/10.1042/0264-6021:3510095

Dawlaty, M. M., Ganz, K., Powell, B. E., Hu, Y. C., Markoulaki, S., Cheng, A. W., … Jaenisch, R. (2011). Tet1 is dispensable for maintaining pluripotency and its loss is compatible with embryonic and postnatal development. *Cell Stem Cell*. https://doi.org/10.1016/j.stem.2011.07.010

De Ganck, Ariane, Corte, V. De, Staes, A., Gevaert, K., Vandekerckhove, J., & Gettemans, J. (2008). Multiple isoforms of the tumor suppressor myopodin are simultaneously transcribed in cancer cells. *Biochemical and Biophysical Research Communications*. https://doi.org/10.1016/j.bbrc.2008.03.086

De Ganck, Ariane, Hubert, T., Van Impe, K., Geelen, D., Vandekerckhove, J., De Corte, V., & Gettemans, J. (2005). A monopartite nuclear localization sequence regulates nuclear targeting of the actin binding protein myopodin. *FEBS Letters*. https://doi.org/10.1016/j.febslet.2005.10.054

De Ganck, Arianne, De Corte, V., Bruyneel, E., Bracke, M., Vandekerckhove, J., & Gettemans, J. (2009). Down-regulation of myopodin expression reduces invasion and motility of PC-3 prostate cancer cells. *International Journal of Oncology*. https://doi.org/10.3892/ijo_00000268

Deller, T., Korte, M., Chabanis, S., Drakew, A., Schwegler, H., Stefani, G. G., … Mundel, P. (2003). Synaptopodin-deficient mice lack a spine apparatus and show deficits in synaptic plasticity. *Proceedings of the National Academy of Sciences of the United States of America*. https://doi.org/10.1073/pnas.1832384100

Deng, S., Bothe, I., & Baylies, M. K. (2015). The Formin Diaphanous Regulates Myoblast Fusion through Actin Polymerization and Arp2/3 Regulation. *PLoS Genetics*. https://doi.org/10.1371/journal.pgen.1005381

Doberstein, S. K., Fetter, R. D., Mehta, A. Y., & Goodman, C. S. (1997). Genetic analysis of myoblast fusion: Blown fuse is required for progression beyond the prefusion complex. *Journal of Cell Biology*. https://doi.org/10.1083/jcb.136.6.1249

Dobi, K. C., Schulman, V. K., & Baylies, M. K. (2015). Specification of the somatic musculature in Drosophila. *Wiley Interdisciplinary Reviews: Developmental Biology*. https://doi.org/10.1002/wdev.182

Doherty, J. T., Lenhart, K. C., Cameron, M. V., Mack, C. P., Conlon, F. L., & Taylor, J. M. (2011). Skeletal muscle differentiation and fusion are regulated by the BAR-containing Rho-GTPase-activating Protein (Rho-GAP), GRAF. *Journal of Biological Chemistry*. https://doi.org/10.1074/jbc.M111.243030

Domingo-Horne, R. M., & Salajegheh, M. K. (2018). An Approach to Myopathy for the Primary Care Clinician. *American Journal of Medicine*. https://doi.org/10.1016/j.amjmed.2017.10.016

Dowling, J. J., Vreede, A. P., Kim, S., Golden, J., & Feldman, E. L. (2008). Kindlin-2 is required for myocyte elongation and is essential for myogenesis. *BMC Cell Biology*. https://doi.org/10.1186/1471-2121-9-36

Duan, H., Skeath, J. B., & Nguyen, H. T. (2001). Drosophila Lame duck, a novel member of the Gli superfamily, acts as a key regulator of myogenesis by controlling fusion-competent myoblast development. *Development (Cambridge, England)*.

Duan, R., & Gallagher, P. J. (2009). Dependence of myoblast fusion on a cortical actin wall and nonmuscle myosin IIA. *Developmental Biology*. https://doi.org/10.1016/j.ydbio.2008.10.035

Duan, R., Jin, P., Luo, F., Zhang, G., Anderson, N., & Chen, E. H. (2012). Group I PAKs function downstream of Rac to promote podosome invasion during myoblast fusion in vivo. *Journal of Cell Biology*. https://doi.org/10.1083/jcb.201204065

Duff, M. O., Olson, S., Wei, X., Garrett, S. C., Osman, A., Bolisetty, M., … Graveley, B. R. (2015). Genome-wide identification of zero nucleotide recursive splicing in Drosophila. *Nature*. https://doi.org/10.1038/nature14475

Duggirala, A., Kimura, T. E., Sala-Newby, G. B., Johnson, J. L., Wu, Y. J., Newby, A. C., & Bond, M. (2015). CAMP-induced actin cytoskeleton remodelling inhibits MKL1-dependent expression of the chemotactic and pro-proliferative factor, CCN1. *Journal of Molecular and Cellular Cardiology*. https://doi.org/10.1016/j.yjmcc.2014.11.012

El-Brolosy, M. A., & Stainier, D. Y. R. (2017). Genetic compensation: A phenomenon in search of mechanisms. *PLoS Genetics*. https://doi.org/10.1371/journal.pgen.1006780

Erickson, M. R. S., Galletta, B. J., & Abmayr, S. M. (1997). Drosophila myoblast city encodes a conserved protein that is essential for myoblast fusion, dorsal closure, and cytoskeletal organization. *Journal of Cell Biology*. https://doi.org/10.1083/jcb.138.3.589

Faul, C., Dhume, A., Schecter, A. D., & Mundel, P. (2007). Protein Kinase A, Ca2+/Calmodulin-Dependent Kinase II, and Calcineurin Regulate the Intracellular Trafficking of Myopodin between the Z-Disc and the Nucleus of Cardiac Myocytes. *Molecular and Cellular Biology*. https://doi.org/10.1128/mcb.00950-07

Faul, Christian, Hüttelmaier, S., Oh, J., Hachet, V., Singer, R. H., & Mundel, P. (2005). Promotion of importin α-mediated nuclear import by the phosphorylation-dependent binding of cargo protein to 14-3-3. *Journal of Cell Biology*. https://doi.org/10.1083/jcb.200411169

Fortier, M., Comunale, F., Kucharczak, J., Blangy, A., Charrasse, S., & Gauthier-Rouvière, C. (2008). RhoE controls myoblast alignment prior fusion through RhoA and ROCK. *Cell Death and Differentiation*. https://doi.org/10.1038/cdd.2008.34

Frank, D., & Frey, N. (2011). Cardiac Z-disc signaling network. *Journal of Biological Chemistry*. https://doi.org/10.1074/jbc.R110.174268

Freudenberg, J., Ghosh, S., … B. L.-N. acids, & 2011, undefined. (n.d.). Acute depletion of Tet1-dependent 5-hydroxymethylcytosine levels impairs LIF/Stat3 signaling and results in loss of embryonic stem cell identity. *Academic.Oup.Com*. Retrieved from https://academic.oup.com/nar/article-abstract/40/8/3364/2411559

Gakis, G., Schwentner, C., Todenhöfer, T., & Stenzl, A. (2012). Current status of molecular markers for prognostication and outcome in invasive bladder cancer. *BJU International*. https://doi.org/10.1111/j.1464-410X.2011.10839.x

Gau, D., & Roy, P. (2018). SRF'ing and SAP'ing - The role of MRTF proteins in cell migration. *Journal of Cell Science*. https://doi.org/10.1242/jcs.218222

Girardi, F., Taleb, A., Giordani, L., CADOT, B., Datye, A., Ebrahimi, M., … Grand, F. Le. (2019). TGFβ signaling curbs cell fusion and muscle regeneration. *BioRxiv*. https://doi.org/10.1101/557009

Goh, Q., & Millay, D. P. (2017). Requirement of myomaker-mediated stem cell fusion for skeletal muscle hypertrophy. *ELife*. https://doi.org/10.7554/ELIFE.20007

Goody, M. F., Carter, E. V., Kilroy, E. A., Maves, L., & Henry, C. A. (2017). "Muscling" Throughout Life: Integrating Studies of Muscle Development, Homeostasis, and Disease in Zebrafish. In *Current Topics in Developmental Biology*. https://doi.org/10.1016/bs.ctdb.2016.11.002

Griffin, C. A., Apponi, L. H., Long, K. K., & Pavlath, G. K. (2010). Chemokine expression and control of muscle cell migration during myogenesis. *Journal of Cell Science*. https://doi.org/10.1242/jcs.066241

Gruenbaum-Cohen, Y., Harel, I., Umansky, K.-B., Tzahor, E., Snapper, S. B., Shilo, B.-Z., & Schejter, E. D. (2012). The actin regulator N-WASp is required for muscle-cell fusion in mice. *Proceedings of the National Academy of Sciences*. https://doi.org/10.1073/pnas.1116065109

Gurevich, D. B., Nguyen, P. D., Siegel, A. L., Ehrlich, O. V., Sonntag, C., Phan, J. M. N., … Currie, P. D. (2016). Asymmetric division of clonal muscle stem cells coordinates muscle regeneration in vivo. *Science*. https://doi.org/10.1126/science.aad9969

Hamoud, N., Tran, V., Croteau, L.-P., Kania, A., & Côté, J.-F. (2014). G-protein coupled receptor BAI3 promotes myoblast fusion in vertebrates. *Proceedings of the National Academy of Sciences*. https://doi.org/10.1073/pnas.1313886111

Haralalka, S., Shelton, C., Cartwright, H. N., Katzfey, E., Janzen, E., & Abmayr, S. M. (2013). Asymmetric Mbc, active Rac1 and F-actin foci in the fusion-competent myoblasts during myoblast fusion in Drosophila. *Development*. https://doi.org/10.1242/dev.092379

Henry, C. A., & Amacher, S. L. (2004). Zebrafish slow muscle cell migration induces a wave of fast muscle morphogenesis. *Developmental Cell*. https://doi.org/10.1016/j.devcel.2004.09.017

Hernández, J. M., & Podbilewicz, B. (2017). The hallmarks of cell-cell fusion. *Development*, *144*(24), 4481–4495. https://doi.org/10.1242/dev.155523

Higgs, H. N., & Pollard, T. D. (2000). Activation by Cdc42 and PIP2 of Wiskott-Aldrich Syndrome protein (WASp) stimulates actin nucleation by Arp2/3 complex. *Journal of Cell Biology*. https://doi.org/10.1083/jcb.150.6.1311

Hirayama, E., & Kim, J. (2008). Identification and characterization of a novel neural cell adhesion molecule (NCAM)-associated protein from quail myoblasts: Relationship to myotube formation and induction of neurite-like protrusions. *Differentiation*. https://doi.org/10.1111/j.1432-0436.2007.00215.x

Holden, L. A., & Brown, K. H. (2018). Baseline mRNA expression differs widely between common laboratory strains of zebrafish. *Scientific Reports*. https://doi.org/10.1038/s41598-018-23129-4

Hollnagel, A., Grund, C., Franke, W. W., & Arnold, H.-H. (2002). The Cell Adhesion Molecule M-Cadherin Is Not Essential for Muscle Development and Regeneration. *Molecular and Cellular Biology*. https://doi.org/10.1128/mcb.22.13.4760-4770.2002

Housley, M. P., Njaine, B., Ricciardi, F., Stone, O. A., Hölper, S., Krüger, M., … Stainier, D. Y. R. (2016). Cavin4b/Murcb Is Required for Skeletal Muscle Development and Function in Zebrafish. *PLOS Genetics*, *12*(6), e1006099. https://doi.org/10.1371/journal.pgen.1006099

Hromowyk, K. (2017). Genetic analysis of skeletal muscle cell fusion in zebrafish. Retrieved from http://rave.ohiolink.edu/etdc/view?acc_num=osu1512114979019823

Huang, S. Y., Tsai, M. L., Wu, C. J., Hsu, J. L., Ho, S. H., & Chen, S. H. (2006). Quantitation of protein phosphorylation in pregnant rat uteri using stable isotope dimethyl labeling coupled with IMAC. *Proteomics*. https://doi.org/10.1002/pmic.200500507

Iakoucheva, L. M., Kimzey, A. L., Ackerman, E. J., Masselon, C. D., Smith, R. D., & Dunker, A. K. (2001). Aberrant mobility phenomena of the DNA repair protein XPA. *Protein Science*. https://doi.org/10.1110/ps.ps.40101

Insall, R. H., & Machesky, L. M. (2009). Actin Dynamics at the Leading Edge: From Simple Machinery to Complex Networks. *Developmental Cell*. https://doi.org/10.1016/j.devcel.2009.08.012

Ishizaki, T., Uehata, M., Tamechika, I., Keel, J., Nonomura, K., Maekawa, M., & Narumiya, S. (2000). Pharmacological properties of Y-27632, a specific inhibitor of Rho-associated kinases. *Molecular Pharmacology*.

Iwasaki, K., Hayashi, K., Fujioka, T., & Sobue, K. (2008). Rho/Rho-associated kinase signal regulates myogenic differentiation via myocardin-related transcription factor-A/Smad-dependent transcription of the Id3 gene. *Journal of Biological Chemistry*. https://doi.org/10.1074/jbc.M710525200

Jacob, A. E., Amack, J. D., & Turner, C. E. (2017). Paxillin genes and actomyosin contractility regulate myotome morphogenesis in zebrafish. *Developmental Biology*. https://doi.org/10.1016/j.ydbio.2017.03.012

Jansen, K. M., & Pavlath, G. K. (2006). Mannose receptor regulates myoblast motility and muscle growth. *Journal of Cell Biology*. https://doi.org/10.1083/jcb.200601102

Jing, L., Liu, L., Yu, Y. P., Dhir, R., Acquafondada, M., Landsittel, D., … Luo, J. H. (2004). Expression of Myopodin Induces Suppression of Tumor Growth and Metastasis. *American Journal of Pathology*. https://doi.org/10.1016/S0002-9440(10)63738-8

Kai, F., Fawcett, J. P., & Duncan, R. (2015). Synaptopodin-2 induces assembly of peripheral actin bundles and immature focal adhesions to promote lamellipodia formation and prostate cancer cell migration. *Oncotarget*. https://doi.org/10.18632/oncotarget.3578

Kai, Fui Boon, & Duncan, R. (2013). Prostate cancer cell migration induced by myopodin isoforms is associated with formation of morphologically and biochemically distinct actin networks. *FASEB Journal*. https://doi.org/10.1096/fj.13-231571

Kai, FuiBoon B., Tanner, K., King, C., & Duncan, R. (2012). Myopodin isoforms alter the chemokinetic response of PC3 cells in response to different migration stimuli via differential effects on Rho-ROCK signaling pathways. *Carcinogenesis*. https://doi.org/10.1093/carcin/bgs268

Kang, J. S., Mulieri, P. J., Hu, Y., Taliana, L., & Krauss, R. S. (2002). BOC, an Ig superfamily member, associates with CDO to positively regulate myogenic differentiation. *EMBO Journal*. https://doi.org/10.1093/emboj/21.1.114

Kang, J. S., Yi, M. J., Zhang, W., Feinleib, J. L., Cole, F., & Krauss, R. S. (2004). Netrins and neogenin promote myotube formation. *Journal of Cell Biology*. https://doi.org/10.1083/jcb.200405039

Kaul, A., Köster, M., Neuhaus, H., & Braun, T. (2000). Myf-5 revisited: Loss of early myotome formation does not lead to a rib phenotype in homozygous Myf-5 mutant mice. *Cell*. https://doi.org/10.1016/S0092-8674(00)00006-4

Kesper, D. A., Stute, C., Buttgereit, D., Kreisköther, N., Vishnu, S., Fischbach, K. F., & Renkawitz-Pohl, R. (2007). Myoblast fusion in Drosophila melanogaster is mediated through a fusion-restricted myogenic-adhesive structure (FuRMAS). *Developmental Dynamics*. https://doi.org/10.1002/dvdy.21035

Kim, J. H., Jin, P., Duan, R., & Chen, E. H. (2015a). Mechanisms of myoblast fusion during muscle development. *Current Opinion in Genetics and Development*. https://doi.org/10.1016/j.gde.2015.03.006

Kim, J. H., Jin, P., Duan, R., & Chen, E. H. (2015b). Mechanisms of myoblast fusion during muscle development. *Current Opinion in Genetics & Development*, *32*, 162–170. https://doi.org/10.1016/j.gde.2015.03.006

Kim, J. H., Ren, Y., Ng, W. P., Li, S., Son, S., Kee, Y. S., … Chen, E. H. (2015). Mechanical Tension Drives Cell Membrane Fusion. *Developmental Cell*. https://doi.org/10.1016/j.devcel.2015.01.005

Kim, J., Jin, P., Duan, R., & Chen, E. (2015). Mechanisms of myoblast fusion during muscle development. *Current Opinion in Genetics &* …. Retrieved from http://www.sciencedirect.com/science/article/pii/S0959437X15000271

Kim, J., Ren, Y., Ng, W., Li, S., Son, S., & Kee, Y. (2015). Mechanical tension drives cell membrane fusion. *Developmental Cell*. Retrieved from http://www.sciencedirect.com/science/article/pii/S1534580715000283

Kim, S., Shilagardi, K., Zhang, S., Hong, S. N., Sens, K. L., Bo, J., … Chen, E. H. (2007). A Critical Function for the Actin Cytoskeleton in Targeted Exocytosis of Prefusion Vesicles during Myoblast Fusion. *Developmental Cell*. https://doi.org/10.1016/j.devcel.2007.02.019

Kitzmann, M., Vandromme, M., Schaeffer, V., Carnac, G., Labbé, J.-C., Lamb, N., & Fernandez, A. (2015). cdk1- and cdk2-Mediated Phosphorylation of MyoD Ser200 in Growing C2 Myoblasts: Role in Modulating MyoD Half-Life and Myogenic Activity. *Molecular and Cellular Biology*. https://doi.org/10.1128/mcb.19.4.3167

Knight, J., & Kothary, R. (2011). The myogenic kinome: protein kinases critical to mammalian skeletal myogenesis. *Skelet Muscle*. Retrieved from http://www.biomedcentral.com/content/pdf/2044-5040-1-29.pdf

Knöll, R., Buyandelger, B., & Lab, M. (2011). The sarcomeric Z-disc and Z-discopathies. *Journal of Biomedicine and Biotechnology*. https://doi.org/10.1155/2011/569628

Kok, F. O., Shin, M., Ni, C. W., Gupta, A., Grosse, A. S., vanImpel, A., … Lawson, N. D. (2015). Reverse genetic screening reveals poor correlation between morpholino-induced and mutant phenotypes in zebrafish. *Developmental Cell*. https://doi.org/10.1016/j.devcel.2014.11.018

Krauss, R. S., Joseph, G. A., & Goel, A. J. (2017). Keep your friends close: Cell–cell contact and skeletal myogenesis. *Cold Spring Harbor Perspectives in Biology*. https://doi.org/10.1101/cshperspect.a029298

Lafreniere, J. F., Mills, P., Bouchentouf, M., & Tremblay, J. P. (2006). Interleukin-4 improves the migration of human myogenic precursor cells in vitro and in vivo. *Experimental Cell Research*. https://doi.org/10.1016/j.yexcr.2006.01.002

Lafuste, P., Sonnet, C., Chazaud, B., Dreyfus, P. A., Gherardi, R. K., Wewer, U. M., & Authier, F.-J. (2005). ADAM12 and α<inf>9</inf>β<inf>1</inf> integrin are instrumental in human myogenic cell differentiation. *Molecular Biology of the Cell*. https://doi.org/10.1091/mbc.E04-03-0226

Landemaine, A., Rescan, P. Y., & Gabillard, J. C. (2014). Myomaker mediates fusion of fast myocytes in zebrafish embryos. *Biochemical and Biophysical Research Communications*. https://doi.org/10.1016/j.bbrc.2014.07.093

Laurin, M., Fradet, N., Blangy, A., Hall, A., Vuori, K., & Cote, J.-F. (2008). The atypical Rac activator Dock180 (Dock1) regulates myoblast fusion in vivo. *Proceedings of the National Academy of Sciences*. https://doi.org/10.1073/pnas.0805546105

Lauter, G., Söll, I., & Hauptmann, G. (2011). Two-color fluorescent in situ hybridization in the embryonic zebrafish brain using differential detection systems. *BMC Developmental Biology*. https://doi.org/10.1186/1471-213X-11-43

Lebedeva, S., de Jesus Domingues, A. M., Butter, F., & Ketting, R. F. (2017). Characterization of genetic loss-of-function of Fus in zebrafish. *RNA Biology*. https://doi.org/10.1080/15476286.2016.1256532

Leikina, E., Gamage, D. G., Prasad, V., Goykhberg, J., Crowe, M., Diao, J., … Millay, D. P. (2018). Myomaker and Myomerger Work Independently to Control Distinct Steps of Membrane Remodeling during Myoblast Fusion. *Developmental Cell*. https://doi.org/10.1016/j.devcel.2018.08.006

Leinweber, B. D., Fredricksen, R. S., Hoffman, D. R., & Chalovich, J. M. (1999). Fesselin: A novel synaptopodin-like actin binding protein from muscle tissue. *Journal of Muscle Research and Cell Motility*. https://doi.org/10.1023/A:1005597306671

Lepper, C., & Fan, C. M. (2010). Inducible lineage tracing of Pax7-descendant cells reveals embryonic origin of adult satellite cells. *Genesis*. https://doi.org/10.1002/dvg.20630

Liang, J., Ke, G., You, W., Peng, Z., Lan, J., Kalesse, M., … Tao, T. (2008). Interaction between importin 13 and myopodin suggests a nuclear import pathway for myopodin. *Molecular and Cellular Biochemistry*. https://doi.org/10.1007/s11010-007-9588-1

Lim, J. A., Li, L., & Raben, N. (2014). Pompe disease: From pathophysiology to therapy and back again. *Frontiers in Aging Neuroscience*. https://doi.org/10.3389/fnagi.2014.00177

Lin, F., Yu, Y. P., Woods, J., Cieply, K., Gooding, B., Finkelstein, P., … Luo, J. H. (2001). Myopodin, a synaptopodin homologue, is frequently deleted in invasive prostate cancers. *American Journal of Pathology*. https://doi.org/10.1016/S0002-9440(10)63006-4

Linnemann, A, & Ven, P. van der. (2010). The sarcomeric Z-disc component myopodin is a multiadapter protein that interacts with filamin and α-actinin. *European Journal of Cell* .... Retrieved from http://www.sciencedirect.com/science/article/pii/S0171933510000890

Linnemann, Anja, Vakeel, P., Bezerra, E., Orfanos, Z., Djinović-Carugo, K., Van Der Ven, P. F. M., … Fürst, D. O. (2013). Myopodin is an F-actin bundling protein with multiple independent actin-binding regions. *Journal of Muscle Research and Cell Motility*. https://doi.org/10.1007/s10974-012-9334-5

Liu, J., Ye, L., Li, Q., Wu, X., Wang, B., Ouyang, Y., … Lin, C. (2018). Synaptopodin-2 suppresses metastasis of triple-negative breast cancer via inhibition of YAP/TAZ activity. *Journal of Pathology*. https://doi.org/10.1002/path.4995

Liu, Z., Wang, C., Liu, X., & Kuang, S. (2018). Shisa2 regulates the fusion of muscle progenitors. *Stem Cell Research*. https://doi.org/10.1016/j.scr.2018.07.004

Luo, W., Li, E., Nie, Q., & Zhang, X. (2015). Myomaker, regulated by MYOD, MYOG and miR-140-3P, promotes chicken myoblast fusion. *International Journal of Molecular Sciences*. https://doi.org/10.3390/ijms161125946

Machesky, L. M., & Insall, R. H. (1998). Scar1 and the related Wiskott-Aldrich syndrome protein, WASP, regulate the actin cytoskeleton through the Arp2/3 complex. *Current Biology*. https://doi.org/10.1016/S0960-9822(98)00015-3

Mancini, A., Sirabella, D., Zhang, W., Yamazaki, H., Shirao, T., & Krauss, R. S. (2011). Regulation of myotube formation by the actin-binding factor drebrin. *Skeletal Muscle*. https://doi.org/10.1186/2044-5040-1-36

Massarwa, R., Carmon, S., Shilo, B. Z., & Schejter, E. D. (2007). WIP/WASp-Based Actin-Polymerization Machinery Is Essential for Myoblast Fusion in Drosophila. *Developmental Cell*. https://doi.org/10.1016/j.devcel.2007.01.016

Matsumura, F., & Hartshorne, D. J. (2008). Myosin phosphatase target subunit: Many roles in cell function. *Biochemical and Biophysical Research Communications*. https://doi.org/10.1016/j.bbrc.2007.12.090

Menon, S. D., & Chia, W. (2001). Drosophila Rolling pebbles: A Multidomain Protein Required for Myoblast Fusion that Recruits D-Titin in Response to the Myoblast Attractant Dumbfounded. *Developmental Cell*. https://doi.org/10.1016/S1534-5807(01)00075-2

Meyer, B. M., Froehlich, J. M., Galt, N. J., & Biga, P. R. (2013). Inbred strains of zebrafish exhibit variation in growth performance and myostatin expression following fasting. *Comparative Biochemistry and Physiology - A Molecular and Integrative Physiology*. https://doi.org/10.1016/j.cbpa.2012.10.004

Millay, D. P., O'Rourke, J. R., Sutherland, L. B., Bezprozvannaya, S., Shelton, J. M., Bassel-Duby, R., & Olson, E. N. (2013). Myomaker is a membrane activator of myoblast fusion and muscle formation. *Nature*, *499*(7458), 301–305. https://doi.org/10.1038/nature12343

Miralles, F., Posern, G., Zaromytidou, A. I., & Treisman, R. (2003). Actin dynamics control SRF activity by regulation of its coactivator MAL. *Cell*. https://doi.org/10.1016/S0092-8674(03)00278-2

Moore, C. A., Parkin, C. A., Bidet, Y., & Ingham, P. W. (2007). A role for the Myoblast city homologues Dock1 and Dock5 and the adaptor proteins Crk and Crk-like in zebrafish myoblast fusion. *Development*. https://doi.org/10.1242/dev.001214

Mundel, P., Heid, H. W., Mundel, T. M., Krüger, M., Reiser, J., & Kriz, W. (1997). Synaptopodin: An actin-associated protein in telencephalic dendrites and renal podocytes. *Journal of Cell Biology*. https://doi.org/10.1083/jcb.139.1.193

Nguyen, N. U. N., & Wang, H. V. (2015). Dual roles of palladin protein in in vitro myogenesis: Inhibition of early induction but promotion of myotube maturation. *PLoS ONE*. https://doi.org/10.1371/journal.pone.0124762

Nishiyama, T., Kii, I., & Kudo, A. (2004). Inactivation of Rho/ROCK signaling is crucial for the nuclear accumulation of FKHR and myoblast fusion. *Journal of Biological Chemistry*. https://doi.org/10.1074/jbc.M403546200

Nord, H., Burguiere, A.-C., Muck, J., Nord, C., Ahlgren, U., & von Hofsten, J. (2014). Differential regulation of myosin heavy chains defines new muscle domains in zebrafish. *Molecular Biology of the Cell*. https://doi.org/10.1091/mbc.e13-08-0486

Nowak, S. J., Nahirney, P. C., Hadjantonakis, A.-K., & Baylies, M. K. (2009). Nap1-mediated actin remodeling is essential for mammalian myoblast fusion. *Journal of Cell Science*. https://doi.org/10.1242/jcs.047597

Padrick, S. B., Doolittle, L. K., Brautigam, C. A., King, D. S., & Rosen, M. K. (2011). Arp2/3 complex is bound and activated by two WASP proteins. *Proceedings of the National Academy of Sciences*. https://doi.org/10.1073/pnas.1100236108

Pajcini, K. V., Pomerantz, J. H., Alkan, O., Doyonnas, R., & Blau, H. M. (2008). Myoblasts and macrophages share molecular components that contribute to cell-cell fusion. *Journal of Cell Biology*. https://doi.org/10.1083/jcb.200707191

Patrie, K. M., Drescher, A. J., Welihinda, A., Mundel, P., & Margolis, B. (2002). Interaction of two actin-binding proteins, synaptopodin and alpha-actinin-4, with the tight junction protein MAGI-1. *The Journal of Biological Chemistry*. https://doi.org/10.1074/jbc.M203072200

Pelosi, M., Marampon, F., Zani, B. M., Prudente, S., Perlas, E., Caputo, V., … Rosenthal, N. (2007). ROCK2 and Its Alternatively Spliced Isoform ROCK2m Positively Control the Maturation of the Myogenic Program. *Molecular and Cellular Biology*. https://doi.org/10.1128/mcb.01735-06

Pizza, F. X., Martin, R. A., Springer, E. M., Leffler, M. S., Woelmer, B. R., Recker, I. J., & Leaman, D. W. (2017). Intercellular adhesion molecule-1 augments myoblast adhesion and fusion through homophilic trans-interactions. *Scientific Reports*. https://doi.org/10.1038/s41598-017-05283-3

Pollard, T. D., Blanchoin, L., & Mullins, R. D. (2002). Molecular Mechanisms Controlling Actin Filament Dynamics in Nonmuscle Cells. *Annual Review of Biophysics and Biomolecular Structure*. https://doi.org/10.1146/annurev.biophys.29.1.545

Powell, G. T., & Wright, G. J. (2011). Jamb and jamc are essential for vertebrate myocyte fusion. *PLoS Biology*. https://doi.org/10.1371/journal.pbio.1001216

Prykhozhij, S. V., Fuller, C., Steele, S. L., Veinotte, C. J., Razaghi, B., Robitaille, J. M., … Berman, J. N. (2018). Optimized knock-in of point mutations in zebrafish using CRISPR/Cas9. *Nucleic Acids Research*. https://doi.org/10.1093/nar/gky674

Quinn, M. E., Goh, Q., Kurosaka, M., Gamage, D. G., Petrany, M. J., Prasad, V., & Millay, D. P. (2017). Myomerger induces fusion of non-fusogenic cells and is required for skeletal muscle development. *Nature Communications*, *8*, 15665. https://doi.org/10.1038/ncomms15665

Reimann, L., Wiese, H., Leber, Y., Schwäble, A. N., Fricke, A. L., Rohland, A., … Warscheid, B. (2017). Myofibrillar Z-discs Are a Protein Phosphorylation Hot Spot with Protein Kinase C (PKCα) Modulating Protein Dynamics. *Molecular & Cellular Proteomics*. https://doi.org/10.1074/mcp.m116.065425

Renegar, R. H., Chalovich, J. M., Leinweber, B. D., Zary, J. T., & Schroeter, M. M. (2009). Localization of the actin-binding protein fesselin in chicken smooth muscle. *Histochemistry and Cell Biology*. https://doi.org/10.1007/s00418-008-0508-6

Richardson, B. E., Beckett, K., Nowak, S. J., & Baylies, M. K. (2007). SCAR/WAVE and Arp2/3 are crucial for cytoskeletal remodeling at the site of myoblast fusion. *Development*. https://doi.org/10.1242/dev.010678

Rosen, G. D., Sanes, J. R., LaChance, R., Cunningham, J. M., Roman, J., & Dean, D. C. (1992). Roles for the integrin VLA-4 and its counter receptor VCAM-1 in myogenesis. *Cell*. https://doi.org/10.1016/0092-8674(92)90633-N

Rossi, A., Kontarakis, Z., Gerri, C., Nolte, H., Hölper, S., Krüger, M., & Stainier, D. Y. R. (2015). Genetic compensation induced by deleterious mutations but not gene knockdowns. *Nature*. https://doi.org/10.1038/nature14580

Rossi, G., & Messina, G. (2014). Comparative myogenesis in teleosts and mammals. *Cellular and Molecular Life Sciences*. https://doi.org/10.1007/s00018-014-1604-5

Rudnicki, M. A., Braun, T., Hinuma, S., & Jaenisch, R. (1992). Inactivation of MyoD in mice leads to up-regulation of the myogenic HLH gene Myf-5 and results in apparently normal muscle development. *Cell*. https://doi.org/10.1016/0092-8674(92)90508-A

Rudnicki, M. A., Schnegelsberg, P. N. J., Stead, R. H., Braun, T., Arnold, H. H., & Jaenisch, R. (1993). MyoD or Myf-5 is required for the formation of skeletal muscle. *Cell*. https://doi.org/10.1016/0092-8674(93)90621-V

Rushton, E., Drysdale, R., Abmayr, S. M., Michelson, A. M., & Bate, M. (1995). Mutations in a novel gene, myoblast city, provide evidence in support of the founder cell hypothesis for Drosophila muscle development. *Development (Cambridge, England)*.

Safi, A., Vandromme, M., Caussanel, S., Valdacci, L., Baas, D., Vidal, M., … Goillot, E. (2004). Role for the Pleckstrin Homology Domain-Containing Protein CKIP-1 in Phosphatidylinositol 3-Kinase-Regulated Muscle Differentiation. *Molecular and Cellular Biology*. https://doi.org/10.1128/mcb.24.3.1245-1255.2004

Sanchez-Carbayo, M., Schwarz, K., Charytonowicz, E., Cordon-Cardo, C., & Mundel, P. (2003). Tumor suppressor role for myopodin in bladder cancer: Loss of nuclear expression of myopodin is cell-cycle dependent and predicts clinical outcome. *Oncogene*. https://doi.org/10.1038/sj.onc.1206616

Sanger, J. W., Wang, J., Fan, Y., White, J., & Sanger, J. M. (2010). Assembly and dynamics of myofibrils. *Journal of Biomedicine and Biotechnology*. https://doi.org/10.1155/2010/858606

Schäfer, G., Weber, S., Holz, A., Bogdan, S., Schumacher, S., Müller, A., … Önel, S. F. (2007). The Wiskott-Aldrich syndrome protein (WASP) is essential for myoblast fusion in Drosophila. *Developmental Biology*. https://doi.org/10.1016/j.ydbio.2007.01.015

Schönichen, A., & Geyer, M. (2010). Fifteen formins for an actin filament: A molecular view on the regulation of human formins. *Biochimica et Biophysica Acta - Molecular Cell Research*. https://doi.org/10.1016/j.bbamcr.2010.01.014

Schröder, R., & Schoser, B. (2009). Myofibrillar Myopathies: A Clinical and Myopathological Guide. *Brain Pathology*. https://doi.org/10.1111/j.1750-3639.2009.00289.x

Schroeter, M., & Chalovich, J. M. (2004). Ca2+-calmodulin regulates fesselin-induced actin polymerization. In *Biochemistry*. https://doi.org/10.1021/bi0487490

Schroeter, M. M., Beall, B., Heid, H. W., & Chalovich, J. M. (2008). In vitro characterization of native mammalian smooth-muscle protein synaptopodin 2. *Bioscience Reports*. https://doi.org/10.1042/BSR20080079

Schroeter, M. M., & Chalovich, J. M. (2005). Fesselin binds to actin and myosin and inhibits actin-activated ATPase activity. *Journal of Muscle Research and Cell Motility*. https://doi.org/10.1007/s10974-005-9009-6

Schroeter, M. M., Orlova, A., Egelman, E. H., Beall, B., & Chalovich, J. M. (2013). Organization of f-actin by fesselin (avian smooth muscle synaptopodin 2). *Biochemistry*. https://doi.org/10.1021/bi4005254

Schroter, R. H. (2004). kette and blown fuse interact genetically during the second fusion step of myogenesis in Drosophila. *Development*. https://doi.org/10.1242/dev.01309

Schröter, R. H., Lier, S., Holz, A., Bogdan, S., Klämbt, C., Beck, L., & Renkawitz-Pohl, R. (2004). kette and blown fuse interact genetically during the second fusion step of myogenesis in Drosophila. *Development*. https://doi.org/10.1242/dev.01309

Schwander, M., Leu, M., Stumm, M., Dorchies, O. M., Ruegg, U. T., Schittny, J., & Müller, U. (2003). β1 integrins regulate myoblast fusion and sarcomere assembly. *Developmental Cell*. https://doi.org/10.1016/S1534-5807(03)00118-7

Segal, D., Dhanyasi, N., Schejter, E. D., & Shilo, B. Z. (2016). Adhesion and Fusion of Muscle Cells Are Promoted by Filopodia. *Developmental Cell*. https://doi.org/10.1016/j.devcel.2016.07.010

Sens, K. L., Zhang, S., Jin, P., Duan, R., Zhang, G., Luo, F., … Chen, E. H. (2010). An invasive podosome-like structure promotes fusion pore formation during myoblast fusion. *Journal of Cell Biology*. https://doi.org/10.1083/jcb.201006006

Shi, J., Bi, P., Pei, J., Li, H., Grishin, N. V., Bassel-Duby, R., … Olson, E. N. (2017). Requirement of the fusogenic micropeptide myomixer for muscle formation in zebrafish. *Proceedings of the National Academy of Sciences*. https://doi.org/10.1073/pnas.1715229114

Si, Y., Wen, H., & Du, S. (2019). Genetic Mutations in jamb, jamc, and myomaker Revealed Different Roles on Myoblast Fusion and Muscle Growth. *Marine Biotechnology*. https://doi.org/10.1007/s10126-018-9865-x

Snow, C. J., Goody, M., Kelly, M. W., Oster, E. C., Jones, R., Khalil, A., & Henry, C. A. (2008). Time-lapse analysis and mathematical characterization elucidate novel mechanisms underlying muscle morphogenesis. *PLoS Genetics*. https://doi.org/10.1371/journal.pgen.1000219

Sohn, R. L., Huang, P., Kawahara, G., Mitchell, M., Guyon, J., Kalluri, R., … Gussoni, E. (2009). A role for nephrin, a renal protein, in vertebrate skeletal muscle cell fusion. *Proceedings of the National Academy of Sciences*. https://doi.org/10.1073/pnas.0904398106

Sotiropoulos, A., Gineitis, D., Copeland, J., & Treisman, R. (1999). Signal-regulated activation of serum response factor is mediated by changes in actin dynamics. *Cell*. https://doi.org/10.1016/S0092-8674(00)81011-9

Srinivas, B. P., Woo, J., Leong, W. Y., & Roy, S. (2007). A conserved molecular pathway mediates myoblast fusion in insects and vertebrates. *Nature Genetics*. https://doi.org/10.1038/ng2055

Stainier, D. Y. R., Raz, E., Lawson, N. D., Ekker, S. C., Burdine, R. D., Eisen, J. S., … Moens, C. B. (2017). Guidelines for morpholino use in zebrafish. *PLOS Genetics*. https://doi.org/10.1371/journal.pgen.1007000

Strünkelnberg, M., Bonengel, B., Moda, L. M., Hertenstein, A., de Couet, H. G., Ramos, R. G., & Fischbach, K. F. (2001). rst and its paralogue kirre act redundantly during embryonic muscle development in Drosophila. *Development (Cambridge, England)*.

Swailes, N. T., Colegrave, M., Knight, P. J., & Peckham, M. (2006). Non-muscle myosins 2A and 2B drive changes in cell morphology that occur as myoblasts align and fuse. *Journal of Cell Science*. https://doi.org/10.1242/jcs.03096

Szabo, L., Morey, R., Palpant, N. J., Wang, P. L., Afari, N., Jiang, C., … Salzman, J. (2015). Statistically based splicing detection reveals neural enrichment and tissue-specific induction of circular RNA during human fetal development. *Genome Biology*. https://doi.org/10.1186/s13059-015-0690-5

Sztal, T. E., McKaige, E. A., Williams, C., Ruparelia, A. A., & Bryson-Richardson, R. J. (2018). Genetic compensation triggered by actin mutation prevents the muscle damage caused by loss of actin protein. *PLoS Genetics*. https://doi.org/10.1371/journal.pgen.1007212

Takada, S., Stark, K. L., Shea, M. J., Vassileva, G., McMahon, J. A., & McMahon, A. P. (1994). Wnt-3a regulates somite and tailbud formation in the mouse embryo. *Genes and Development*. https://doi.org/10.1101/gad.8.2.174

Takaesu, G., Kang, J. S., Bae, G. U., Yi, M. J., Lee, C. M., Premkumar Reddy, E., & Krauss, R. S. (2006). Activation of p38α/β MAPK in myogenesis via binding of the scaffold protein JLP to the cell surface protein Cdo. *Journal of Cell Biology*. https://doi.org/10.1083/jcb.200608031

Tamir-Livne, Y., Mubariki, R., & Bengal, E. (2017). Adhesion molecule Kirrel3/Neph2 is required for the elongated shape of myocytes during skeletal muscle differentiation. *International Journal of Developmental Biology*. https://doi.org/10.1387/ijdb.170005eb

Totsukawa, G., Wu, Y., Sasaki, Y., Hartshorne, D. J., Yamakita, Y., Yamashiro, S., & Matsumura, F. (2004). Distinct roles of MLCK and ROCK in the regulation of membrane protrusions and focal adhesion dynamics during cell migration of fibroblasts. *Journal of Cell Biology*. https://doi.org/10.1083/jcb.200306172

Tsuchiya, M., Hara, Y., Okuda, M., Itoh, K., Nishioka, R., Shiomi, A., … Umeda, M. (2018). Cell surface flip-flop of phosphatidylserine is critical for PIEZO1-mediated myotube formation. *Nature Communications*. https://doi.org/10.1038/s41467-018-04436-w

Tsukamoto, Y., Hijiya, N., Yano, S., Yokoyama, S., Nakada, C., Uchida, T., … Moriyama, M. (2008). Arpp/Ankrd2, a member of the muscle ankyrin repeat proteins (MARPs), translocates from the I-band to the nucleus after muscle injury. *Histochemistry and Cell Biology*. https://doi.org/10.1007/s00418-007-0348-9

Turczyńska, K. M., Swärd, K., Hien, T. T., Wohlfahrt, J., Mattisson, I. Y., Ekman, M., … Albinsson, S. (2015). Regulation of Smooth Muscle Dystrophin and Synaptopodin 2 Expression by Actin Polymerization and Vascular Injury. *Arteriosclerosis, Thrombosis, and Vascular Biology*. https://doi.org/10.1161/ATVBAHA.114.305065

Ulbricht, A., Eppler, F., & Tapia, V. (2013). Cellular mechanotransduction relies on tension-induced and chaperone-assisted autophagy. *Current Biology*. Retrieved from http://www.sciencedirect.com/science/article/pii/S0960982213001334

Van Impe, K., De Corte, V., Eichinger, L., Bryneel, E., Mareel, M., Vandekerckhove, J., & Gettemans, J. (2003). The nucleo-cytoplasmic actin-binding protein CapG lacks a nuclear export sequence present in structurally related proteins. *Journal of Biological Chemistry*. https://doi.org/10.1074/jbc.M209946200

Vasyutina, E., Martarelli, B., Brakebusch, C., Wende, H., & Birchmeier, C. (2009). The small G-proteins Rac1 and Cdc42 are essential for myoblast fusion in the mouse. *Proceedings of the National Academy of Sciences*. https://doi.org/10.1073/pnas.0902501106

Vasyutina, Elena, Martarelli, B., Brakebusch, C., Wende, H., & Birchmeier, C. (2009). The small G-proteins Rac1 and Cdc42 are essential for myoblast fusion in the mouse. *Proceedings of the National Academy of Sciences of the United States of America*. https://doi.org/10.1073/pnas.0902501106

Vizcarra, C. L., Bor, B., & Quinlan, M. E. (2014). The role of formin tails in actin nucleation, processive elongation, and filament bundling. *Journal of Biological Chemistry*. https://doi.org/10.1074/jbc.M114.588368

von Hofsten, J., Elworthy, S., Gilchrist, M. J., Smith, J. C., Wardle, F. C., & Ingham, P. W. (2008). Prdm1- and Sox6-mediated transcriptional repression specifies muscle fibre type in the zebrafish embryo. *EMBO Reports*. https://doi.org/10.1038/embor.2008.73

Wallace, M. A., Della Gatta, P. A., Mir, B. A., Kowalski, G. M., Kloehn, J., McConville, M. J., … Lamon, S. (2016). Overexpression of striated muscle activator of Rho Signaling (STARS) Increases C2C12 skeletal muscle cell differentiation. *Frontiers in Physiology*. https://doi.org/10.3389/fphys.2016.00007

Weins, A., Schwarz, K., Faul, C., Barisoni, L., Linke, W. A., & Mundel, P. (2001). Differentiation- and stress-dependent nuclear cytoplasmic redistribution of myopodin, a novel actin-bundling protein. *Journal of Cell Biology*. https://doi.org/10.1083/jcb.200012039

White, R. M., Sessa, A., Burke, C., Bowman, T., LeBlanc, J., Ceol, C., … Zon, L. I. (2008). Transparent Adult Zebrafish as a Tool for In Vivo Transplantation Analysis. *Cell Stem Cell*. https://doi.org/10.1016/j.stem.2007.11.002

Wong, J. S., Iorns, E., Rheault, M. N., Ward, T. M., Rashmi, P., Weber, U., … Mundel, P. (2012). Rescue of tropomyosin deficiency in Drosophila and human cancer cells by synaptopodin reveals a role of tropomyosin α in RhoA stabilization. *EMBO Journal*. https://doi.org/10.1038/emboj.2011.464

Xia, E., Zhou, X., Bhandari, A., Zhang, X., & Wang, O. (2018). Synaptopodin-2 plays an important role in the metastasis of breast cancer via PI3K/Akt/mTOR pathway. *Cancer Management and Research*, *10*, 1575–1583. https://doi.org/10.2147/CMAR.S162670

Xu, H., Xiao, T., Chen, C. H., Li, W., Meyer, C. A., Wu, Q., … Liu, X. S. (2015). Sequence determinants of improved CRISPR sgRNA design. *Genome Research*. https://doi.org/10.1101/gr.191452.115

Yamamoto, A., Nagano, T., Takehara, S., Hibi, M., & Aizawa, S. (2005). Shisa promotes head formation through the inhibition of receptor protein maturation for the caudalizing factors, Wnt and FGF. *Cell*. https://doi.org/10.1016/j.cell.2004.11.051

Yin, H., Price, F., & Rudnicki, M. (2013). Satellite cells and the muscle stem cell niche. *Physiological Reviews*. Retrieved from http://physrev.physiology.org/content/93/1/23.short

Yu, Y. P., & Luo, J. H. (2011). Phosphorylation and interaction of myopodin by integrin-link kinase lead to suppression of cell growth and motility in prostate cancer cells. *Oncogene*. https://doi.org/10.1038/onc.2011.200

Yu, Yan Ping, & Luo, J. H. (2006). Myopodin-mediated suppression of prostate cancer cell migration involves interaction with zyxin. *Cancer Research*. https://doi.org/10.1158/0008-5472.CAN-06-0227

Yue, F., Cheng, Y., Breschi, A., Vierstra, J., Wu, W., Ryba, T., … Ren, B. (2014). A comparative encyclopedia of DNA elements in the mouse genome. *Nature*. https://doi.org/10.1038/nature13992

Yura, Y., Amano, M., Takefuji, M., Bando, T., Suzuki, K., Kato, K., … Kaibuchi, K. (2016). Focused Proteomics Revealed a Novel Rho-kinase Signaling Pathway in the Heart. *Cell Structure and Function*. https://doi.org/10.1247/csf.16011

Zeng, L., Kempf, H., Murtaugh, L. C., Sato, M. E., & Lassar, A. B. (2002). Shh establishes an Nkx3.2/Sox9 autoregulatory loop that is maintained by BMP signals to induce somitic chondrogenesis. *Genes and Development*. https://doi.org/10.1101/gad.1008002

Zhang, Q., Vashisht, A. A., O'Rourke, J., Corbel, S. Y., Moran, R., Romero, A., … Sampath, S. C. (2017). The microprotein Minion controls cell fusion and muscle formation. *Nature Communications*, *8*, 15664. https://doi.org/10.1038/ncomms15664

Zhang, W., & Roy, S. (2017). Myomaker is required for the fusion of fast-twitch myocytes in the zebrafish embryo. *Developmental Biology*. https://doi.org/10.1016/j.ydbio.2017.01.019

Zismanov, V., Chichkov, V., Colangelo, V., Jamet, S., Wang, S., Syme, A., … Crist, C. (2016). Phosphorylation of eIF2α is a Translational Control Mechanism Regulating Muscle Stem Cell Quiescence and Self-Renewal. *Cell Stem Cell*. https://doi.org/10.1016/j.stem.2015.09.020

APPENDIX A: LIST OF DIFFERENTIALLY REGULATED GENES

ENSEMBLE ID (ENSDARG)	Gene ID	Gene description	logFC	pValue
00000097973	si:ch1073-190k2.1		-11.94	2.45E-36
00000038248	ggact.2	gamma-glutamylamine cyclotransferase, tandem duplicate 2	-11.41	1.58E-08
00000092833	si:dkeyp-1h4.8		-10.62	5.97E-09
00000098699	si:ch211-11c3.9		-9.85	7.47E-05
00000100552	taco1	translational activator of mitochondrially encoded cytochrome c oxidase I	-9.52	2.22E-34
00000095522	si:dkey-71b5.3		-9.28	1.63E-07
00000069276	pimr132	Pim proto-oncogene, serine/threonine kinase, related 132	-9.20	3.59E-16
00000102848	si:dkey-31n13.3		-9.02	5.14E-17
00000090847	si:ch211-209l18.4		-8.90	5.36E-37
00000093111	si:ch211-209l18.2		-8.83	2.97E-11
00000022525	mchr1b	melanin-concentrating hormone receptor 1b	-8.61	1.17E-08
00000104174	NA		-8.34	6.32E-08
00000100964	si:ch211-57b15.2		-8.27	2.01E-06
00000080001	NA		-8.25	3.75E-39
00000104268	NA		-8.24	4.72E-10
00000077571	zgc:174862		-8.22	0.000419121
00000093153	NA		-8.19	2.38E-06
00000098570	si:ch211-8c17.2		-8.11	1.05E-06
00000105279	si:ch211-108c17.2		-7.93	2.26E-37
00000093998	si:ch73-7i4.2		-7.76	5.24E-07
00000102528	AL935126.1		-7.45	2.00E-05
00000004939	mtdhb	Metadherin	-7.41	9.28E-48
00000096541	BX901942.1		-7.39	1.48E-08
00000103260	si:ch211-57b15.1		-7.39	1.36E-06

00000079703	si:dkey-18p12.4		-7.38	4.05E-08
00000098036	si:ch211-69l10.4		-7.34	1.44E-36
00000097541	CU137680.1	lincRNA	-7.29	1.15E-06
00000041433	si:dkey-7c18.24		-7.01	2.24E-09
00000103319	si:ch73-359m17.7		-7.00	4.79E-07
00000103555	si:ch211-8c17.4		-6.94	5.99E-05
00000093365	NA		-6.85	2.92E-16
00000099419	CABZ01025780.1		-6.75	0.000127669
00000102364	si:dkey-202l22.6		-6.67	4.26E-05
00000098557	BX323564.1		-6.50	0.000504064
00000099521	NA		-6.36	0.000492483
00000097728	CR388132.1	lincRNA	-6.35	0.000472072
00000102282	CABZ01063298.1		-6.00	2.54E-08
00000095883	BX001026.1	lincRNA	-5.89	2.83E-09
00000056502	si:ch73-334d15.4		-5.89	6.71E-13
00000071648	zgc:113298		-5.82	1.70E-12
00000101040	ccl20a.3	chemokine (C-C motif) ligand 20a, duplicate 3	-5.79	5.87E-21
00000078551	zgc:171242		-5.67	9.59E-07
00000069566	mucms1	mucin, multiple PTS and SEA group, member 1	-5.62	7.03E-09
00000077090	si:ch211-127b11.1		-5.58	1.63E-14
00000098976	CU457778.1		-5.46	0.000748978
00000078001	kbtbd7	kelch repeat and BTB (POZ) domain containing 7	-5.39	0.000170812
00000099417	NA		-5.35	9.55E-14
00000070991	mlpha	melanophilin a	-5.25	5.37E-13
00000093416	BX470229.1		-5.25	0.000458133
00000105556	NA		-5.24	2.05E-10
00000094937	CR450833.1		-4.99	3.88E-05

00000086522	zp2.5	zona pellucida glycoprotein 2, tandem duplicate 5	-4.92	1.33E-09
00000069830	NA		-4.87	3.11E-07
00000100023	NA		-4.86	1.22E-05
00000071651	NA		-4.80	6.09E-13
00000099864	si:ch73-170d6.2		-4.76	1.03E-05
00000104950	NA		-4.76	2.15E-05
00000093019	si:dkey-83k24.5		-4.75	1.05E-26
00000059786	NA		-4.74	2.44E-06
00000096014	znf1146	zinc finger protein 1146	-4.65	7.14E-09
00000101756	im:7141269		-4.43	1.56E-10
00000093926	CR855277.3	lincRNA	-4.42	6.43E-05
00000033854	abrab	actin binding Rho activating protein b	-4.38	1.74E-09
00000099006	CABZ01029938.1		-4.34	1.21E-10
00000068609	NA		-4.33	1.97E-06
00000093974	CR933734.2		-4.32	0.000175505
00000002722	ankrd2	ankyrin repeat domain 2 (stretch responsive muscle)	-4.31	0.0009102 6
00000045453	f13a1a.1	coagulation factor XIII, A1 polypeptide a, tandem duplicate 1	-4.31	3.18E-09
00000091235	CABZ01015525.1		-4.30	2.78E-10
00000097137	CR753876.1	lincRNA	-4.28	5.40E-05
00000096545	si:ch211-191a16.5		-4.26	3.59E-07
00000097229	si:ch211-226h8.15		-4.22	1.13E-05
00000075225	si:ch211-223a10.1		-4.17	2.56E-05
00000070845	si:dkey-56d12.4		-4.16	1.96E-09
00000103634	CU914622.2		-4.04	3.75E-05
00000074001	crygmxl2	crystallin, gamma MX, like 2	-3.96	8.31E-06
00000092692	pimr133	Pim proto-oncogene, serine/threonine kinase, related 133	-3.92	0.000100002
00000089021	si:dkey-7f16.3		-3.91	2.16E-06

00000085497	RF00009		-3.88	2.29E-05
00000090108	si:ch1073-174d20.1	dysbindin domain-containing protein 1 (from NCBI)	-3.78	3.41E-05
00000089515	si:dkeyp-46h3.5		-3.77	1.79E-08
00000088885	si:ch1073-340i21.3		-3.67	1.00E-10
00000068124	opn7d	opsin 7, group member d	-3.67	1.88E-05
00000105408	BX248082.1		-3.55	0.00093747
00000100740	CU179702.2		-3.51	9.46E-06
00000089049	NA		-3.45	3.35E-10
00000096599	si:ch211-160d14.9		-3.42	0.00047941
00000105391	si:cabz01059983.1		-3.41	2.75E-08
00000097611	CU896691.2		-3.32	0.000296994
00000087407	si:ch73-304f21.1		-3.30	9.61E-05
00000086337	si:dkey-102g19.3		-3.27	1.39E-05
00000037789	pvalb1	Parvalbumin 1	-3.24	2.96E-07
00000103437	NA		-3.21	6.59E-05
00000073821	znf1177	zinc finger protein 1177	-3.21	8.04E-09
00000086351	NA		-3.20	0.000223349
00000039351	ccl19b	chemokine (C-C motif) ligand 19b	-3.16	0.000332423
00000101748	si:ch211-24o8.4		-3.16	3.33E-05
00000104652	NA		-3.14	1.16E-08
00000095200	si:ch211-197e7.1		-3.12	1.33E-07
00000022817	pvalb3	Parvalbumin 3	-3.11	6.34E-06
00000014803	cryba1l2	crystallin, beta A1, like 2	-3.11	7.96E-06
00000098095	CT027696.1	lincRNA	-3.08	0.000177748
00000078728	znf1068	zinc finger protein 1068	-3.08	2.01E-07
00000103248	CABZ01064771.1		-3.08	2.16E-05
00000080675	si:dkey-71b5.7		-3.07	8.62E-05
00000060034	tmem151ba	transmembrane protein 151Ba	-3.06	7.59E-06

00000032836	pvalb5	parvalbumin 5	-3.05	5.32E-05
00000090526	zgc:158404		-3.02	1.80E-08
00000104670	NA		-2.98	4.42E-08
00000091996	tcnbb	transcobalamin beta b	-2.92	0.000265732
00000068457	tnnt3b	troponin T type 3b (skeletal, fast)	-2.91	6.84E-07
00000096189	si:dkey-54j5.2		-2.89	2.31E-07
00000089963	NA		-2.87	1.01E-07
00000060345	apoda.1	apolipoprotein Da, duplicate 1	-2.85	2.53E-05
00000092378	BX571809.1		-2.84	0.000858011
00000092885	zgc:171977		-2.82	0.000124348
00000039436	il13ra2	interleukin 13 receptor, alpha 2	-2.80	0.000402202
00000091627	si:dkey-271j15.3		-2.77	0.000207891
00000103013	pcdh1g22	protocadherin 1 gamma 22	-2.74	1.01E-05
00000101623	znf992	zinc finger protein 992	-2.73	6.59E-08
00000096936	BX005461.2		-2.72	0.000272834
00000100213	NA		-2.71	5.33E-09
00000095595	si:ch211-283e2.7		-2.71	1.05E-05
00000034705	pvalb7	Parvalbumin 7	-2.70	2.06E-05
00000079227	plekhs1	Pleckstrin Homology Domain Containing S1	-2.69	1.83E-05
00000027355	slc25a4	Solute Carrier Family 25 Member 4	-2.66	6.48E-06
00000007769	sult5a1	sulfotransferase family 5A, member 1	-2.66	6.19E-06
00000092578	si:ch211-222e20.4		-2.66	8.64E-07
00000091119	fbxo40.2	F-box protein 40, tandem duplicate 2	-2.63	0.000451509
00000043085	alox5b.1	arachidonate 5-lipoxygenase b, tandem duplicate 1	-2.59	0.000106219
00000089627	si:ch211-160d20.5		-2.58	0.00027772
00000052949	NA		-2.57	0.000321786

00000088432	NA		-2.56	4.61E-05
00000103790	NA		-2.53	7.94E-07
00000099736	CABZ01075078.1		-2.52	8.23E-05
00000087999	BX664625.3		-2.52	8.47E-07
00000098987	znf1071	zinc finger protein 1071	-2.49	1.93E-05
00000006568	kcnmb2	Potassium Calcium-Activated Channel Subfamily M Regulatory Beta Subunit 2	-2.48	2.44E-05
00000045230	cox6b1	cytochrome c oxidase subunit 6B1	-2.47	9.72E-06
00000011259	trpm1a	transient receptor potential cation channel, subfamily M, member 1a	-2.47	0.000259815
00000012610	saga	S-antigen; retina and pineal gland (arrestin) a	-2.43	0.000690042
00000029069	tnni2a.4	troponin I type 2a (skeletal, fast), tandem duplicate 4	-2.42	1.95E-05
00000103237	si:ch73-299h12.8		-2.40	4.62E-06
00000100859	NA		-2.39	4.31E-08
00000096091	BX927253.2		-2.38	0.000152003
00000098743	NA		-2.37	0.000100434
00000076146	si:ch211-285c6.4		-2.36	1.45E-06
00000077497	igsf10	immunoglobulin superfamily, member 10	-2.35	4.19E-05
00000103371	si:dkey-190j3.6		-2.34	0.000358863
00000053875	cryba1b	crystallin, beta A1b	-2.33	7.73E-05
00000035438	myhc4	myosin heavy chain 4	-2.33	3.68E-07
00000035891	acana	aggrecan a	-2.31	6.38E-07
00000024433	pvalb4	Parvalbumin 4	-2.31	0.000197804
00000091099	NA		-2.31	6.42E-05
00000092945	si:ch211-250g4.3		-2.31	0.000836342
00000081702	RF00092		-2.30	4.16E-05
00000096688	CU660013.1	lincRNA	-2.28	0.000653372

00000104890	si:dkey-82i20.1		-2.27	1.18E-05
00000095930	myha	myosin, heavy chain a	-2.27	1.10E-05
00000027523	trpc7a	transient receptor potential cation channel, subfamily C, member 7a	-2.27	0.000363929
00000099097	NA		-2.27	8.78E-05
00000105411	si:ch211-113d11.5		-2.27	0.00012517
00000100340	NA		-2.26	6.51E-06
00000101695	si:dkey-26m3.3		-2.24	9.38E-06
00000099440	CR936249.1		-2.22	0.000488652
00000087318	NA		-2.22	2.32E-05
00000101817	si:dkey-5i16.5		-2.18	8.60E-05
00000101426	NA		-2.17	4.43E-06
00000056028	slc22a7a	solute carrier family 22 (organic anion transporter), member 7a	-2.15	0.000108205
00000037285	mipa	major intrinsic protein of lens fiber a	-2.14	0.000128949
00000045180	acta2	actin, alpha 2, smooth muscle, aorta	-2.12	3.21E-06
00000096273	si:dkey-3n22.9		-2.12	2.75E-06
00000102326	NA		-2.12	0.000281329
00000075527	zgc:174154		-2.10	0.000947859
00000084991	RF00091		-2.08	0.000573473
00000059412	zgc:111976		-2.05	0.000193275
00000104919	si:ch211-153b23.3		-2.03	4.61E-09
00000093068	c3b.1	complement component c3b, tandem duplicate 1	-2.03	1.14E-05
00000057426	oard1	O-acyl-ADP-ribose deacylase 1	-2.03	0.000196299
00000067848	nmrk2	nicotinamide riboside kinase 2	-2.02	3.06E-07
00000102004	apoea	apolipoprotein Ea	-2.02	0.000516444
00000006456	pdgfrl	Platelet Derived Growth Factor Receptor Like	-2.02	9.61E-07

00000101760	znf1016	zinc finger protein 1016	-2.00	0.000903726
00000044212	NA		-2.00	0.000709821
00000102304	NA		-1.99	4.23E-05
00000105274	CABZ01074130.1		-1.99	1.38E-05
00000074308	lrrc75ba	leucine rich repeat containing 75Ba	-1.99	0.000208789
00000016793	crybb1l2	crystallin, beta B1, like 2	-1.96	0.00022268
00000094017	znf1137	zinc finger protein 1137	-1.96	0.000454427
00000087061	si:ch211-71k14.1		-1.90	0.000414841
00000092358	BX469930.1		-1.89	0.000468762
00000002768	pvalb2	Parvalbumin 2	-1.87	4.68E-05
00000037747	fscn1b	fascin actin-bundling protein 1b	-1.87	0.000602353
00000093317	si:ch211-209j10.6		-1.86	5.69E-05
00000099644	NA		-1.85	3.70E-06
00000104814	NA		-1.84	3.00E-07
00000068263	csf1b	colony stimulating factor 1b	-1.83	0.000192396
00000070770	her4.3	hairy-related 4, tandem duplicate 3	-1.83	0.000107442
00000012944	myhz2	myosin, heavy polypeptide 2, fast muscle specific	-1.83	4.36E-07
00000068507	crybb1	crystallin, beta B1	-1.82	0.000211315
00000098884	BX649355.1		-1.82	0.000396406
00000094175	znf1027	zinc finger protein 1027	-1.81	2.03E-05
00000096216	NA		-1.81	0.000775878
00000097091	si:dkey-7j22.2		-1.80	0.000237064
00000100491	BX511111.1	lincRNA	-1.78	0.000357373
00000002589	mylpfb	Myosin Light Chain, Phosphorylatable, Fast Skeletal Muscle	-1.77	2.54E-05

00000028306	prph	peripherin	-1.77	5.72E-06
00000089875	zgc:173705		-1.77	0.000346182
00000090169	NA		-1.75	0.000490962
00000070331	muc5.1	mucin 5.1, oligomeric mucus/gel-forming	-1.75	0.000137205
00000090399	NA		-1.74	0.000280088
00000070000	txnipb	thioredoxin interacting protein b	-1.73	1.59E-06
00000006848	si:ch211-219a4.6		-1.73	0.000100565
00000103796	NA		-1.70	0.000770805
00000067995	myhz1.2	myosin, heavy polypeptide 1.2, skeletal muscle	-1.70	1.05E-06
00000105651	BX323060.3	lincRNA	-1.70	0.000512692
00000087180	ubxn2a	UBX domain protein 2A	-1.70	0.000341116
00000007275	si:ch211-251b21.1		-1.69	0.000521709
00000078828	npb	neuropeptide B	-1.69	7.14E-07
00000074583	grid1a	glutamate receptor, ionotropic, delta 1a	-1.68	0.000772182
00000076075	myh7ba	myosin, heavy chain 7B, cardiac muscle, beta a	-1.65	7.77E-06
00000018105	casq1b	Calsequestrin 1	-1.65	0.000173862
00000056464	fitm1	fat storage-inducing transmembrane protein 1	-1.64	5.36E-09
00000094428	si:dkey-31f5.8		-1.62	0.000505911
00000042641	cyp51	cytochrome P450, family 51	-1.62	2.83E-05
00000102725	CABZ01081909.1	coiled-coil domain-containing protein 34-like	-1.61	0.000490299
00000100829	pcdh1g32	protocadherin 1 gamma 32	-1.59	5.18E-05
00000086157	NA		-1.59	0.000550453
00000038716	casq1a	calsequestrin 1a	-1.59	2.66E-05

00000056108	ndufa4	NADH:ubiquinone oxidoreductase subunit A4	-1.58	0.000141965
00000088514	and1	actinodin1	-1.58	8.36E-05
00000071445	myoz1b	myozenin 1b	-1.57	0.000146721
00000079302	and2	actinodin2	-1.56	0.000677937
00000019521	mpx	Myeloperoxidase	-1.55	0.000453426
00000058848	mcoln1b	mucolipin 1b	-1.55	0.000230064
00000069559	muc13a	mucin 13a, cell surface associated	-1.53	0.000206557
00000077157	synpo2b	Synaptopodin-2b	-1.53	8.16E-05
00000103380	si:ch73-21k16.1		-1.51	0.000644684
00000091243	znf975		-1.50	0.000745944
00000003797	asb2a.1	Ankyrin Repeat And SOCS Box Containing 2	-1.50	0.000732128
00000096152	NA		-1.49	0.000320626
00000015876	npas1	Neuronal PAS Domain Protein 1	-1.43	0.000518058
00000039099	aep1	aerolysin-like protein	-1.43	0.000345517
00000094426	her4.2	hairy-related 4, tandem duplicate 2	-1.43	3.71E-07
00000062045	il1rapl1a	interleukin 1 receptor accessory protein-like 1a	-1.42	4.84E-06
00000099860	pkmb	pyruvate kinase M1/2b	-1.40	0.000961033
00000057903	si:ch211-266g18.10		-1.40	0.000730325
00000007407	barx1	BARX Homeobox 1	-1.40	0.000730789
00000029105	ftr51	finTRIM family, member 51	-1.39	0.000261005
00000070157	tgm2a	transglutaminase 2, C polypeptide A	-1.38	7.34E-05
00000093957	si:dkey-251i10.2		-1.38	0.000916438
00000093773	si:ch1073-296i8.2		-1.37	0.000179598

00000030270	tnnt3a	troponin T type 3a (skeletal, fast)	-1.37	0.000425006
00000056729	her4.2	hairy-related 4, tandem duplicate 2	-1.35	3.29E-06
00000071877	dhrs7cb	dehydrogenase/reductase (SDR family) member 7Cb	-1.35	0.000299978
00000017441	mylz3	myosin, light polypeptide 3, skeletal muscle	-1.34	7.53E-05
00000095675	ccdc141	coiled-coil domain containing 141	-1.34	1.07E-05
00000099420	nme2b.2	NME/NM23 nucleoside diphosphate kinase 2b	-1.32	8.44E-05
00000096257	si:ch73-367p23.2		-1.30	1.90E-05
00000030844	klf11a	Kruppel-like factor 11a	-1.30	6.59E-05
00000062788	irg1l	immunoresponsive gene 1, like	-1.29	8.79E-06
00000056732	her4.1	hairy-related 4, tandem duplicate 1	-1.27	0.000387948
00000069775	fbxo40.1	F-box protein 40, tandem duplicate 1	-1.27	0.00079567
00000061977	ppfibp2a	PTPRF interacting protein, binding protein 2a (liprin beta 2)	-1.27	0.000372101
00000035629	parvab	parvin, alpha b	-1.25	0.00088718
00000036671	tnni4b.2	troponin I4b, tandem duplicate 2	-1.24	0.000503144
00000090268	krtt1c19e	keratin type 1 c19e	-1.24	0.000185723
00000103442	NA		-1.23	3.86E-05
00000103586	si:dkey-65j6.2		-1.21	4.16E-05
00000038559	h1f0	H1 histone family, member 0	-1.21	1.04E-08
00000022399	ntmt1	N-terminal Xaa-Pro-Lys N-methyltransferase 1	-1.21	0.000146853
00000061249	myom1a	myomesin 1a (skelemin)	-1.17	3.35E-05
00000058003	wfdc1	WAP four-disulfide core domain 1	-1.16	0.000152567
00000067990	myhz1.1	myosin, heavy polypeptide 1.1, skeletal muscle	-1.14	0.000158331
00000058548	bves	blood vessel epicardial substance	-1.13	0.00011815

00000006588	zgc:111983		-1.12	0.000223553
00000099974	ldb3b	LIM domain binding 3b	-1.12	0.000462244
00000035327	ckma	creatine kinase, muscle a	-1.11	0.000162246
00000037618	ddit4	DNA-damage-inducible transcript 4	-1.09	0.000172267
00000044968	vcla	vinculin a	-1.06	0.000368395
00000054560	her15.2	hairy and enhancer of split-related 15, tandem duplicate 2	-1.05	0.000335093
00000099154	CABZ01032488.1		-1.04	0.000545637
00000034933	chchd3b	coiled-coil-helix-coiled-coil-helix domain containing 3b	-1.04	0.000786766
00000016357	fmo5	Flavin Containing Monooxygenase 5	-1.03	0.000242196
00000099101	gch2	GTP cyclohydrolase 2	-1.02	6.32E-05
00000000804	rassf6	Ras Association Domain Family Member 6	-1.01	0.000862192
00000036028	arrdc3b	arrestin domain containing 3b	-0.98	2.86E-05
00000040565	ckmb	creatine kinase, muscle b	-0.98	0.000618743
00000055618	acta1b	actin, alpha 1b, skeletal muscle	-0.95	0.000322095
00000013755	actn3a	actinin alpha 3a	-0.94	0.000482184
00000054058	h1fx	H1 histone family, member X	-0.93	0.000521292
00000009822	her4.4	hairy-related 4, tandem duplicate 4	-0.92	0.000586415
00000022456	eno1a	enolase 1a, (alpha)	-0.90	0.000770769
00000037030	casz1	castor zinc finger 1	-0.85	0.000530775
00000035519	histh1l	histone H1 like	-0.85	0.000449798
00000020574	atp2a1	ATPase sarcoplasmic/endoplasmic reticulum Ca2+ transporting 1	-0.84	0.000533733

00000035859	angptl4	angiopoietin-like 4	-0.84	0.000172514
00000036107	txnipa	thioredoxin interacting protein a	-0.82	0.000143515
00000039052	klhl40a	kelch-like family member 40a	-0.79	0.000761587
00000039007	eno3	enolase 3, (beta, muscle)	-0.76	0.000572783
00000068995	h2afx1	H2A histone family member X1	-0.75	0.000869343
00000076962	gdpd5b	glycerophosphodiester phosphodiesterase domain containing 5b	0.79	0.000788867
00000039117	tefa	thyrotrophic embryonic factor a	0.79	7.06E-05
00000012968	rhoub	ras homolog family member Ub	0.79	0.000913571
00000076239	si:ch211-74f19.2		0.81	0.000527354
00000070546	msgn1	mesogenin 1	0.85	0.000786775
00000097663	BX324206.2	lincRNA	0.87	0.000423201
00000075048	lonrf1	LON peptidase N-terminal domain and ring finger 1	0.87	0.000908189
00000093463	CU693484.1	lincRNA	0.94	0.000263501
00000035559	tp53	tumor protein p53	0.97	0.000426799
00000076839	ftr86	finTRIM family, member 86	0.97	6.74E-05
00000103512	NA		1.02	0.000268338
00000002609	rnf145a	RING finger protein 145	1.04	1.79E-05
00000078882	slc22a31	solute carrier family 22, member 31	1.06	0.000889364
00000105445	CR769769.2	lincRNA	1.08	8.30E-07
00000096990	si:ch1073-340i21.2		1.09	0.000642134
00000091902	b3gnt2b	UDP-GlcNAc:betaGal beta-1,3-N-acetylglucosaminyltransferase 2b	1.12	0.000555103
00000100513	rps27l	ribosomal protein S27 like	1.13	0.000528251

00000076667	ccng1	cyclin G1	1.16	7.79E-05
00000073799	zgc:194210		1.19	6.79E-05
00000092900	BX927258.1		1.21	0.000369893
00000074844	CABZ01061495.1		1.27	7.22E-06
00000078567	lonrf1l	LON peptidase N-terminal domain and ring finger 1, like	1.29	2.72E-08
00000037804	phlda3	pleckstrin homology-like domain, family A, member 3	1.30	6.01E-05
00000052846	fsta	follistatin a	1.31	2.20E-09
00000091657	CT573256.1	serine/threonine-protein kinase VRK1-like	1.34	0.000785091
00000045636	rbl2	retinoblastoma-like 2 (p130)	1.35	6.17E-05
00000045768	cry1aa	cryptochrome circadian regulator 1aa	1.35	4.88E-08
00000055715	capn8	calpain 8	1.36	2.45E-05
00000102226	gpr19	G protein-coupled receptor 19	1.37	0.000173486
00000095556	CR318588.4		1.39	8.14E-05
00000018980	zgc:91890		1.48	9.27E-06
00000042221	mthfd1l	methylenetetrahydrofolate dehydrogenase (NADP+ dependent) 1 like	1.48	0.00047043
00000034503	per2	period circadian clock 2	1.51	2.05E-08
00000077178	zgc:152977		1.51	0.000228283
00000058325	casp8	caspase 8, apoptosis-related cysteine peptidase	1.53	7.95E-06
00000025679	comtb	catechol-O-methyltransferase b	1.54	0.000842599
00000069654	ppp6r2b	protein phosphatase 6, regulatory subunit 2b	1.55	7.88E-05
00000059885	frmd3	FERM domain containing 3	1.56	0.000377503
00000076321	col28a2a	collagen, type XXVIII, alpha 2a	1.58	5.82E-05
00000097694	CU137681.3	lincRNA	1.60	0.000814047
00000043624	pqlc2	PQ loop repeat containing 2	1.62	0.000514273

00000093699	si:ch73-27e22.4		1.63	0.000770715
00000014309	spaw	southpaw	1.70	0.00034525
00000007421	ftcd	Formimidoyltransferase Cyclodeaminase	1.72	0.00013524
00000044253	paqr3b	progestin and adipoQ receptor family member IIIb	1.73	7.68E-08
00000105655	BX571811.2	lincRNA	1.80	2.08E-05
00000095893	si:dkey-85n7.7		1.84	0.000790109
00000077903	NA		1.91	0.000396839
00000094408	si:ch1073-110a20.1		1.91	0.0001013
00000093289	si:dkey-9i23.14		1.94	1.72E-05
00000062943	taco1	translational activator of mitochondrially encoded cytochrome c oxidase I	1.96	3.41E-05
00000095161	AL590134.1		1.98	0.000472302
00000086839	NA		2.01	6.80E-05
00000036471	dand5	DAN domain family, member 5	2.06	0.000478549
00000083519	NC_002333.24		2.14	6.45E-05
00000104340	rspo1	R-spondin 1	2.15	8.59E-05
00000009018	rhbg	Rh Family B Glycoprotein	2.21	2.03E-05
00000079403	si:dkey-204l11.1		2.21	2.44E-05
00000104166	si:ch211-232d10.1		2.21	0.000301387
00000051912	zgc:152945	hemopexin b	2.22	2.39E-05
00000097693	si:ch211-248a14.8		2.25	4.25E-07
00000059053	slc13a4	solute carrier family 13 (sodium/sulfate symporter), member 4	2.29	8.20E-05
00000071103	si:dkey-222p3.1		2.29	0.000878821
00000062508	cplx3a	complexin 3a	2.31	0.000288363
00000068731	rxfp2l	relaxin family peptide receptor 2, like	2.35	2.40E-05

00000102552	NA		2.36	0.000139683
00000078258	CABZ01049847.1	gamma-glutamyltransferase 5b	2.36	0.00032111
00000094135	BX936305.1	lincRNA	2.45	0.000899637
00000017880	kcnip3b	Potassium Voltage-Gated Channel Interacting Protein 3	2.45	2.65E-05
00000071588	BX539307.1		2.46	2.77E-07
00000040194	NA		2.46	0.000635986
00000094508	CR925709.2		2.50	0.000434879
00000097929	si:dkey-117j14.6		2.54	9.81E-05
00000094212	si:dkey-179k24.1		2.55	9.23E-05
00000094719	CR318588.3		2.66	2.11E-05
00000008788	camk1gb	calcium/calmodulin-dependent protein kinase Igb	2.73	0.000207703
00000095963	si:ch73-361h17.1		2.75	6.31E-10
00000090945	si:ch211-170d8.8		2.83	4.38E-05
00000019093	si:ch73-160i9.2		2.89	0.000438947
00000063078	abcg5	ATP-binding cassette, sub-family G (WHITE), member 5	2.89	0.000318879
00000039747	BX914200.1		2.89	0.000244953
00000030307	hspa12b	heat shock protein 12B	2.90	9.67E-15
00000042010	pklr	pyruvate kinase L/R	2.92	6.92E-10
00000103309	BX664625.4		2.96	4.49E-07
00000101790	si:ch73-299h12.3		2.97	8.75E-06
00000043002	vmo1a	vitelline membrane outer layer 1 homolog a	3.10	0.000155617
00000037613	lgals8b	galectin 8b	3.16	8.19E-11
00000102488		lincRNA	3.44	5.68E-06
00000037195	tshr	thyroid stimulating hormone receptor	3.86	6.29E-10
00000100520	si:dkey-25o1.7		3.86	7.40E-06

00000092806	si:ch1073-110a20.2		4.37	2.36E-15
00000104440	cdh30	cadherin 30	4.41	0.000151996
00000039682	si:ch211-121a2.2		4.74	4.98E-09
00000093639	BX537282.1		4.83	5.02E-16
00000040781	sult3st4	sulfotransferase family 3, cytosolic sulfotransferase 4	5.17	0.000607189
00000093787	CR450686.3	lincRNA	5.41	8.83E-10
00000100796	na		5.53	1.17E-09
00000011983	zgc:136908		5.89	3.70E-05
00000027587	htr7b	5-hydroxytryptamine (serotonin) receptor 7b	6.17	3.15E-09
00000039164	mhc1uma	major histocompatibility complex class I UMA	7.50	1.75E-05
00000104985	zgc:110249		8.02	1.03E-10
00000059039	mhc1ula	major histocompatibility complex class I ULA	8.27	1.90E-06
00000071543	SHISA4 (1 of many)	shisa family member 4	9.25	1.60E-16